

# **Delineating genetic underpinnings and disease pathogenesis of primary microcephaly and Filippi syndrome**

Inaugural-Dissertation  
zur  
Erlangung des Doktorgrades  
der Mathematisch-Naturwissenschaftlichen Fakultät  
der Universität zu Köln



vorgelegt von

**Maria Asif**

aus

**Peshawar, Pakistan**

Köln, 2020

Vorsitzender: Prof. Dr. Siegfried Roth  
1. Berichterstatter: Prof. Dr. Peter Nürnberg  
2. Berichterstatter: Prof. Dr. Ludwig Eichinger  
Beisitzer: Dr. Birgit Budde

Mündliche Prüfung voraussichtlich: 25.06.2020

The present research work was carried out from January 2017 to April 2020 at the Institute of Biochemistry I, Medical Faculty, University of Cologne, Germany and the Cologne Center for Genomics (CCG), under the supervision of Prof. Dr. Peter Nürnberg, Prof. em. Dr. Angelika A. Noegel and Dr. Muhammad Sajid Hussain.

Die vorliegende Arbeit wurde in der Zeit von Januar 2017 bis April 2020 unter der Anleitung von Prof. Dr. Peter Nürnberg, Prof. em. Dr. Angelika A. Noegel und Dr. Muhammad Sajid Hussain am Zentrum für Biochemie I, Medizinischen Fakultät, Universität zu Köln und des Cologne Center for Genomics (CCG) angefertigt.

**Dedicated to**  
**The Participating Families**  
**And Science**

# Acknowledgements

The period of Ph.D. has been probably one of the best chapters of my life. I have to thank all the people who have contributed to the realization of this work, may that be in the field, the bench, in reflection, or just simply by their presence in everyday life.

First of all, I would like to thank **Prof. Dr. Peter Nürnberg**, founding director Cologne Center for Genomics (CCG), University of Cologne, for the confidence he granted me by agreeing to supervise my doctoral journey. I am forever grateful that you welcomed me to the group and maintained intellectually stimulating environment. I especially enjoyed brainstorming science with you; your advice, comments have been very valuable for progress this challenging work has made. I hope this work meets your expectation and testify my profound admiration.

With all my admiration, I sincerely thank Prof. **Dr. Shahid Mahmood Baig**, Deputy Chief Scientist, Head Health Biotechnology, National Institute for Biotechnology and Genetic Engineering (NIBGE), Faisalabad, Pakistan. His scientific input and vision have always guided my scientific ventures. I have been equally appreciating of his qualities as human, his generosity, leadership, professionalism and open-mindedness have been exemplary to me.

**Prof. em. Dr. Angelika Anna Noegel** (former head, Institute of Biochemistry I, Medical Faculty, University of Cologne)! Believe in my eternal respect and my sincere gratitude. I thank you for the interest you showed in my work particularly NUP proteins, found time to critically review it and the precious advice you gave me throughout of my doctoral work.

My deepest gratitude goes to **Dr. Muhammad Sajid Hussain**, Group Leader, Cologne Center for Genomics (CCG), University of Cologne. I am grateful for your availability, your intelligent criticism — which allowed me to mature as a young researcher — and above all your patience throughout my experimental work. I sincerely thank you for the intellectual input and the time you have spent for designing my experiments and correcting the drafts of this dissertation. This thesis was, undoubtedly, not possible without the kind of insights you have provided.

I can never thank enough my friends, especially, **Dr. Uzma Abdullah** who had been supporting me unconditionally and helped me greatly in all my personal and academic matters. Uzma, your suggestions, ideas, technical assistance during my thesis write up and reviews were precious. I owe you my life! I am also very thankful to **Dr. Ambrin Fatima** for her very recent and lively addition to my life!

To all my colleagues, staff and faculty at Institute of Biochemistry I, CCG, CMMC and CECAD! thank you for the exchange of knowledge and your support and encouragement. I am highly indebted to **Gabriele Thorn**, for being extra ordinary nice and taking care of all my official documentation. I especially thank CECAD proteomic and imaging facility and bioinformatics team of CCG for their technical contribution in data generation.

I sincerely thank my collaborators, especially, **Prof. Dr. Francesco Brancati**, University of L'Aquila, L'Aquila, Italy, **Prof. Dr. Marwan Shinawi**, Washington University School of Medicine, **Prof. Dr. Karsten Niefind**, University of Cologne and **Prof. Dr. Joachim Jose** and **Anna Nickelson** from University of Münster for sharing patient material and technical expertise that gave this work the scientific depth and strength that wasn't possible otherwise.

Finally, I have no words to thank my loving father, **Syed Asif Bukhari**, my loving mother **Tahira Asif** and my loving **siblings** for trusting me and listening to my cries and boosting my energies.

My most profound thanks go to **patients and their families** who have agreed to participate in this work. Thank you for the generosity with your time and your stories. It is only because of your collaboration, interest and will to help, that we can continue the search for answers. You are my true source of inspiration!

**Maria Asif**

# Table of Contents

1.	Summary .....	1
2.	Zusammenfassung .....	3
3.	Introduction .....	5
3.1	Human genetics: a brief history and future .....	5
3.2	Genetic disorders .....	6
3.3	<i>Fons et origo</i> of genetic disorders .....	7
3.3.1	Inherited familial mutations .....	7
3.3.2	Sporadic <i>de novo</i> mutations .....	8
3.4	Human brain development .....	10
3.4.1	Neurogenesis .....	10
3.4.2	Mode of cell division during neurogenesis .....	11
3.5	Congenital microcephaly (Small head) .....	13
3.5.1	Environmental factors .....	14
3.5.2	Genetics of MCPH .....	14
3.5.3	Pathomechanism of MCPH .....	16
3.5.4	Centriolopathy .....	17
3.5.5	Wnt signaling .....	17
3.5.6	DNA damage response (DDR) .....	18
3.5.7	Organ specificity of CM associated variations .....	18
3.5.8	Brain-specific phenotype .....	19
3.6	Syndromic microcephaly .....	20
3.7	Filippi syndrome (FLPIS) .....	21
3.7.1	Clinical features .....	21
3.7.2	Genetics of Filippi syndrome .....	22
3.7.3	<i>CKAP2L</i> — The first candidate gene of Filippi syndrome .....	22
3.7.4	Features of <i>CKAP2L</i> protein .....	23
3.7.5	<i>CAKP2L</i> in relation to digital anomaly .....	23
3.7.6	<i>CSNK2B</i> — the second candidate gene of Filippi syndrome .....	24
3.7.7	<i>CK2β</i> Protein — A subunit of <i>CK2</i> holoenzyme .....	24
3.7.8	<i>CK2</i> and human diseases .....	25
3.8	Nucleoporopathies .....	27
3.8.1	Microcephaly associated nephrotic syndrome .....	27
4.	Aims of the study .....	29

5.	Results .....	30
5.1	Preview of investigated families .....	30
5.2	Novel mutation in <i>STIL</i> causes MCPH in family MCP1 .....	31
5.3	<i>SH2D3C</i> is a novel candidate gene identified in family MCP2 .....	33
5.3.1	Genetic investigation .....	33
5.3.2	Splice site mutation in <i>SH2D3C</i> causes primary microcephaly .....	35
5.4	Mutation in novel gene <i>NUP37</i> causes primary microcephaly .....	36
5.4.1	Effects of <i>NUP37</i> nonsense mutation at transcript level .....	36
5.4.2	Effects of mutation on protein level .....	38
5.4.3	Effects of reduced <i>NUP37</i> on its binding partners .....	38
5.4.4	Investigating the effect of mutation on nuclear pore density .....	39
5.4.5	Abnormalities observed in <i>NUP37</i> mutated fibroblasts .....	40
5.4.6	Alteration in chromatin organization .....	41
5.4.7	Misshapen nuclei .....	41
5.4.8	Abnormal nucleoli .....	42
5.4.9	Verification of abnormalities using transmission electron microscopy (TEM) .....	43
5.4.10	Effect of mutation on cellular proliferation .....	44
5.5	Recapitulating cellular phenotype of <i>NUP37</i> mutants in <i>NUP107</i> mutated LCLs .....	45
5.6	Clinical features of FLPIS and FLS cases .....	47
5.6.1	Identification of disease-causing variants in studied cohort of FLPIS and FLS .....	48
5.6.2	Identification of six novel candidate genes of FLPIS .....	49
5.7	Novel mutations identified in <i>CSNK2B</i> causing a phenotype distinguished from Poirier-Bienvenu neurodevelopmental syndrome (POBINDS) .....	52
5.7.1	Family FP28 .....	52
5.7.2	Family FP30 .....	53
5.7.3	<i>In silico</i> predictions of <i>CSNK2B</i> variants .....	54
5.7.4	Validation of <i>CSNK2B de novo</i> mutations in etiology of Filippi syndrome .....	55
5.7.5	Prediction of effects of mutation on structure of CK2 $\beta$ .....	55
5.7.6	Prediction of effects of mutation on stability of CK2 $\beta$ .....	57
5.8	Influence of mutations on cellular expression of CK2 $\beta$ .....	59
5.8.1	Subcellular localization of endogenous and overexpressed CK2 $\beta$ .....	59
5.8.2	CK2 $\beta$ in whole cell lysate, cytosolic and nuclear fractions in patient LCLs .....	59



5.8.3	Transient expression of wild-type and CK2 $\beta$ mutants in HeLa cells.....	60
5.8.4	CK2 $\alpha$ and CKAP2L in <i>CSNK2B</i> mutated LCLs.....	62
5.9	Influence of CK2 $\beta$ mutations on association with CK2 $\alpha$ .....	64
5.9.1	Microscale thermophoresis (MST).....	65
5.10	Protein-protein interactome — probing interacting partners of CK2 $\beta$ .....	65
5.10.1	Known and novel binding partners of CK2 .....	66
5.10.2	Pathway enrichment of 38 binding partners showing compromised interaction of CK2 $\beta$ .....	66
5.11	Investigating regulators of Wnt signaling pathway.....	69
5.11.1	Cellular expression of $\beta$ -Catenin .....	69
5.11.2	Investigating the dynamics of active $\beta$ -Catenin by confocal imaging...	69
5.11.3	Investigating the dynamics of inactive $\beta$ -Catenin by confocal imaging	69
5.11.4	Confirmation of active and inactive $\beta$ -Catenin by immunoblotting .....	71
5.11.5	Interaction of CK2 $\beta$ with $\beta$ -Catenin .....	71
5.11.6	Phosphorylation of $\beta$ -Catenin by CK2 containing mutant CK2 $\beta$ .....	72
5.11.7	Capillary Electrophoresis based CK2 activity assay .....	73
5.11.8	Exploring the behavior of DVL3 in CK2 $\beta$ mutated LCLs .....	75
5.12	Investigating key regulators of DNA damage response pathway .....	76
5.12.1	Upregulation of $\gamma$ H2AX in p.Asp32His mutant LCL.....	76
5.12.2	Upregulation of 53BP1 in p.Asp32His mutant LCLs.....	77
5.12.3	Upregulation of CHK1 in p.Asp32His patient LCLs.....	78
5.13	Fate of <i>CSNK2B</i> mutated cells .....	79
5.13.1	Effect of p.Asp32His mutation on cell cycle in patient LCLs.....	79
5.13.2	Cellular apoptosis detected by TUNEL assay in p.Asp32His mutant LCLs.....	79
5.14	Phosphoproteome analysis of CK2 $\beta$ .....	81
5.14.1	Pathway enrichment of CK2 substrates lacking phosphorylation in p.Asp32His mutant.....	82
5.14.2	Reported CK2 substrates lack phosphopeptides in p.Asp32His mutant	83
5.14.3	Phosphoproteomic perturbations in p.Asp32His mutant .....	86
5.15	Whole transcriptome profiling — connecting the dots in bigger picture....	87
5.15.1	Pathway enrichment using PANTHER (protein analysis through evolutionary relationships) .....	88
5.15.2	Wnt target genes .....	89
5.15.3	DNA damage response and repair regulators .....	90
5.15.4	Transcription regulators .....	91

5.15.5	Immune response genes .....	92
5.16	Proposed disease model.....	94
6.	Discussion .....	95
6.1	Prediction tools are effective for determinig pathogenecity at gene and protein level.....	96
6.2	Microcephaly — extensive phenotypic and genotypic spectra.....	96
6.2.1	A novel variant of <i>STIL</i> — addition to the existing knowledge.....	97
6.2.2	<i>SH2D3C</i> is a promising novel candidate gene of primary microcephaly ...	97
6.2.3	Mutations in NUP genes — presenting non-syndromic and syndromic microcephaly .....	98
6.2.4	Reduced nucleoporin proteins cause gross cellular abnormalities leading to disease phenotype.....	99
6.2.5	Variable phenotypic spectra in NUP mutated individuals .....	99
6.3	The shift from non-syndromic to syndromic microcephaly remains unsolved .....	101
6.4	Filippi Syndrome — microcephaly remains part of a severe syndrome ...	102
6.4.1	The wild card regulator of kinases, <i>CSNK2B</i> , is the second disease causing gene of Filippi syndrome.....	103
6.4.2	Expanding the mutational and phenotypic horizon of <i>CSNK2B</i> .....	103
6.5	Why <i>CSNK2B</i> is chosen as the strongest candidate gene for this study?..	104
6.5.1	Extensive genetic investigations .....	104
6.5.2	<i>In silico</i> prediction of pathogenicity of <i>CSNK2B</i> variants in relation with CK2 $\beta$ protein domains .....	104
6.5.3	CK2 $\beta$ being a chief regulatory subunit for many proteins indicates its functional relevance with a syndromic condition.....	105
6.6	Mutations in the beta subunit of CK2 — the master of all kinases — causes impaired Wnt signaling .....	106
6.7	Delayed DNA damage response plays a significant role in pathogenicity of Filippi syndrome .....	108
6.8	Whole phosphoproteomic profiling validated and expanded knowledge to dysregulation of mutant CK2 .....	109
6.9	Transcriptome profiling authenticates findings obtained at protein level.	110
6.10	Implications of upregulated mutant CK2 $\beta$ (p.Asp32His and p.Asp32Asn) in patient LCLs .....	111
6.11	Hunting novel candidate genes for FLPIS .....	111
6.12	Concluding remarks and future prospects .....	113
7.	Materials and Methods .....	114
7.1	Data collection.....	114

7.2	Pedigree Construction .....	114
7.3	Genetic Investigations .....	114
7.3.1	Blood sampling and DNA extraction and quantification .....	114
7.3.2	Polymerase chain reaction (PCR) and gel electrophoresis.....	115
7.3.3	Homozygosity mapping .....	115
7.3.4	Whole-exome sequencing .....	116
7.3.5	Sanger sequencing.....	117
7.3.6	RNA isolation.....	118
7.3.7	Reverse transcriptase PCR (RT-PCR).....	118
7.3.8	Quantitative real-time PCR (qRT-PCR).....	118
7.4	Functional studies.....	119
7.4.1	Cell culture .....	119
7.4.2	Establishment of dermal fibroblasts from skin biopsies .....	119
7.4.3	Establishment of LCLs from blood.....	119
7.4.4	Cell culture conditions.....	120
7.4.5	Immunofluorescence of adherent cells.....	120
7.4.6	Immunofluorescence of cell suspension (LCLs).....	121
7.5	Microscopy.....	122
7.5.1	Electron microscopy.....	122
7.5.2	Confocal imaging .....	122
7.5.3	Confocal laser scanning microscope .....	122
7.6	Cell cycle assay by FACS .....	122
7.7	Proliferation assay .....	123
7.8	TUNEL assay .....	123
7.9	Investigating DNA Damage response .....	123
7.10	Immunoblot analysis .....	123
7.10.1	Protein extraction from eukaryotic cells .....	123
7.10.2	Immunoblotting.....	124
7.11	Site-directed mutagenesis to generate mutant constrcuts.....	125
7.11.1	Growing bacterial culture .....	126
7.11.2	Transformation of competent bacterial cells.....	127
7.11.3	Plasmid DNA purification from prokaryotic cells.....	127
7.12	Expression and purification of recombinant GST fused proteins from prokaryotic cells .....	128
7.12.1	Thrombin cleavage of GST tag from fusion proteins .....	129

7.13	Transient transfection of GFP-tagged constructs in eukaryotic cells.....	129
7.14	Pull-down assay.....	130
7.15	Mass spectrometry analysis.....	131
7.16	Experiments conducted for determining the kinase activity of CK2 $\beta$ variants .....	131
7.16.1	ADP-Glo assay.....	131
7.16.2	Capillary Electrophoresis.....	132
7.17	Microscale thermophoresis (MST).....	132
7.18	Whole transcriptome analysis .....	132
7.19	Whole phosphoproteome analysis.....	133
8.	Web resources .....	135
9.	Abbreviations .....	136
10.	References .....	138
11.	Erklärung .....	155
12.	Lebenslauf .....	156

# List of Tables

Table 3.1: List of genes involved in etiology of MCPH.....	15
Table 3.2: Reported <i>de novo</i> variants of <i>CSNK2B</i> .....	26
Tabel 5.1: Preview of investigated families.....	30
Table 5.2: Clinical and molecular investigation of <i>STIL</i> mutated individuals. ....	32
Table 5.3: Genetic information of the variants selected in MCP2 family along with their segregation pattern.....	35
Table 5.4: MaxEntScan prediction scores showing the scores obtained by different models.....	36
Table 5.5: Clinical profile of cases manifesting FLPIS and FLS .....	47
Table 5.6: Genetic information of studied cases.....	49
Table 5.7: pLI, Z and CADD scores of novel genes proposed for FLPIS.....	50
Table 5.8: Pathogenicity prediction scores of CK2 $\beta$ mutations by various <i>in silico</i> tools.....	55
Table 5.9: Protein thermostability scores predicted by I-Mutant2.0 and MUpro.....	58
Table 5.10: Proteins losing interaction with mutant CK2 $\beta$ . ....	68
Table 5.11: List of the reported proteins containing CK2 phosphosites, hypophosphorylated in mutant LCLs.....	84
Table 5.12: Whole phosphoproteome analysis of p.Asp32His patient LCLs.....	87
Table 6.1: Reported phenotypes caused due to variations in NUP genes.....	101
Table 7.1: List of primary antibodies used in this study.....	133
Table 7.2: List of secondary antibodies used in this study .....	134
Table 7.3: List of primers used in this study.....	134

# Tabel of Figures

Figure 3.1: Global distribution of consanguineous marriages. ....	8
Figure 3.2: An overview of interkinetic nuclear migration of different neuronal cell types. ....	11
Figure 3.3: Depiction of the mode of division and cleavage planes of progenitor cells. ....	12
Figure 3.4: Images of Flippi patient mutated with <i>CSNK2B</i> . ....	24
Figure 3.5: Structure of CK2 holoenzyme (Niefind et al, 2001). ....	25
Figure 5.1: Genetic and clinical analyses of MCP1 having mutation in <i>STIL</i> . ....	31
Figure 5.2: Gene structure of <i>STIL</i> (NM_001048166.1) showing reported disease-causing variations. ....	32
Figure 5.3: Genetic and clinical analyses of a family having mutation in <i>SH2D3C</i> . ..	33
Figure 5.4: Identification of pathogenic variation of <i>SH2D3C</i> . ....	34
Figure 5.5: Effects of mutation on protein level observed in <i>NUP37</i> mutated primary fibroblasts. ....	37
Figure 5.6: Effects of mutation, c.916C>T in <i>NUP37</i> at transcript level. ....	38
Figure 5.7: Effects of reduced <i>NUP37</i> on the localization and amounts of its binding partners. ....	39
Figure 5.8: Reduced nuclear pore density in <i>NUP37</i> mutated fibroblasts. ....	40
Figure 5.9: Immunostaining of heterochromatin in patient fibroblasts. ....	41
Figure 5.10: Abnormal shape of nuclear envelop in <i>NUP37</i> mutated fibroblasts. ....	42
Figure 5.11: Nucleolar abnormality in <i>NUP37</i> mutated primary fibroblasts. ....	42
Figure 5.12: TEM images of control versus mutant fibroblasts. ....	43
Figure 5.13: Proliferation of mutant fibroblasts. ....	44
Figure 5.14: Investigation of <i>NUP107</i> mutated LCLs. ....	46
Figure 5.15: Genetic and clinical analyses of Brazilian family having presumably pathogenic variation in <i>CDKL5</i> (Family FP14). ....	51

Figure 5.16: Genetic and clinical analyses of FP28 family having novel mutation in <i>CSNK2B</i> .....	52
Figure 5.17: Gene structure of <i>CSNK2B</i> (NM_001320.6).....	53
Figure 5.18: Clinical analysis of FP30 family having novel mutation in <i>CSNK2B</i> .....	53
Figure 5.19: Effects of mutations on the structure of CK2 $\beta$ .....	57
Figure 5.20: Effects of mutation(s) in patient LCLs on protein level.....	60
Figure 5.21: Localization of GFP tagged wild-type and mutants of CK2 $\beta$ .....	61
Figure 5.22: CK2 $\alpha$ and CKAP2L in <i>CSNK2B</i> mutated LCLs.....	63
Figure 5.23: Purification of GST fused CK2 $\beta$ and obtaining the cleaved protein product.....	64
Figure 5.24: Interaction of CK2 subunits analyzed by MST.....	65
Figure 5.25: Mass spectrometry data of wild-type and mutant, p.Asp32His, CK2 $\beta$ ...	67
Figure 5.26: Cellular localization and amount of $\beta$ -Catenin in patient derived and wild-type LCLs.....	70
Figure 5.27: Interaction of GST fused CK2 $\beta$ with $\beta$ -Catenin in HeLa cells.....	72
Figure 5.28: Kinase activity of CK2 having mutated beta subunits.....	73
Figure 5.29: Kinase activity of CK2 wild type and mutants based on capillary electrophoresis based assay.....	74
Figure 5.30: Analysis of DVL3 protein in wild-type and p.Asp32His mutant LCLs and validation of interaction with mutant CK2 $\beta$ .....	75
Figure 5.31: Investigation of $\gamma$ H2AX in p.Asp32His patient on DNA damage induction.....	77
Figure 5.32: Investigation of 53PB1 in p.Asp32His patient LCLs on DNA damage induction.....	77
Figure 5.33: Investigation of CHK1 in p.Asp32His patient derived LCLs on DNA damage induction.....	78
Figure 5.34: Effects of p.Asp32His mutation on cell cycle and apoptosis of LCLs....	80
Figure 5.35: Phosphoproteome analysis of wild-type and mutant LCLs.....	81
Figure 5.36: Pathway enrichment analysis of hypophosphorylated substrates of CK2 in patient derived LCLs.....	83
Figure 5.37: Pathway enrichment of differentially expressed genes.....	88

Figure 5.38: Heatmap of differentially expressed Wnt target genes in p.Asp32His mutant LCLs compared to control. ....	89
Figure 5.39: Heat map of differentially regulated DNA damage and repair genes in p.Asp32His mutant LCLs compared to control. ....	90
Figure 5.40: Heatmap of differentially regulated transcription factors in p.Asp32His mutant LCLs compared to control. ....	92
Figure 5.41: Heatmap of differentially regulated immune response genes in p.Asp32His mutant and control LCLs. ....	93
Figure 5.42: Proposed disease model of FLPIS caused due to variations in <i>CSNK2B</i> . ....	94



# 1. Summary

The genetic underpinnings of autosomal recessive genetic disorders have been extensively scrutinized for decades. Nevertheless, the requisites for dissecting the role of causative gene variants are indispensable for elucidation of underlying disease pathogenesis. Since thoroughgoing research has been conducted to decipher complexities of brain development, congenital microcephaly (CM) stands prominent as an immaculate model of the *in utero* development of the brain. The isolated form of CM — primary microcephaly (MCPH) — is a rare disorder portrayed by reduced brain size and intellectual disability. Contrarily, the syndromic form of CM has a shared genetic architecture and expounds additional roles of CM proteins in other organ systems.

This study aimed to comprehend the underlying pathology of 17 families afflicted with different inherited conditions. A consanguineous Pakistani MCPH family was characterized to harbour a mutation in *NUP37*. The mutational consequences of this gene, along with *NUP107* — mutated in syndromic microcephaly — were studied in patient derived cells to delineate the pathomechanisms. Both genes encode crucial components of the outer rings of the nuclear pore complex (NPC). Mutant proteins were discerned to be unstable and dislocated from the nuclear envelope in patient cells. Comparable mutational effects were observed on *NUP160* and *NUP133* — further components of the NPC. Consequently, abnormalities of the nuclear shape, chromatin organization, nucleoli as well as reduction of nuclear pore density were revealed in primary fibroblasts carrying a mutation in *NUP37*. My observations accentuate that the components of the NPC play a pivotal role in embryonic brain development and that a defective function of nuclear pore proteins leads to congenital microcephaly with or without associated anomalies.

CM is also a prominent feature of an extremely rare disorder, Filippi syndrome (FLPIS) typically characterized by craniodigital features (syndactyly of fingers and/or toes), short stature, intellectual disability and peculiar facial gestalt. A slight variability in clinical presentation causes an allelic disorder called Filippi like syndrome (FLS). Hitherto, only *CKAP2L* has been biochemically characterized for unraveling disease pathogenesis of FS. In this study, mutational consequences of *CSNK2B* — a novel candidate gene based on twomissense and a nonsense mutation identified in three unrelated cases of FS and FLS — were explored. *CSNK2B* encodes the  $\beta$  subunit of CK2, which is the master regulator of all kinases. Mutant *CSNK2B* showed abnormal expression at transcript as well as

protein level. One of the missense mutations resulted in an impaired cross talk between  $\alpha$  and  $\beta$  subunits and both missense mutations compromised the kinase activity of CK2. Delving deeper into the mutational effects, two crucial pathways were mainly investigated; canonical Wnt signaling (CWS) and DNA damage response (DDR). In CWS, a compromised interaction of CK2 $\beta$  with two key regulators of Wnt signaling, DVL3 and  $\beta$ -Catenin (along with its dysregulated expression) was observed. The likely effects of  $\beta$ -Catenin dysregulation on Wnt and DDR related genes were traced by transcriptional profiling. Furthermore, cell cycle arrest and elevated apoptosis were observed in mutant LCLs due to delayed DDR. Additionally, whole proteome profiling demonstrated disturbed interaction of 38 proteins crucial for pivotal cellular pathways, specifically CWS. Intriguingly, whole phosphoproteome profiling revealed impaired phosphorylation of more than 300 CK2 substrates in patient LCLs, thus suggesting global mutational effects. In general, it was noticed that the impact of both missense mutations slightly differed from each other on protein level. Data suggest that mutations in *CSNK2B* exert pleiotropic mutational effects, thereby causing FS and FSL.

In the remaining families of FS and MCPH, whole-exome sequencing and subsequent bioinformatics analyses revealed strong novel candidate genes for each of them. Taken together, this study provides novel insights into the genetic and functional bases of MCPH and FS. It lays the foundation for future genomic and therapeutic investigations for these and related disorders.

## 2. Zusammenfassung

Die Ursachen autosomal rezessiver Erkrankungen wurden in den letzten Jahrzehnten intensiv untersucht. Daneben ist die Analyse der Funktion der auslösenden Genvarianten eine herausragende Aufgabe, um die zugrunde liegenden Mechanismen der Entstehung und Entwicklung der jeweiligen Erkrankung zu verstehen. Im Zentrum unseres Interesses steht die angeborene Mikrozephalie (CM). Die autosomal rezessive primäre Mikrozephalie (MCPH), die isolierte Form der CM, ist eine seltene angeborene Erkrankung, die durch eine Störung der Gehirnentwicklung, eine reduzierte Gehirngröße und damit einhergehend einen reduzierten Kopfumfang und eine unterschiedlich stark ausgeprägte geistige Behinderung gekennzeichnet ist. Die syndromische Form der CM ist ebenfalls durch Mikrozephalie charakterisiert, es sind jedoch gleichzeitig auch andere Organsysteme betroffen. Darüber hinaus ist die Mikrozephalie für die Aufklärung der Gehirnentwicklung von erheblicher Bedeutung.

Ziel dieser Arbeit war die Analyse von siebzehn pakistanischen Familien, die verschiedene erblich bedingte Erkrankungen aufwiesen. In einer blutsverwandten MCPH-Familie konnten wir eine Mutation im Gen für das Kernporenprotein NUP37 identifizieren. Die Konsequenzen dieser Mutation und einer weiteren im Gen für NUP107, die eine syndromische Mikrozephalie verursacht, wurden in Patientenzellen analysiert. NUP37 und NUP107 sind beides Komponenten des äußeren Rings des Kernporenkomplexes (NPC). Die Proteine waren instabil und nur gering mit der Kernhülle assoziiert. NUP160 und NUP133 zeigten ein ähnliches Verhalten. Eine Analyse des Zellkerns in Mutantenfibroblasten ergab Veränderungen der Kernform, der Chromatinorganisation, der Nukleoli und eine geringere Kernporendichte. Zusammengefasst kann man sagen, dass Komponenten des NPC eine entscheidende Rolle in der embryonalen Gehirnentwicklung spielen und eine Fehlfunktion von Kernporenproteinen zur angeborenen Mikrozephalie mit oder ohne assoziierten Anomalien führt.

Das Filippi Syndrom (FS), eine weitere sehr seltene Erkrankung, ist ebenfalls durch CM charakterisiert und durch craniodigitale Defekte (Syndaktylie der Finger und/oder Zehen), Kleinwuchs, geistige Retardierung und eine charakteristische Gesichtsform. Das Filippi like Syndrome (FLS) ist durch eine variable Klinik gekennzeichnet. Bis jetzt waren nur

Mutationen in *CKAP2L* als Ursache für FS bekannt und untersucht. In dieser Arbeit wurde die Konsequenz von Mutationen in *CSNK2B* untersucht. *CSNK2B* ist ein neues Kandidatengen für FS und FLS, in dem zwei Missensmutationen und eine Nonsensmutation in drei unabhängigen Fällen von FS und FLS identifiziert wurden. *CSNK2B* kodiert für die  $\beta$ -Untereinheit der Proteinkinase CK2, dem Regulator aller Kinasen. Das mutierte *CSNK2B* zeigte eine veränderte Expression sowohl auf der Transkript- als auch auf der Proteinebene. Zudem führte eine der Missensmutationen zu einer Veränderung der Interaktion zwischen der  $\alpha$ - und der  $\beta$ -Untereinheit der CK2, und beide Missensmutationen beeinträchtigten die Kinaseaktivität der CK2. Um die Effekte der Mutationen weiter zu untersuchen, wurden mit dem kanonischen Wnt-Signalweg (CWS) und dem Reparaturweg nach DNA-Schädigung (DDR) zwei wichtige Signalwege ausgewählt, die durch CK2 beeinflusst werden. Für den CWS fanden wir, dass die Interaktion von CK2 $\beta$  mit den zwei Schlüsselregulatoren des Wnt-Signalwegs, nämlich DVL3 und  $\beta$ -Catenin, gestört war zusätzlich zu deren veränderter Expression. Die Auswirkungen der  $\beta$ -Catenin-Dysregulation auf die Wnt- and DDR-assoziierten Gene wurden durch eine Analyse der Transkriptionsprofile verfolgt. Darüber hinaus wurden bei mutierten LCLs aufgrund verzögerter DDR ein Stillstand des Zellzyklus und eine erhöhte Apoptose beobachtet. Eine Proteomanalyse zeigte eine gestörte Interaktion von 38 Proteinen an, die in zentrale zelluläre Signalwege involviert sind, insbesondere in den CWS, und eine Phosphoproteomanalyse zeigte eine Beeinträchtigung der Phosphorylierung von mehr als 300 CK2-Substraten in Patienten-LCLs. Das verweist auf globale Effekte der Mutationen. Generell konnten wir feststellen, dass beide Missensmutationen in ihren Auswirkungen geringfügig voneinander abwichen. Unsere Daten weisen darauf hin, dass Mutationen in *CSNK2B* pleiotrope Effekte haben und so FS und FSL verursachen.

Schließlich haben wir in den verbleibenden FS- und MCPH-Familien durch Exom-Sequenzierung und bioinformatische Analyse neue Kandidatengene identifiziert. Zusammenfassend haben wir mit dieser Arbeit neue Daten zu den genetischen und funktionellen Ursachen von MCPH und FS gezeigt. Sie bilden die Grundlage für weitere Untersuchungen, die möglicherweise zu einer Behandlung dieser und verwandter Erkrankungen führen können

## 3. Introduction

### 3.1 Human genetics: a brief history and future

Human has always been inquisitive about its existence and mysteries evolving along with his generations. As quoted by Theodore Dobzhansky, *nothing in biology makes sense except in the light of evolution* (Dobzhansky 2013). This idea stems from the concept of the origin of species and their divergence as explained by Charles Robert Darwin and Alfred Russel Wallace. They explained the phenomenon of natural selection on existing variations in specific populations resulting in evolution of new forms of living beings (Vogel and Motulsky 1997). In this regard, philosophers of ancient times were also intrigued and critically observing certain traits running in families and theorizing human origin as blend of male and female fluids (Vogel and Motulsky 1997). As early as 400 B.C. the first idea of how traits are transmitted through the generations was given by Hippocrates. He stated that, “*semen is produced by whole body, healthy by healthy parts, sick by sick parts. Baldheaded begets baldheaded, blue-eyed begets blue-eyed, and squinting, squinting*”. On the contrary, Aristotle claimed that the ‘matter’ is contributed by both sexes (Vogel and Motulsky 1997). In early 19<sup>th</sup> century, the concept of genetics and hereditary was more pronounced and a few diseases like hemophilia and color blindness were advocated to have hereditary components (Wynbrandt and Ludman 2010). As technologies became more sophisticated in the late 19<sup>th</sup> century, Gregor Mendel — the father of genetics — conducted experiments with sweet pea (*Pisum sativum*) and proposed laws of inheritance. Although, oversimplified, he devised Laws of Segregation and Independent Assortment of the investigated traits (shape and color of sweet pea) which ushered a new era of genetics (Weldon 1902).

In the journey of exploration, the Human Genome Project (HGP) in June 2003 happened to be the biggest achievement revolutionizing the field of genetics. This project documented the human genome sequence for the first time and mapped around 3 billion bases of DNA covering 99% of human genome (Collins, Morgan et al. 2003). This knowledge paved ways for subsequent efforts to gain insights into variations in the genome that cause diversity and evolution of living organisms. Soon

after that, the 1000 Genome project was launched which sequenced genomes of over 2,504 unidentified individuals from all over the world and provided a resource of genetic variants, including single nucleotide polymorphisms (SNPs) and structural variants (Sudmant, Rausch et al. 2015). With the advancement of sequencing technologies the focus is now diverted towards the efficient diagnosis and ultimately provides insights into the complexity of genetic disorders which are necessary for devising treatment strategies (Valencia, Husami et al. 2015).

Scientists are investing all their energies to devise methods and tools for treatment of these diseases. Recently, the cutting-edge technology of clustered regularly interspaced short palindromic repeats (CRISPR/Cas9) offers to manipulate the sequence of the genome and shows potential for disease treatment in future (Barrangou and Horvath 2017). In this regard, efforts have been made for proposing treatment of the  $\beta$ -thalassemia — lethal inherited condition caused by mutations in *HBB* gene — using CRISPR/Cas9. This technology has been efficiently used to correct two different  $\beta$ -thalassemia mutations, and changed homozygous (pathogenic) to the heterozygous (normal) state in patient derived iPSCs without observing any off-target effects. The corrected iPSCs showed restoration of *HBB* expression, thus providing a potential source for transplantation in patients of  $\beta$ -thalassemia (Xie et al. 2014a). Similarly, CRISPR/Cas9 technology has also marked success by correcting the Cystic Fibrosis Transmembrane Conductance Regulator (CFTR) locus in intestinal stem cells of patients with cystic fibrosis (Schwank et al. 2013), an inherited condition affecting the lungs and digestive system. These examples show increased chances of treatment for monogenic disorders in future.

### **3.2 Genetic disorders**

The human genome has sophisticatedly arranged 3 billion nucleotides which are replicated in a highly accurate, yet error prone manner (Chial 2008). Changes in the sequence of coding or regulatory parts of DNA due to environmental factors or mistakes during replication may result in medical conditions called genetic disorder (Lewis 2016). These variations in the sequence vary from a single base pair to a large fragment being modified. Disorders that are caused due to mutation(s) in a single gene are called monogenic whereas those which are caused by more than one gene

including the environmental factors are termed as complex disorders. Undoubtedly, these mutations can affect phenotypes such that it may lead to disease condition in individuals. However, such variations offer the possibility of exploring the genetics of human beings (Weischenfeldt, Symmons et al. 2013).

### **3.3 *Fons et origo* of genetic disorders**

#### **3.3.1 Inherited familial mutations**

One of the leading causes of genetic disorders (Mendelian) is pathogenic familial mutations; these range from point mutations to larger fragments of DNA being altered, segregated by one founder mutant within a family (Speicher, Antonarakis et al. 2009). The segregation of mutations follows two patterns; autosomal recessive, when both copies of mutant allele manifest disease in an individual, each inherited from both parents. However, in autosomal dominant, only one mutant allele is sufficient to cause genetic anomaly in offspring (Griffiths, Wessler et al. 2005). Inbreeding is one of the most prominent causes of Mendelian disorders explaining why a mutant allele keeps segregating through the generations; it is defined as the union between two close biological relatives — second cousin or closer (Bittles and Black 2010). The consanguineous couple has one or more common ancestors within the preceding three generations. The effect is predominantly noticeable for rare recessive disorders (Corry 2014).

Globally, at least 20% of the human population prefers consanguineous marriages with an estimate of at least 8.5% of children having consanguineous parents (Organization 1985; Bittles 1990). Highly frequent consanguineous marriages occur in North and sub-Saharan Africa, the Middle East, and West, Central, and South Asia. In these regions even unrelated couples may exhibit high levels of homozygosity, as marriages within tribe or caste boundaries has been a deep-rooted tradition (Bittles and Black 2010). As far as European and American countries are concerned, cousin marriages are unlikely, however, in Western Europe at least 10 million residents have migrated from regions where consanguinity is preferential, therefore their progenies are more prone to genetic diseases (Dyer 2005; Bittles 2008).

Pakistan is highlighted in the list of countries where consanguinity is followed as long established practice and thus remains center of attention for studying rare or complex genetic disorders running in the families, as indicated in (Hussain and Bittles 1998). In Pakistani population,  $\approx 50\%$  of marriages are between first cousins where there is a chance of 22/1,000 extra monogenic disorders are likely to occur (Hussain and Bittles 1998). The higher rate of consanguinity results in increased incidence of genetic anomalies, as 1 in 1,200 children is diagnosed with some rare inherited disorders (<https://www.dawn.com/news/1208993>). Findings of an investigation of consanguinity-associated morbidity in a Pakistani community in the United Kingdom show that there would be a  $\approx 7/1,000$  increase in autosomal recessive disorders for every 0.01 increase in the mean coefficient of inbreeding (Christianson, Howson et al. 2006). Thus, Pakistani population offers extended pedigrees and multiple affected individuals for revealing extensive genetic information as well as studying the pathomechanism of a specific disease in the variety of phenotypes, predominantly, autosomal recessive disorders for instance, microcephaly and intellectual disability (Sajid Hussain, Marriam Bakhtiar et al. 2013; Riazuddin, Hussain et al. 2017).

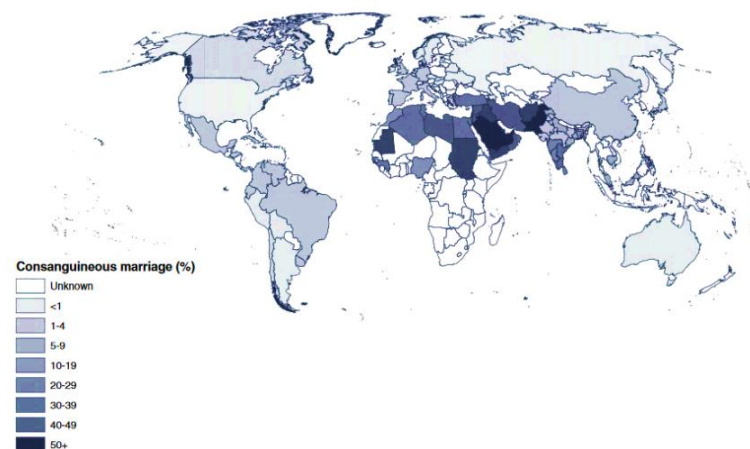


**Figure 3.1: Global distribution of consanguineous marriages.**

The map shows Pakistan among one of those countries having high consanguineous marriages ( $>50\%$ ) (Bittles and Black 2010).

### 3.3.2 Sporadic *de novo* mutations

In addition to inheriting half of the genome from each of our parents, a few numbers of novel genetic changes — *de novo* variations — may also occur during the formation of gametes or postzygotically acquired by the offspring (Lynch 2010). *De*



*novo* mutations arise due to the erroneous incorporation of nucleotides by DNA polymerases during DNA replication (Ségurel, Wyman et al. 2014). In addition, DNA lesions can also spontaneously appear as a result of exogenous or endogenous mutagens such as UV or ionizing radiation (Ségurel, Wyman et al. 2014).

A typical human genome contains 40,000 to 200,000 rare variants occurring in less than 0.5% of the population (Consortium 2015); all of these variations must have once arisen as a *de novo* germ-line mutation in an individual occurring once in human evolution (Lupski, Belmont et al. 2011). The number of *de novo* single-nucleotide variations (SNVs) on average in an individual is 44 to 82 out of which only one or two might be present in the protein coding sequence (Acuna-Hidalgo, Veltman et al. 2016). These mutations, though occur less frequently in coding regions, yet represent the most life-threatening forms of rare genetic variations as well as aneuploidies which, also arise as *de novo* events; the reason is that these are exposed to more stringent evolutionary selection (Gilissen, Hoischen et al. 2012; Corry 2014).

Previously, the focus of geneticists was mainly on inherited diseases, leaving sporadic disorders largely unexplored. New advents in sequencing techniques and their wide spread availability have given the opportunity to enlighten the medical relevance of *de novo* mutations. According to previous studies in year 2012-13, more than 500 novel genes are attributed to several different disorders due to pathogenic *de novo* mutations (Gilissen, Hoischen et al. 2012; Boycott, Vanstone et al. 2013). In addition, sporadic cases receiving clinical diagnosis at molecular level explain 60 to 75% of them are caused by *de novo* mutations (Yang, Muzny et al. 2014; Posey, Rosenfeld et al. 2016). Those *de novo* events occurring in the coding region of the genome present phenotypes of intellectual disability, neurodevelopmental disorders, epilepsy and autism spectrum disorders which make 1% of the world population (Yang, Muzny et al. 2014). Taking into account the severity of disease caused by *de novo* mutations, it is reported that most severe phenotype of dominant neurodevelopmental disorders are contributed by germline *de novo* events (Gilissen, Hehir-Kwa et al. 2014). Regarding larger copy number variations, which arise at a frequency of only 0.01 to 0.02 events per generation, which is very low (Gilissen, Hoischen et al. 2012), *de novo* germline SNVs in single genes still remain the leading cause of rare sporadic syndromes such as Schinzel–Giedion syndrome and Kabuki syndrome (Bilgüvar, Öztürk et al. 2010;

Hoischen, van Bon et al. 2010). Taken together, the high occurrence of *de novo* events causing phenotypic lethality draws attention towards deeper exploration of these variations.

## **3.4 Human brain development**

### **3.4.1 Neurogenesis**

The brain is the most complex organ of the human body, formed in a highly organized fashion by a process called neurogenesis. It is followed by a series of events; starting from formation of neural plate leading to production of neurons and followed by successive differentiation, migration, dendrite and axon formation, synaptogenesis, and the establishment of connectivity networks between the neurons (Kriegstein and Noctor 2004; Götz and Huttner 2005; Mora-Bermúdez, García et al. 2013). There are a few non neuronal processes as well; gliogenesis, myelination and angiogenesis, playing their part to successfully achieve the formation of a normal functional brain (Taverna, Götz et al. 2014) Tight regulation of neurogenic events is highly crucial for normal brain development. Over 100 billion neurons are produced during human fetal brain development out of which 21.4 to 26.3 billion reside in the cerebral cortex (Pelvig, Pakkenberg et al. 2008). These are folded in gyral layers in a highly defined pattern where the number and length of neurons matters for adjustment in limited space (Zecevic, Chen et al. 2005).

Typically, the mammalian neocortex shows the greater extent of phylogenetic expansion and is composed of six layers (Kriegstein, Noctor et al. 2006; Borrell and Reillo 2012). It starts with the formation of the neural plate that is composed of neuroepithelial cells, which are highly polarized along their apical–basal axis and form a single layer of neuroepithelium. Following to this, transformation of neuroepithelium takes place with generation of neurons (Götz and Huttner 2005). As the process goes on, the neuroepithelial cells differentiate into radial glial cells, which are more fate restricted progenitors, and can give rise to astrocytes, oligodendrocytes and microglia (Grove, Williams et al. 1993). In addition, another type of neural progenitor cell, basal progenitor, originates from the mitotic division of neuroepithelial and radial glial cells at the apical surface of the ventricular zone. After differentiation, neuroepithelial cells and radial glial cells undergo a hallmark

phenomenon, interkinetic nuclear migration, in the specified zones present in the layers; the nuclei divide mitotically at the apical surface of the ventricular zone and migrate basally during S phase of the cell cycle depending on the cell type (Figure 3.2A, 3.2B and 3.2C) (Götz and Huttner 2005). Several rounds of symmetric and asymmetric divisions of neuroepithelial and glial cells increase the pool of neurons in the developing brain and eventually their migration towards the cortex lead to the formation of a six-layers laminar neocortex (Haubensak, Attardo et al. 2004).

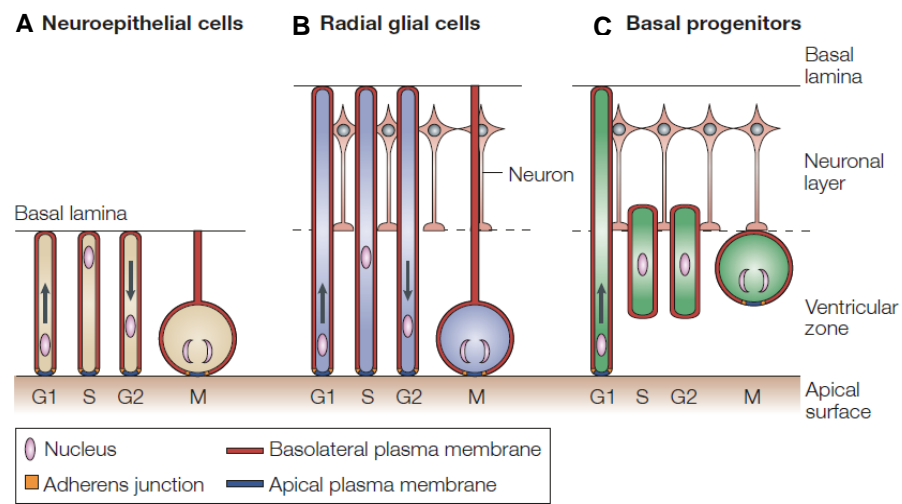


**Figure 3.2: An overview of interkinetic nuclear migration of different neuronal cell types.**

(A) Apical–basal axis migration of neuroepithelial cells; the nucleus migration during G1 is basal and remains at the basal side in S phase. During G2 phase it is apical, and mitosis occurs at the apical surface. (B) Partially basal migration of radial glial cells; it remains to the between the apical surface and the basal boundary of the ventricular zone. (C) Migration of basal progenitors; the nucleus migrates from the apical to the basal boundary of the ventricular zone (dashed line) during S phase and mitosis. Note: Image adopted from Kaundl et al, 2010.

### 3.4.2 Mode of cell division during neurogenesis

Depending on the daughter cell identity, progenitor cells divide in four different manners; (a) symmetric proliferative, (b) symmetric consumptive, (c) asymmetric self-renewing, and (d) asymmetric consumptive division. In case of symmetric proliferative, (Figure 3.3A) a neuroprogenitor cell divides into two identical daughter progenitor cells and so generates a whole progenitor pool (Kaundl, Passemar et al. 2010). However, if the mother progenitor cell doesn't generate identical daughter cells

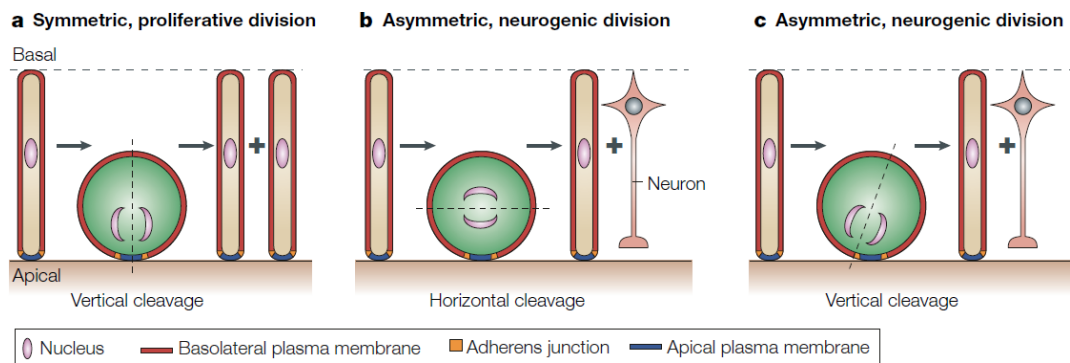


**Figure 3.3: Depiction of the mode of division and cleavage planes of progenitor cells.**

(A) Symmetric proliferative division showing vertical cleavage. (B) Asymmetric neurogenic division showing horizontal cleavage. (C) Asymmetric neurogenic division showing vertical cleavage (Figure adopted from Kaindl et al, 2010).

such as a basal progenitor divides to form two neurons (Figure 3.3B), the division is called symmetric consumptive (Taverna, Götz et al. 2014). In this mode, the cleavage plane of a dividing cell is vertically orientated in the radial dimension of the ventricular zone so that crucial apical and basal constituents are distributed equally to the daughter cells (Götz and Huttner 2005). However, in asymmetric self-renewal division (Figure 3.3C) a progenitor cell produces one progenitor cell identical to the mother progenitor (which becomes a radial glial cell) and a committed precursor (which gives rise to a neuron). In case of asymmetric consumptive division, the daughter cells differ in identity from one another, as well as from the mother progenitor cell (Fish, Dehay et al. 2008; Taverna, Götz et al. 2014). The cleavage planes, in this case, can be horizontal or vertical and are parallel to the apical surface of the ventricular zone as the apical constituent will be inherited by one daughter cell and the basal constituents by the precursor cell. Eventually, after a series of symmetric and asymmetric divisions, development of a six-layer laminar neocortex occurs as a result of neuronal migration to the cortex (Taverna, Götz et al. 2014).

### **3.5 Congenital microcephaly (Small head)**

Congenital microcephaly is a rare neurodevelopmental disorder generally defined by reduction in occipital-frontal head circumference (OFC) of less than  $-3$  SD, thus results in the reduced cerebral cortex and diminution of brain volume (Shaheen, Maddirevula et al. 2019). Although at birth, OFC of microcephaly patient tends to be at least  $-2$  SD, it worsens until 6 months of age and reaches  $-3$  SD. In older individuals the range falls between  $-8$  SD to  $-12$  SD (mean  $-8$  SD) (Passemar, Kaindl et al. 2013). As 55% of the human brain is comprised of cerebral cortex, therefore, abnormal brain development in microcephaly is frequently associated with intellectual disability and impaired cognitive skills (Woods 2004).

Microcephaly has heterogeneous global prevalence; one study carried out in the United States showed pooled prevalence of microcephaly as 8.7 per 10,000 live births (Cragan, Isenburg et al. 2016). Several studies highlight the global incidence of microcephaly; it varies from 1.3 to 150 per 100,000 depending upon the ethnic group and clinical features defining microcephaly (Komai, Kishimoto et al. 1955; Van den Bosch 1958; Tolmie, McNay et al. 1987).

Given the onset of disease, microcephaly is categorized into primary microcephaly which can be diagnosed in the 24<sup>th</sup> week of gestation using ultrasound or magnetic resonance imaging (MRI) and secondary manifested after birth of affected individuals and it is progressive and degenerative in nature (Zaqout, Morris-Rosendahl et al. 2017). Neuroimaging shows that in certain cases of primary or true microcephaly some structural brain malformations such as gyrification issues, agenesis of corpus callosum, pituitary abnormalities resulting in craniosyntosis can also be observed (Alcantara and O'driscoll 2014). On the basis of segregation pattern, primary microcephaly is further categorized; autosomal dominant and autosomal recessive primary microcephaly (MCPH [MIM 251200]) (Passemar, Kaindl et al. 2013). Globally, MCPH has been reported in more than 300 families and individual patients (Zaqout, Morris-Rosendahl et al. 2017; Létard, Drunat et al. 2018). In comparison to incidence of MCPH in western population (Yorkshire region of Britain) which is one per million, the prevalence in Asian population (northern region of Pakistan) is 1/1,000 (Woods, Bond et al. 2005; Thornton and Woods 2009).

Beside intellectual disability (IQ between 30 and 70–80) as a neurological condition, a few other signs are also commonly observed in MCPH patients, such as, hyperactivity and attention deficit, speech delay, seizures and rarely epilepsy (Kraemer, Picker-Minh et al. 2016). Neuroimaging studies show some additional abnormalities including pachygyria with cortical thickening, lissencephaly, and schizencephaly (Bilgüvar, Öztürk et al. 2010). Etiology of congenital microcephaly (CM) – Do all roads lead to Rome?

The etiology of MCPH is heterogeneous mainly because of its broad clinical phenotype. Mendelian Inheritance in Man (MIM) retrieves 666 entries with microcephaly in a clinical synopsis section (Barkovich, Guerrini et al. 2012). These can be categorized into cases having environmental and genetic etiology.

### **3.5.1 Environmental factors**

Several environmental factors are involved in causing microcephaly such as intrauterine infections, prenatal radiation exposure, maternal phenylketonuria, and drugs taken during pregnancy (Kaindl, Passemard et al. 2010; Gilmore and Walsh 2013). Most prominent example is a recent outbreak of Zika virus (ZIKV) infection in Brazil emerged which was reported to cause MCPH (Mlakar, Korva et al. 2016). The cellular defects and brain size of ZIKV infected individuals strikingly resembled MCPH phenotype. Studies showed a decreased proliferation and increased cell death due to structurally abnormal centrosomes in interphase of Zika infected neural progenitor cells (Souza, Sampaio et al. 2016). In addition, ZIKV injection in the developing mouse brain resulted in a smaller brain size with a thinner cortex (Li, Saucedo-Cuevas et al. 2016).

### **3.5.2 Genetics of MCPH**

The majority of microcephaly cases present genetic etiology which provide insights into basic processes of brain development and neurogenic mitosis (Kousar, Hassan et al. 2011). All reported 25 MCPH genes (Table 3.1) are highly conserved among species and are expected to play roles in brain evolution (Woods, Bond et al. 2005). The majority of mutations reported in these genes are frameshifts or nonsense, eventually leading to truncated nonfunctional proteins (Barbelanne and Tsang 2014). These mutations mainly affect neural progenitor cells to prematurely switch from

asymmetric to symmetric cell division, reducing the progenitor pool and thus the number of neurons as a whole. MCPH proteins are ubiquitously expressed and many of them have particular roles in mitosis and are expressed in the neuroepithelium during embryonic neurogenesis (Cox, Jackson et al. 2006). As most of them are associated with the centrosomes, mitotic spindles and nuclear envelope proteins, which were recently discovered, (Barbelanne and Tsang 2014; Braun, Lovric et al. 2018) truncation of these proteins cause dysregulation of crucial cellular processes such as, centrosomal duplication and maturation, Wnt signaling, DNA damage response, mitotic checkpoints and transmembrane transport (Chellas-Gery, Wolf et al. 2011). The genes can be divided on the basis of the above mentioned pathways, three of which, centriolopathy, Wnt signaling and DNA damage response, are discussed below in detail (section 1.5.6, 1.5.7, 1.5.8).

**Table 3.1: List of genes involved in etiology of MCPH.**

Locus	Location	Gene	Protein	Subcellular Localization	Ref.
MCPH1	8p23.1	<i>MCPH1</i>	Microcephalin 1	Nucleus/chromatin; centrosome	(Jackson, McHale et al. 1998)
MCPH2	19q13.12	<i>WDR62</i>	WD-repeat containing protein 62	Spindle poles during mitosis; nucleus during interphase	(Bhat, Girimaji et al. 2011)
MCPH3	9q33.2	<i>CDK5RAP2</i>	Cyclin-dependent kinase 5 regulatory subunit-associated protein 2	Centrosome	(Issa, Mueller et al. 2013)
MCPH4	15q15.1	<i>KNL1*</i>	Kinetochore scaffold 1	Kinetochore	(Genin, Desir et al. 2012)
MCPH5	1q31.3	<i>ASPM</i>	Abnormal spindle-like microcephaly-associated protein	spindle poles during mitosis, nucleus during interphase	(Passemard, Titomanlio et al. 2009)
MCPH6	13q12.2	<i>CENPJ</i>	Centromere protein J	Centrosome	(Bond and Woods 2006)
MCPH7	1p33	<i>STIL</i>	SCL/TAL1-interrupting locus protein	Centriole	(Kumar, Girimaji et al. 2009)
MCPH8	4q12	<i>CEP135</i>	Centrosomal protein of 135 kDa	Centrosome	(Hussain, Baig et al. 2012)
MCPH9	15q21.1	<i>CEP152</i>	Centrosomal protein of 152 kDa	Pericentriolar marker	(Guernsey, Jiang et al. 2010)
MCPH10	20q13.12	<i>ZNF335</i>	Zinc finger protein 335	component of H3K4 methyltransferase complex (chromatin remodeling)	(Yang, Baltus et al. 2012)
MCPH11	12p13.31	<i>PHC1</i>	Polyhomeotic-like protein 1	component of polycomb (chromatin remodeling)	(Awad, Al-Dosari et al. 2013)
MCPH12	7q21.2	<i>CDK6</i>	Cyclin-dependent kinase 6	centrosome during mitosis, cytosol and nucleus during interphase	(Hussain, Baig et al. 2013)
MCPH13	4q24	<i>CENPE</i>	Centromere-associated protein E	Centromere, kinetochore	(Mirzaa, Vitre et al. 2014)

MCPH14	1p21.2	<i>SASS6</i>	Spindle assembly abnormal protein 6 homolog	Centriole	(Khan, Rupp et al. 2014)
MCPH15	1p34.2	<i>MFSD2A</i>	Sodium-dependent lysophosphatidylcholine symporter 1	Cell membrane, endoplasmic reticulum membrane	(Alakbarzade, Hameed et al. 2015)
MCPH16	12q24.33	<i>ANKLE2</i>	Ankyrin repeat- and LEM domain-containing protein 2	Endoplasmic reticulum	(Yamamoto, Jaiswal et al. 2014)
MCPH17	12q24.23	<i>CIT</i>	Citron Rho-interacting kinase	Cleavage furrow and midbody	(Basit, Al-Harbi et al. 2016)
MCPH18	4q21.23	<i>WDFY3</i>	WD repeat and FYVE domain-containing protein 3	Cytosol	(Kadir, Harel et al. 2016)
MCPH19	3q23	<i>COPB2</i>	Coatomer subunit beta	Inclusion membrane	(Chellas-Gery, Wolf et al. 2011; DiStasio, Driver et al. 2017)
MCPH20	1q32.1	<i>KIF14</i>	Kinesin-like protein KIF14	Midbody	(Ahmad, Baig et al. 2017)
MCPH21	12p13.31	<i>NCAPD2</i>	Condensin complex subunit 1	Nucleus (cytoplasm only in interphase)	(Beck and Hurt 2016)
MCPH22	11q25	<i>NCAPD3</i>	Condensin-2 complex subunit D3	Nucleus (cytoplasm only in interphase)	(Beck and Hurt 2016)
MCPH23	2q11.2	<i>NCAPH</i>	Condensin-2 complex subunit H2	Mainly localized to the cytosol. In addition localized to the nucleoplasm.	(Beck and Hurt 2016)
MCPH24	12q23.2	<i>NUP37</i>	Nucleoporin Nup37	Nuclear envelop membrane	(Braun, Lovric et al. 2018)
MCPH25	7q22.1	<i>MAP11</i>	Microtubule-associated protein 11	Microtubule	(Perez, Bar-Yaacov et al. 2019)

Note; gene and their respective encoded protein names are verified from HUGO (Human Genome Organization), Gene Nomenclature Committee (HGNC) and UniProt Knowledgebase (UniProtKB), respectively. \* This gene was previously known as *CASC5*.

### 3.5.3 Pathomechanism of MCPH

During neurogenesis the formation of neural tube requires particular temporal and spatial arrangements (Kriegstein and Noctor 2004). This process is highly sophisticated and demands organized fashion and proper regulation at every step. A few studies propose the pathomechanism of MCPH; conceivably, any dysregulation in balance between symmetric and asymmetric division, such as premature switching from symmetric proliferative to asymmetric apical progenitor division (Fish et al. 2006), and from asymmetric self-renewing to symmetric consumptive apical progenitor division, considerably reduces the number of neuroprogenitor cells thus appearing as microcephaly brain (Fish, Kosodo et al. 2006; Fei, Haffner et al. 2014). In addition, other factors causing underdevelopment of brain include abnormal neuronal migration and differentiation. Although these are some of the most prominent and well explained pathomechanisms of MCPH, other additional mechanisms notably, cell proliferation defects, aneuploidy and enhanced apoptosis may also impair brain development (Kaindl, Passemard et al. 2010).



### **3.5.4 Centriolopathy**

The centrosome is mainly composed of a pair of centrioles which are responsible for microtubule organization during mitosis and overall internal spatial organization of somatic cells (Chavali, Pütz et al. 2014).

The known functions of microcephaly associated genes (*MCPH1*, *CDK5RAP2*, *STIL*, *CEP135*, *CEP152*, *CDK6*, *SASS6* and *CENPE*), suggest a major contribution of defects in centrosome organization or function (Hussain, Baig et al. 2013; Chavali, Pütz et al. 2014). Centrosomes play indispensable roles in a variety of processes during brain development such as neurogenesis, neuronal migration and polarity (Kuijpers and Hoogenraad 2011). MCPH mutations cause abnormalities in centriole biogenesis by dysregulating the process of centriole duplication or affecting the essential components involved in this pathway (Chavali, Pütz et al. 2014), resulting in impaired cell cycle progression, cell cycle arrest and eventually cell death (Barbelanne and Tsang 2014).

### **3.5.5 Wnt signaling**

Wnt signaling is one of the pivotal pathways to ensure proper regulation of embryogenesis — particularly embryonic as well as adult brain development (Zhang, Yang et al. 2011). The differentiation and maturation of neural progenitors, growth of lateral-to-medial and anterior-to-posterior of neocortex is tightly regulated by initiation of transcription of target genes and controlled apoptosis by Wnt signaling (Wang and Wynshaw-Boris 2004; Machon, Backman et al. 2007). In addition to determine the cellular fate in the developing cortex, Wnt signal transduction also plays a critical part in cellular events related to the hippocampus (Machon, Backman et al. 2007). Mutations in two of the MCPH genes, *ASPM* and *ALFY*, are known to deregulate Wnt signaling and cause microcephaly. A study reported that, upon knockdown of *ASPM*, decreased Wnt mediated transcription was observed which was rescued by stable expression of stabilized  $\beta$ -Catenin — the focal protein of Wnt signal transduction. Regarding *ALFY*, it is involved in autophagy dependent removal of DVL3, a protein which is also the main player of Wnt signaling. Mutation in this gene causes aggregation of DVL3 which leads to impaired Wnt signaling and thus diminution of brain size (Buchman, Durak et al. 2011; Keaney and Campbell 2015; Kadir, Harel et al. 2016).

There are three different types of Wnt signal transduction; canonical, non-canonical and calcium dependent pathway, though the canonical pathway is most studied and well understood for its role in neurogenesis. Several proteins are involved in this pathway; Axin, adenomatous polyposis coli (APC), glycogen synthase kinase 3 (GSK3), casein kinase 2 (CK2), disheveled (dsh) and  $\beta$ -Catenin, which is the master player of this pathway (Huelsenken and Behrens 2002).  $\beta$ -Catenin is constantly degraded by proteasomal activity when Wnt signaling is switched off whereas it is activated on Wnt signal received by frizzled receptor protein, and transported to the nucleus for initiation of transcription of target genes. This phenomenon requires cascades of highly specific phosphorylation and ubiquitination of  $\beta$ -Catenin for proper functioning (Huelsenken and Behrens 2002).

### **3.5.6 DNA damage response (DDR)**

Genomic stability is achieved by regulation of DNA damage response by repairing DNA lesions, activation of cell cycle checkpoint and/or apoptosis of damaged cell (Branzei and Foiani 2010). As the cell cycle checkpoint is most crucial during neurogenesis and brain development, mutations in DDR genes, such as *MCPHI*, *ATR*, *NBS1* and *PCNT*, result in increased apoptotic rate and reduced proliferation of neural progenitor cells to cause microcephaly and associated syndromes in humans (Lin, Rai et al. 2005; O'Driscoll and Jeggo 2008). *MCPHI* is the first gene identified to cause MCPH and its knockdown leads to defective DDR, decreased chromosomal condensation and dysregulation of cell cycle checkpoints (Lin, Rai et al. 2005). Like *MCPHI* mutant cells, both Seckel and Nijmegen breakage syndrome cells also have impaired checkpoint signaling (Lin, Rai et al. 2005). Interestingly, defects in two of the centrosomal proteins, Cep152 and CDK5RAP2, also cause delayed DDR; Cep152 mutated patient fibroblasts develop aneuploidy in culture and excessive cell death has been observed in the mouse model lacking *Cdk5rap2* (Gilmore and Walsh 2013).

### **3.5.7 Organ specificity of CM associated variations**

It is notable that most of the mutations in microcephaly associated genes manifest brain specific phenotype in non-syndromic form (Woods, Bond et al. 2005). Nonetheless, the syndromic form of microcephaly is also commonly reported, showing heterogeneity of phenotypic spectra. In such cases, different organs are affected such as in case of microcephalic primordial dwarfism (MIM 210600), where

the patient has global growth retardation along with facial dysmorphism (Shaheen, Abdel-Salam et al. 2015). Smith-Lemli-Opitz Syndrome is another representative example of syndromic form where diverse phenotypes such as digital anomaly, heart defect as well as characteristic facial features are observed in the patient (Abuelo 2007). Taking the cases of non-syndromic microcephaly, most of the MCPH mutated genes are globally expressed; however, the phenomenon that these genes specifically compromise brain development is vaguely understood (Shaheen, Maddirevula et al. 2019).

### **3.5.8 Brain-specific phenotype**

Brain specific phenotype of CM can be justified by the following arguments:

#### ***Site of expression***

MCPH genes products are highly and specifically expressed in the ventricular zone of the cerebral cortex, dedicated to proliferation of neural progenitor cells and localize on centrosome/spindle pole which is one good explanation of brain specific phenotype (Bond and Woods 2006; Duerinckx and Abramowicz 2018).

#### ***Fragility of asymmetric neuronal division***

Spindle pole formation and centrosome duplication are extremely crucial events in neuronal duplication for the sake of maintaining polarity of neuronal cells. It is apparent that neuronal cells are specifically sensitive to centrosomal defects as any abnormality in proteins involved in asymmetric neuronal division causes depletion of neural progenitor pool. Centrosomal abnormalities, on the other hand, show a less dramatic influence in case of extra neurogenic mitosis as has been shown by studies of neuroblasts in *Drosophila* too (Basto, Brunk et al. 2008). This is interesting to notice that most of the centrosomal proteins are functioning together; MCPH1 and WDR62 are physically interacting partners and make a complex with Cep63 as well; the knockdown of *CEP63* abolishes MCPH1-WDR62 interaction. In addition, Cep63, Asp homolog, also known as ASPM, and WDR62 recruit CENP-J, also known as CPAP/SAS-4, for carrying out centriole biogenesis (Jayaraman, Bae et al. 2018). If we place these centrosomal proteins together, it is clearly seen that all of them are highly expressed in cerebral cortex, localized in closed vicinity of each other (centrosome/spindle pole) and are interconnected in a network having influence on

each other. Not only that they make complexes but also regulate each other and functions, together, collectively supports the idea of sensitivity of asymmetric division towards dysfunctioning of either of them.

### ***Altered splicing events***

The concept of alternative splicing events is well explained by different studies and can be speculated as to describe brain specific phenotype (Barbosa-Morais, Irimia et al. 2012). This fact is comprehensively explained in a recent study where one of the MCPH-protein *KNL1* has been investigated in patient derived cerebroids and neural progenitor cells. They explained the fact that reported *KNL1* mutation generated an exonic splicing silencer site, which causes differential expression of *KNL1* protein in different cell types due to formation of transcripts by usual splicing event occurring only in the brain.

The mutant protein was found downregulated, resulting in aneuploidy and consequently reduced cell growth and apoptosis. Moreover, the cerebroids also showed reduction in the overall size. However, the mutant fibroblasts and neural crest cells obtained from the same parental stem cell line did not show any of the above mentioned abnormality (Javed, Li et al. 2018). Obviously, *KNL1* is not the only gene having splice site variants; there are others few examples of MCPH genes such as *CEP135*, *ASPM*, *WDR62*, *CIT*, *STIL* and *KIF14* with splice site variants reported in MCPH patients (Bond, Scott et al. 2003; Kumar, Girimaji et al. 2009; Nicholas, Khurshid et al. 2010; Farooq, Fatima et al. 2016; Ahmad, Baig et al. 2017).

## **3.6 Syndromic microcephaly**

Microcephaly is also observed in syndromic forms where it is associated with other clinical conditions such as growth or skeletal abnormalities and is recognized as distinct clinical conditions like Filippi syndrome, microcephaly associated steroid resistant nephrotic syndrome and Smith-Lemli-Opitz Syndrome (Abuelo 2007; Hussain, Battaglia et al. 2014). More than 700 clinical syndromes are recorded with microcephaly in the London Dysmorphology Database and OMIM (Passemar, Kaindl et al. 2013). Identification of mutations responsible for syndromic congenital microcephaly has greatly expanded the repertoire of pathways involved in early brain development. Examples include DNA damage repair in Fanconi anemia and nuclear

pore complex formation in Galloway–Mowat syndrome (Alcantara and O'driscoll 2014). As microcephaly associated syndromes feature additional clinical conditions, it helps in correct clinical diagnosis. Two of the microcephaly syndromes will be discussed in details below.

### **3.7 Filippi syndrome (FLPIS)**

Filippi syndrome (HP:0000007) [MIM 272440], first introduced by G. Filippi in 1985, is characterized as facial dysmorphism (HP:0001999), intellectual disability (HP:0001249), microcephaly (HP:0000252), developmental delay (HP:0008897) and syndactyly of fingers (HP:0012725) and toes (HP:0010714) (Filippi, Fraser et al. 1985; Battaglia, Filippi et al. 2008). It was identified in a family where three of the eight siblings were diagnosed with this disorder. This disease is manifested in both sexes and thus shows autosomal recessive mode of inheritance (Goyal, Goyal et al. 2015). All the studies until now reported phenotypic variations, thus Filippi syndrome is clinically very heterogeneous. This aspect is described below in detail.

#### **3.7.1 Clinical features**

Being the rarest of syndromes, to date, only 32 affected individuals from consanguineous and non-consanguineous families have been reported worldwide (Sharif and Donnai 2004; Battaglia, Filippi et al. 2008; Hussain, Battaglia et al. 2014; Capecchi, Baldassarri et al. 2018; Sabir, Walker et al. 2019). Dysmorphic facial characteristics of Filippi patients include arched eyebrows (HP:0002553), big ear pinnae with irregular left helix, wide nasal bridge (HP:0000431), bulging tip of nose with hypoplastic alae nasi (HP:0000430), long medial cleft of upper lip (HP:0000161), small wide-spaced teeth (HP:0000307) and sharply pointed chin (HP:0000307) (Capecchi, Baldassarri et al. 2018). In addition to these typical rather prominent features, variations in symptoms of Filippi patients reported by some studies are seizures (HP:0001250), plagiocephaly (HP:0001357), thin hair (HP:0001357) with high hairline, visual defects (HP:0000505), ectodermal anomaly, cryptorchidism (HP:0000028), hypodontia (HP:0000668) and hair abnormalities (Woods, Crouchman et al. 1992; Orrico and Hayek 1997).

Although, there are overlapping features (such as behavioral and neurological) of this syndrome with some other namely Chitayat syndrome (MIM 617180), Scott

Syndrome (MIM 262890), Kelly syndrome, Zerres syndrome and Woods syndrome, still Filippi syndrome can be distinguished with the most typical feature of syndactyly of 3-4 finger and toes. One study has compared the overlapping features of Filippi syndrome with Rubinstein–Taybi syndrome (RTS, [MIM 180849]) in detail where the patient presented with intellectual disability, short stature, visual impairment, bilateral syndactyly of hands and feet, broad thumbs, and characteristic facial features whereas microcephaly was not observed in the investigated patient. The patient was also characterized genetically; no pathogenic variant of *CKAP2L* (see below in section 1.6.4) was found by WES and both syndromes were proven distinct (de Vries, Monroe et al. 2016).

### **3.7.2 Genetics of Filippi syndrome**

Previously, efforts were made by scientists to reveal the genetic cause of Filippi syndrome using several techniques such as karyotyping, Fluorescent In Situ Hybridization (FISH) analysis and Array-Comparative Genomic Hybridization (array-CGH), but none of these could unravel the genetic determinants (Sharif and Donnai 2004). Although, a microdeletion was identified in various syndromes having overlapping features of Filippi syndrome; one study reported it in a Filippi-like patient featuring overlapping symptoms with microdeletion syndrome which included characteristic facial features such as long eyelashes, undersized jaw, strawberry shaped chin and low set ears (Lazier, Chernos et al. 2014). With the advent of new sequencing technologies, two causative genes, *CKAP2L* and *CSNK2B* were proposed which are discussed below in detail.

### **3.7.3 *CKAP2L* — The first candidate gene of Filippi syndrome**

The first extensive molecular investigation was carried out by Hussain et al. in 2014, where they reported six loss-of-function mutations (two of them being compound heterozygous) in *CKAP2L*, from five families of varied origins, manifesting Filippi syndrome. These mutations are likely to cause premature termination of transcription which may results in non-sense mediated mRNA decay, thus depleting *CKAP2L* protein in patient derived lymphoblastoid cell lines (LCLs) confirming loss-of-function (Hussain, Battaglia et al. 2014). Other cellular defects, observed in patient LCLs as well as knockdown in NIH 3T3/13C7 cells, were multipolar spindles and abnormal chromosome segregation. Intrauterine growth restriction was observed as

additional clinical symptoms of cases and thus attributed to loss-of-function mutation of *CKAP2L* (Yumoto, Nakadate et al. 2013; Hussain, Battaglia et al. 2014).

#### **3.7.4 Features of CKAP2L protein**

*CKAP2L*, also, called Radmis (radial fiber and mitotic spindle) is a cytoskeleton-associated protein 2-like. In addition to centrioles, it is localized on microtubules of spindle poles and highly expressed in neuroepithelial cells during neurogenesis as well as in adult brain throughout the life (Yumoto, Nakadate et al. 2013). Regarding its localization during embryonic development, it is present on radial fibers and mitotic spindles of the dividing neural progenitor cells during perinatal phase and found in the proliferative region and subventricular zone during postnatal brain formation (Yumoto, Nakadate et al. 2013).

The localization of Radmis suggest that it is one of the essential proteins which carry out vital role in neurogenesis for proper brain development (Hussain, Battaglia et al. 2014). A study reports that overexpressed Radmis causes abnormal monopolar spindles at the mitotic phase, and hyper-stabilized cytoplasmic bundles whereas knockdown in developing brain of mouse embryo results in abnormal mitotic spindle formation, abnormal division of centrosomes as well as impaired chromosomal segregation (Yumoto, Nakadate et al. 2013). Centrosomal abnormalities are relatable to Radmis protein malfunctioning as these are mostly known to contribute in isolated form of microcephaly as well as Seckel syndrome, which is a typical example of microcephaly syndromes.

#### **3.7.5 CAKP2L in relation to digital anomaly**

As digital anomaly is the characteristic feature of Filippi syndrome, *CKAP2L* has also been investigated in murine embryos where it is reported to localize in the developing limb bud region (Hussain, Battaglia et al. 2014). Although, the exact mechanism is not known but it may be considered that the process of webbing in limbs is a result of apoptotic activity of *CKAP2L* which is impaired in Filippi patient thus the interdigital spaces are not formed (Jordan, Hindocha et al. 2012).

### 3.7.6 *CSNK2B* — the second candidate gene of Filippi syndrome

My study is a further continuation of this research which will be comprehensively discussed in the following section of results. The second candidate gene of Filippi syndrome has been described recently (Emrah Kaygusuz: Thesis abstract available on <https://kups.ub.uni-koeln.de/8139/>) The patient is a 12-year-old Italian female manifested with typical features of Filippi syndrome including microcephaly, intellectual disability, facial dysmorphism and syndactyly of fingers and toes. Additional clinical features being clinically distinguished in the patient are hypodontia, dysarthria, generalized epilepsy, Ebstein's anomaly and inter atrial septal defect (Figure 3.4).

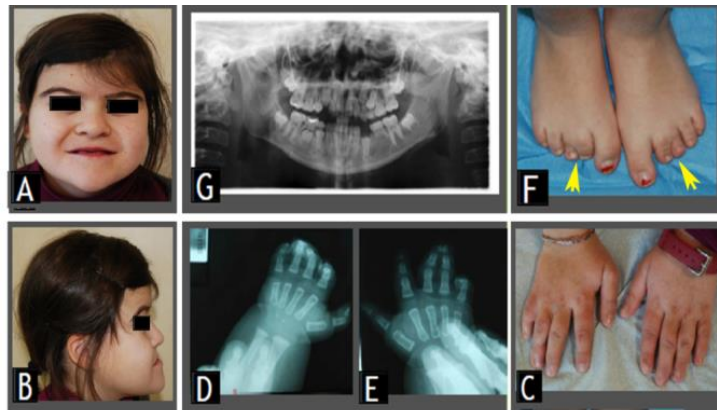


**Figure 3.4: Images of Filippi patient mutated with *CSNK2B*.**

(A) Front view showing facial dysmorphic features. (B) Side view showing microcephaly, (C) Syndactyly of hands. (D) Radiographs of left hand. (E) Radiograph of left hand. (F) Syndactyly of toes. (G) Radiograph showing hypodontia. Image adopted from <https://kups.ub.uni-koeln.de/8139/>.

Trio whole-exome sequencing revealed a *de novo* missense mutation (c.94G>C; p.Asp32His) in *CSNK2B* (NM\_001282385.1 and NM\_001320.6) encoding casein kinase 2 beta (CK2 $\beta$ ). The study shows an up-regulation of mutant transcript as well as protein in patient derived LCLs having an impact on overall growth of mutant cells which was found retarded as compared to wild-type LCLs.

### 3.7.7 CK2 $\beta$ Protein — A subunit of CK2 holoenzyme

CK2 is a ubiquitously expressed Ser/Thr holoenzyme comprised of two catalytic alpha subunits ( $\alpha$  or  $\alpha'$ ) and two regulatory beta ( $\beta$ ) subunits (Marin, Meggio et al. 1997)



(Figure 3.5). It is a highly conserved pleotropic protein kinase dedicated for phosphorylation activity of diverse substrates involved in multiple crucial cellular activities including cell proliferation, apoptosis, transcription, translation, DNA damage response and Wnt signaling. Since this protein kinase CK2 was discovered, a repertoire of above 450 physiological substrates has been identified and the list is still growing (Ahmed, Issinger et al. 2015). The crystallographic structure of CK2 was first demonstrated by Karsten Niefind and colleagues which expanded the functional knowledge of this kinase including autophosphorylation capacity of CK2 $\beta$ , independent function of both subunits and stable tetramerization of all subunits. This study also shows that catalytic activity of CK2 is dependent on the interaction of  $\alpha$  and  $\beta$  subunits (BODENBACH, FAUSS et al. 1994; Niefind, Guerra et al. 2001).

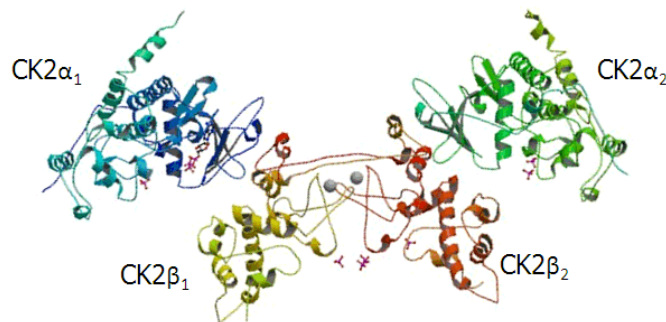


**Figure 3.5: Structure of CK2 holoenzyme (Niefind et al, 2001).**

Alpha subunits are shown in blue and green color at the top and yellow and green color depicts beta subunits of CK2 holoenzyme.

### 3.7.8 CK2 and human diseases

As far as human diseases are concerned, CK2 has remained in the spot light as a drug target for cancer therapy (Ahmad, Wang et al. 2005). Nonetheless, the role of CK2 in neurological diseases, such as Alzheimer's and Parkinson's diseases, has also been well explained as well as it is proposed as target for treatment for such clinical conditions (Perez, Gil et al. 2011). It is highly expressed in brain tissues as compared to other body tissues and phosphorylates a myriad of substrates which are essential for maintaining synaptic plasticity, neurogenesis and ultimately crucial pathways such as Wnt signaling which are involved in human survival and development (Logan and Nusse 2004).

It has been reported that mutations in *CSNK2B* show impaired functions of proteins to cause global developmental delay and epilepsy (Nakashima, Tohyama et al. 2019).

This condition has been termed as Poirier-Bienvenu neurodevelopmental syndrome (POBINDS, [MIM 618732]). A recent study showed 10 *de novo* pathogenic mutations of *CSNK2B* in nine affected individuals (Alvarado, Bos et al. 2019). These pathogenic variations were associated with epilepsy with or without intellectual disability and developmental delay. All the reported variants of *CSNK2B* are listed below (Table 3.2).

**Table 3.2: Reported *de novo* variants of *CSNK2B*.**

<b>Mutations</b>	<b>Phenotype</b>	<b>Reference</b>
c.560T>G, p.(Leu187Arg)	Epilepsy, profound intellectual disability , Delayed developmental milestones	(Li et al, 2019)
c.13G>T p.(Glu5*)	Epilepsy, mild developmental delay and moderate intellectual disability	(Li et al, 2019)
c.256C>T p.(Arg86Cys)	Epilepsy, mild developmental delay and moderate intellectual disability	(Li et al, 2019)
c.621dupC p.(Phe207Phefs*39)	Epilepsy, mild ID	(Li et al, 2019)
c.265delC p.(Ile88Ilefs*46)	Epilepsy	(Li et al, 2019)
c.410G>T p.(Cys137Phe)	Epilepsy	(Li et al, 2019)
c.332G>C p.(Arg111Pro)	Epilepsy, mild developmental delay	(Li et al, 2019)
c.368-2A > G	Epilepsy, mild developmental delay	(Li et al, 2019)
c.409T>G p.(Cys137Gly)	Epilepsy	(Li et al, 2019)
c.494A>G p.(His165Arg)	Intellectual disability, developmental delay, epilepsy	(Nakashima, Tohyama et al. 2019)
c.533_534insGT, p.(Pro179Tyrf*49)	Intellectual disability, developmental delay, epilepsy	(Nakashima, Tohyama et al. 2019)
c.108dup p.(Thr37fs*)	Myoclonic epilepsy	(Nakashima, Tohyama et al. 2019)
c.175+2T>G p.(Leu98Alafs*11)	Myoclonic epilepsy, intellectual disability, cerebral atrophy	(Poirier, Hubert et al. 2017)
c.367+2T>C p.(Val25Metfs*13)	Myoclonic epilepsy, intellectual disability, facial dysmorphism	(Poirier, Hubert et al. 2017)

Note; Mutations c.620\_621insC and c.264delC are corrected according to the rules of HGVS (Human Genome Variation Society) guidelines and are renamed as c.621dupC and c.265delC, respectively.

## **3.8 Nucleoporopathies**

Nucleoporopathies are the diseases which are caused due to mutations in genes encoding nuclear pore complex proteins called nucleoporins (NUPs). Mutations in NUPs caused severe developmental defects observed in zebrafish (Zheng, Yang et al. 2012), mice (del Viso, Huang et al. 2016) and frogs (Lupu, Alves et al. 2008).

The nuclear pore complex (NPC) is a large (100 MDa) macromolecular assembly present at the nuclear envelope serving as gateway between the cytoplasm and the nucleoplasm for trafficking of proteins and mRNA to and from the cell (Beck and Hurt 2017). The basic unit of central channel of the NPC is repeating modules of the NUP93 subcomplex and the NUP107-160 complex/Y complex, arranged as inner and outer ring respectively and is filled with intrinsically disordered proteins, which are rich in phenylalanine-glycine (FG) amino acid residues (von Appen, Kosinski et al. 2015). These FG rich NUPs provide the binding sites for nuclear transport receptors (importins, and exportins) following the signal transduction process of the cell (Beck and Hurt 2017). Studies suggest that NUPs play an additional regulatory roles during growth and maturation of tissue specific progenitor cell maturation (Lupu, Alves et al. 2008). Abnormal function of NUPs can cause microcephaly; steroid resistant nephrotic syndrome is most frequently reported with microcephaly caused by abnormalities in NUPs (Cragan, Isenburg et al. 2016).

### **3.8.1 Microcephaly associated nephrotic syndrome**

Nephrotic syndrome is clinically characterized by abnormal renal glomerular filtration, proteinuria, edema, and hypo albuminemia. Well characterized form of nephrotic syndrome known as Finnish type is the infantile micro-cystic disease which appears as early as in the first year after birth or sometimes during pregnancy (Lenkkeri, Männikkö et al. 1999). Nephrotic syndrome, in general, is curable through drug treatment but sometimes the disease does not respond to drug treatment and this condition is known as steroid resistant nephrotic syndrome (SRNS), abnormal podocyte migration being its surrogate phenotype. As the drug treatment is not effective, diffuse mesangial sclerosis occurs, which indicates irreversible damage to the glomerulus and thus leads to end stage kidney failure (Braun, Lovric et al. 2018).

The association of microcephaly with nephrotic syndrome appears to be a distinct syndrome with an autosomal recessive mode of inheritance (Garty, Eisenstein et al. 1994). This association is particularly reported in several studies with additional clinical manifestation of seizures and psychomotor retardation (Palm, Hägerstrand et al. 1986; Yalçinkaya, Tümer et al. 1994; de Vries, van't Hoff et al. 2001; Braun, Lovric et al. 2018).

### ***Genetics of microcephaly associated nephrotic syndrome***

A study presented the largest international cohort of SRNS where more than 50 genes were declared to be causative in monogenic form of SRNS (Warejko, Tan et al. 2018). Most of the proteins encoded by these genes are highly and exclusively expressed in podocytes which are the specialized epithelial cells for carrying out glomerular filtration and remain the main affected site of mutational consequence. These proteins include lysosomal, mitochondrial, cytoskeletal, metabolic, slit diaphragm associated and nuclear pore complex proteins (Preston, Stuart et al. 2019).

Regarding the role of nucleoporins in podocyte functioning, a study presented nine unrelated SRNS families and three sporadic cases which were found to have mutations in the *NUP107* gene encoding a component of nuclear pore protein complex (Cragan, Isenburg et al. 2016). Another study proved that mutations in four different nucleoporins encoding genes (*NUP107*, *NUP85*, *NUP133* and *NUP160*) being the cause of defective kidney functioning and reduced brain size strengthening the role of nucleoporins in disease pathogenesis of SRNS syndrome (Braun, Lovric et al. 2018).

## 4. Aims of the study

Autosomal recessive primary microcephaly (MCPH) is an increasingly, heterogeneous genetic disorder and thus demands further exploration of causative genes and their functions. Mutations in several genes have been demonstrated to cause MCPH but scientists are far from understanding the precise pathomechanism. Adding to the challenge, the scientific community is still chasing the mechanism of the bifurcation between its non-syndromic to syndromic form. To bridge this gap of knowledge, families afflicted both isolated and syndromic form — Flippi syndrome — of microcephaly were investigated in this study. The study aimed mainly to unravel the genetic and biochemical bases of primary microcephaly and Filippi syndrome which could provide important insights to understand the pathomechanism of these rare disorders.

The specific scope of this dissertation includes

1. Identification of disease causing genes in families afflicted MCPH and dissecting their underlying mechanisms.
2. Biochemical characterization of disease causing mutation in *CSNK2B* — candidate gene of Filippi syndrome.
3. Identification and biochemical characterizations of further novel disease causing variants of *CSNK2B*.
4. Exploring novel candidate genes of cohort manifesting Filippi syndrome

For achieving these aims, complimentary multiomics approaches of genomic, bioinformatics and biochemical techniques were adopted.

## 5. Results

### 5.1 Preview of investigated families

This chapter will brief a total number of 17 families; five families (MCP3, MCP4, FP2, FP28, FP30) were investigated for unraveling the mutational consequences on biochemical level whereas rest of the families were explored only on genetic grounds. The detailed overview of all families is given in the table below (Table 5.1).

**Table 5.1: Preview of investigated families.**

Family ID	Phenotype	Gene	Ethnicity	Consanguinity
MCP1	MCPH	<i>STIL</i>	Pakistani	Yes
MCP2	MCPH	<i>SH2D3C</i>	Pakistani	Yes
MCP3	MCPH	<i>NUP37</i>	Pakistani	Yes
MCP4	MCP,SRNS	<i>NUP107</i>	Pakistani	Yes
FP2	FLPIS	<i>CSNK2B</i>	Italian	No
FP28	FLS	<i>CSNK2B</i>	Caucasian	No
FP30	FLS	<i>CSNK2B</i>	Israeli	No
FP14	FLPIS	<i>CDKL5</i>	Brazilian	No
FP3	FLPIS	Not identified	Polish	No
FP12	FLPIS	Not identified	Newzealander	No
FP13	FLPIS	<i>PTPN23</i>	Omani	No
FP15	FLPIS	<i>PSENI</i>	Finland	No
FP16	FLPIS	<i>DNM3</i>	Turkish	Yes
FP18	FLS	Not identified	German	No
FP19	FLPIS	<i>TRIM35</i>	French	No
FP20	FLPIS	Not identified	Mexican	No
FP22	FLS	<i>CDKL2</i>	British	No

MCPH = autosomal recessive primary microcephaly, MCP = microcephaly, SRNS = steroid resistant nephrotic syndrome, FLPIS = Filippi syndrome, FLS = Filippi-like syndrome

On the basis of phenotype — microcephaly and Filippi syndrome — this chapter is divided into two parts:

## Part 1A: Molecular investigation of primary microcephaly families

### 5.2 Novel mutation in *STIL* causes MCPH in family MCP1

A family, having affected individuals featuring typical symptoms of primary microcephaly (ORPHA:2512), was recruited from Punjab, Pakistan. All the three patients were born to consanguineous parents (Figure 5.1A and 5.1B). Clinical investigations showed that, in addition to reduced head circumference all the patients also showed mild to moderated intellectual disability (HP:0001256, HP:0002342) accompanied with impaired speech. Whole exome sequencing revealed a novel variant (NM\_001048166.1;c.3694C>T; p.(Arg1232\*)) of a previously reported MCPH gene — *STIL* (Kumar, Girimaji et al. 2009). Detailed clinical and molecular data of all the three patients is mentioned in the table below (Table 5.2). Sanger sequencing was performed to validate the segregation of this variant. Sanger sequencing confirmed the segregation of variant in homozygous form in all patients and heterozygous state in both parents (Figure 5.1C).

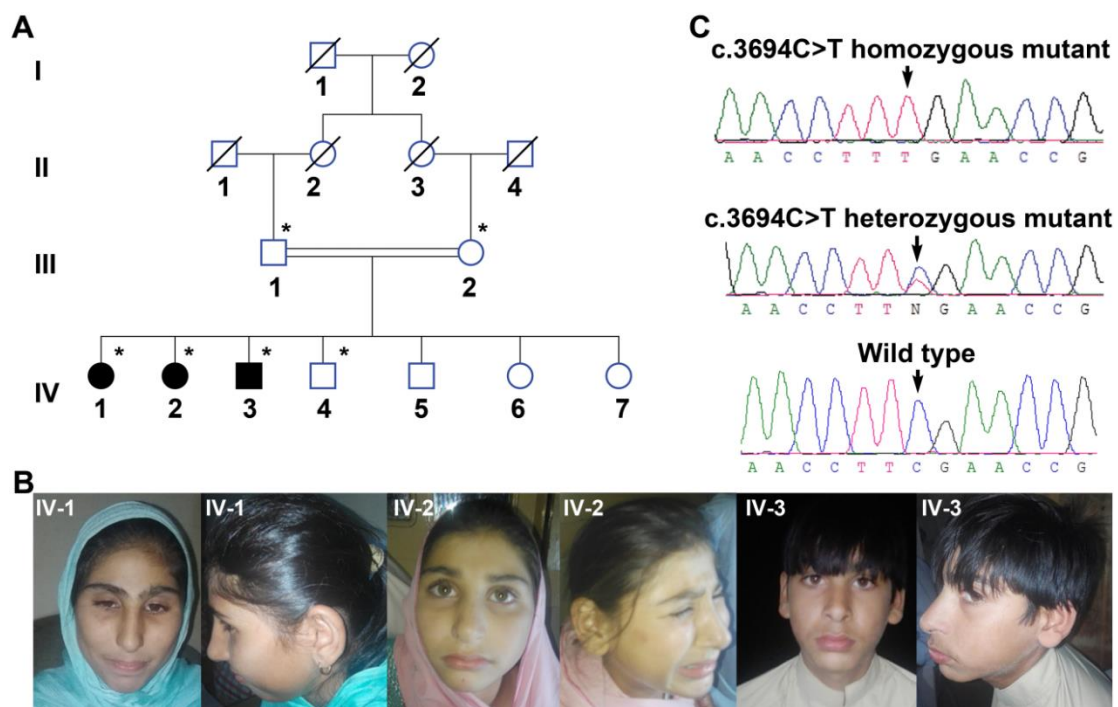


Figure 5.1: Genetic and clinical analyses of MCP1 having mutation in *STIL*.

(A) A Four generation pedigree of family carrying mutation in *STIL*. Asterisk (\*) indicates the samples which were subjected in this study. (B) Front and side views of patients showing microcephaly. (C) Sanger traces of index patient along with her heterozygous parent and wild type showing mutation (NM\_001048166.1;c.3694C>T; p.(Arg1232\*)) of *STIL*.

**Table 5.2: Clinical and molecular investigation of *STIL* mutated individuals.**

Family Individual	Gene	Mutation information	Age at examination (years)	OFC (cm)	OFC (SD)	Observed clinical manifestation
-IV-1	<i>STIL</i>	NM_001048166.1; c.3694C>T	15	45	-6	-Mild intellectual disability, able to perform personal care
-IV-2		p.(Arg1232*)	11	44	-4.66	-Mild intellectual disability, able to perform self-care functions
-IV-3			13	44	-6.66	-Epileptic shocks started at the age of 10 years, aggressive behavior, speech impairment

Previously, 11 variants of *STIL* have been reported in the regard of pathogenesis of primary microcephaly (Kumar, Girimaji et al. 2009; Darvish, Esmaeeli-Nieh et al. 2010; Papari, Bastami et al. 2013; Bennett, Presti et al. 2014; Mouden, de Tayrac et al. 2015) (Figure 5.2). *STIL* encodes a ubiquitously expressed protein, SCL-interrupting locus protein, containing 18 exons. The mutation was found in exon 18 and predicted to be highly pathogenic with maximum CADD (Combined Annotation Dependent Depletion) score i.e., 36.

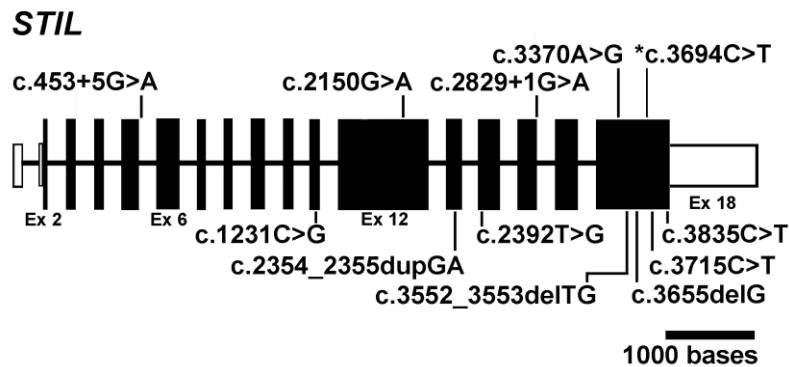


**Figure 5.2: Gene structure of *STIL* (NM\_001048166.1) showing reported disease-causing variations.**

Asterisk (\*) shows the novel mutation identified in this study. Vertical black bars represent the coding exons and white show the non-coding exons which are constructed according to the scale whereas introns are shown by horizontal lines and are drawn arbitrary.



**Explication;** It may be assumed that due to nonsense mutation in *STIL*, a premature stop codon may result in the formation of truncated protein product, if being made, or it may be subjected to degradation of mutant mRNA by nonsense mediated mRNA decay.

### 5.3 *SH2D3C* is a novel candidate gene identified in family MCP2

Two MCPH patients (a male and a female), born to Pakistani consanguineous parents showed typical features of microcephaly (ORPHA:2512) (Figure 5.3A and 5.3B). Further clinical examination revealed moderate to severe intellectual disability (HP:0001256, HP:0002342). Notably, both affected members showed aggressive behavior. HC determined for male patient was -6.6 SD, whereas, it was -8 SD in case of female patient. No other disability was noticed in both affected individuals except imprecise speech articulation (HP:0009088).

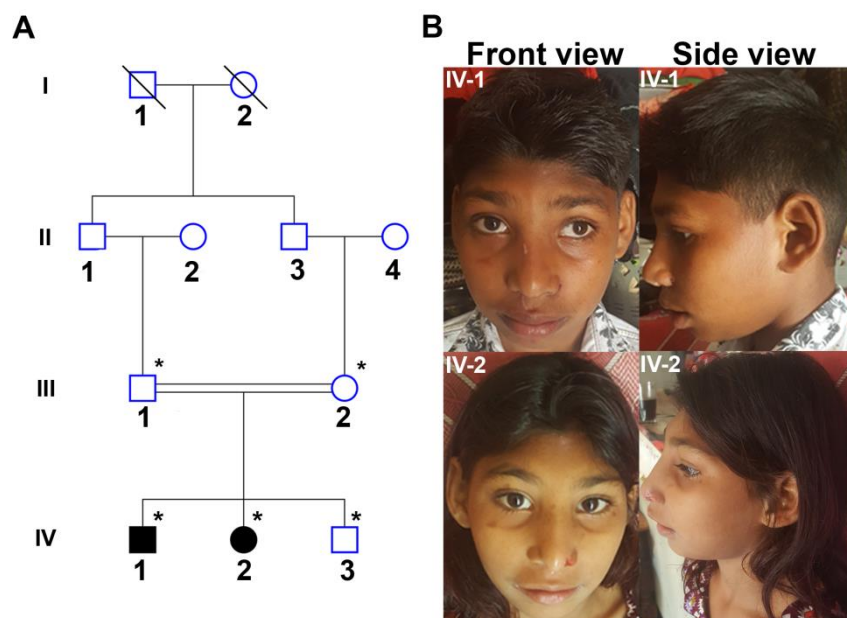


**Figure 5.3: Genetic and clinical analyses of a family having mutation in *SH2D3C*.**

(A) Four generation pedigree of *SH2D3C* mutated family. Asterisk (\*) indicates the samples which were available to this study. (B) Front and side views of patients showing microcephaly.

#### 5.3.1 Genetic investigation

For investigating the genetic determinant(s) of congenital microcephaly in MCP2, exome sequencing was combined with linkage analysis. Linkage analysis was performed by genotyping the DNA of five family members, two affected members, their asymptomatic brother and both parents, with Axiom Precision Medicine Research Array from Affymetrix

(Santa Clara, CA). Data analysis revealed three peaks, on chromosomes 7, and one of each chromosomes 9 and 11 reaching the theoretical maximum possible LOD score of 1.9 (Figure 5.4A). Three homozygous segments of chromosome 7 were identified which are as follows: 0.26 Mb region, rs2190383-rs6963111 (14,184,011-14,447,940 bp); 1.41 Mb region, rs58021112-rs1295136 (14,897,078-16,308,583 bp); and 0.21 Mb region, rs7806392-rs17627078 (16,528,409-16,741,280 bp). Only one linkage interval of 5.41 Mb was identified at chromosome 9, bounded by the markers rs41331550 (121,669,089 bp) and rs4838161 (127,079,253 bp). Finally, 2.82 Mb region was also seen at chromosome 11, where recombinations were observed for the markers, rs3862611 (121,831,524 bp) and rs68065265 (124,657,596 bp).

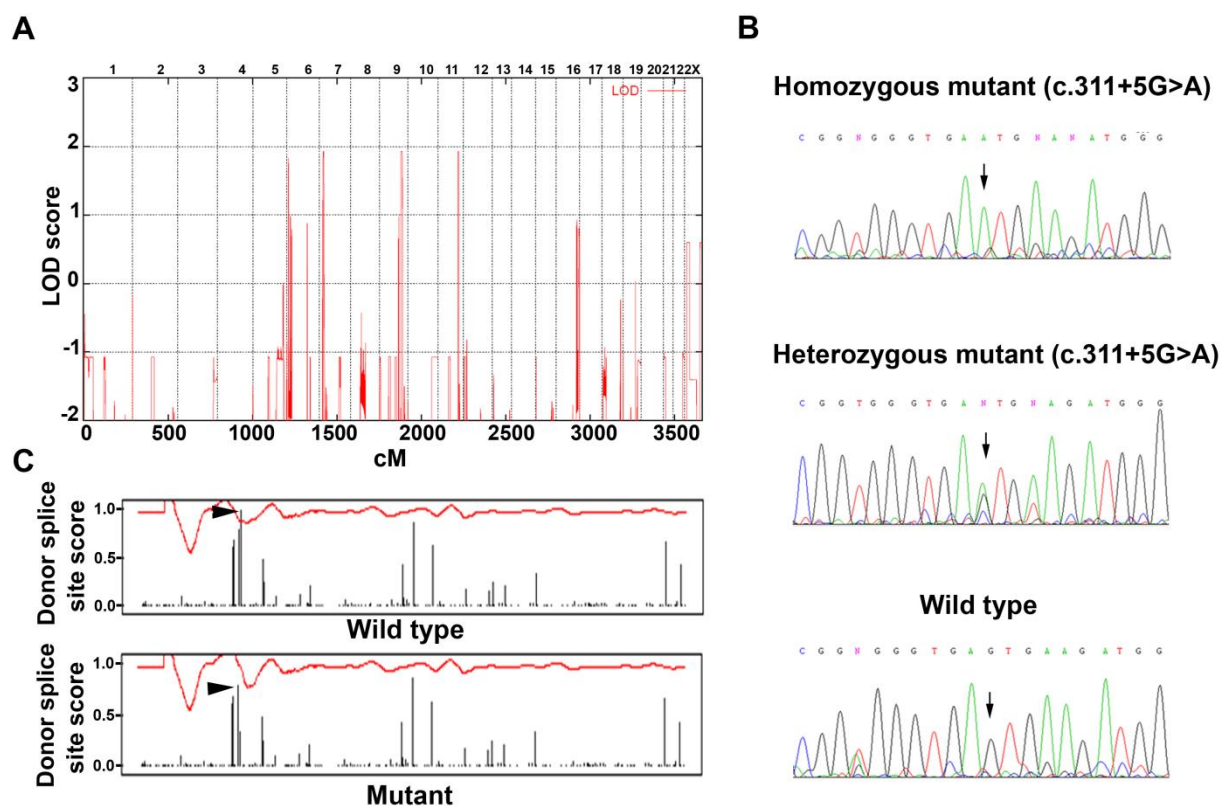


**Figure 5.4: Identification of pathogenic variation of *SH2D3C*.**

(A) Genome-wide linkage graph obtained by genotyping the DNA with Axiom Precision Medicine Research Array from Affymetrix (Santa Clara, CA). Maximum LOD score was obtained on chromosomes 7, 9 and 11. (B) Sanger chromatograms showing the splice site variant of *SH2D3C*. Sanger traces of an index patient, his asymptomatic mother and from control individual are shown. (C) Prediction of NetGene2 Server showing the drop of peak (arrow head) depicting the position of *canonical* splice donor site which otherwise was accurately detected in the wild-type sequence (arrow head).

Keeping in view the linked regions, whole-exome sequencing of one affected individual was performed. Unfortunately, exome data did not reveal any strong candidate gene having homozygous or compound heterozygous variations located within the identified linkage regions. Due to this reason, the search for candidate gene(s) was extended in regions situated outside the linkage regions. Three genes *DNAH11*, *AJMI* and *SH2D3C* having homozygous variations were chosen for co-segregation analysis on the basis of their low allele frequency and pathogenicity predicted by *in silico* tools (Table 5.3). Among them, only splice variant, c.311+5G>A, located in intron 2 of *SH2D3C* (NM\_001252334.1) was found to be segregated in the family (Figure 5.3B).

**Table 5.3: Genetic information of the variants selected in MCP2 family along with their segregation pattern.**

Gene symbol	Transcript ID	Mutation at cDNA level	Mutation at protein level	Allele frequency (in-house)	Allele frequency (gnomAD)	CADD score	CSA
<i>DNAH11</i>	NM_001277115.1	c.13075C>T	p.(Arg4359*)	0.000162	5 heterozygotes	58	NS
<i>AJMI</i> ( <i>C9orf172</i> )	NM_001080482.2	c.1535C>T	p.(Ser512Leu)	0.000142	Absent	25.4	NS
<i>SH2D3C</i>	NM_001252334.1	c.311+5G>A	-	0.000842	Absent	3.3	S

Note: Our in-house database of Cologne Center for Genomics (CCG) with >1,600 exomes. The observed allele frequency was shown as zero heterozygotes, in our in-house database, for all the three genes (*DNAH11*, *AJMI* and *SH2D3C*), CSA = Co-segregation analysis, NS = Not segregated, S = Segregated.

### 5.3.2 Splice site mutation in *SH2D3C* causes primary microcephaly

The effect of splice site mutation was further predicted using NetGene2 Server (Hebsgaard, Korning et al. 1996), MaxEntScan::score5ss for human 5' splice sites (Yeo and Burge 2004) and Human Splice Finder (HSF) Version 3.0 (Desmet, Hamroun et al. 2009). NetGene2 Server predicted that this variant could alter the *canonical* splice donor site (Figure 5.4C).

Similarly, HSF predicted alteration of splice donor site with possible consequences of splicing errors. In addition, MaxEntScan showed decreased scores in case of mutant compared to wild-type sequence thus suggesting the pathogenic effects of this mutation (Table 5.4). It was hence supposed that the creation of new splice donor site may result in aberrant splicing, most likely resulting in intron retention.

**Table 5.4: MaxEntScan prediction scores showing the scores obtained by different models**

Sequence	MAXENT score	MDD	MM	WMM
Wild type (TGGgtgagt)	8.73	13.18	8.36	7.38
Mutant (TGGgtgaat)	1.20	4.28	3.89	3.92

Maximum Entropy Model (MAXENT), Maximum Dependence Decomposition Model (MDD), First-order Markov Model (MM), Weight Matrix Model (WMM). Red color is given to the *canonical* splice donor site and blue to the mutated residues.

*SH2D3C* encodes for Shep1 protein already reported to be highly expressed in brain (Wang, Vervoort et al. 2010). It should also be noted that the mutation is present only in one transcript (NM\_001252334.1) of *SH2D3C*.

**Explication;** *SH2D3C* is a novel candidate gene for microcephaly being stated on the basis of co-segregation analysis and pathogenicity anticipated by different *in silico* prediction tools. It can be assumed if the expression of this transcript (NM\_001252334.1) is higher in the brain then aberrant splicing may lead to microcephaly.

## 5.4 Mutation in novel gene *NUP37* causes primary microcephaly

The genetic delineation of MCP3 family originated from Pakistan was previously carried out. A consanguineous family having four affected individuals born from consanguineous parents, manifesting microcephaly associated with clinodactyly, which is a minor digital curvature of fifth finger. Kidney malfunctioning was investigated as per the knowledge of NUPs involvement in kidney pathogenesis. No clinical symptoms were observed in any of the three affected individuals. A stop gained mutation, c.916C>T;p.Arg306\*, was found in *NUP37* (NM\_024057.3) which encodes nucleoporin Nup37 (Braun, Lovric et al. 2018) (Figure 5.5A). I had tasks to reveal the mutational consequences of this identified variant on transcript as well protein level in patient derived cells.

### 5.4.1 Effects of *NUP37* nonsense mutation at transcript level

Analysis of the *NUP37* genomic regions, both from wild type and mutant, with the help of NetGene2 Server for the possibility of any alteration in the splicing event, showed the

ablation of a *canonical* splice acceptor site near the intron upstream to the mutant exon. To test the possibility of any cryptic splicing activation due to mutation, RT-PCR was carried out which showed no splice variant of *NUP37*, as bands of PCR product were observed at similar sizes (437 bp) in case of wild type as well as in mutant (Figure 5.5B). Sanger sequencing of PCR products obtained from both wild type and mutant did not reveal any differences except the mutant nucleotide was observed in the product belonging to the affected member.

Further, quantification of *NUP37* transcripts from cDNA obtained from wild-type and patient derived primary fibroblasts was carried out where two sets of primers were used; set-1 designed in the region upstream to the mutation and set-2 referred to the region spanning the mutation (Figure 5.5A). Results depicted that compared to wild type, mutant transcript showed 62% reduction when tested with primers pair 1 and 53% reduction in case when the second set of primers was used to quantify the product (Figure 5.5C).

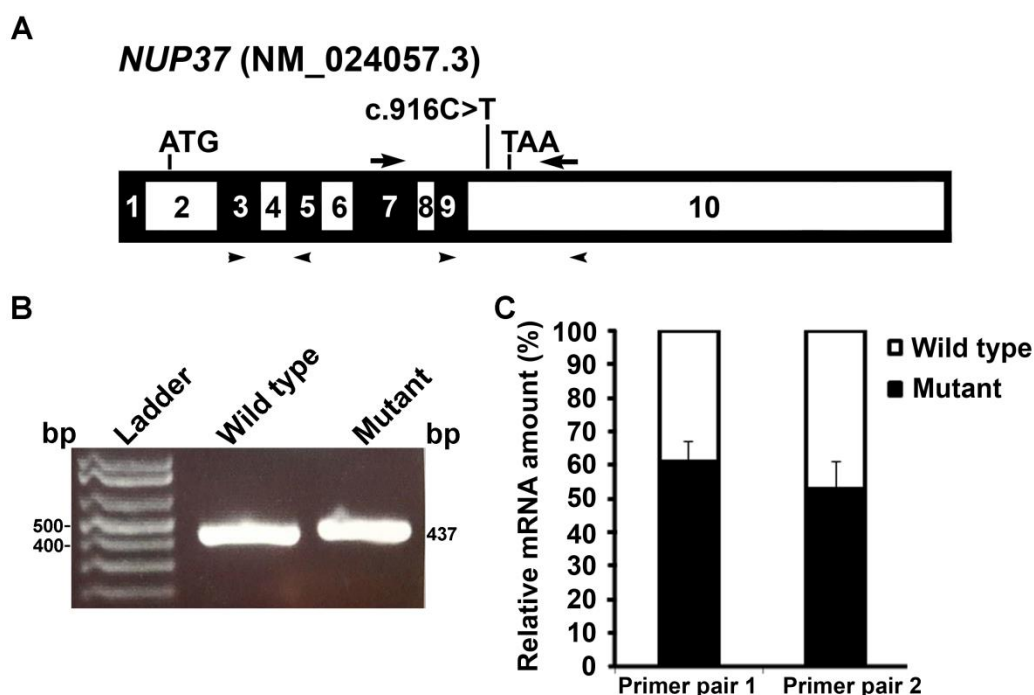


**Figure 5.5: Effects of mutation on protein level observed in *NUP37* mutated primary fibroblasts.**

(A) Gene structure of *NUP37* showing location of primers used for RT PCR (arrows on exon 7 and 10) and qPCR (primer set-1: exon 3 and 5, primer set-2: exon 9 and 10, shown by arrow heads). (B) Agarose gel (2%) image showing similar bands of PCR product with equal sizes. (C) Bar graph showing decreased relative mRNA amount of *NUP37* in mutant fibroblasts compared to wild-type. Error bar depicts SEM. Note:  $p$  values  $> 0.05$  (Student's  $t$  test). Figure is adopted from Braun et al, 2018.

### 5.4.2 Effects of mutation on protein level

As reduction of *NUP37* was seen at transcripts level, western blot and immunofluorescence were performed to observe the similar effect at the protein level. Immunoblotting revealed the reduction in the amount of **nucleoporin Nup37 (p37)** seen in protein lysate obtained from patient derived fibroblasts as compared to wild type (Figure 5.6A). Further, immunofluorescence showed fine staining of NUP37 around the nucleus, particularly at the nuclear envelop, of wild type whereas it was barely visible in the mutant fibroblasts (Figure 5.6B).

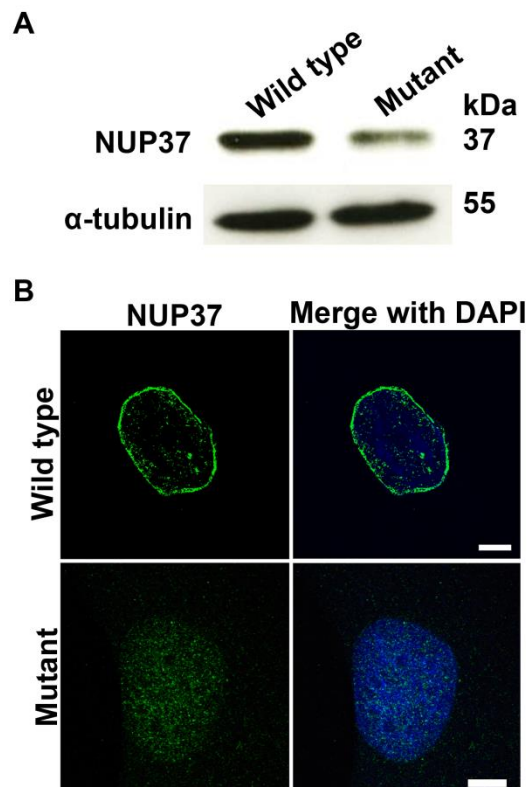


**Figure 5.6: Effects of mutation, c.916C>T in *NUP37* at transcript level.**

(A) Immunoblotting shows reduced nucleoporin Nup37 (p37), also known as NUP37, in mutant fibroblasts as compared to wild type.  $\alpha$ -tubulin serves as loading control. (B) Immunofluorescence shows reduced NUP37 in mutant primary fibroblasts as compared to wild-type. Scale bar is 5  $\mu$ m, DAPI (blue) is used for staining nucleus. Figure is adopted from Braun et al, 2018.

### 5.4.3 Effects of reduced NUP37 on its binding partners

NUP37 is a component of the Y complex and shares localization with other nucleoporins (Kelley, Knockenhauer et al. 2015), therefore the effects of reduced NUP37 was further inquired on its binding partners located at the nuclear envelop. For this purpose, two of the



direct physical partners, NUP107 and NUP160, were investigated. Immunoblotting performed on cell lysates obtained from wild-type and patient derived primary fibroblasts revealed reduction of both NUP107 and NUP160 (Figure 5.7A and B). Immunofluorescence analysis coupled with confocal microscopy of both binding partners corroborated the immunoblotting data. Both proteins were found reduced at nuclear envelop as well as mislocalized in patient fibroblasts as compared to wild type, their faint signal was detected within the nuclei of the mutant primary fibroblasts (Figure 5.7C and D).

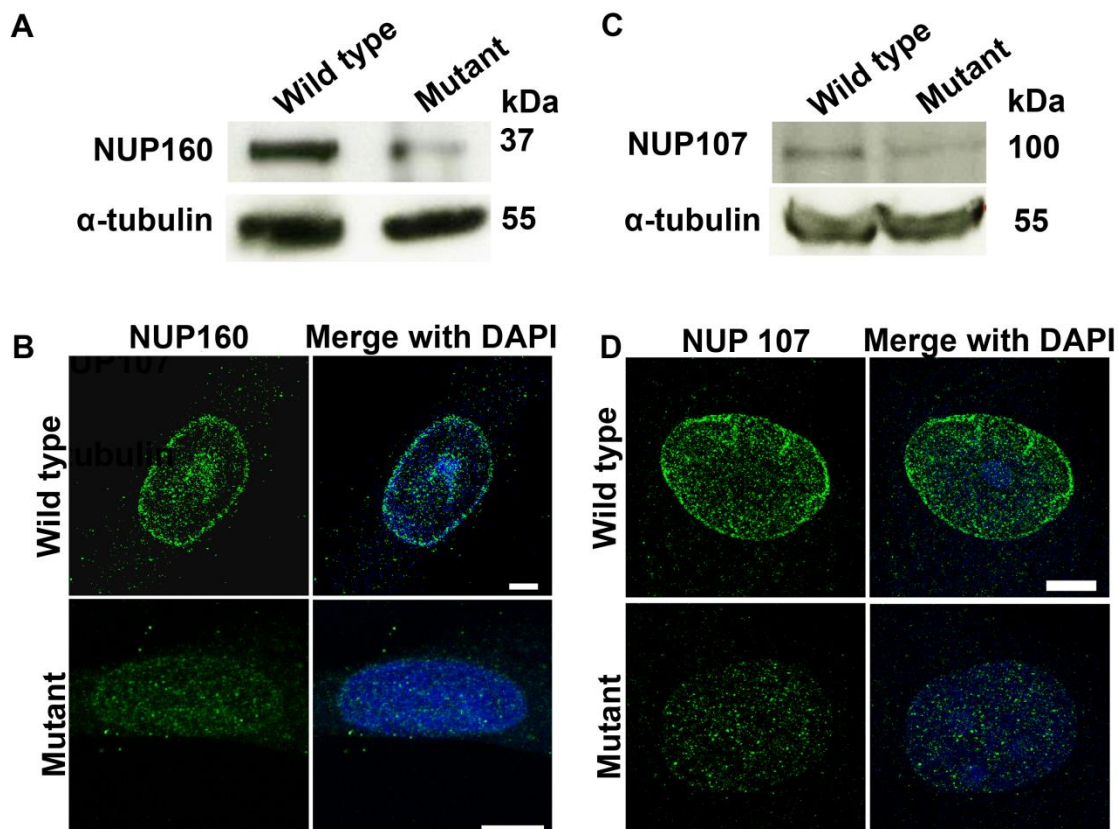


**Figure 5.7: Effects of reduced NUP37 on the localization and amounts of its binding partners.**

(A and B) Immunoblotting shows reduced NUP160 and NUP107 in NUP37 mutated primary fibroblasts as compared to wild type.  $\alpha$ -tubulin was used to observe equal protein loading. (C and D) Immunofluorescence shows reduced NUP160 and NUP107 in NUP37 mutated fibroblasts as compared to wild type. Scale bar is 5  $\mu$ m, DAPI (blue) is used for staining DNA. Figure is adopted from Braun et al, 2018.

#### 5.4.4 Investigating the effect of mutation on nuclear pore density

After finding reduction of NUP37 and its binding partners, the overall nuclear pore density was expected to be decreased. For this purpose, images of both wild-type and mutant primary

fibroblasts were taken using a confocal laser scanning microscope (TCS SP8 gSTED, Leica Microsystems) which showed a reduced intensity of the mAb414 (binds to common FG repeats of nuclear pores) antibody signal (Figure 5.8A). Nuclear pore density was analyzed using the “particle analysis” tool of ImageJ (version 1.51z; NIH). Statistical analysis suggested a lower number of nuclear pores in mutant fibroblasts i.e, 13 pores per  $\mu\text{m}^2$  as compared to control cells showing 20 pores per  $\mu\text{m}^2$  (Figure 5.8B).

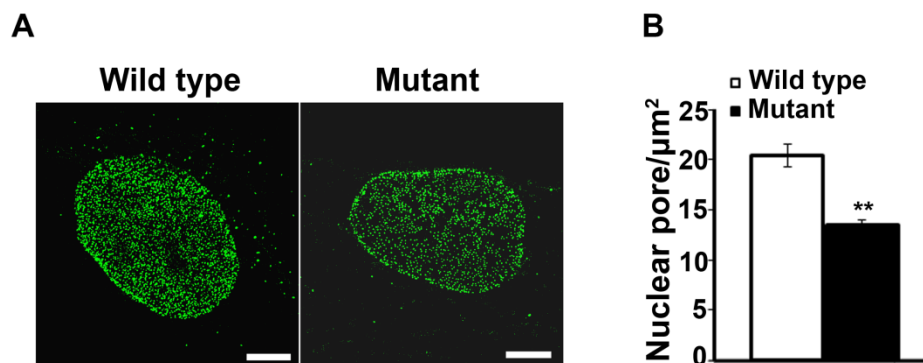


**Figure 5.8: Reduced nuclear pore density in NUP37 mutated fibroblasts.**

(A) Immunostaining with an antibody against several FG-repeat nucleoporins (mAb414) in wild-type versus mutant primary fibroblasts. Scale bar is 5  $\mu\text{m}$ , DAPI (blue) is used for staining nucleus. (B) Bar graph demonstrates a significant reduction in the number of NPCs per square micrometer in mutant versus control cells. Data were obtained for 100 cells from 3 different experiments. Error bars denote SEM.  $P$  value = 0.0048 (Student’s  $t$  test). Figure is adopted from Braun et al, 2018.

**Explication;** The genetic data obtained by exome sequencing reveals *NUP37* as causative gene of primary microcephaly. Further investigation on RNA and protein obtained by patient derived primary fibroblasts strongly supports the idea that reduced amount of NUP37 and its binding partners (NUP107 and NUP160) may have even deleterious cellular effects in a broader sense.

#### 5.4.5 Abnormalities observed in NUP37 mutated fibroblasts

Nuclear abnormalities have been associated with dysfunction of nuclear pore proteins demonstrated previously (Sheffield, Miskiewicz et al. 2006). It also intrigued me to investigate the effects of reduced NUP37 on structure and functions of the nucleus. Such abnormalities observed in the NUP37 mutated fibroblasts are explained in this section.



#### 5.4.6 Alteration in chromatin organization

Arrangement of heterochromatin was being investigated using antibody specific for HP1 $\beta$  (histone protein 1 beta). Images taken with the help of confocal microscopy showed nicely arranged chromatin in the close vicinity of nuclear membranes in wild-type fibroblasts. However, alteration in the organization of chromatin in patient derived fibroblasts was notable, where it was found scattered in whole nucleoplasm (Figure 5.9).

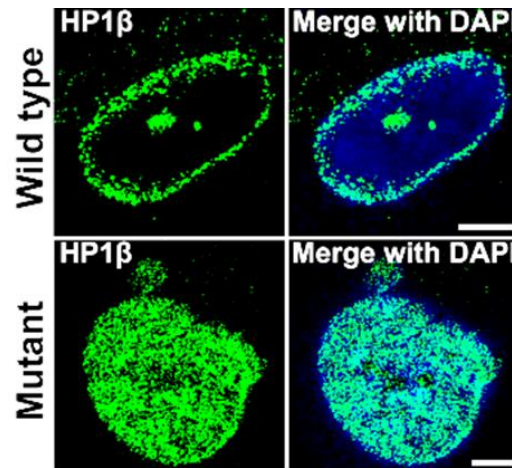


**Figure 5.9: Immunostaining of heterochromatin in patient fibroblasts.**

Staining HP1 $\beta$  (green), demonstrates an altered pattern in mutant versus control fibroblasts. Scale bar is 5  $\mu$ m, DAPI (blue) is used for staining nucleus. Figure is adopted from Braun et al, 2018.

#### 5.4.7 Misshapen nuclei

To investigate the nuclear morphology in NUP37 mutated fibroblasts; LAP2 $\beta$  (lamina-associated polypeptide 2) antibody was used to stain nuclear membrane which showed distorted nuclei as well as blebbing of the nuclear envelope in case of patient fibroblasts as compared to wild type (Figure 5.10A). Considering the statistical data, 10.6% of patient fibroblasts showed abnormal shape of nuclei which were significantly higher as compared to wild-type where 1.5% cells were found with abnormal nuclear shape (Figure 5.10B).

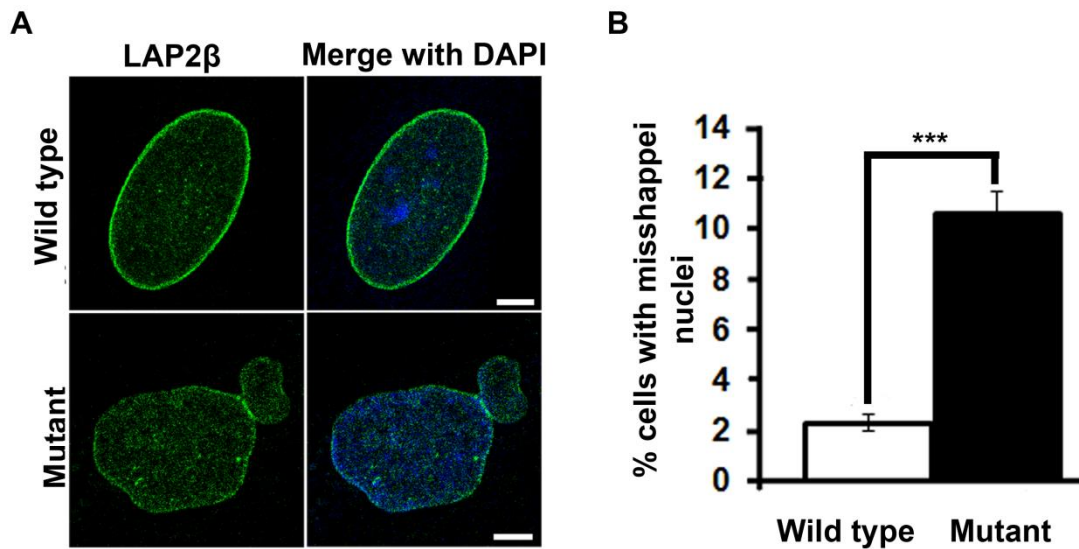


**Figure 5.10: Abnormal shape of nuclear envelop in NUP37 mutated fibroblasts.**

(A) LAP2 $\beta$  (green) was used to stain nuclear membrane. Note mutant fibroblasts show abnormal shape of nuclei. Scale bar is 5  $\mu$ m, DAPI (blue) is used to stain DNA. (B) Quantification of 150 cells from 3 independent experiments demonstrates a significantly increased percentage of nuclei with misshapen nuclei in mutant versus control cells. Error bars represent SEM. *P* value = 0.0009 (Student's *t* test). Figure is adopted from Braun et al, 2018.

#### 5.4.8 Abnormal nucleoli

Nucleolar abnormalities, particularly morphology of the nucleoli, were also analyzed using antibody specific for nucleolar protein fibrillarin. Data revealed that nucleoli in patient fibroblasts were misshapen and less prominent as compared to wild-type fibroblasts (Figure 5.11A). The statistical data suggested that about 13% of the patient fibroblasts featured nucleoli with abnormal shape and appearance whereas only 1% of wild-type primary fibroblasts showed abnormal shaped nucleoli (Figure 5.11B).

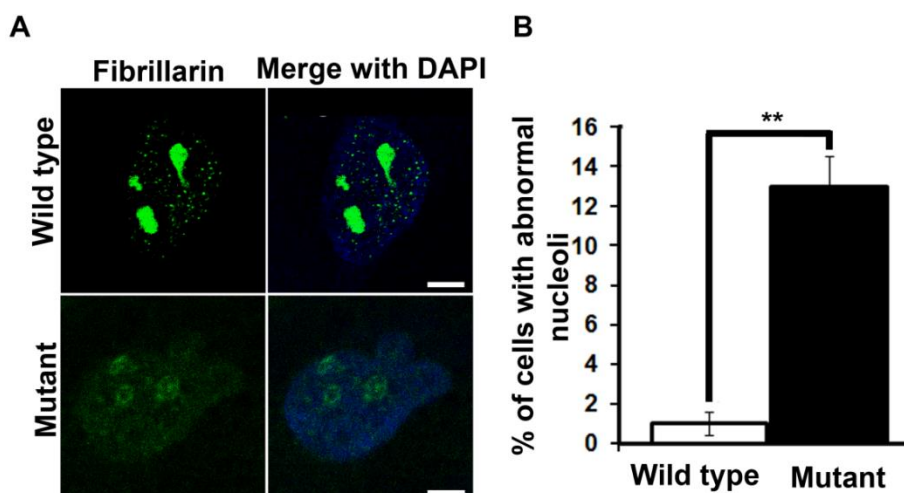


**Figure 5.11: Nucleolar abnormality in NUP37 mutated primary fibroblasts.**

(A) Fibrillarlin (green) was used to stain nucleoli. Note that fibrillarlin staining was more dispersed in mutant fibroblasts. Scale bar is 5  $\mu\text{m}$ , DAPI (blue) is used to detect nucleus. (B) Bar graph demonstrating a significantly increased percentage of cells with abnormal shaped nucleoli in mutant versus control cells.  $n=3$  (150 cells/experiment). Error bars represent SEM.  $P$  value = 0.0018 (Student's  $t$  test). Figure is adopted from Braun et al, 2018.

#### 5.4.9 Verification of abnormalities using transmission electron microscopy (TEM)

For validation of abnormalities found in patient derived fibroblasts by immunofluorescence, TEM was carried out to validate the data. Data showed a regular nuclear envelope (arrowhead outside the nucleus) and well-arranged heterochromatin in the proximity of the nuclear envelope (arrowhead inside the nucleus) seen the wild-type cells. Additionally, these cells also showed regular shaped nucleoli (arrows) (Figure 5.12A). Whereas patient derived fibroblasts showed irregular heterochromatin, misshapen nuclei and abnormal shaped nucleoli (Figure 5.12B). Wild-type primary fibroblasts exhibited well-arranged perinuclear space (Figure 5.12C), however widened perinuclear space and bulbous invasions of nuclear envelope was observed in patient derived fibroblasts (Figure 5.12D).

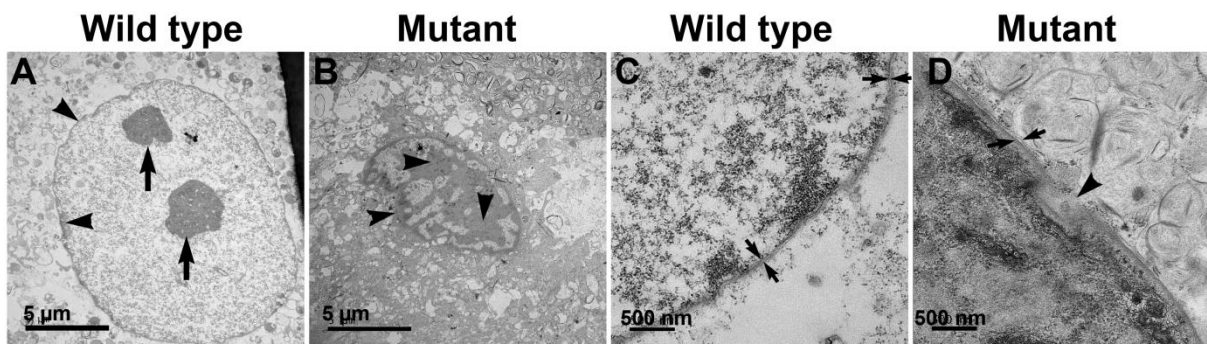


**Figure 5.12: TEM images of control versus mutant fibroblasts.**

(A) Control (WT) cell with regular nuclear envelope and well-arranged heterochromatin. (B) Depiction of the altered nuclear architecture of mutant fibroblasts; specifically, there is an abnormal arrangement of heterochromatin and nucleoli (shown by arrowheads). (C) Well-arranged perinuclear space, indicated by arrows. (D) Widened and irregular perinuclear space in mutant fibroblasts indicated by arrows. Arrowhead indicates bulbous invasions of the nuclear envelope. Scale bars are defined in each image. Figure is adopted from Braun et al, 2018.

**Explication;** The abnormalities found in NUP37 mutated fibroblasts on cellular level may lead to severe effects on organ level. Based on these data it may also be assumed that brain may show sensitivity towards dosage of NUP37 which may cause microcephaly.

#### 5.4.10 Effect of mutation on cellular proliferation

As, nucleoporins (NUPs) are relocated to kinetochore during cell division for proper chromosomal segregation, reduced level of NUP37 may delay cell cycle and ultimately effect cellular proliferation. Keeping this fact, proliferation assay was performed to find out the influence of mutation on the proliferation rate of the cells. Both, wild-type and patient derived fibroblasts were grown for 8 days and counted. The data revealed that there was a decreased count of patient fibroblasts after day four and cells showed slower growth rate whereas the number of wild-type fibroblasts followed a progressive pattern. Statistical data showed that the number of patient cells remained in the range of 10,000 to 15,000, from 4<sup>th</sup> day onwards whereas wild-type fibroblast increased up to 25,000 cells until 8<sup>th</sup> day (Figure 5.13).

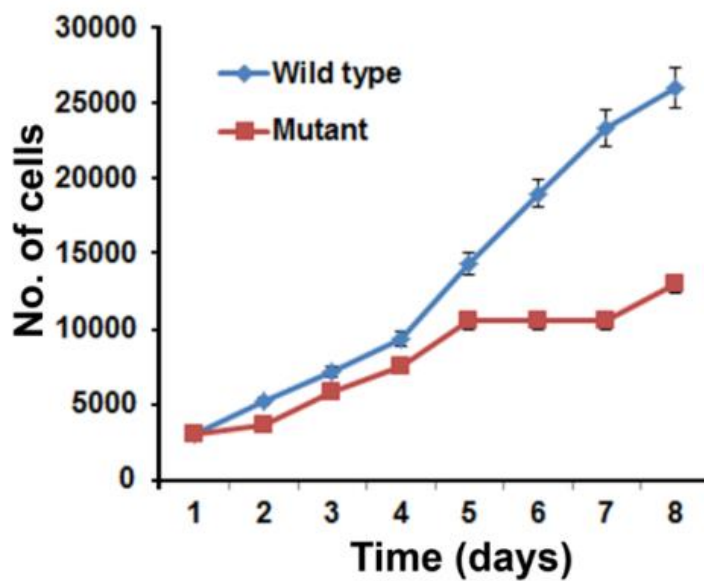


**Figure 5.13: Proliferation of mutant fibroblasts.**

The assay was performed in the fibroblasts obtained from the index patient and control cells. Data is based on three independent experiments, error bars denote SEM. Figure is adopted from Braun et al, 2018.

**Explication;** As, cell division and proliferation, during neurogenesis, is more sensitive and crucial, the mutation might have even severe effects on neurons thus disturbing the neurogenesis.

## **Part 1B: Molecular investigation of microcephaly associated nephrotic syndrome (SRNS) in family MCP4**

This part comprehends the biochemical characterization of an already reported NUP107 mutated family manifested as microcephaly associated SRNS (Braun, Lovric et al. 2018)

### **5.5 Recapitulating cellular phenotype of NUP37 mutants in NUP107 mutated LCLs**

As a matter of fact, NUP37 and NUP107 are binding partners; it was feasible to recapitulate the cellular phenotypes of NUP37 mutated fibroblasts in *NUP107* mutated lymphoblastoid cell lines (LCLs). NUP133 and NUP160, which are the direct binding partners of NUP107, were investigated in wild-type and mutant LCLs. In addition, NUP37 was also examined on protein level. Immunofluorescence revealed that NUP37, NUP133 and NUP160 were localized on nuclear envelop of the wild-type LCLs, whereas in patient derived LCLs not only the intensities of all of these tested proteins were found reduced but also, they were mislocalised with faint staining observed within the nuclei (Figure 5.14A, B and C). Immunoblotting showed that all the above-mentioned partners of NUP107 were reduced in patient fibroblasts as compared to wild type, thus validating the immunofluorescence data (Figure 5.14D).

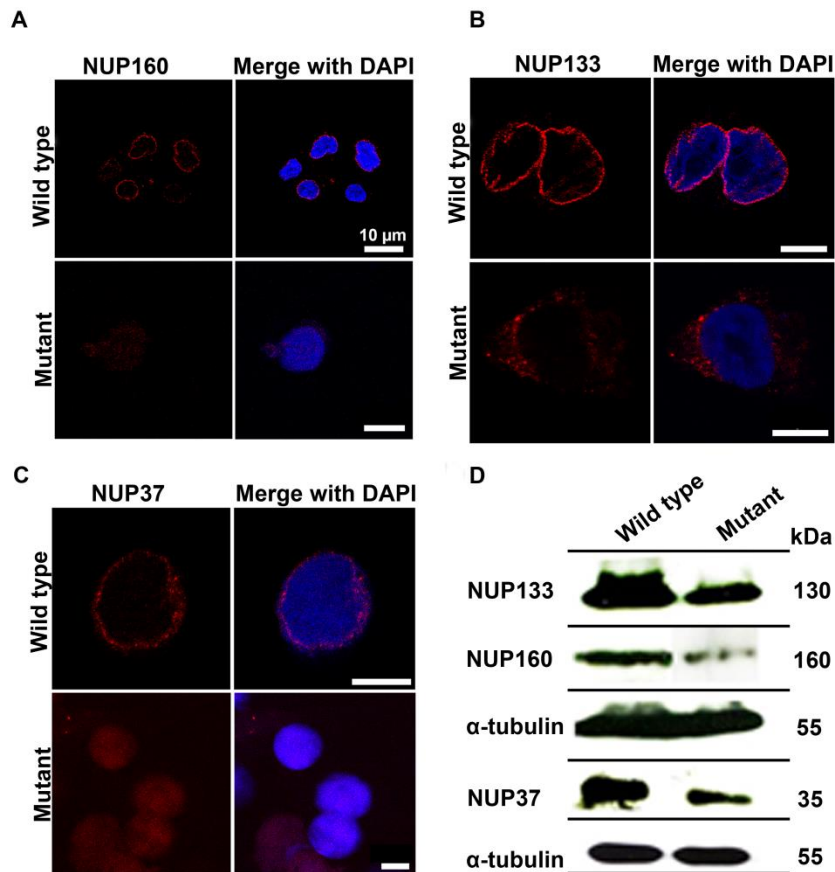


**Figure 5.14: Investigation of NUP107 mutated LCLs.**

(A, B and C) NUP107 mutated LCLs showing absence of NUP160 (red), NUP133 (red), and NUP37 (red) whereas wild-type LCLs show their localization at the nuclear envelope. DAPI was used for staining of nucleus. Scale bar is 5  $\mu\text{m}$ , otherwise defined in the image. (D) Western blots performed on protein lysates from mutant and control LCLs demonstrates reduction in the amount of NUP107, NUP133, NUP160, and NUP37 as compared to control LCLs. To demonstrate equal protein loading,  $\alpha$ -tubulin antibody was used. NUP133 and NUP160 were tested on the same blot. Figure is adopted from Braun et al, 2018.

**Explication;** Data obtained by NUP107 mutated LCLs validates the findings of NUP37 proving that the reduction of either of these proteins results in the drastic reduction of its binding partners. It can be speculated that reduction of NUP107 and its binding partners (NUP37, NUP133 and NUP160) may also cause reduction of the overall density of nuclear pores as we observed in NUP37 mutated fibroblasts.

## Part 2: Molecular investigation of cases manifesting Filippi and Filippi-like syndrome

This part includes genetic investigation of a cohort of Filippi syndrome (FLPIS) (HP:0000007) and cases manifesting Filippi-like syndrome (FLS). A detailed biochemical characterization of an already known variant (c.94G>C;p.His32Asp) of *CSNK2B* (NM\_001320.6) — causative gene of Filippi syndrome — is demonstrated in this part. In addition, two novel variants of *CSNK2B* identified in two unrelated cases born from non-consanguineous parents are also characterized on genetic and biochemical levels. Additionally, I also proposed a few novel candidate genes of FLPIS, which are also included in this section.

### 5.6 Clinical features of FLPIS and FLS cases

By the team efforts, we recruited a cohort of 12 unrelated cases, from different continents, manifesting features of FLPIS and FLS. Additionally, a published uncharacterized case was also included in this cohort for functional characterization of the identified *CSNK2B* variant (<https://kups.uni-koeln.de/8139/>). Typical features of Filippi syndrome (FLPIS) including, microcephaly (HP:0001999), syndactyly of fingers (HP:0012725) and/or toes (HP:0010714), peculiar facial features (HP:0001999), short stature (HP:0004322) and intellectual disability (HP:0001249) were noticed in majority of the studied cases of this cohort. Though, variations in cranio-digital features and severity of intellectual disability were also observed. Some additional clinical conditions recorded in each patient are given below (Table 5). Four of the (FP22, FP18, FP28 and FP30) cases which showed slight phenotypic variability in terms of microcephaly and/or syndactyly were grouped under the category of Filippi-like syndrome (FLS). The similarities observed in both syndromes were facial dysmorphism, developmental delay (HP:0008897) and intellectual disability (HP:0001249) (Table 5. 5).

**Table 5.5: Clinical profile of cases manifesting FLPIS and FLS**

Patients ID	Microcephaly	Digital anomaly	Facial dysmorphism	Intellectual disability	Other symptoms
FP3	+	Syndactyly of 3 <sup>rd</sup> and 4 <sup>th</sup> finger and 4 <sup>th</sup> and 5 <sup>th</sup> of toe	+	+	No epilepsy, imprecise articulation
FP12	+	Syndactyly of 2 <sup>nd</sup> and 3 <sup>rd</sup> toe	+	+	Developmental delay, Atrial septal defect

FP13	+	Syndactyly of 2 <sup>nd</sup> and 3 <sup>rd</sup> toe	+	+	Developmental delay
FP14	+	Syndactyly of 2 <sup>nd</sup> and 3 <sup>rd</sup> toe	+	+	Severe speech impairment, cryptorchidism, short stature
FP15	+	Syndactyly of 3 <sup>rd</sup> and 4 <sup>th</sup> finger and 2 <sup>nd</sup> and 3 <sup>rd</sup> toe	+		Short stature
FP16	+	Syndactyly of 2 <sup>nd</sup> and 3 <sup>rd</sup> toe	+	+	Brachcephaly, developmental delay
FP18	-	Syndactyly of 3 <sup>rd</sup> and 4 <sup>th</sup> finger and 4 <sup>th</sup> and 5 <sup>th</sup> of toe	+	+	Bradycardia, mild peripheral pulmonary stenosis,
FP19	+	Syndactyly of 3 <sup>rd</sup> and 4 <sup>th</sup> finger and 2 <sup>nd</sup> and 3 <sup>rd</sup> toe	+	+	Scoliosis
FP20	+	Syndactyly of 3 <sup>rd</sup> and 4 <sup>th</sup> of left toe and 4 <sup>th</sup> and 5 <sup>th</sup> of right toe	+	+	Developmental delay, ear lobes, and linear hypochromic pigmentation on upper and lower extremities, enamel hypoplasia, hypoplasia of fifth fingers with single palmar creases in both hands
FP22	-	Syndactyly of 3 <sup>rd</sup> , 4 <sup>th</sup> and 5 <sup>th</sup> of hands and 2 <sup>nd</sup> and 3 <sup>rd</sup> of toes	Data not available	+	Behavioral problems
FP28	-	Clinodactyly of 4 <sup>th</sup> and 5 <sup>th</sup> digit of toes	+	+	Micrognathia, developmental delay
FP30	-	-	+	+	Global developmental delay and epilepsy

The symbol of plus indicates presence of phenotype, whereas minus indicates otherwise.

### 5.6.1 Identification of disease-causing variants in studied cohort of FLPIS and FLS

A total of 12 clinically characterized Filippi and FLS cases were subjected to pathogenic genetic variants identification by using different techniques including whole-exome sequencing (WES), trio whole-exome sequencing (Trio-WES), CytoScan HD array (Affymetrix, Santa Clara, CA) and Sanger sequencing (SS). Out of 12, 4 cases remained unsolved; no causal variant was identified as well as these were also negative for pathogenic variations in the two known candidate genes of FLPIS, *CAKP2L* and *CSNK2B*. Interestingly, 2 cases revealed novel mutations (c.94G>A;Asp32Asn and c.374C>G;p.Ser125\*) in *CSNK2B* (NM\_001320.6) were being identified by trio-WES in FP28 and FP30, respectively. Additionally, I am going to propose 6 novel candidate genes of this rare disorder with identification of pathogenic DNA variations in highly constrained genes (Table 5.6). In this section, eight of these solved families, FP13, FP14, FP15, FP16, FP19, FP22, FP28 and FP30 will be discussed further.



### 5.6.2 Identification of six novel candidate genes of FLPIS

Six novel candidate genes (*PTPN23*, *CDKL5*, *PSEN1*, *DNM3*, *TRIM35*, and *CDKL2*) were proposed in FLPIS cases (Table 5.6). These candidate genes were selected based on their highest expression and critical roles during embryogenesis and their low allele frequencies or absence in the public databases of genomic variants (Table 5.6). Among them the co-segregation analysis was only performed for variations of *CDKL5* and *DNM3*, which were segregated in their respective family members corresponding to their proposed disease model. Detailed description for *CDKL5* mutated family is given in the section below. For rest of the families, blood samples of parents were unavailable for co-segregation analysis. Therefore, further analyses are necessary to prove the causality of the proposed variants.

**Table 5.6: Genetic information of studied cases**

Filippi patients ID	Gene	Transcript ID	cDNA Variation	Protein variation	Zygoty/allele frequency gnomAD
FP3	NI	-	-	-	-
FP12	NI	-	-	-	-
FP13	<i>PTPN23</i>	NM_015466.3, NM_001304482.1	c.4634_4635delinsTA	p.(Pro1545Leu)	Homo/5.42e-4
FP14	<i>CDKL5</i>	NM_001037343.1, NM_001323289.1, NM_003159.2	c.146-19A>G		Hemi/0
FP15	<i>PSEN1</i>	NM_000021.4	c.29A>C	p.(Tyr10Ser)	Het/0
FP16	<i>DNM3</i>	NM_001278252.1, NM_015569.4, NM_001136127.2	c.494C>T	p.(Thr165Met)	Homo/2.15e-5
FP18	NI	-	-	-	
FP19	<i>TRIM35</i>	NM_171982.4, NM_001304495.1	c.4G>T	p.(Glu2*)	CH/0
			c.-6C>T	p.(?)	
FP20	NI	-	-	-	
FP22	<i>CDKL2</i>	NM_003948.3	c.908_909delAA c.906A>T	p.(Lys303Serfs*12) p.(Leu302Phe)	CH/0
FP28	<i>CSNK2B</i>	NM_001320.6 NM_001282385.1	c.94G>A	p.Asp32Asn	<i>De novo</i> /0
FP30	<i>CSNK2B</i>	NM_001320.6 NM_001282385.1	c.374G>C	p.Ser125*	<i>De novo</i> /0

NI = none identified, Homo = homozygous, Hemi = hemizygous, CH = compound heterozygous, Het = heterozygous.

The *in silico* pathogenicity scores of all the novel proposed genes of FLPIS were noted their pLI and Z score documented in gnomAD suggest that these genes are highly intolerant to loss-of-function as well as for missense variations (Table 5.7). In addition, CADD score also

demonstrate the high pathogenicity of all the identified variations found in the proposed genes except for *CDKL5* (Table 5.7).

**Table 5.7: pLI, Z and CADD scores of novel genes proposed for FLPIS**

Filippi patients ID	Gene	pLI	Z score	CADD score
FP3	NI	-	-	-
FP12	NI	-	-	-
FP13	<i>PTPN23</i>	pLI = 0.03 o/e = 0.25 (0.17 - 0.37)	Z = 1.33 o/e = 0.88 (0.83 - 0.93)	21.4
FP14	<i>CDKL5</i>	pLI = 1 o/e = 0.09 (0.04 - 0.23)	Z = 2.74 o/e = 0.62 (0.55 - 0.68)	8.700
FP15	<i>PSENI</i>	pLI = 0.97 o/e = 0.12 (0.06 - 0.32)	Z = 2.16 o/e = 0.62 (0.55 - 0.71)	22.7
FP16	<i>DNM3</i>	pLI = 0 o/e = 0.3 (0.2 - 0.48)	Z = 2.7 o/e = 0.65 (0.59 - 0.72)	22.1
FP18	NI			
FP19	<i>TRIM35</i>	pLI = 0 o/e = 0.4 (0.24 - 0.7)	Z = 0.74 o/e = 0.89 (0.81 - 0.97)	23.9
FP20	NI			
FP22	<i>CDKL2</i>	pLI = 0 o/e = 1.02 (0.75 - 1.43)	Z = -0.25 o/e = 1.04 (0.94 - 1.16)	23
FP28 and FP30	<i>CSNK2B</i>	pLI = 0.92 o/e = 0.08 (0.03 - 0.38)	Z = 3.13 o/e = 0.21 (0.16 - 0.3)	32

Note: Loss-of-function intolerant (pLI).

### ***CDKL5 is a novel candidate gene segregating in a FLPIS afflicted family***

A 10-year-old male patient, born to non-consanguineous parents, was recruited from Brazil. Patient presented typical features of Filippi syndrome including microcephaly and bilateral complete syndactyly of second and third toes (HP:0001770) and underdeveloped alae nasi (HP:0000430) (Figure 5.15A and B). In addition, other clinical conditions observed in patient were failure to thrive (HP:0001508), severe speech impairment (HP:0009088), cryptorchidism (HP:0000028) and short stature (HP:0004322) (Table 5.5). Whole-exome sequencing revealed an X-linked hemizygous variant (NM\_001037343.1\_c.146-19A>G) of cyclin dependent kinase like 5 (*CDKL5*) (Table 5.6). This gene encodes a serine/threonine kinase

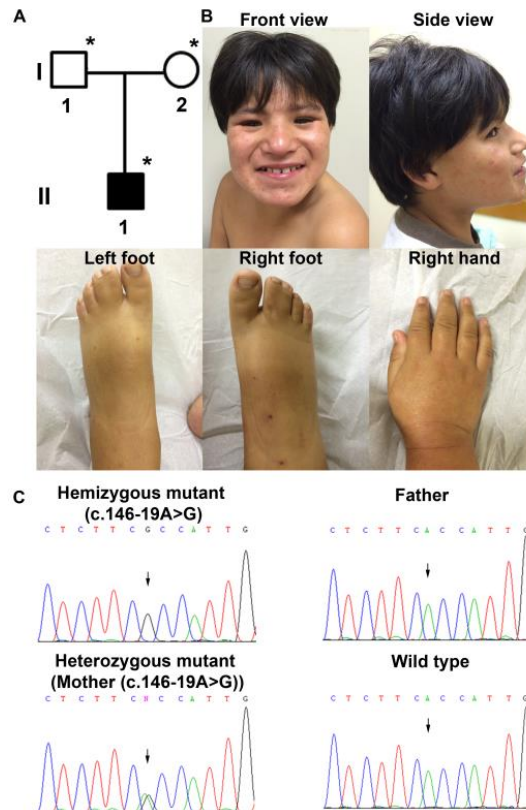


**Figure 5.15: Genetic and clinical analyses of Brazilian family having presumably pathogenic variation in *CDKL5* (Family FP14).**

(A) Pedigree of FP14 family. (B) Photos of *CDKL5* mutated patient showing front and side view. Notably syndactyly of toes is indicated. (C) Sanger traces of *CDKL5* mutated individual along with heterozygous mother, control and father having wild-type allele.

known as cyclin-dependent kinase-like 5 which is hugely expressed in the brain and associated with neurodevelopmental disorders such as early-onset epileptic encephalopathy and severe mental retardation (Zhao, Zhu et al. 2019; Yan, He et al. 2020). The role of *CDKL5* has been elaborated in regulation of axon outgrowth, dendritic morphogenesis, and synapse formation (Zhao, Zhu et al. 2019). This variant of *CDKL5* is not present in gnomAD, our in-house database of CCG with >1,600 exomes, the Greater Middle Eastern Variome, Iranome and dbSNP153. Sanger sequencing confirmed co-segregation of variant within the family (Figure 5.15C). Defects of *CDKL5* has already been reported for inherited disorders such as Rett syndrome and early-onset epileptic encephalopathy (Rodriguez, Contreras et al. 2008). Like *CSNK2B* this gene also encodes for a serine/threonine kinase and holds great potential to further unravel the pathomechanism of Filippi syndrome.

## 5.7 Novel mutations identified in *CSNK2B* causing a phenotype distinguished from Poirier-Bienvenu neurodevelopmental syndrome (POBINDS)

Two patients were recruited through a freely accessible web source — available for searching common interests of researchers in same gene(s) — GeneMatcher (<https://genematcher.org/>). Clinical and genetic investigations of these two cases are comprehensively explained below:

### 5.7.1 Family FP28

In family 28, a 9-year-old Caucasian female presented facial dysmorphism including deep set eyes, micrognathia (HP:0000307) and asymmetric ears (HP:0010722) — the right ear was more prominent than left ear; no tags or pits were observed (Figure 5.16A and B). It was interesting to notice that this patient showed striking similarity with facial gestalt of FP2 patient (Chapter 3, Figure 3.4). EEG of the patient demonstrated excessive fast frequencies and interictal discharges (posterior predominant). This type of phenotype is most consistent with generalized or mixed epilepsy (HP:0001250). Among digital anomalies, although syndactyly was absent yet other features were noted including, bilateral tapering of fingers (HP:0001182) (most prominent on fifth digit) and bilateral clinodactyly (HP:0001863) of 3<sup>rd</sup> and 5<sup>th</sup> toe (Figure 5.16B). In addition, pronation of both feet and a 1-2 cm poorly circumscribed firm mass on plantar aspect of left heel was also notable (Figure 5.16B). Clinical features of this affected member are distinct from patients manifesting Poirier-Bienvenu neurodevelopmental syndrome (POBINDS, [MIM 618732]).



**Figure 5.16: Genetic and clinical analyses of FP28 family having novel mutation in *CSNK2B*.**

(A) Pedigree of family FP28 with one affected female born to unaffected non-consanguineous parents. (B) Photos of FP28 patient (II-1) showing front and side views (left panel) along with her feet and right hand (right panel).

Trio-WES of the affected member revealed a novel pathogenic *de novo* variant, NM\_001320.6\_c.94G>A;p.Asp32Asn in *CSNK2B* as a causal variant (Figure 5.17).

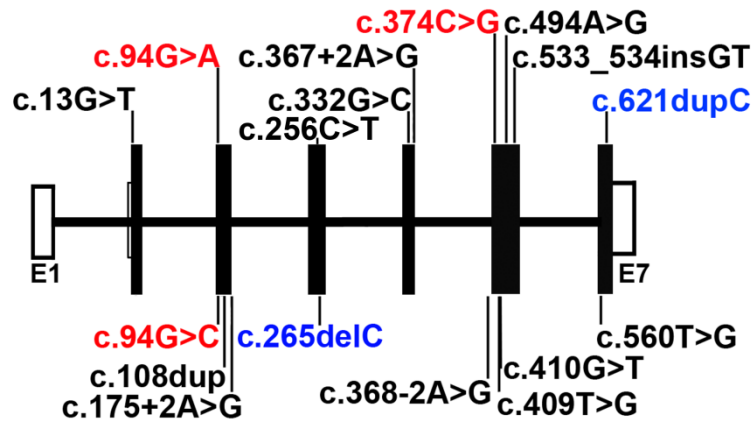


**Figure 5.17: Gene structure of *CSNK2B* (NM\_001320.6).**

Shown are already reported 14 variations, three of them are novel (indicated in red color) identified in this study. Blue color is given to those variations which are renamed according to the HGVS (Human Genome Variation Society) guidelines. Vertical black bars represent the coding exons and white show the non-coding exons which are constructed according to the scale (1 kb = 1cm) whereas introns are shown by horizontal lines and are drawn arbitrary.

### 5.7.2 Family FP30

The second case in our cohort recruited from GeneMatcher was a 6-year-old male from Israel (Figure 5.18). He presented phenotypes including prominent facial dysmorphic features including, long face (HP:0000276), protruding ears (HP:0000411), high forehead (HP:0000348), broad nasal bridge (HP:0000431) and hair hypopigmentation (HP:0005599) (center of head) (Figure 5.18A and B). In addition, low muscle tone (HP:0001252) and

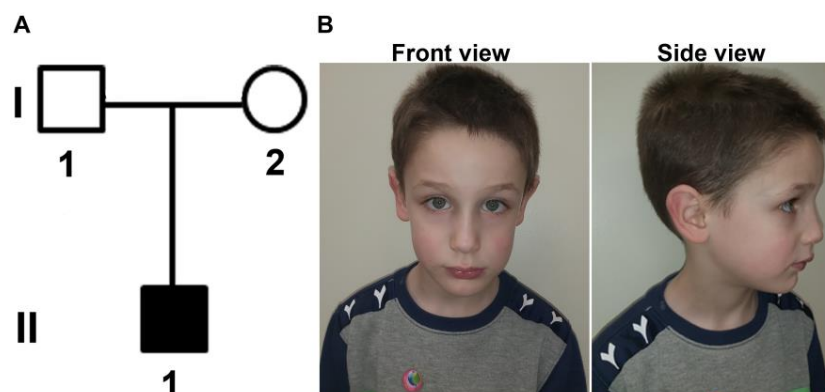


**Figure 5.18: Clinical analysis of FP30 family having novel mutation in *CSNK2B*.**

(A) Pedigree of family FP30 with one affected male born from asymptomatic non-consanguineous parents. (B) Photos of FP30 patient (II-1) showing front view and side view.

ligament laxity (HP:0001388) was also noted. Regarding intellectual abilities, intelligence quotient was noted around 70 which denote mild intellectual disability; low speech intelligibility, learning disability, emotional regulation disorder, low attention span and verbal performance were also recorded. Electroencephalogram showed centro temporal spike waves signifying epilepsy. Carnitine level in patient's blood test was higher than normal i.e., 42.3 micro mol/L suggesting mild cardiac defect. On the other hand, the patient did not show any symptoms of craniodigital or teeth anomaly. MRI showed normal brain morphology (data not shown).

For genetic investigation, chromosomal microarray analysis was performed which showed normal number of chromosomes. Furthermore, this case was also found negative for pathogenic mutations in *SCN1A* and *FMRI*, later is a causative gene of fragile X syndrome (Siomi, Choi et al. 1994). Eventually, WES revealed a novel pathogenic *de novo* variant c.374C>G;p.Ser125\* in *CSNK2B* (NM\_001320.6) causing Filippi-like syndrome (Figure 5.18). This mutation may produce the truncated protein, if stably expressed, will lack the domain that interacts with CK2 $\alpha$  and thus the catalytic activity of the mutated CK2 may be reduced or completely abolished.

**Explication;** The features of epilepsy and developmental delay (POBINDS) had been recently associated with mutations in *CSNK2B* (Pagano, Sarno et al. 2005). However, additional prominent features diagnosed in FP28 and FP30 families are distinguished from POBINDS and representing a novel disorder which I indicated as Filippi-like syndrome.

### 5.7.3 *In silico* predictions of *CSNK2B* variants

Pathogenicity score of *CSNK2B* variants was calculated using *in silico* prediction tool, CADD. The tool scored *CSNK2B* variant c.94G>C as 31 and 32 for c.94G>A; scores above 30 falls in the range of highly pathogenic by the set criteria of the tool. In case of c.374C>G, the predicted score is 39 which signifies the highest pathogenicity of this variant among the other identified in this study. Notably, *CSNK2B* is an essential and highly contained gene with Z score = 3.13 and pLI score = 0.92, which signifies that this gene is highly intolerant for any missense or loss-of-function variants. American College of Medical Genetics (ACMG) classified c.94G>C;p.Asp32His as likely pathogenic (PM1, PM2, PM5, PP3, BP1), c.94G>A;p.Asp32Asn as a variant of uncertain significance (PM1, PM2, PP3, BP1) and c.374C>G;p.Ser125\*, a pathogenic variant (PVS1, PM2, PP3).

The effects of these three mutations were further predicted on protein level using various prediction tools; PROVEAN, SNAP<sup>2</sup>, SNPs&GO, PANTHER, PhD-SNP, SIFT, SNAP and Meta-SNP. All of them anticipated that histidine or asparagine instead of aspartic acid at position 32 in mutant CK2 $\beta$  is deleterious and disease causing and have pathogenic effect. The respective pathogenicity scores provided by these tools are given below (Table 5.7). For the nonsense mutation, the prediction was only available by PROVEAN which anticipated it as deleterious (Table 5.7).

**Table 5.8: Pathogenicity prediction scores of CK2 $\beta$  mutations by various *in silico* tools**

Prediction tool	Function	Prediction		
		p.Asp32His	p.Asp32Asn	p.Ser125*
<b>PROVEAN</b>	Protein variation effect analyzer	Deleterious	Deleterious	Deleterious
<b>SNAP<sup>2</sup></b>	Functional effect classifier on the basis of neural networks	Pathogenic	Pathogenic	-
<b>SNAP&amp;GO</b>	Variant effect prediction using gene ontology terms	Disease causing	Disease causing	-
<b>PANTHER</b>	Protein analysis through evolutionary Relationships	Disease causing (0.9)	Disease causing (0.9)	-
<b>PhD-SNP</b>	Predictor of human deleterious single nucleotide polymorphisms	Disease causing (0.8)	Disease causing (0.8)	-
<b>SIFT</b>	Predict effects of nonsynonymous / missense variants	Disease causing (0.03)	Disease causing (0.03)	-
<b>SNAP</b>	Prediction of nonsynonymous functional effects	Disease causing (0.6)	Disease causing (0.6)	-
<b>Meta-SNP</b>	Meta-predictor of disease causing variants	Disease causing (0.74)	Disease causing (0.74)	-

Note: Values given in the parentheses indicate the scores obtained from respective tool.

#### 5.7.4 Validation of *CSNK2B* *de novo* mutations in etiology of Filippi syndrome

The reported missense variants of *CSNK2B* were thoroughly characterized for elucidation of their pathogenic aspects on protein level.

#### 5.7.5 Prediction of effects of mutation on structure of CK2 $\beta$

Consequences of the mutations on the structure of CK2 $\beta$  protein were also taken into account and predicted using a structure prediction tool called PyMOL (version 2.3.2). To be noted that lysine at position 49 of CK2 $\alpha$  interacts with aspartate 32 of CK2 $\beta$  is being modeled in the figure below (<https://kups.uni-koeln.de/8139/>) (Figure 5.19A).

A wizard of PyMOL called 'mutagenesis' allows mutating an amino acid *in silico*. After creating the desired mutations, p.Asp32His and p.Asp32Asn, all possible rotamers (adjustments of newly incorporated amino acids appear along with their probabilities of positioning in specific site. In case of p.Asp32His, seven different rotamers appeared with highest probability of 25% which is too low for adjustment in the existing protein structure (Figure 5.19B). The red blocks present significantly in each rotamer indicate the clashes of mutated residue. Regarding p.Asp32Asn mutation, 9 rotamers were suggesting the clashes of newly incorporated amino acid, asparagine. However, in this case the mutational effects on the structure of CK2 $\beta$  were observed slightly weaker, shown by the red blocks (Figure 5.19C), as compared to p.Asp32His mutation. One reason could be that the mutant residue asparagine is of the same size as compared to histidine which has a benzene ring. Furthermore, both mutant residues have no charge as compared to aspartic acid having negative charge which leads the assumption that the interaction with neighboring amino acids might have been influenced due to neutral charge. Furthermore, another *in silico* tool, HOPE (<https://www3.cmbi.umcn.nl/hope/input/>) (Sajnaga, Szyszka et al. 2013), predicted that both mutant amino acids may lose interaction with phenylalanine at 34 position in beta subunit of CK2.



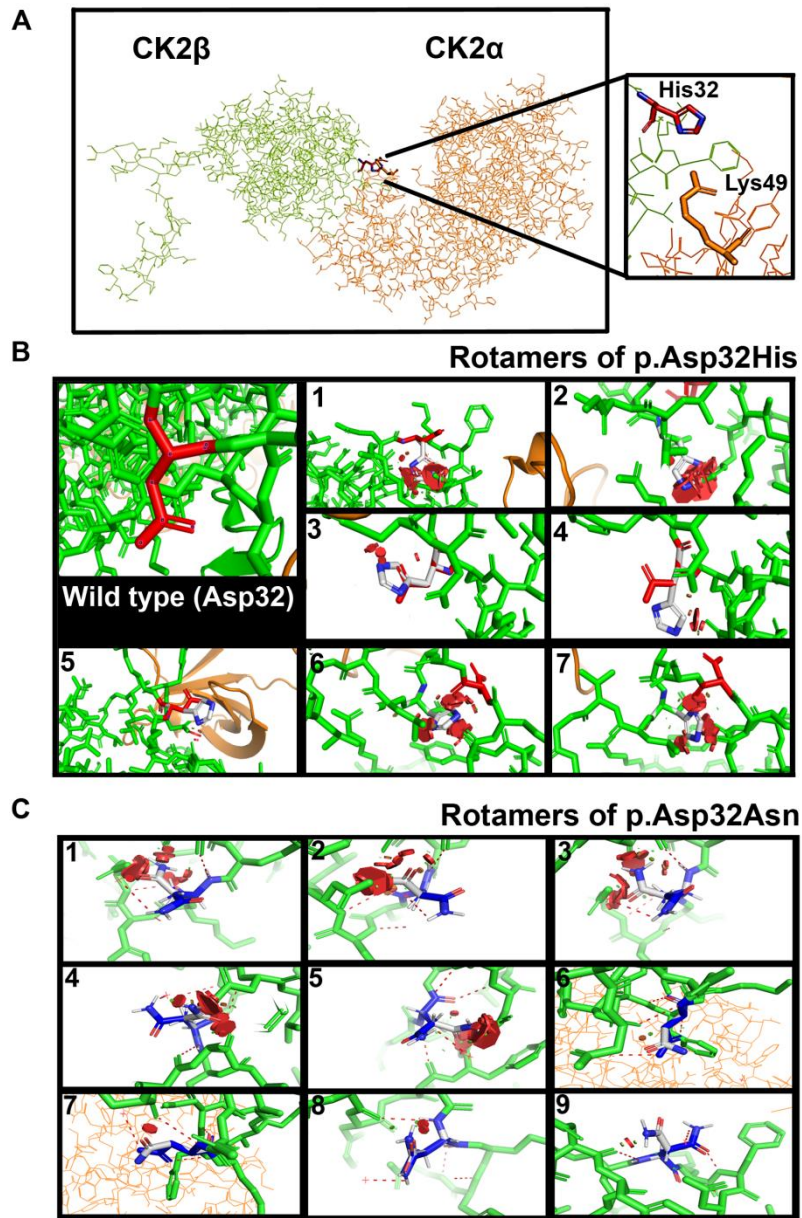


**Figure 5.19: Effects of mutations on the structure of CK2 $\beta$ .**

(A) Dimer of CK2 $\alpha$  (orange) and CK2 $\beta$  (green) is shown. Note that lysine at position 49 of CK2 $\alpha$  (orange) is shown in the zoomed image. (B) Amino acid structure of wild type and possible rotamers of CK2 $\beta$  due to the mutation p.Asp32His shown in white and red color. (C) Possible rotamers of CK2 $\beta$  due to mutation p.Asp32Asn. Note: red blocks show clash of mutant amino acid with neighboring amino acids.

### 5.7.6 Prediction of effects of mutation on stability of CK2 $\beta$

Moreover, the effects of missense mutations on the protein stability was predicted using two online tools, MUpro: Prediction of protein stability changes for single site mutations from

sequences (Marin, Meggio et al. 1997) and I-Mutant 2.0 (Rodriguez, Contreras et al. 2008). I-Mutant 2.0 predicted decrease stability of CK2 $\beta$  mutants, p.Asp32His and p.Asp32Asn, at given conditions (pH: 7, temperature: 25 °C). This tool measures the DDG (delta delta G) value calculated from the unfolding Gibbs free energy value of the mutated protein minus the unfolding Gibbs free energy value of the wild type (Kcal/mol). Given the conditions of same pH but increased temperature (37 °C, 60 °C, 80 °C), the stability of p.Asp32His and p.Asp32Asn was predicted to be increased. It should be noted that DDG<0 signifies decreased stability, whereas, DDG>0 showed increased stability. Additionally, MUpro predicted decreased stability for p.Asp32His and p.Asp32Asn mutants (Table 5.8).

**Table 5.9: Protein thermostability scores predicted by I-Mutant2.0 and MUpro.**

Tool	Position	Wild type amino acid	Mutant amino acid	DDG value	Temperature (°C)	Stability
I-Mutant	32	Asp	His	-0.41	25	Decreased
				0.30	60	Increased
				0.65	80	Increased
	32	Asp	Asn	-0.53	25	Decreased
				0.16	60	Increased
				0.50	80	Increased
MUpro	32	Asp	His	-1.2239963	NA	Decreased
	32	Asp	Asn	-1.045697	NA	Decreased

DDG = delta delta G

**Explication;** The *in silico* predictions indicate that effects of mutations are damaging and disease causing on protein level as well as it leaves an influence on the structure of CK2 $\beta$  which may compromise its function and thus pathogenic. The prediction clearly means that histidine or asparagine in position of aspartate may disturb the overall structure of CK2 $\beta$  protein. Moreover, the stability of mutant proteins may also be affected due to mutations predicted by *in silico* tools.

## **5.8 Influence of mutations on cellular expression of CK2 $\beta$**

Mutational consequences on cellular expression of CK2 $\beta$  were noticed by conducting the following experiment.

### **5.8.1 Subcellular localization of endogenous and overexpressed CK2 $\beta$**

To find out the subcellular localization of CK2 $\beta$  protein, immunofluorescence was carried out in wild-type LCLs and LCLs derived from two patients carrying p.Asp32His and p.Asp32Asn. After performing confocal microscopy, CK2 $\beta$  protein was observed to localize inside the nucleus as well as at Golgi apparatus in wild-type LCLs whereas the mutant CK2 $\beta$  (p.Asp32His and p.Asp32Asn) proteins were present hugely in the nucleus as well as cytoplasm of both mutants' LCLs (Figure 5.20A). However, the abundance of p.Asp32Asn mutant CK2 $\beta$  protein was comparatively less in patient as compared to p.Asp32Asn mutant protein (Figure 5.20A and B).

### **5.8.2 CK2 $\beta$ in whole cell lysate, cytosolic and nuclear fractions in patient LCLs**

To corroborate the data of impaired subcellular localization detected by immunofluorescence, immunoblotting was performed to observe the amount of CK2 $\beta$  in whole cell lysate of wild-type LCLs in comparison with both mutants (p.Asp32His and p.Asp32Asn). Results show that as observed in the immunofluorescence, the amount of mutant CK2 $\beta$  was found increased in the whole cell lysate of both mutants (Figure 5.20B). To analyze which cellular fraction contained more mutant protein, fractionation assay was performed in case of only p.Asp32His mutant. The result shows an increased amount of mutant protein in both, cytosolic and nuclear fraction as compared to wild type (Figure 5.20C). Fractionation assay could not be performed for p.Asp32Asn mutant due to unavailability of patient LCLs.

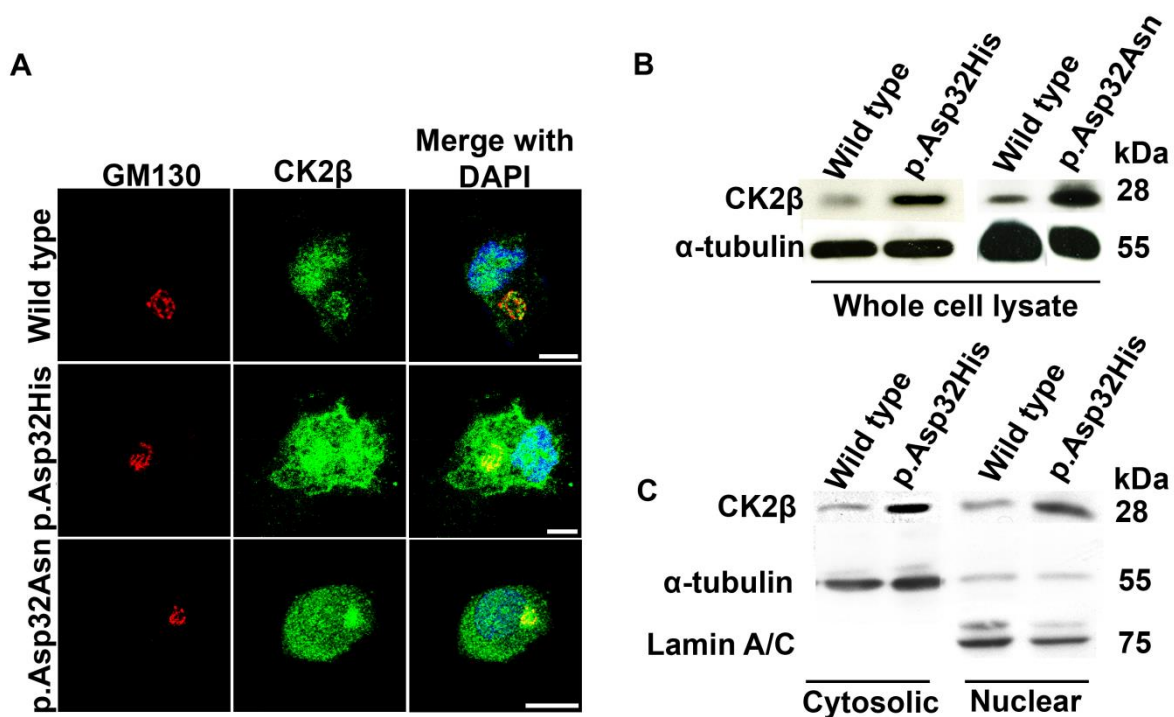


**Figure 5.20: Effects of mutation(s) in patient LCLs on protein level.**

(A) Immunofluorescence shows increased amount of mutant CK2β (green) in nucleus as well as in cytoplasm as compared to wild-type LCLs. GM130 (red) serves as marker of Golgi apparatus and DAPI (blue) indicates staining of nucleus and scale bar is 10 μm. (B) Immunoblotting shows an increased amount of CK2β in whole cell lysates obtained from mutant (p.Asp32His and p.Asp32Asn) LCLs versus wild-type. α-tubulin is used as loading controls. (C) Immunoblotting shows an increased amount of CK2β in cytosolic and nuclear fraction in p.Asp32His mutant versus wild-type LCLs. Loading controls are α-tubulin and lamin A/C, for cytosol and nucleus, respectively.

### 5.8.3 Transient expression of wild-type and CK2β mutants in HeLa cells

To gain insights into the behavior of overexpressed wild-type and mutant CK2β proteins and to reproduce the results of subcellular localization of endogenous proteins observed in immunofluorescence, GFP tagged CK2β wild type and three mutants were transiently expressed in HeLa cells. Transient expression of wild-type CK2β was found in the nucleus as well as on Golgi apparatus (Figure 5.21A). As expected, ectopic expression showed abnormal localization of all three CK2β mutants. Two of the mutants, p.Asp32His and p.Asp32Asn, were found in cytosol and nuclei in the form of aggregates as tracked by GFP fluorescence (Figure 5.21A). Regarding the truncated mutant p.Ser125\*, the protein expression is reduced in both cytosol as well as in the nucleus as compared to the wild type. It was also observed

that the morphology of Golgi apparatus was distorted in cells transfected with the CK2 $\beta$  truncated mutants (Figure 5.21B). This abnormality was also noticed in cells transfected with GFP-tagged p.Asp32Asn mutant, but seemed mild as compared to the cells overexpressing p.Ser125\* mutant (Figure 5.21B). The expression of GFP tagged wild-type and mutants of CK2 $\beta$  were also confirmed on immunoblot, where increased amounts of mutants, p.Asp32His and p.Asp32Asn, proteins were noted compared to wild type (Figure 5.21C). Analysis of the band intensities indicates a 1.4 and 1.7 fold increase in p.Asp32His and p.Asp32Asn mutants, respectively (Figure 5.21D). The data also showed a faint band of truncated protein at expected size (~37 kDa). Statistical data showed a reduction of truncated protein to 0.2 folds shown by the band intensities (Figure 5.21D).

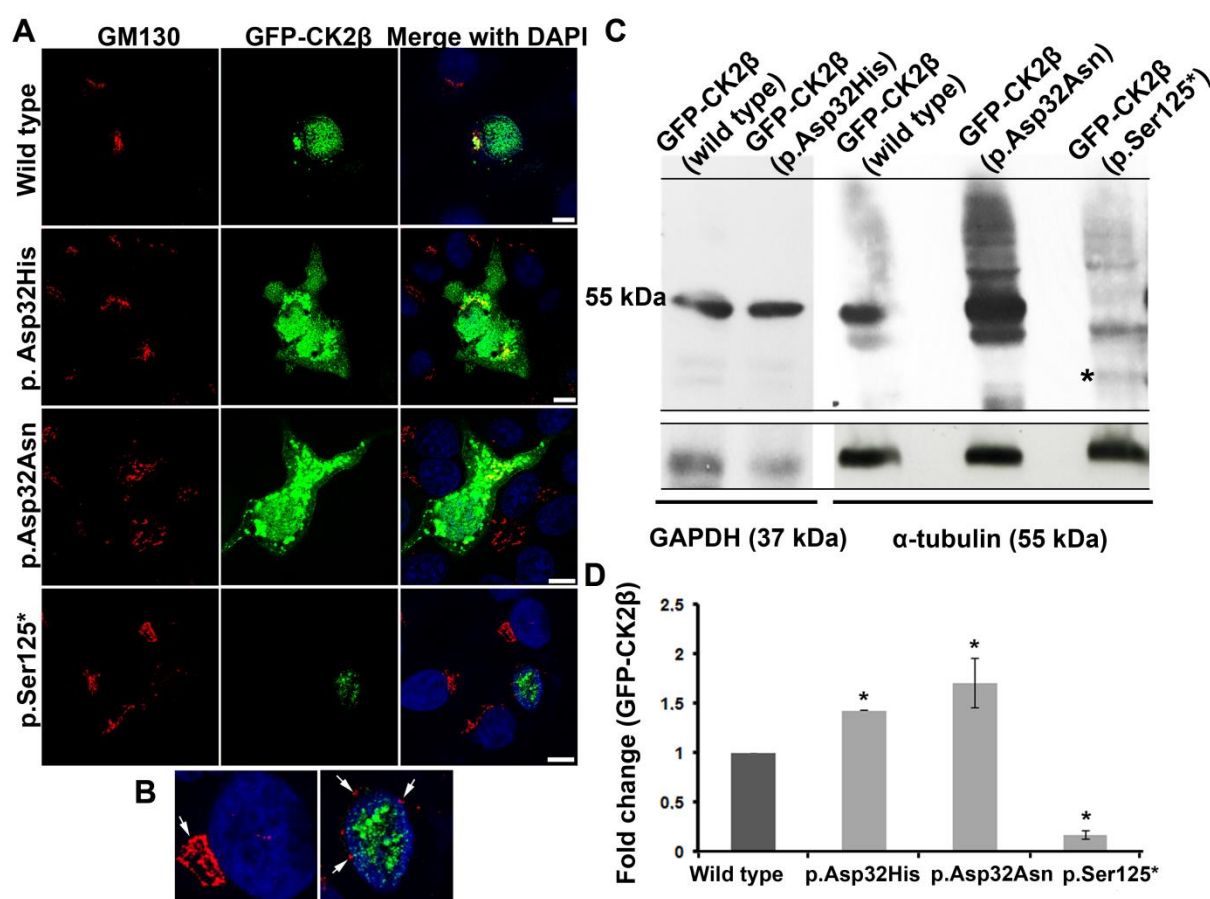


**Figure 5.21: Localization of GFP tagged wild-type and mutants of CK2 $\beta$ .**

(A) Immunofluorescence showing mislocalized mutant GFP tagged CK2 $\beta$  as compared to wild type in HeLa cells. Scale bar is 10  $\mu$ m. (B) CK2 $\beta$  mutant (p.Ser125\*), shown at the right hand side, revealing abnormal morphology of Golgi apparatus pointed by white arrows as compared to wild-type cell shown at the left hand side. (C) Immunoblotting shows GFP tagged CK2 $\beta$  on 55 kDa band size in both wild type and mutant. Note that loading control is

$\alpha$ -tubulin (55 kDa) except for p.Asp32His, where GAPDH, 37 kDa, was used for loading control. Asterisk (\*) shows the expected band of truncated protein (p.Ser125\*). **(D)** Graph showing the fold change of GFP tagged CK2 $\beta$  wild type in comparison with all three mutants, p.Asp32His, p.Asp32Asn and p.Ser125\*. Note: n = 2 and asterisk (\*) shows *p* values of 0.05 (Student's *t* test).

**Explication;** On the basis of experiments performed for analyzing the subcellular localization of CK2 $\beta$ , it is interpreted that missense mutations in *CSNK2B* causes abnormal localization of mutant CK2 $\beta$  and upregulation in both cytosolic and nuclear fraction. In addition, the truncating mutation may create an unstable protein product, thus causing reduced expression of mutant protein.

#### **5.8.4 CK2 $\alpha$ and CKAP2L in *CSNK2B* mutated LCLs**

The impact of mutation, p.Asp32His, was investigated on CK2 $\alpha$  for the fact that it is one of the subunit of CK2 holoenzyme and upregulation of CK2 $\beta$  might cause differential regulation of CK2 $\alpha$ . On the contrary to the localization of mutant CK2 $\beta$ , immunofluorescence showed that the localization of CK2 $\alpha$  was found similar in mutant and wild-type LCLs (Figure 5.22A). Also, immunoblotting results did not show any change in the quantity of CK2 $\alpha$  in both mutant and wild-type LCLs (Figure 5.22B). In addition, CKAP2L, binding partner of CK2 $\beta$  as well as reported in causation of Filippi syndrome was investigated on protein level (<https://kups.ub.uni-koeln.de/10093/>). Interestingly, immunoblotting showed that CKAP2L was found reduced in mutant LCLs compared to wild type (Figure 5.22B). Analysis of the CKAP2L band intensities revealed 0.5 folds (50%) reduction in mutant as compared to wild-type LCLs (Figure 5.22C).



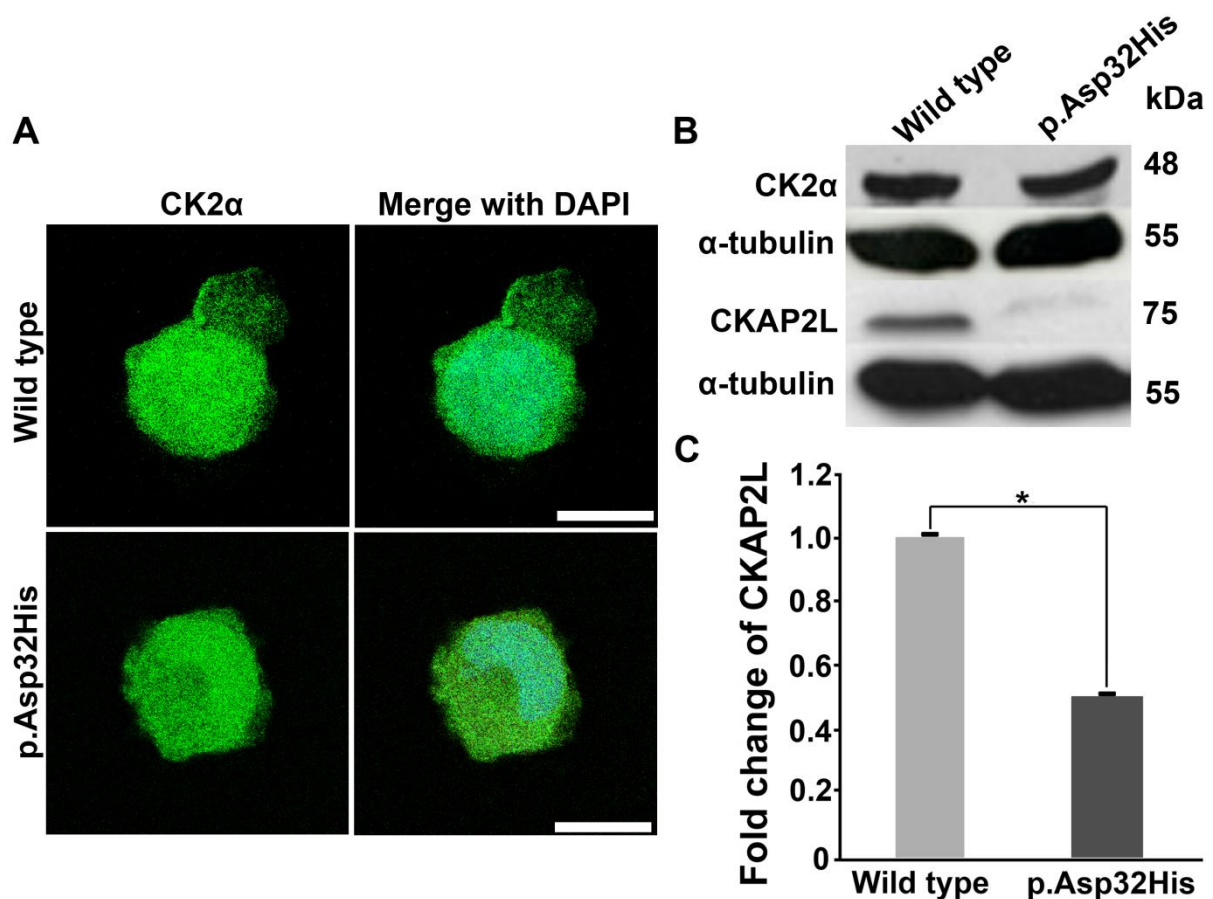


**Figure 5.22: CK2 $\alpha$  and CKAP2L in CSNK2B mutated LCLs.**

(A) Immunofluorescence shows localization of CK2 $\alpha$  (green) in p.Asp32His mutant and wild-type LCLs. Note that staining looks similar in both cases. Scale bar is 5  $\mu$ m and DAPI is used for staining nucleus. (B) Immunoblotting shows similar amount of CK2 $\alpha$  in both wild-type and mutant LCLs, upper panel, however reduced CKAP2L observed in p.Asp32His mutant LCLs, lower panel, as compared to wild-type. (C) Bar graph showing 0.5 folds reduction of CKAP2L in p.Asp32His mutant as compared to wild type. Note that  $n = 3$  and  $p$  value is 0.0447 shown by the asterisk (\*).

**Explication;** the investigation of CK2 $\alpha$  at protein level validates that upregulation of mutant, p.Asp32His, CK2 $\beta$  does not influence the amount or localization of CK2 $\alpha$ . In addition, the reduction of CKAP2L depicts that it might play a role in manifestation or severity of FLPIS. As earlier study (Hussain, Battaglia et al. 2014) also showed reduction of CKAP2L in Filippi patient. Nonetheless, more data in this regard would be necessary for drawing a strong conclusion.

## 5.9 Influence of CK2 $\beta$ mutations on association with CK2 $\alpha$

For studying the influence of mutation on association of  $\alpha$  and  $\beta$  subunits of CK2, microscale thermophoresis (MST) was performed. For this purpose, GST-tagged recombinant CK2 $\beta$  wild-type and mutant proteins were purified in bacteria (Figure 5.23A). Later on, GST was successfully cleaved off from all the proteins (wild type and the mutants) shown in the coomassie stained SDS-PAGE gel image below (Figure 5.23B).

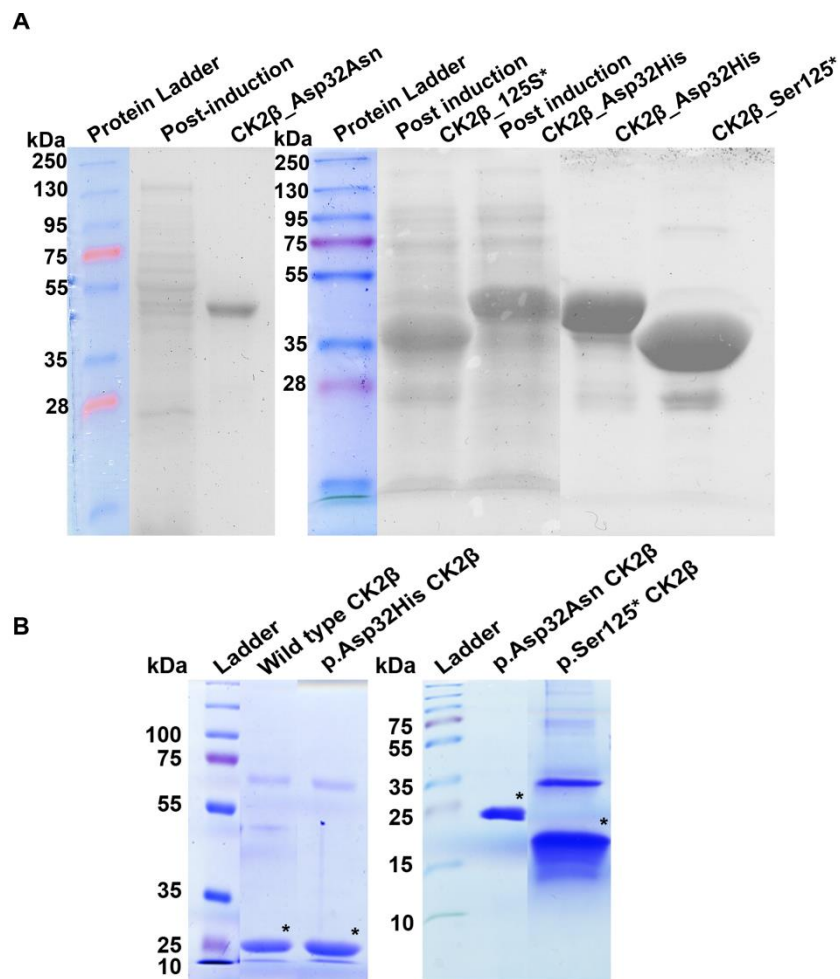


**Figure 5.23: Purification of GST fused CK2 $\beta$  and obtaining the cleaved protein product.**

(A) Coomassie stained SDS-PAGE gel showing purified GST tagged wild-type CK2 $\beta$  and its mutants (p.Asp32His, p.Asp32Asn and p.Ser125\*). Note: Image is obtained by two different gels (B) SDS-PAGE showing purified cleaved protein of wild-type CK2 $\beta$  and its mutants (p.Asp32His, p.Asp32Asn and p.Ser125\*) indicated by asterisks. Note: Image is obtained by two different gels.



### 5.9.1 Microscale thermophoresis (MST)

In this case, CK2 $\alpha$  was tagged with a fluorophore DBCO-Sulfo-Cy5 with tyrosine at position 239 of an unnaturally incorporated amino acid and mixed with wild type as well as mutant  $\beta$  subunits. After recording the intensities,  $K_D$  values of the complexes were calculated which showed a clear difference; the  $K_D$  value of wild-type complex was  $694.6 \pm 2.0$  nM (Figure 5.24A) and significantly higher ( $1174 \pm 2.4$  nM) in case of mutant complex (Figure 5.24B) which signifies impaired interaction between mutant  $\beta$  subunit with  $\alpha$  as compared to wild-type,

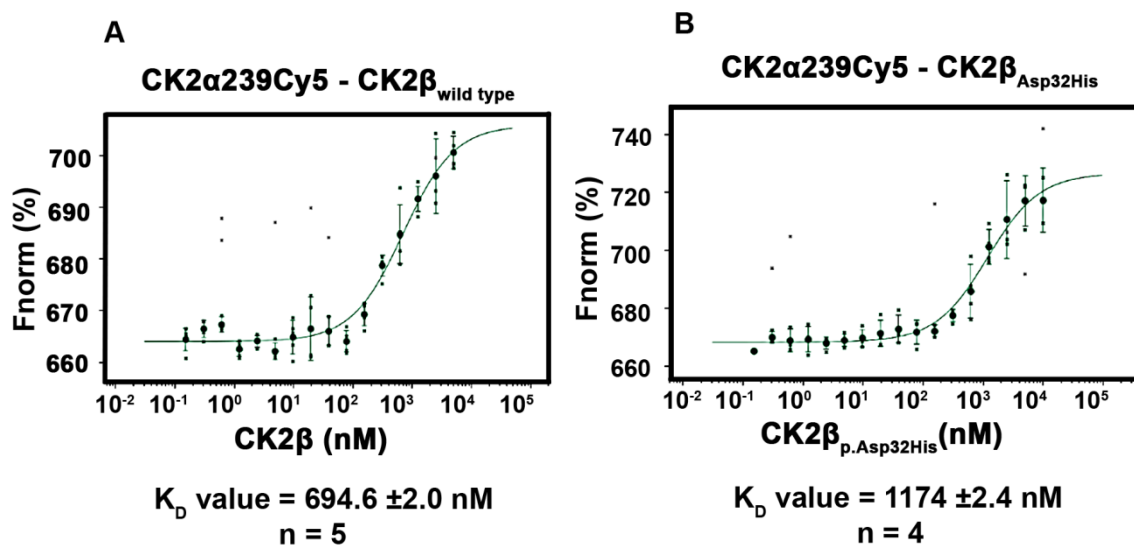


**Figure 5.24: Interaction of CK2 subunits analyzed by MST.**

**Figure 24:** (A) MST shows decreased  $K_D$  value ( $694.6 \pm 2.0$  nM) in wild-type CK2 $\beta$  bound to CK2 $\alpha$ 239<sub>Cy5</sub>. Note: n=5 (B) MST results show increased  $K_D$  value ( $1174 \pm 2.4$  nM) in mutant CK2 $\beta$  bound to CK2 $\alpha$ 239<sub>Cy5</sub>. Note: n=4.

## 5.10 Protein-protein interactome — probing interacting partners of CK2 $\beta$

Motivation behind this experiment was to precisely explore the cellular pathways on the basis of those interacting partners which would lose interaction with mutant CK2 $\beta$ . For this purpose, GST tagged wild-type and mutant CK2 $\beta$  were pulled down with HeLa cell lysate and subjected to mass spectrometry for protein interactome analysis.

### **5.10.1 Known and novel binding partners of CK2**

The data provided a total list of 224 proteins (Figure 5.25A). Interaction was analyzed on the basis of log<sub>2</sub> LFQ (Label-free quantification; signifies the relative amount of proteins in two or more biological replicates) intensity and number of peptides pulled down with purified GST tagged CK2 $\beta$  wild type and mutant. Out of 224 proteins, 30 proteins were found in negative control and thus excluded. The remaining 194 proteins were considered as the CK2 independent partners of CK2 $\beta$  thus adding more knowledge to the already existing data. 47 out of 194 were already reported as CK2 substrates (de Villavicencio-Díaz, Mazola et al. 2015). These interacting partners were distinguished on the basis of protein class. Classes were assigned using Gene Ontology (GO) categories and literature curation.

Based on the number of peptides, 156/194 showed normal binding affinity with p.Asp32His mutant of CK2 $\beta$ , whereas, 38 presented reduced binding (Figure 5.25A and B). Interestingly, out of these 38 proteins, 20 (RBBP6, DDX5, POLR2A, KAT7, BRD3, STED2, GPATCH2, ACIN1, ZC3H18, IWS1, SRRM2, BCLAF1, PNN, DDX47, DVL3, DVL1, TCOF1, SLC25A5, THRAP3, LENG8) are those which are already reported as CK2 substrates by two independent studies (Bian, Ye et al. 2013; de Villavicencio-Díaz, Mazola et al. 2015; Franchin, Salvi et al. 2015). In addition, KIAA1522, DDX46, BRD2, DROSHA and CLASRP are also mentioned in the unsorted list of 4062 interacting partners of CK2 $\beta$  obtained by affinity purification. Collectively, 25 (65.79%) out of 38 are known interacting partners of CK2. Rests of the 35% stand a fair chance to be substrates/binding partners of CK2 more specifically for beta subunit (Figure 5.25C). It was noted that, comparing with wild type, the lowest number (three folds) of peptides observed in p.Asp32His mutant were for DVL1, DVL1P1, CFAP20, PRICKL3 and RBBP6 thus showing weakest interaction with mutant CK2 $\beta$  (Figure 5.25C).

### **5.10.2 Pathway enrichment of 38 binding partners showing compromised interaction of CK2 $\beta$**

Proteins showing compromised interaction with mutant CK2 $\beta$  were enriched with respect to biological process, using FunRich (functional enrichment analysis tool, version 3.1.3) (Figure 5.25D). Data showed that highly enriched proteins were involved in the biological pathways including RNA regulatory pathway, translation, Wnt signaling, and pathways involved in apoptosis such as NF-related apoptosis-inducing ligand (IL3 and mTOR pathway (Figure 5.25D and Table 5.9). Studies show that withdrawal of IL-3 activates caspase proteases which

ultimately lead to cell death (Johnson 1998). Similarly, mTOR pathway is involved in inhibition of apoptosis, therefore, it is likely that loss of interaction might cause increased apoptosis in patient LCLs (Guernsey, Jiang et al. 2010).

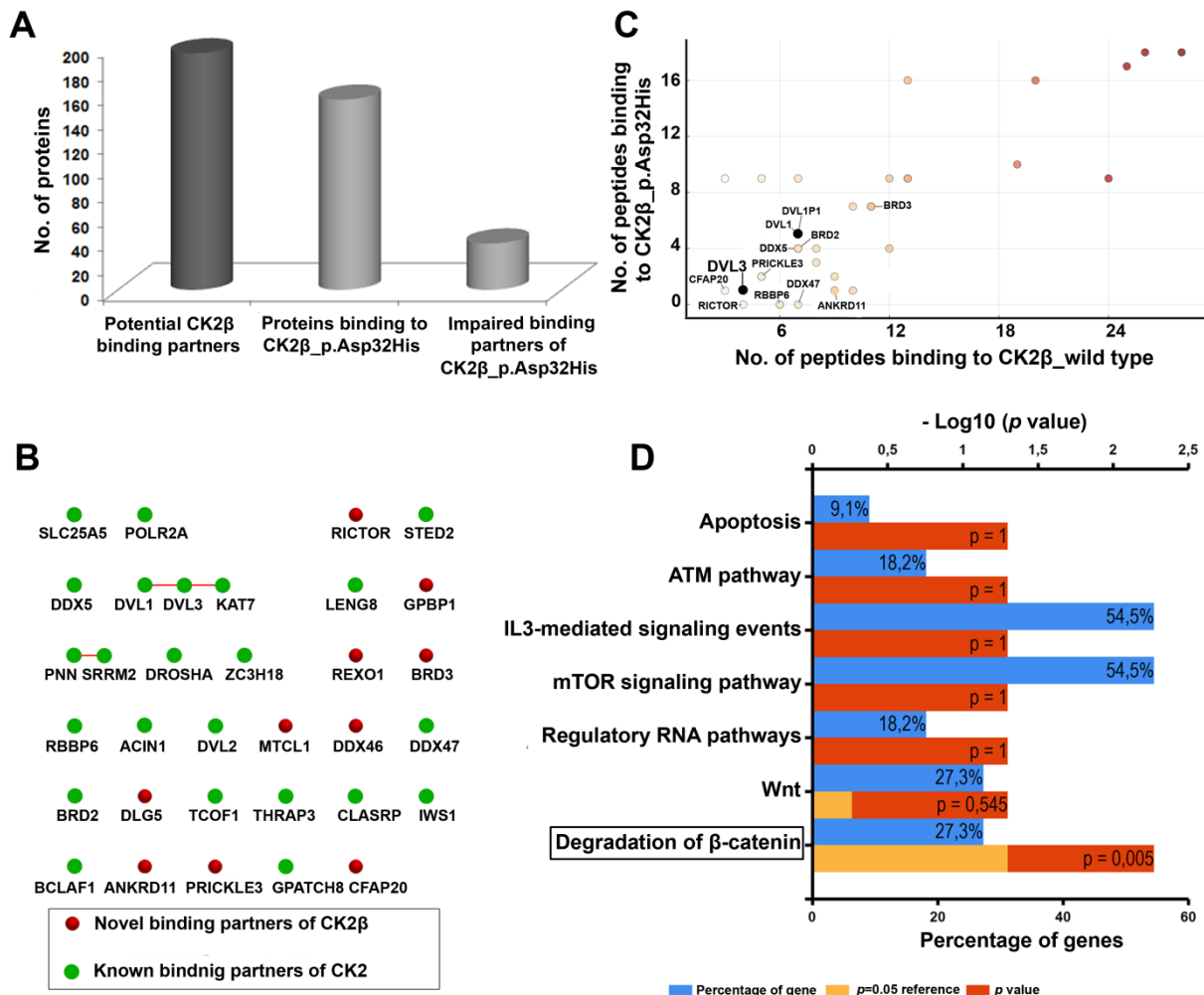


**Figure 5.25: Mass spectrometry data of wild-type and mutant, p.Asp32His, CK2β.**

(A) Graph shows total number of proteins (194) detected in mass spectrometry data. 156 proteins showed interaction whereas 38 proteins showed no interaction with mutant GST tagged CK2β as compared to wild type. (B) Protein-protein interactome generated by FunRich 3.1.3 showing red spheres as proteins losing interaction with mutant CK2β. Green colored are already known partners of CK2 and a few of CK2β only. (C) Scatter plot illustrates number of peptides of proteins bound to wild-type GST tagged CK2β (X-axis) compared to mutant CK2β (Y-axis). DVL3 is indicated here showing zero peptides in case of mutant CK2β as compared to wild type. Note:  $p$  value = 0.05. (D) Pathway enrichment of proteins showing compromised interaction with mutant CK2β. Color code of bars is given under the graph.

Interestingly, the function of CK2 in activation of interleukines and mTOR pathway response is already established by previous studies (Aparicio-Siegmund, Sommer et al. 2014; Gibson, Yang et al. 2017).

Among the proteins losing interaction with mutant CK2 $\beta$  were, most notably (as shown by the most significant  $p$  value ( $>0.001$ )), the regulators of Wnt signaling. More specifically, these proteins are involved in degradation of  $\beta$ -Catenin (Figure 5.25D). As a matter of fact,  $\beta$ -Catenin is one of the main regulators of Wnt signaling and regarding the proteins involved in degradation activity of  $\beta$ -Catenin, are the members of disheveled proteins, DVL1, DVL1P1 and DVL3 (Table 5.10). Thus, on the basis of relevance with Wnt signaling, DVL3 and  $\beta$ -Catenin (Figure 5.25D), both of these proteins were considered for further comprehensive investigation. The other well-characterized Wnt signaling proteins found were PRICKLE3 and bromodomain containing proteins (BRD2 and BRD3). Three of these proteins showed reduced binding with CK2B\_p.Asp32His up to 3 folds (Figure 5.25C).

**Table 5.10: Proteins losing interaction with mutant CK2 $\beta$ .**

Pathway	No. of proteins involved	Names of proteins
IL3 mediated/ mTOR pathway	6	DDX5, DVL1, DROSHA, DVL3, RICTOR, KAT7
Regulatory RNA pathways	7	ANKRD11, GPBP1, DDX47, GPATCH2, GPATCH8, DDX46, THRAP3
Translation	3	SRRM2, IWS1, REXO1
Apoptosis	2	BCLAF1, ACIN1
ATM pathway	5	DDX5, DROSHA, THRAP3, BCLAF1, SETD2
Wnt signaling pathway	7	DVL1, DVL1P1, DVL3, PRICKL3, DDX5, BRD2, BRD3
Degradation of $\beta$ -Catenin	2	DVL1, DVL3

**Explication;** Data analysis of mass spectrometry showed that mutation influences crucial cellular processes, most significantly, Wnt signaling. This data also provides a list of crucial binding partners of CK2 $\beta$ .

## **5.11 Investigating regulators of Wnt signaling pathway**

Mass spectrometry results intrigued me, further, to investigate the dynamics of Wnt signaling. Both proteins,  $\beta$ -Catenin and DVL3, were thoroughly analyzed by the following experiments.

### **5.11.1 Cellular expression of $\beta$ -Catenin**

Localization of non-active  $\beta$ -Catenin and its active form was analyzed in patient LCLs by immunofluorescence coupled with confocal microscopy. It should be noted that active form of  $\beta$ -Catenin is referred to the nuclear or dephosphorylated form (on Ser33, Ser37 and T41) (Liu, Li et al. 2002; Gao, Xiao et al. 2014) whereas; the non-active  $\beta$ -Catenin is cytoplasmic or phosphorylated form on the same sites. CK2 is already proven to participate in maintaining the balance of  $\beta$ -Catenin pool (nuclear and cytoplasmic) by phosphorylation activity (Song, Sussman et al. 2000).

### **5.11.2 Investigating the dynamics of active $\beta$ -Catenin by confocal imaging**

Confocal microscopy imaging showed that the active form or nuclear  $\beta$ -Catenin was found drastically reduced inside the nucleus of both mutants (p.Asp32His and p.Asp32Asn) as compared to the wild type (Figure 5.26A and B). It was also noticed that the reduced amount of  $\beta$ -Catenin was mislocalised as well in both mutants; In case of p.Asp32His mutant, it was observed near the nuclear membrane whereas in p.Asp32Asn it was visibly scattered in cytoplasm near the periphery of nucleus (Figure 5.26A and B). However, in both mutant cells  $\beta$ -Catenin was consistently invisible inside the nucleus. These results indicated the disturbance in translocation of  $\beta$ -Catenin into the nucleus for downstream activities.

### **5.11.3 Investigating the dynamics of inactive $\beta$ -Catenin by confocal imaging**

Regarding the cytoplasmic or non-active  $\beta$ -Catenin, confocal microscopy showed that it was abundant in the cytoplasm of both mutants (p.Asp32His and p.Asp32Asn) as compared to the wild type (Figure 5.26A and B). Further confirming the inactivity of  $\beta$ -Catenin in p.Asp32Asn mutant, another phosphorylation specific (at Ser33 and Ser37) antibody was used. This antibody could indicate the  $\beta$ -Catenin which should be degraded by proteosomal activity. p- $\beta$ -Catenin is hardly detectable in normal cultured cells (Alvarado, Bos et al. 2019), yet in Asp32Asn mutant cells it was very prominent as compared to wild-type LCLs where it was barely visible (Figure 5.26C). For further confirmation, the same antibody was tested on immunoblotting for p.Asp32Asn mutant, which complemented the results of confocal

imaging and showed that p- $\beta$ -Catenin was abundant in whole cell lysate of p.Asp32Asn mutant as compared to wild type (Figure 5.26D). The p- $\beta$ -Catenin antibody could not be used for p.Asp32His mutant due to unavailability of cells.

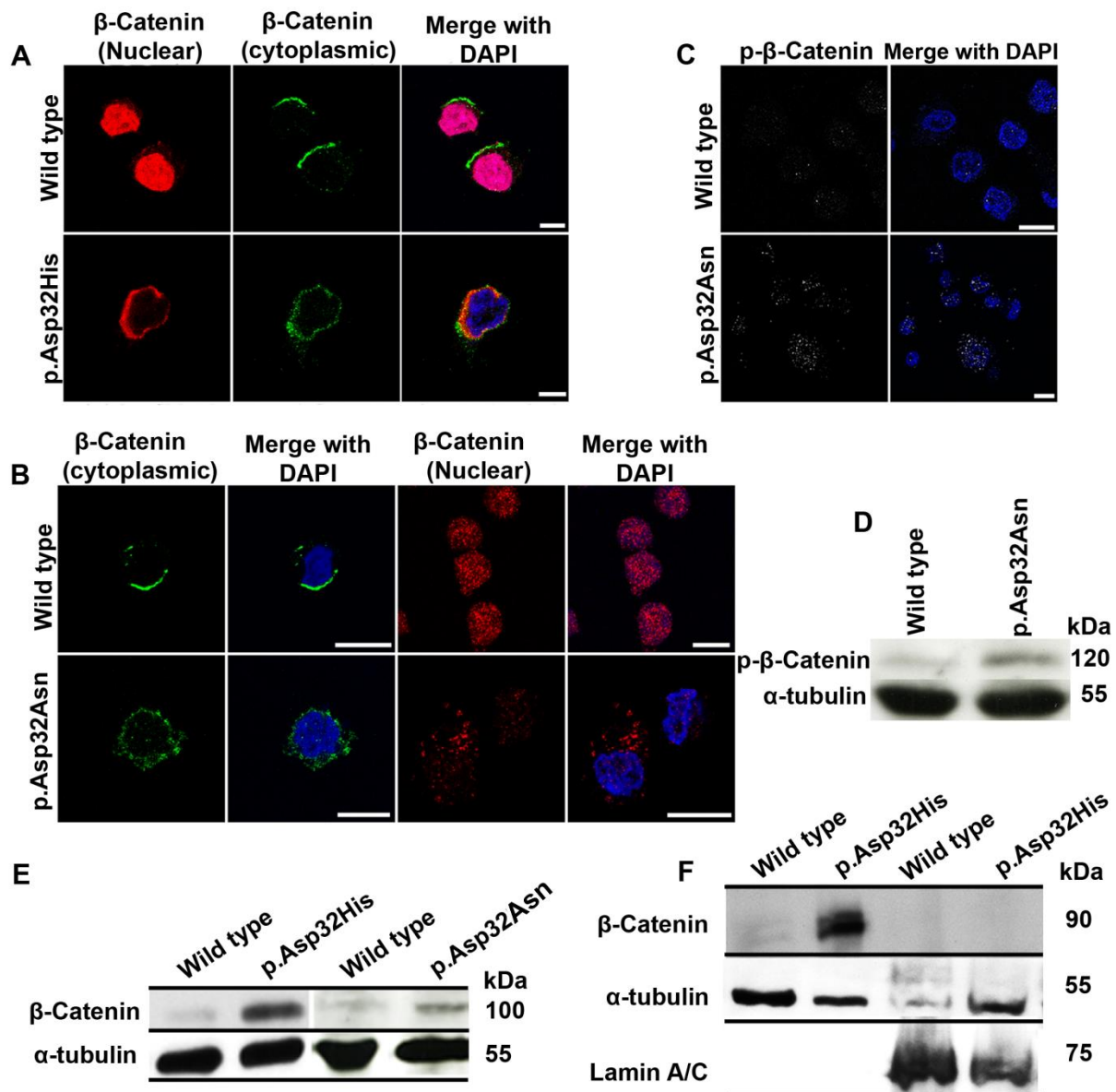


**Figure 5.26: Cellular localization and amount of  $\beta$ -Catenin in patient derived and wild-type LCLs.**

(A) Immunofluorescence shows decreased amount of active  $\beta$ -Catenin (red) in nucleus of p.Asp32His LCLs as compared to the wild type. Non-active  $\beta$ -Catenin (green) is increased in cytoplasm of mutant LCLs as compared to the wild type. DAPI (blue) indicates staining of nucleus. Scale bar, 5  $\mu$ m. (B) Immunofluorescence shows decreased amount of active  $\beta$ -Catenin (red) in nucleus of p.Asp32Asn LCLs as compared to the wild type. Non-active  $\beta$ -Catenin (green) is increased in cytoplasm of mutant LCLs as compared to the wild type.

DAPI (blue) indicates staining of nucleus. Scale bar, 10  $\mu$ m. **(C)** Immunofluorescence shows increased amount of p- $\beta$ -Catenin (white dots) in nucleus of p.Asp32Asn mutant LCLs as compared to the wild type. DAPI (blue) indicates staining of nucleus. Scale bar, 10  $\mu$ m. **(D)** Immunoblotting shows an increased amount of p- $\beta$ -Catenin in whole cell lysate of p.Asp32Asn mutant versus wild-type LCLs.  $\alpha$ -tubulin serves as loading control. **(E)** Immunoblotting shows an increased amount of cytoplasmic  $\beta$ -Catenin in whole cell lysate of p.Asp32Asn mutant versus wild-type LCLs.  $\alpha$ -tubulin serves as loading control. **(F)** Immunoblotting shows an increased amount of cytoplasmic  $\beta$ -Catenin in cytosolic fraction of p.Asp32Asn mutant versus wild-type LCLs, left two columns, whereas absent in the nuclear fraction, right two columns.  $\alpha$ -tubulin and lamin A/C serves as loading controls for cytosol and nucleoplasm, respectively.

#### **5.11.4 Confirmation of active and inactive $\beta$ -Catenin by immunoblotting**

Furthermore, immunoblotting of cytoplasmic  $\beta$ -Catenin was carried out for confirming the results observed by immunofluorescence analysis. Data showed that the cytoplasmic  $\beta$ -Catenin was substantially increased in the whole cell lysates of both mutants (Figure 5.26E) as observed in immunofluorescence (Figure 5.26A and B). For further confirmation fractionation assay was performed in case of p.Asp32His mutant which showed that the amount of cytoplasmic  $\beta$ -Catenin was found substantially higher in the cytosolic fraction (Figure 5.26F). This experiment confirmed that the antibody was very specific for detecting the cytoplasmic  $\beta$ -Catenin only as it was totally absent in nuclear fraction of both wild type and p.Asp32His mutant. Furthermore, signal of antibody specific for detecting active  $\beta$ -Catenin could not be obtained on immunoblots even after multiple trials.

#### **5.11.5 Interaction of CK2 $\beta$ with $\beta$ -Catenin**

Impaired localization as well as amounts of  $\beta$ -Catenin observed in the mutants derived LCLs intrigued me to analyze the consequences of CK2 $\beta$  mutation on binding efficiency with  $\beta$ -Catenin. As previous studies provided enough evidences that  $\beta$ -Catenin is a binding partner/substrate of CK2 and  $\beta$ -Catenin dependent regulation of Wnt signaling is also based on phosphorylation performed by CK2, therefore it was logical to investigate the influence of mutated CK2 $\beta$  protein on association with  $\beta$ -Catenin.

Interaction of both proteins was analyzed by pull-down assay where GST tagged CK2 $\beta$  wild type and p.Asp32His mutant were pulled down with HeLa cells lysates. Immunoblotting showed that the interaction of  $\beta$ -Catenin with mutated GST tagged CK2 $\beta$  was reduced as

compared to wild type (Figure 5.27A). This data validated the interaction of wild-type CK2 $\beta$  with  $\beta$ -Catenin. For further validation of this reduced interaction due to mutation of CK2 $\beta$ , another strategy of pull-down was experimented where GST tagged CK2 $\beta$  wild type and mutant were pulled down with HeLa cell lysates expressing GFP tagged  $\beta$ -Catenin. As expected, this pull-down recapitulated the reduction of mutant CK2 $\beta$  interaction with  $\beta$ -Catenin as observed in the previous experiment (Figure 5.27B).

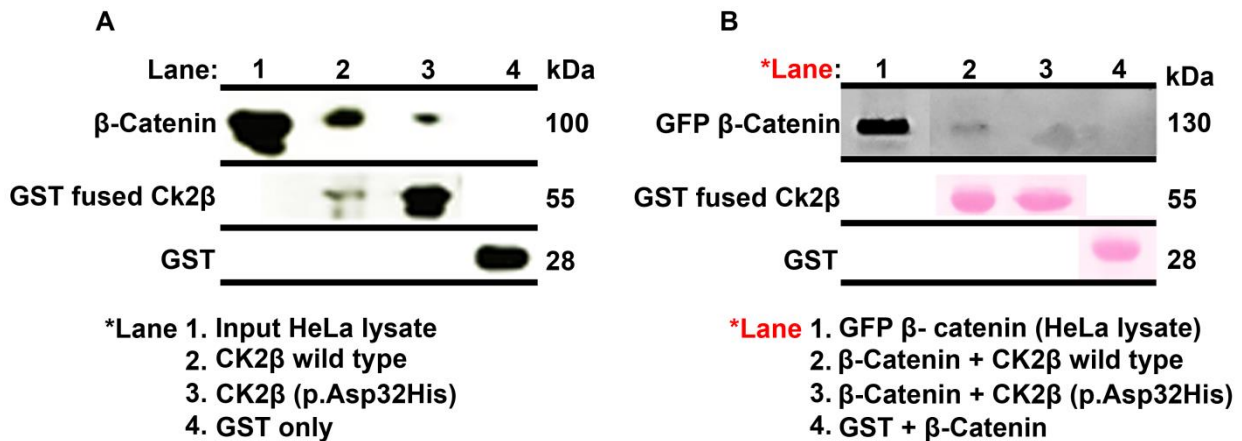


**Figure 5.27: Interaction of GST fused CK2 $\beta$  with  $\beta$ -Catenin in HeLa cells.**

(A) Pull-down assay indicates reduced interaction of endogenous  $\beta$ -Catenin with mutant GST tagged CK2 $\beta$  as compared to wild type in HeLa cells. GST serves as negative control. Key of lanes is mentioned in the figure. (B) Pull-down assay indicates reduced interaction of over expressed GFP tagged  $\beta$ -Catenin with mutant GST tagged CK2 $\beta$  as compared to wild type in HeLa cells. GFP antibody was used to detect GFP-fused proteins. Membrane was stained with Ponceau S to observe the equal amount of GST tagged proteins used in this assay. GST serves as negative control. Key of lane (red with asterisk) is shown below in the figure.

### 5.11.6 Phosphorylation of $\beta$ -Catenin by CK2 containing mutant CK2 $\beta$

As the interaction of CK2 $\beta$  and  $\beta$ -Catenin was found compromised, the next question was obviously marked on the phosphorylation capacity of CK2 having mutated beta subunit as compared to the wild type. It was hypothesized that the reduced interaction may cause reduced phosphorylation of  $\beta$ -Catenin. To answer the question of the impaired enzymatic activity of mutant CK2 holoenzyme, containing mutated  $\beta$  subunit, ADP-Glo assay was conducted. For this purpose,  $\beta$ -Catenin was taken as substrate. The CK2 tetrameric holoenzyme composed of CK2 $\alpha$  and wild-type CK2 $\beta$  showed the highest phosphorylation rate in presence of  $\beta$ -Catenin (set to 100 %) compared to the mutant CK2 holoenzymes containing



mutant  $\beta$  subunits, p.Asp32His (28 %) and p.Asp32Asn (35 %). The kinase activity of the CK2 holoenzymes with mutants CK2 $\beta$  (p.Asp32His and p.Asp32Asn) was reduced by more than half compared to wild-type CK2 with a significance level of  $\leq 1$  % (Figure 5.28).

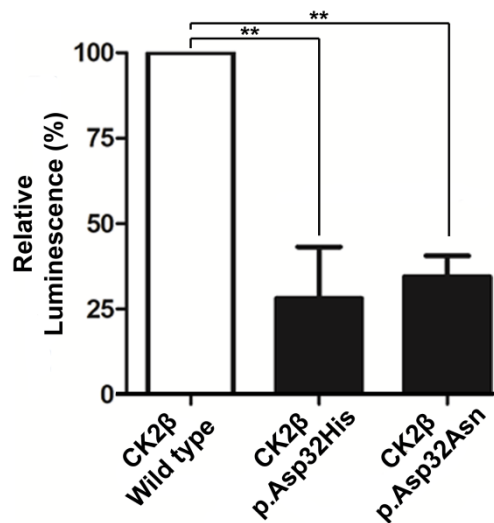


**Figure 5.28: Kinase activity of CK2 having mutated beta subunits.**

Graph showing reduced kinase activity of mutant CK2 $\beta$  as compared to wild type. Note that  $\beta$ -Catenin was used as substrate. Note that  $p$  value is  $> 0.05$ .

**Explication;** These findings overall support the idea that the mutated CK2 $\beta$  protein has an influence on expression and regulation of  $\beta$ -Catenin which is considerably upregulated and mislocalized in mutant LCLs in non-active state and reduced in its active form. Furthermore, the data validates that the physical interaction of mutant CK2 $\beta$  with  $\beta$ -Catenin is being compromised which was expected due to drastically reduced kinase activity of mutant CK2 $\beta$ . This hypothesis was proven by analyzing the kinase activity of mutated CK2 $\beta$  which confirmed that phosphorylation of its substrate ( $\beta$ -Catenin) was significantly reduced. Reduced kinase activity could be due to reduced interaction of CK2 $\alpha$  with mutated CK2 $\beta$  as it was observed that at 37 °C, only the holoenzyme catalytic subunit showed activity. Taken together it may be concluded that the interaction of CK2 $\beta$  and  $\beta$ -Catenin is weakened by the mutations in  $\beta$  subunit.

### 5.11.7 Capillary Electrophoresis based CK2 activity assay

For further validation of kinase activity measured by ADP Glo assay, capillary electrophoresis (CE) based assay was performed. For this purpose, a CK2 target peptide (RRRDDDSDDD) was used (Wünsch, Kröger et al. 2020). Results demonstrated that CK2 $\alpha$  alone showed low

phosphorylation activity against the substrate peptide. In presence of CK2 $\beta$  wild type, the kinase activity of CK2 $\alpha$  is increased due to tetrameric complex building (Figure 5.29A), which could also be seen in the amount of phosphorylated peptide (Figure 5.29B). Compared to CK2 $\beta$  wild type, the presence of the p.Asp32His CK2 $\beta$  mutant showed a decreased phosphorylation of substrate peptide (Figure 5.29A) and thus decreased amount of product observed in the given time (Figure 5.29B); it was only up to the level of free CK2 $\alpha$  kinase activity, showing that this particular mutant subunit drastically influence the phosphorylation activity to the extent which is comparable to activity observed for CK2 $\alpha$  alone. Here, it can be assumed that low kinase activity could be due to the weaker interaction of CK2 $\alpha$  with CK2 $\beta$  mutant, p.Asp32His. On the contrary, the addition of p.Asp32Asn CK2 $\beta$  mutant to CK2 $\alpha$  showed no significant differences with respect to phosphorylation activity (Figure 5.29A) and product formation (Figure 5.29B) as compared with CK2 $\beta$  wild type. However, the kinase activity for this particular mutant observed in ADP-Glo assay was found compromised as compared to kinase activity observed in this experiment. The reason could be the substrate specificity because different substrates had been used in both experiments. Hence, I concluded that p.Asp32Asn mutation may have milder effects and the mutant protein.

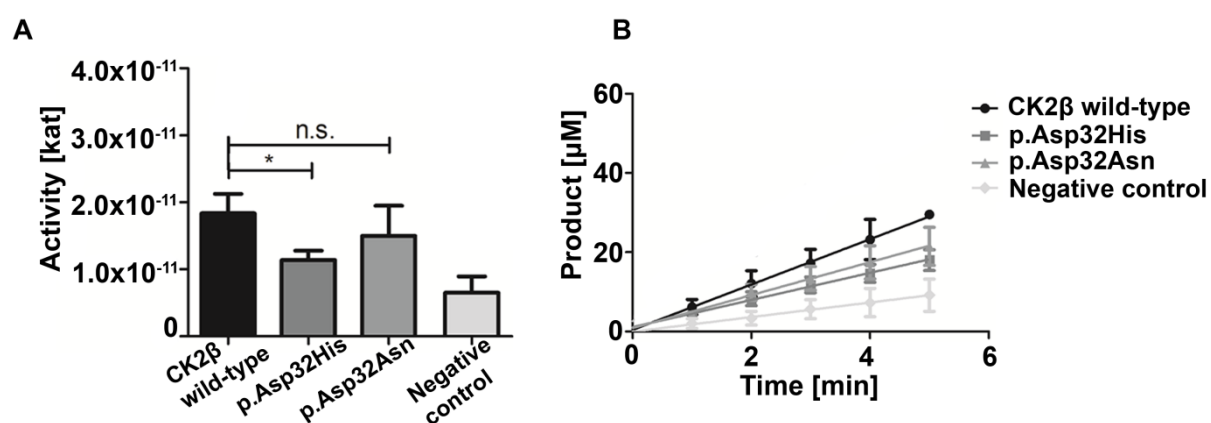


**Figure 5.29: Kinase activity of CK2 wild type and mutants based on capillary electrophoresis based assay.**

(A) Bar graph showing kinase activity of CK2 containing wild-type and mutant beta subunits (p.Asp32His and p.Asp32Asn). Note that the activity of CK2 containing p.Asp32His is reduced as compared to wild type but CK2 containing Asp32Asn mutant does not show any significant difference. *P* value is > 0.05 denoted by asterisk (\*) and n.s. stands for not significant. (B) Graph showing the amount of phosphorylated substrate peptide in the given time. Note that CK2 containing p.Asp32His shows decreased amount of phosphorylated peptide as compared to wild type whereas CK2 containing p.Asp32Asn shows no significant differences. The color and shape key denoting all the samples given in the figure.

**Explication;** Combined with the information from the ADP-Glo and the CE assays, the mutation, p.Asp32His of CK2 $\beta$  seems to inhibit the interaction of CK2 $\alpha$  and CK2 $\beta$  leading to hypophosphorylation of  $\beta$ -Catenin and of the substrate peptide compared to the wild-type CK2 $\beta$ . However, p.Asp32Asn mutation may have milder effects as compared to p.Asp32His mutation and could still phosphorylate one of the substrate used in CE. Thus, structural changes in CK2 $\beta$  leading to a deterioration of the interaction sites of CK2 $\beta$  and  $\beta$ -Catenin may explain the variable kinase activity.

### 5.11.8 Exploring the behavior of DVL3 in CK2 $\beta$ mutated LCLs

After confirming the mutational consequences on regulation of  $\beta$ -Catenin, DVL3 was followed as the second key regulator of Wnt signaling pathway.

#### *Cellular dynamics of DVL3 in p.Asp32His patient LCLs*

As shown by the protein interactome data that DVL3 was one of the proteins losing interaction with mutated CK2 $\beta$ , further investigations were carried out to analyze the amount of DVL3 as well the data of impaired localization was validated by performing pull-down assay. In this regard, immunoblotting was carried out which showed that the amount of DVL3 remains the same in patient LCLs as compared to wild type (Figure 5.30A), however, when the interaction of DVL3 with CK2 $\beta$  was analyzed by pulling down wild-type and p.Asp32His mutant GST tagged CK2 $\beta$  with protein lysate of wild-type LCLs, it was noted that the interaction was considerably reduced in case of p.Asp32His mutant CK2 $\beta$  compared to wild-type (Figure 5.30B).

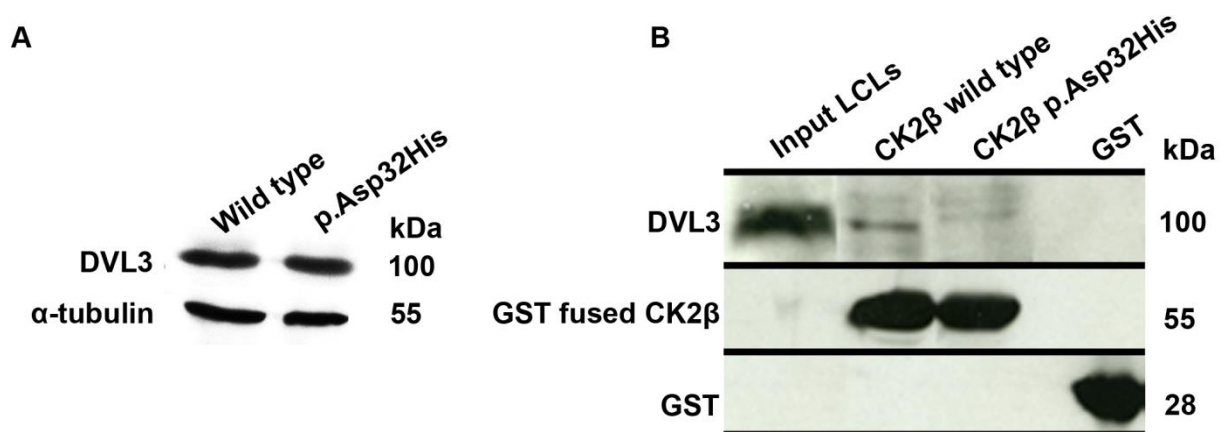


**Figure 5.30: Analysis of DVL3 protein in wild-type and p.Asp32His mutant LCLs and validation of interaction with mutant CK2 $\beta$ .**

(A) Immunoblotting shows equal amount of DVL3 in wild type as well as mutant LCLs.  $\alpha$ -tubulin serves as loading control. (B) Pull-down assay shows reduced interaction of DVL3

with p.Asp32His mutant GST fused CK2 $\beta$  as compared to wild-type. GST was used as negative control.

## **5.12 Investigating key regulators of DNA damage response pathway**

After investigating Wnt signaling pathway, the second pathway followed in this study was DNA damage response (DDR) pathway. The motivation behind this investigation was relevance of CK2 functions in this pathway. Well established and key regulators of DDR pathway were examined in the patient derived LCLs in comparison with wild type. Among the sensor proteins of DNA damage,  $\gamma$ H2AX was studied whereas 53BP1 and CHK1 were taken in the account of mediator and checkpoint proteins, respectively. To be noted here, that all of the three regulators are binding partners of CK2 $\beta$  (Guerra, Issinger et al. 2003; Mason 2011). Therefore, all the three proteins could be used as sensitive protein markers indicating response of cell towards DNA damage.

### **5.12.1 Upregulation of $\gamma$ H2AX in p.Asp32His mutant LCL**

Activation of H2AX as a result of phosphorylation is an early response of the cell for induced DNA double-strand breaks (Boumil, Letts et al. 2010). Detection of this phosphorylation event was analysed by induction of DNA damage using hydroxyurea for 24 hours in wild-type as well patient LCLs followed by immunofluorescence and immunoblotting. Results indicated that number of  $\gamma$ H2AX foci (stained by phosphorylation specific antibody at Ser139) were significantly increased upon treatment in patient LCLs (Figure 5.31A) i.e, 8 foci per cell as compared to control where 1.8 foci per cell were recorded (Figure 5.31B), whereas,  $\gamma$ H2AX in the untreated wild-type and patient LCLs did not show any significant difference i.e 1 focus per cell ( $P$  value = 0.7156) (Figure 5.31A and B). Immunoblotting validated the same results as obtained by immunofluorescence (Figure 5.31C).

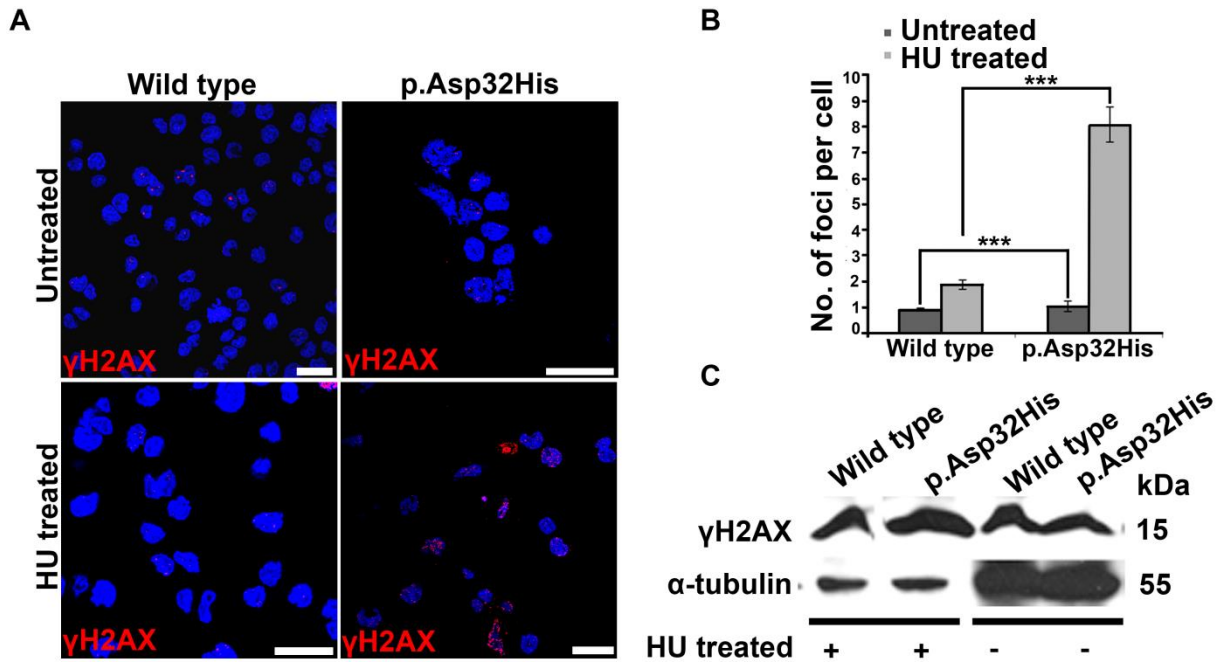


**Figure 5.31: Investigation of  $\gamma$ H2AX in p.Asp32His patient on DNA damage induction.**

(A) Immunofluorescence shows number of foci in case of hydroxyurea (HU) treated mutant LCLs as compared to wild type whereas there was no significant difference in case of untreated wild-type and mutant LCLs. (B) Graph shows 8 foci per mutant LCL as compared to wild type upon hydroxyl urea treatment, whereas, without treatment, there were 1-2 foci in wild-type as well as in mutant LCLs. Note:  $p$  values  $>0.05$  (Student's  $t$  test), number of experiments performed were three, 150 cells were counted per experiment. (C) Immunoblotting shows increased amount of  $\gamma$ H2AX in hydroxyurea treated mutant LCLs as compared to wild type. No significant differences were observed in protein level of  $\gamma$ H2AX in wild-type and mutant LCLs without HU treatment.

### 5.12.2 Upregulation of 53BP1 in p.Asp32His mutant LCLs

53BP1 protein is also a sensitive marker for DNA double breaks; during cellular stress, it is re-localized to the sites of DNA damage and accumulates there (Pryde, Khalili et al. 2005). Immunoblotting shows increased amount of 53BP1 in hydroxyurea treated mutant LCLs as compared to wild type. No significant difference was observed in protein level of 53BP1 in wild-type and mutant LCLs without treatment.

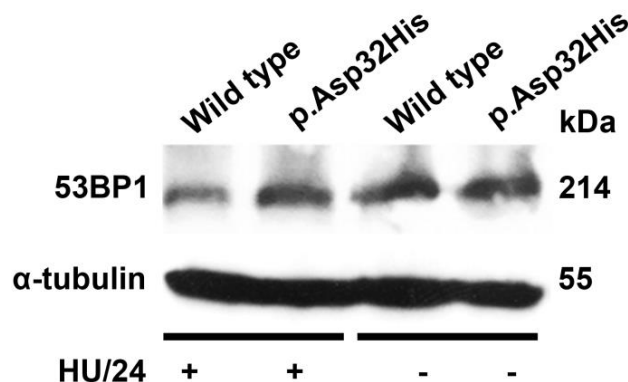


**Figure 5.32: Investigation of 53BP1 in p.Asp32His patient LCLs on DNA damage induction.**

For further validation of data obtained in case of  $\gamma$ H2AX, 53BP1 was also analysed in patient LCLs. Similar to  $\gamma$ H2AX, upon treatment of hydroxyurea, the amount of 53BP1 was found increased in the treated patient LCLs as compared to wild type, whereas, no difference in the amount of 53BP1 was observed in untreated case (Figure 3.32).

### 5.12.3 Upregulation of CHK1 in p.Asp32His patient LCLs

Phosphorylation events of CHK1 maintain the cell cycle arrest after DNA damage. (Narayanaswamy, Tkachuk et al. 2016). In addition, one interesting aspect of CK2 $\beta$  is that it works as docking protein and has several binding partners which are CK2 independent binding partners; these are activated by binding to CK2 $\beta$  and do not depend on formation of CK2 holoenzyme. One of those CK2 $\beta$  dependent partners is CHK1 protein. This fact was considered for checking the concentration of CHK1 quantity in the wild-type and mutant LCLs in both hydroxyurea treated and non-treated LCLs. Secondly, the phosphorylated CHK1 at position Ser345 is an indicator of DNA damage response pathway activation (Arrigoni, Pagano et al. 2008) that is why Ser345 specific CHK1 antibody was used.

Both phosphorylated (p.Ser345) and non-phosphorylated CHK1 (Cell Signaling technology, 2360) were examined on inducing DNA damage in wild-type and patient LCLs. Interestingly, the phosphorylated CHK1 showed similar response as  $\gamma$ H2AX and 53BP1 showed and was increased in patient LCLs as compared to wild type. On the contrary, the non-phosphorylated CHK1 was found decreased in the patient LCLs, which clearly meant that more amount of CHK1 is being phosphorylated as a result of DNA damage induction (Figure 5.33).

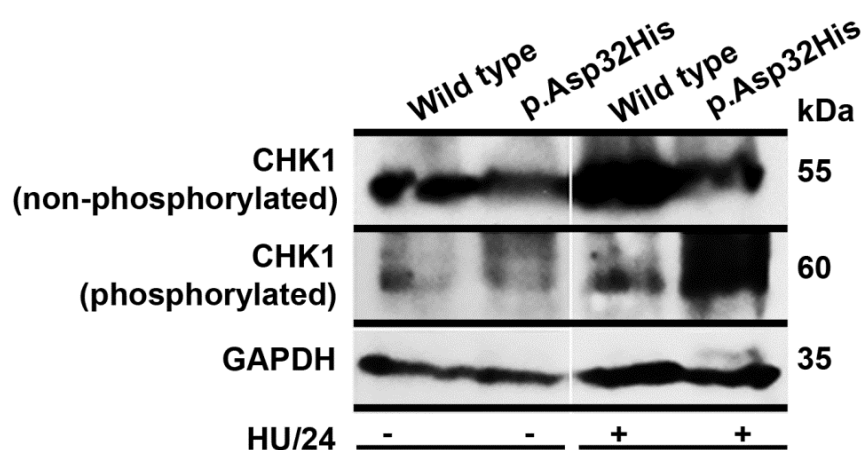


**Figure 5.33: Investigation of CHK1 in p.Asp32His patient derived LCLs on DNA damage induction.**

Immunoblotting shows decreased amount of CHK1 and increased amount of p.CHK1 in hydroxyurea treated mutant LCLs as compared to wild type. No significant difference was observed in protein level of 53BP1 in wild-type and mutant LCLs without treatment.

**Explication;** These findings suggest that all the investigated key regulators of DNA damage response are found upregulated on induction of injury to DNA in CK2 $\beta$  mutant cells. Also, all of the three regulators are strong binding partners of CK2 $\beta$ ; it can be assumed that the role of CK2 $\beta$  in DNA damage kinase cascade is being compromised. This upregulation also suggests that the response to injury is delayed and as a result of impairment of DNA repair mechanism.

### **5.13 Fate of *CSNK2B* mutated cells**

Based on the delayed DNA damaged response observed in p.Asp32His mutant LCLs, it was further intended to explore the cellular fate. For this purpose, cell cycle and apoptosis by terminal deoxynucleotidyl transferase-mediated dUTP nick-end labeling (TUNEL) assay was performed; both are discussed as following.

#### **5.13.1 Effect of p.Asp32His mutation on cell cycle in patient LCLs**

The role of CK2 has been demonstrated regarding cell viability and proliferation by several studies, especially in mouse embryonic development, showing that overexpression as well as depletion of mutant CK2 $\beta$  causes growth inhibition. Also, the patient LCLs in culture seemed to grow slower than wild type. So, it was reasonable to perform an experiment to find the reasons of slower growth rate of mutant LCLs. For this purpose, the statuses of cells were observed at different cell cycle stages. To accomplish this task, cells were incubated with Nuclear-ID™ Red DNA stain (Enzo Life Sciences) and then subjected to fluorescence-activated cell sorter (FAC) analysis which showed that mutant LCLs were found 7% more in G0/G1 phase. Whereas in S phase, the mutant LCLs were found 7.05% lesser than the wild type. However, the data of M phase were statistically insignificant (Figure 5.34A). This data shows that majority of the mutant cells are arrested in G0/G1, therefore lesser cells entered into S-phase.

#### **5.13.2 Cellular apoptosis detected by TUNEL assay in p.Asp32His mutant LCLs**

TUNEL assay was also performed for detecting the apoptotic cells in p.Asp32His mutant. Immunofluorescence reflected significantly more TUNEL positive p.Asp32His LCLs as compared to the wild type (Figure 5.34B). Statistical data was taken after counting the cells in

three independent experiments which showed that 7.5% of mutant LCLs underwent apoptosis which is significantly more as compared to wild type which were 1.2% (Figure 5.34C).

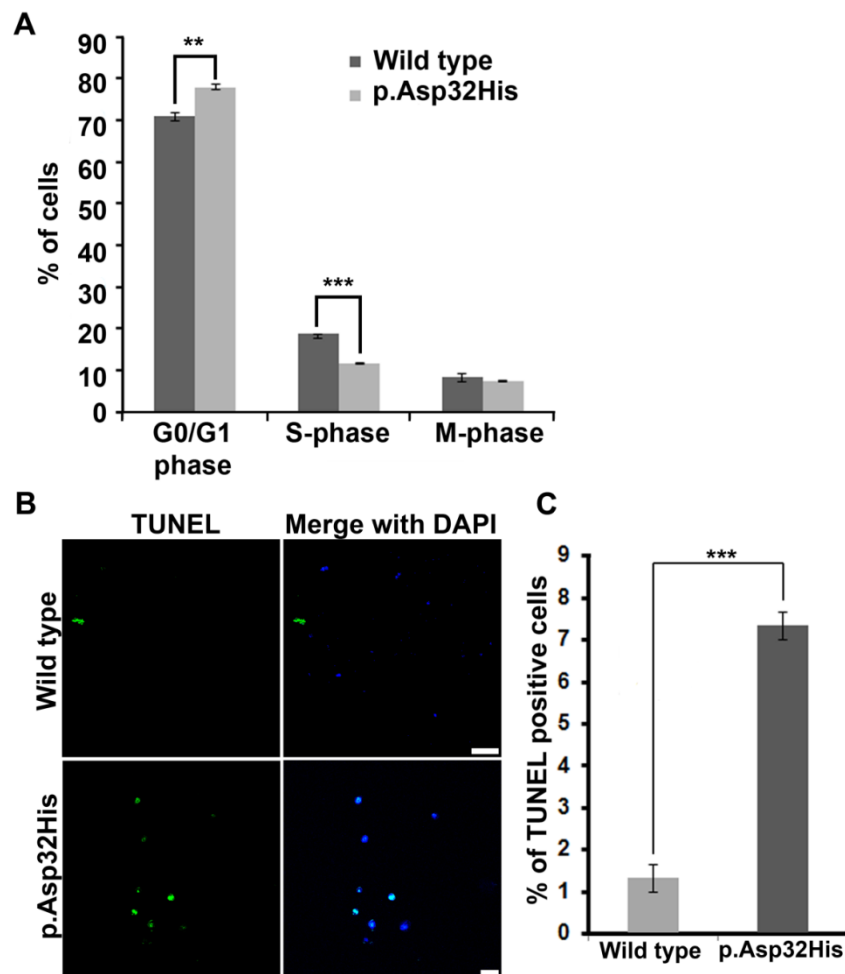


**Figure 5.34: Effects of p.Asp32His mutation on cell cycle and apoptosis of LCLs.**

(A) Cell cycle assay performed by FACS. Note the  $p$  value (indicated by Asterisks) for G0/G1 phase is 0.0047, S-phase is 0.0001 (Student's  $t$  test) and M phase was not significant. (B) Immunofluorescence showing TUNEL positive cells in p.Asp32His mutant. Note that the mutant shows more TUNNEL positive cells as compared to wild type. Scale bar is 20  $\mu\text{m}$  (C) Graph showing TUNNEL positive cells being increased in mutant as compared to wild type. Note that,  $n = 3$ , 100 cells counted in each experiment and  $p > 0.005$  (Student's  $t$  test).

**Explication;** Data suggested that the cellular fate of mutant cells due to delayed DNA damage response is cell cycle arrest in G0/G1 phase as well as increased cellular apoptosis.



## 5.14 Phosphoproteome analysis of CK2 $\beta$

As earlier experiments were performed for analyzing the phosphorylation activity of CK2, which showed compromised kinase activity, therefore, whole phosphoproteome analysis was conducted to recapitulate the data and to further extend the information in a bigger scenario. Principle component analysis (PCA) of the data was performed for the validation of datasets of wild-type and p.Asp32His patient LCLs (Figure 5.35A). Further data analysis was carried out by using an online available tool Perseus, which revealed a total of 2241 enriched phosphorylated protein peptides (Figure 5.35B and C). Considering the significant values ( $q < 0.05$ ), 762 phosphorylated peptides were further filtered out; intriguingly, 344 of the protein peptides, including DVL3 and APC, were

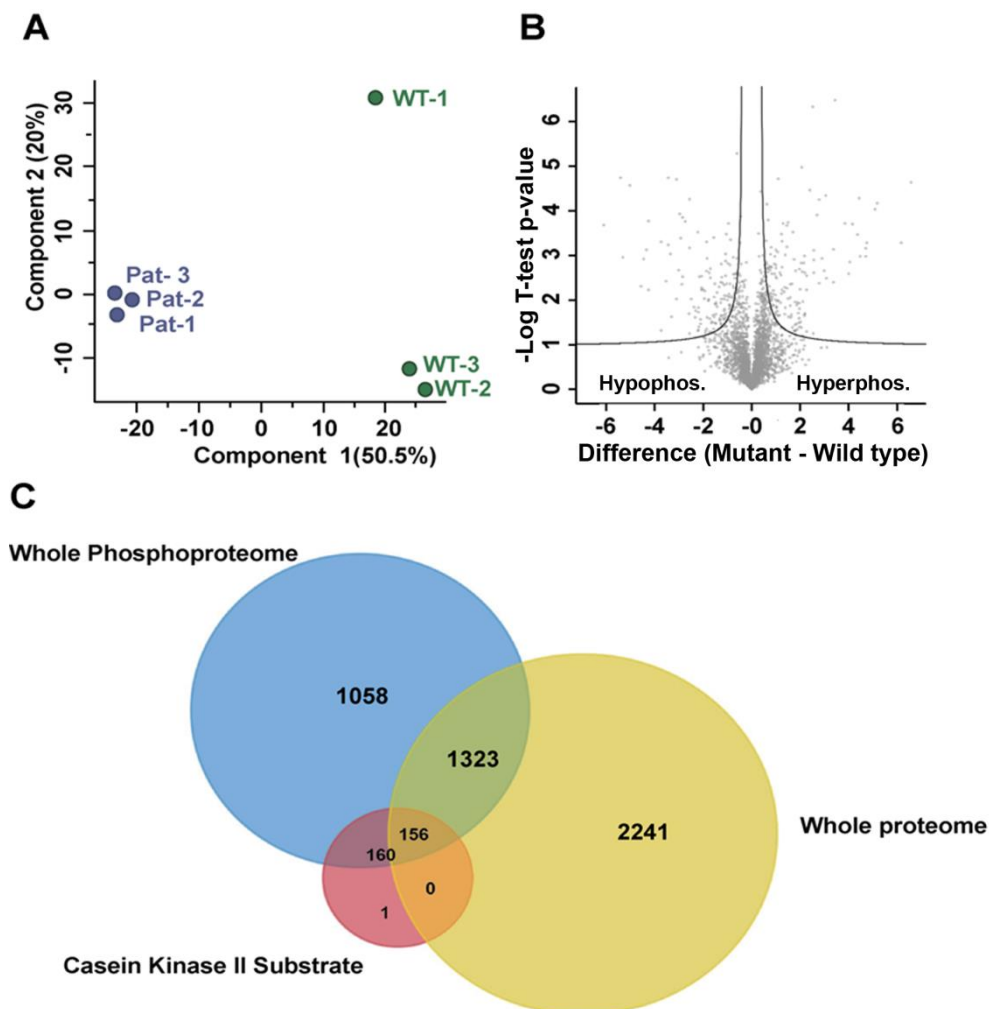


**Figure 5.35: Phosphoproteome analysis of wild-type and mutant LCLs.**

(A) PCA of three replicates of wild-type and mutant samples submitted for phosphoproteome. (B) Volcano plot of proteins enriched in phosphoproteome. (C) Venn diagram showing

number of proteins obtained in whole proteome (yellow), phosphoproteome (blue) and substrates of CK2 (pink).

those which showed phosphorylation at casein kinase II substrate motif only in the wild type, whereas, in patient cells all the enriched protein peptides remained non-phosphorylated at all (Table 5.10). This figure of 344 proteins lacking phosphorylation in patient cells is convincing enough to suggest the impaired kinase activity of CK2 having mutated  $\beta$  subunit and provides a strong back to my findings of impaired kinase activity of CK2 containing mutant beta subunit (Figure 5.35C). Rest of the 424 protein motifs, out of 762, were found substrates of casein kinase I, AKT kinase, ATM kinase and  $\beta$ -adrenergic receptor kinase (Table 5.11).

#### **5.14.1 Pathway enrichment of CK2 substrates lacking phosphorylation in p.Asp32His mutant**

The proteins (344) which showed no phosphorylated peptides were enriched on functional basis to observe their roles in specific pathways. Interestingly, FunRich generated donut graph revealed that 7.2% of total proteins (BRCA1, HNRNPA1, CCND2, RANBP9, SKP1, APC, INCENP, PELP1) were involved specifically in regulation of nuclear  $\beta$ -Catenin and transcription of the target genes. This again strongly supported my findings related to trends of nuclear  $\beta$ -Catenin in p.Asp32His and p.Asp32Asn mutant.

Other pathways depicted by enrichment included mTOR, ATM pathway, BMP receptor pathway and gene expression (Figure 5.36A). Note that mTOR, ATM pathway and gene expression pathway were also enriched in the data of proteins showing reduced interaction with GST fused CK2 $\beta$ \_p.Asp32His mutant thus reconfirming the impaired interaction of CK2 $\beta$  due to mutation (Table 5.9).

Enrichment of cellular processes was also performed using GOrilla, a tool for identifying and visualizing enriched gene ontology terms. It showed that these genes are mostly enriched in the process of cell development and differentiation (Figure 5.36B); this provides logic and strength to my findings related to cell cycle (Figure 5.34).

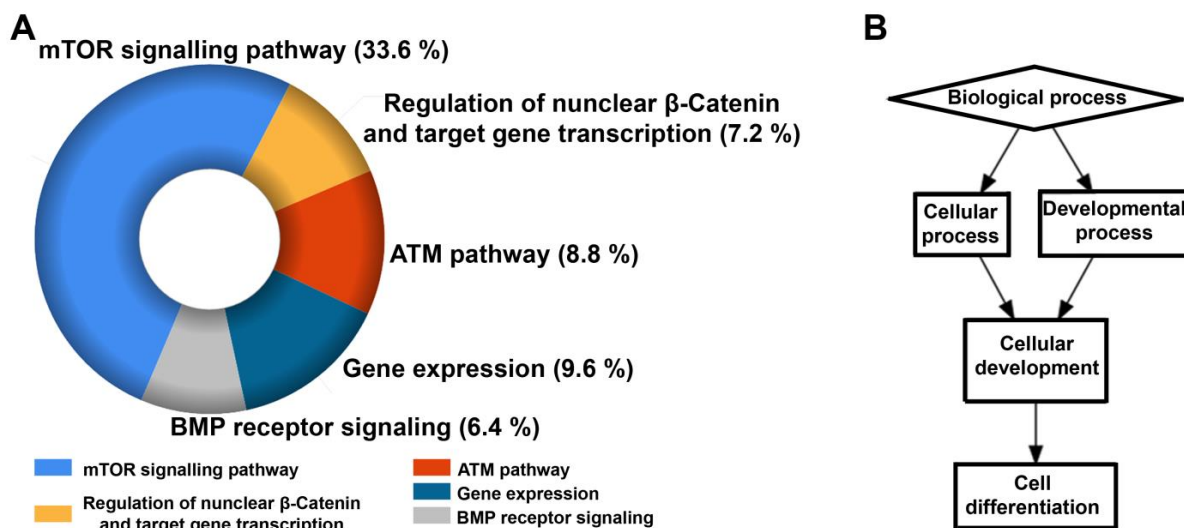


**Figure 5.36: Pathway enrichment analysis of hypophosphorylated substrates of CK2 in patient derived LCLs.**

(A) Donut graph generated by Funrich shows the percent of genes involved in a biological pathway. Note that each pathway is color coded and the key is given in the figure. (B) Graph generated by PANTHER shows pathway enrichment of those protein peptides which showed no phosphorylation in case of p.Asp32His mutant CK2 $\beta$ . Y-axis shows the percentage of the protein involved in specific pathway shown on the X-axis.

#### 5.14.2 Reported CK2 substrates lack phosphopeptides in p.Asp32His mutant

The 344 CK2 substrates showing no phosphorylated peptides, were further analysed by comparing them with already known substrates of CK2 reported in other comprehensive studies (Bian, Ye et al. 2013; de Villavicencio-Díaz, Mazola et al. 2015; Franchin, Salvi et al. 2015; Rusin, Adamo et al. 2017). In addition, these were further compared with substrates of CK2 given on phosphositeplus v6.5.9 (<https://www.phosphosite.org/homeAction>) and Phospho.ELM version 9.0 (<http://phospho.elm.eu.org/dataset.html>). Interestingly, 71 of these 344 were those of already reported proteins containing CK2 phosphorylation motifs (Table 5.11). Although, these are the mutual substrates of other kinases (Casein kinase I, AKT kinase, ATM kinase and  $\beta$ -adrenergic receptor kinase) as suggested by the literature and data provided by the whole phosphoproteome facility yet the fact is obvious that only the mutant cells significantly lack phosphopeptides (0 peptides in all the three mutant replicates) of the given proteins (Table 5.11). Moreover, it is also interesting to notice that 17 of the proteins are also common between those obtained in protein-protein interactome data and whole phosphoproteome data of p.Asp32His mutant. These proteins are ARL6IP4, ATRX, BCLAF1, CEP170, FAM120A, GPATCH2, HDGFRP2, HIRIP3, IWS1, PPIG, RBBP6,

RPL13, SRRM1, SRRM2, SSRP1, TCOF1 and THRAP3. Among them BCLAF1, GPATCH2, IWS1 and RBBP6 are those showing significantly compromised interaction with p.Asp32His CK2 $\beta$ .

**Table 5.11: List of the reported proteins containing CK2 phosphosites, hypo-phosphorylated in mutant LCLs.**

Unique identifier	Gene name	Protein name	-Log T-test p-value Mut_W T	-Log T-test difference Mut_W T	Mean log2 Mut	Mean log2 Mut	Position	A. A	Motif sequence
UID878	<i>MATR3</i>	A0A0R4J2E8	1,84661	-2,90348	0	25,3679	604	S	KDKSRKRSYSPDGKESPSDKKSKTDGSGQKTE
UID1267	<i>SRRM1</i>	A9Z1X7	2,24326	-3,37243	0	25,9	724	S	VRRGASSSPQRRQSPSPSTRPIRRVSRTPPEP
UID2107	<i>TCOF1</i>	J3KQ96	3,16556	-3,70411	0	26,4862	349	S	KPEEDSESSSEESSDSEETPAAKALLQAKA
UID2831	<i>HNRNPAL</i>	F8W6I7	1,67231	-1,38036	0	24,3194	298	S	FAKPRNQGGYGGSSSSSYGSGRRF_____
UID3058	<i>CEP170</i>	H0Y2V6	1,85526	-2,24501	0	24,2167	922	S	LVTGETERKSTQKRKSFTSLYKDRCSSTGSPS
UID3358	<i>PML</i>	H3BT57	1,72813	-2,80895	0	25,1201	38	S	MPPPETPSEGRQSPSPSPTERAPASEEEEFQ
UID5310	<i>CTPS1</i>	P17812	3,32585	-8,23113	0	30,665	562	S	SVGRLSHYLQKGCRLSPRDYSDRSGSSSPD
UID5428	<i>LMNB1</i>	P20700	2,48576	-0,919029	0	23,3732	278	S	ELEQTYHAKLENARLSSEMNTSTVNSAREEL
UID5578	<i>RPL13</i>	P26373	1,36496	-1,8067	0	23,8933	106	S	ARTIGISVDPRRRNKSTESLQANVQRLKEYR
UID5814	<i>DEK</i>	P35659	1,96599	-1,40587	0	24,0236	231	S	KAKRTRKCEILSDESSSDEDEKKNKEESSDD
UID5846	<i>RBMX</i>	P38159	1,47344	-1,66209	0	24,2072	221	S	YLSPRDDGYSTKDSYSSRDYPSRRDTRDYAP
UID5867	<i>BRCA1</i>	P38398	3,5814	-2,36493	0	24,7581	1642	S	AMEESVSREKPELTASTERVKNRMSMVVSGL
UID6696	<i>SPTBN1</i>	Q01082	1,60399	-1,43035	0	23,9776	825	S	LPQEHAESPDVRGRSLGIEERYKEVAELTRL
UID6945	<i>SSRP1</i>	Q08945	1,56733	-1,97234	0	24,6804	659	S	SRGSSSKSSSRQLSESFKSKEFVSSDESSSG
UID7394	<i>SQSTM1</i>	Q13501	2,01105	-2,56307	0	24,852	266	S	LGIEVDIDVEHGGKRSRLTPVSPESSTEEK
UID7746	<i>GAPVD1</i>	Q14C86	1,74977	-2,42111	0	24,8049	914	S	RSRSDIVSSVRRPMSDPSWNRPRGNEEREL
UID7874	<i>SKIV2L</i>	Q15477	1,51594	-1,923	0	24,4506	245	S	AVGQPGGPRGDTVASPCAPLARASSLEDL
UID8348	<i>ZC3H13</i>	Q5T200	1,85281	-1,75648	0	24,1883	325	S	KRDKPRSTPAGQHHSPISSRHSSSSQSGS
UID8683	<i>ARL6IP4</i>	Q66PI3	3,53654	-2,2089	0	25,173	239	S	TSQGRKASTAPGAEASPCITERSKQKARR
UID10997	<i>IWS1</i>	Q96ST2	1,9635	-1,80155	0	24,6343	261	S	RISDSESEDPPRHQASDSENEELPKPRISDS
UID1134	<i>HIRIP3</i>	Q9BW71	2,11588	-2,53742	0	24,673	305	S	DSEEEQKEAASSGDDSGRDREPPVQRKSE

0						8			DR
UID1154 7	<i>KLC2</i>	Q9H0B6	2,47137	-2,56392	0	24,678 4	507	S	VELLKDGGRRGDRSSSRDMAGGAGPRS ESD
UID1277 8	<i>SRRM2</i>	Q9UQ35	3,20399	-5,75498	0	28,101	353	S	KDKDKKEKSATRPSPPERSSTGPEPPAPT P
UID1312 8	<i>THRAP3</i>	Q9Y2W1	2,32333	-2,48784	0	24,700 2	560	S	RDKLGAKGDFPTGKSSFSITREAQVNVRM DS
UID1424 2	<i>ANP32A</i>	P39687	2,42683	-5,44456	0	28,025	15	T	_MEMGRRIHLELRNRTPSDVKELVLDNSR SN
UID1455 2	<i>IF116</i>	Q16666	1,964	-1,70463	0	24,285 3	779	T	RKNKKDILNPDSSMETSPDFFF_____
UID2606 5	<i>CHAMP1</i>	Q96JM3	1,9457	-2,00867	0	24,796 3	386	S	KSSSVSPSSWKSPASPESWKSQPPELRKT A
UID1219 6	<i>FAM120 A</i>	Q9NZB2	2,50489	-1,5054	0	24,409 7	1023	S	YKNQAAIQGRPPYAASAEVAKELKSKSG ES
UID1250 7	<i>FAM208 A</i>	Q9UK61	3,65328	-2,67363	0	25,507 6	673	S	SRGEAIIISGKQRSSHSLDYDKDRVKELINLI
UID1139 4	<i>FANCD2</i>	Q9BXW9	2,68882	-1,90693	0	24,545 4	891	S	GSKTSSSDTLSEEKNSECPTPSHRGQLNK E
UID1208 6	<i>GPATCH 2</i>	Q9NW75	2,09749	-1,82992	0	24,459 5	54	S	SSEQARGGFAETGDHSRSISCLKRQARK RR
UID2447 4	<i>HDGFRP 2</i>	Q7Z4V5	2,08159	-2,05645	0	24,575 7	369	S	RERADRGEAERGSGSSGDELREDDEPVK KR
UID7122	<i>ILF3</i>	Q12906	4,37204	-2,47526	0	24,875 3	810	S	GGGSDYNYESKFNYSGSGGRSGGNSYG SGG
UID2530 3	<i>KDM2B</i>	Q8NHM5	2,00112	-3,10998	0	25,493 3	474	S	KKPKAPALRFLKRTLSNESEESVKSTTLA VD
UID4291	<i>KIF1C</i>	O43896	4,14194	-5,04269	0	27,467 2	1092	S	RYPPYTTTPRMRQRSAPDLKESGAAV_ —
UID2852 3	<i>PAXBP1</i>	Q9Y5B6	1,42533	-3,80199	0	26,757 4	557	S	AREQTGKMADHLEGLSSDDEETSTDITNF NL
UID2491 7	<i>PELP1</i>	Q8IZL8	2,17346	-3,27119	0	26,075 6	485	S	ADALKLRSRPGSPDGLQTGKPSAPKCLK LD
UID7149	<i>PRDM2</i>	Q13029	1,75865	-1,59707	0	24,461 8	739	S	SMLPVTSSRFKRTSSPPSPQHSPALRDF G
UID9258	<i>RBBP6</i>	Q7Z6E9	3,86433	-2,66185	0	25,311	1699	S	QVGISRNQSHSPSPSRSHSPSGSQTRSH
UID6526	<i>RPS3A</i>	P61247	2,09668	-2,08137	0	24,582 7	236	S	PKFELGKLMELHGEGSSGKATGDETGAKE VE
UID1805 6	<i>SCAF11</i>	F8VXG7	3,02145	-1,931	0	24,900 8	688	S	RSPKRDTTRESRRSELSPRRETSRENKRS Q
UID1773	<i>SRRT</i>	C9JUL9	2,12054	-1,95044	0	24,661 5	11	S	____MAPSDRAMGDSDEYDRRRRDKFR RE
UID6864	<i>SRSF11</i>	Q05519	4,17754	-9,0552	0	31,972 9	449	S	SEKEKKEKKPIETGSPKTKESVKEGTGD S
UID8408	<i>UBR4</i>	Q5T4S7	3,89185	-3,93232	0	26,272 5	1760	S	FQSEPRIESLVRHASTSSPADKAKVTISD G
UID1568	<i>USP39</i>	B9A018	2,45224	-2,63278	0	25,371 9	43	S	VKREDREREPEAASSRGPVVRVKREFEP AS
UID1195 9	<i>ANLN</i>	Q9NQW6	2,4176	-3,46981	0	26,190 5	65	S	QQPLSGGEEKSCTKPSKRCSDNTEVE VS
UID1717 4	<i>CLASP2</i>	E3W994	2,82457	-3,43792	0	25,677 5	529	S	ARSSRIPRPSVSGQCSREASRESSRDTSPVR
UID2714 4	<i>CWC22</i>	Q9HCG8	3,27482	-1,9837	0	24,961 3	61	S	FDYSRSDYEHRRGRSYDSSMESRNRDRE KR

UID8000	<i>DBNI</i>	Q16643	2,52321	-2,23062	0	24,990	339	S	SHRRMAPTPIPTRSPSDSSTASTPVAEQIER
UID4122	<i>FYB</i>	O15117	2,69347	-2,25251	0	25,244	209	S	PKPAFGQKPLSTENSHEDESPMKNVSSS KG
UID2462 2	<i>KTNI</i>	Q86UP2	1,9361	-2,04979	0	24,776	75	S	KKNKKKEIQNGLHESDSESVPRDFKLS DAL
UID2447	<i>LMO7</i>	E9PMS6	4,33436	-4,71109	0	27,290	316	S	QKWQDDLAKWKDRRKSYSIDLQKKKEE REEI
UID9371	<i>LUZP1</i>	Q86V48	2,76122	-3,51584	0	25,824	440	S	SFTNRRAAKASHMGVSTDSGTQETKKTE DRF
UID7357	<i>MYO9B</i>	Q13459	2,86149	-3,56847	0	26,747	1972	S	GDEDREKEILIERIQSIKEEKEDITYRLPEL
UID9136	<i>SETX</i>	Q7Z333	2,15569	-1,95276	0	24,290	642	S	MGKTSRKDMHCLEASSPTFSKEPMKVQD SVL
UID981	<i>TJP2</i>	A0A1B0GT W1	1,37164	-2,40028	0	25,054	229	S	YSERSRLNSHGGRSRWEDSPERGRPHER AR
UID6983	<i>AHNAK</i>	Q09666	1,75803	-2,2796	0	25,435	5731	S	KFNFSKPKGKGGVTGSPEASISGSKGDLK SS
UID2134 7	<i>ATRX</i>	P46100	2,21981	-2,68854	0	25,395	675	S	KTTPLRRPTETNPVTSNSDEECNETVKEK QK
UID6628	<i>BASPI</i>	P80723	3,10991	-4,6497	0	27,290	194	S	AAPSSKETPAATEAPSTPKAQGPAASAE P
UID2679	<i>CCDC82</i>	F5H777	1,53395	-2,06881	0	24,969	219	S	KVGVKRPRRVVEDEGSSVEMEQTPEKT LAA
UID1438 3	<i>CENPC</i>	Q03188	4,39618	-2,24372	0	25,193	130	T	EVHQKILATDVSSKNTPDSSKISSRNINDH H
UID902	<i>DENND4 A</i>	A0A0U1RR2 7	2,22261	-2,58959	0	24,786	966	S	GYNSLSKDEVRRGDTSTEDIQEEKDKKGS DC
UID8794	<i>DHX57</i>	Q6P158	3,56005	-2,8242	0	25,112	74	S	DDGDDFCIFESRRSRPSNSNISKGESRPK
UID2934 4	<i>EIF3G</i>	O75821	1,43218	-1,71542	0	23,648	41	T	VTSELLKGIPLATGDTSPPELLPGAPLPPP
UID2894 1	<i>HMX3</i>	A6NHT5	2,0436	-2,70737	0	25,868	149	T	ASEKALLRDSSPASGTDSDRDSPELLKADP DH
UID1306 2	<i>INPP5F</i>	Q9Y2H2	1,77021	-1,20438	0	24,219	907	S	CGIIASAPRLGSRSQLSSTDSVHAPSEIT
UID7325	<i>PPIG</i>	Q13427	1,77154	-2,08697	0	25,283	745	S	NDHVHEKNKKFDHESSPGTDEDKSG____ —
UID501	<i>RRBP1</i>	A0A0A0MR V0	2,5356	-1,67658	0	24,363	1277	S	KSHVEDGDIAGAPASSPEAPPAEQDPVQL KT
UID7670	<i>RRP1B</i>	Q14684	1,82784	-2,40115	0	24,347	513	S	SQSGPSGSHQGRGSPGTGGAQLLKRKRK LG
UID5331	<i>SON</i>	P18583	2,0521	-1,5906	0	24,263	2129	S	QSKEDDDVIVNKPVSDEEEEEPPFYHHP FK
UID8638	<i>ZMYM4</i>	Q5VZL5	2,88464	-1,65957	0	24,049	1256	S	SPRSDPLGSTQDHALSQESSEPGCRVRSIK L
UID785	<i>MEF2C</i>	A0A0D9SGI5	2,09559	-2,85107	0	25,218	419	S	TPSRYPQHTRHEAGRSPVDSLSSCSSSYDG S

Mut = Mutant\_p.Asp32His, WT = Wild type, A.A = amino acid.

### 5.14.3 Phosphoproteomic perturbations in p.Asp32His mutant

Data analysis after applying FISHER test, revealed some interesting facts about certain kinases showing dysregulation of phosphorylation activity in mutant LCLs; foremost, 189

motifs belong to Calmodulin-dependent protein kinase II substrate are found hyper-phosphorylated in patient derived LCLs as compared to the wild type. Moreover, 377 substrates motifs of protein kinase A were found hyper-phosphorylated whereas 385 of its substrates were hypo-phosphorylated in patient cells. Similarly, 362 substrates of protein kinase C are hyper-phosphorylated whereas 375 are observed hypo-phosphorylated. In addition, 61 of  $\beta$ -Adrenergic Receptor kinase substrates and Casein kinase I substrates are also found hyperphosphorylated. To be noted that 68 of the Casein kinase I substrates are hypophosphorylated as well (Table 5.12).

**Table 5.12: Whole phosphoproteome analysis of p.Asp32His patient LCLs.**

Substrates	Hyper-phosphorylated Substrates	Hypo-phosphorylated Substrates	P value	Benjamini-Hochberg False discovery rate (FDR)
PKA kinase substrate	377	385	3.30E-06	7.58E-05
PKC kinase substrate	362	375	1.64E-06	5.03E-05
Calmodulin-dependent protein kinase II substrate	189	0	0.0033738	0.038799
$\beta$ -Adrenergic Receptor kinase substrate	61	0.59746	3.81E-07	3.51E-05
Casein kinase I substrate	61	68	0.0014452	0.018993

Note: Student t-test difference  $> -2$ . P values and Benjamini-Hochberg false discovery rate (FDR) is mentioned in the table.

## 5.15 Whole transcriptome profiling — connecting the dots in bigger picture

For revealing the effects of *CSNK2B* mutation on whole transcriptome of c. 94G>A; p.Asp32His mutant, RNA sequencing was carried out on wild type and mutant LCLs, in two replicates. Regarding sequence libraries, an average reads mapped were 131.8 M and 105.8 M whereas aligned reads obtained were 127.3 M and 100.5 M for wild type and c mutant RNA, respectively. In addition, ambiguous reads, obtained in all replicates of wild type and patient, were around 10.5 M which showed relatively good quality of data for further processing.

Data was being normalized using by DESEQ2 and FPKM (fragments per kilobase per million) were calculated. Data analysis showed 1022 DEGs (differentially expressed RefSeq

genes) (FC >5, P value <0.05) in wild-type and patient LCLs, where 650 of these DEGs were downregulated in patient LCLs whereas 362 were showing upregulation. Genes were filtered on the basis of pathways these were involved and trends of expression were noted. Heatmaps were generated based on FPKM values, using Heatmapper {Babicki, 2016 #189} to visualize the DEGs in Wnt signaling pathway and HOX cluster genes.

### 5.15.1 Pathway enrichment using PANTHER (protein analysis through evolutionary relationships)

Differentially expressed genes (FC >5, P value <0.05) were taken into account for pathway enrichment. For this purpose, an online available pathway enrichment tool PANTHER was utilized which provided the information that maximum number of genes was involved in Wnt signaling and immune response pathway shown by the highest peaks in the graphs generated by the above mentioned tool (Figure 5.37A). The genes involved in WNT signaling, were further explored where it was observed that three highest peaks were of those genes expressing cadherins, NFAT target genes and Wnt target genes (Figure 5.37B).

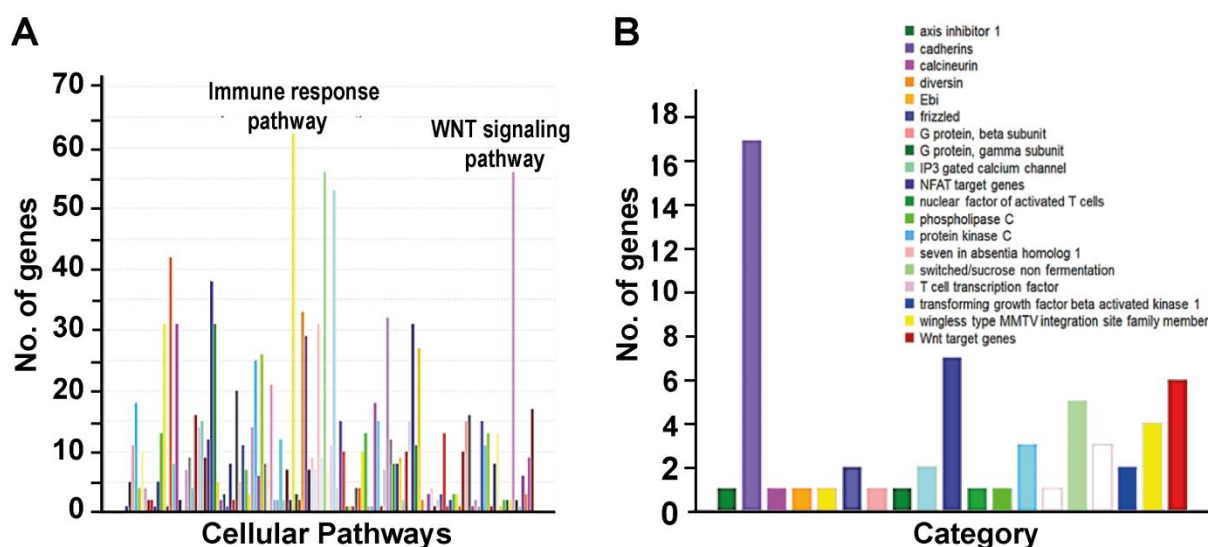


**Figure 5.37: Pathway enrichment of differentially expressed genes.**

(A) Graph depicts pathway enrichment of significantly differentially expressed genes obtained from RNA-seq data. Note that two of the highest peaks are related to the genes involved in immune response pathway and WNT signaling. X-axis shows number of genes and Y-axis shows cellular pathways. Fold Change (FC) >5, and P values <0.05. (B) Graph shows number of differentially expressed genes involved in WNT signaling pathway. X-axis shows number of genes and Y-axis shows category of the genes involved. Color scheme of each category is mentioned in the graph. Fold Change (FC) was >5, and P value <0.05.



### 5.15.2 Wnt target genes

It was interesting to notice that all the Wnt target genes (*CDH3*, *TCF7*, *WNT2*, *EPHX2*, *SMN*, *WNT2B*, *KLF4*, *TCF7L1*, *NR4A2*, *DVL2*, *APC2*, *AXIN2*, *RARG*, *WNT11*, *WNT2B*, *SDC2*, *FZD9*, *TCF7L1*, *TCF7L2*, *TCF7*, *EPHB4*, *BMP4*, *SOX9*, *SOX13*, *SALL4*, *TBX6*) were downregulated including *DVL3* (Figure 5.38). These results, once again, support the idea that CK2 $\beta$  is playing a pivotal role in the dysregulation of Wnt signaling. All of the Wnt target genes are highly expressed in brain such as *CDH3* and *TCF* and are considered crucial during events of brain development (Hirano and Takeichi 2012; Wisniewska 2013).

In addition, according to a study dysregulation of *BMP4* causes brain, bone and digit anomalies in humans (Bakrania, Efthymiou et al. 2008) which are certainly evident in the Filippi patient investigated in this study. Nonetheless, SOX genes are also highly expressed in brain; dysregulation due to mutation in *SOX9* is reported to cause a severe dwarfism associated with brain defects (Pompolo and Harley 2001).

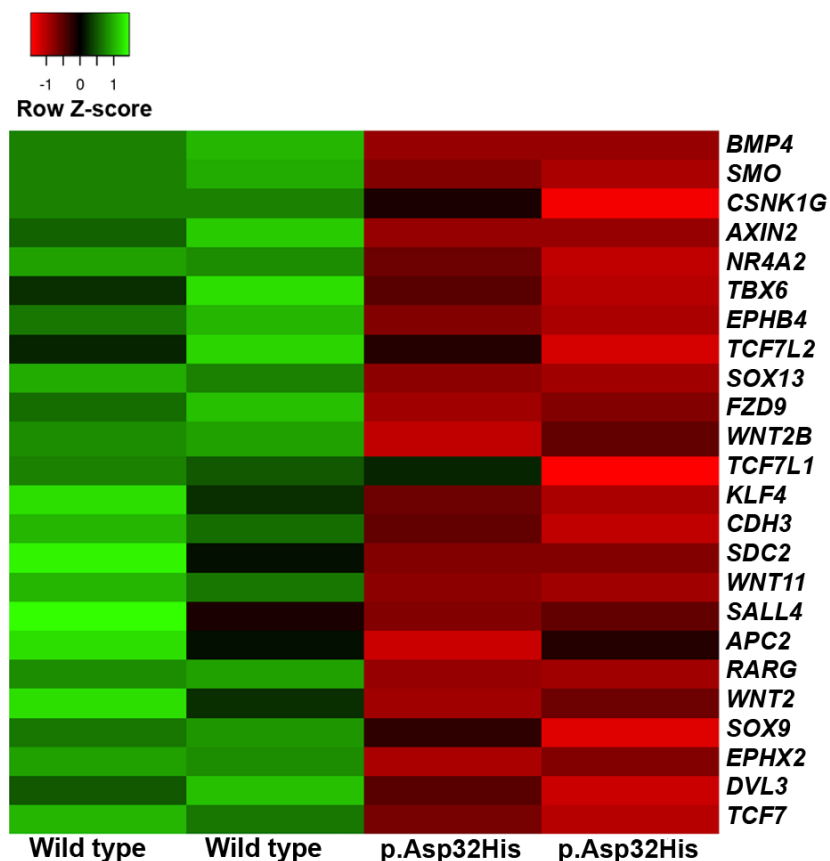


Figure 5.38: Heatmap of differentially expressed Wnt target genes in p.Asp32His mutant LCLs compared to control.

Color code is mentioned in the figure above. Fold Change (FC) was >5, and *P* values <0.05.

### 5.15.3 DNA damage response and repair regulators

The genes involved in DNA damage response are found upregulated including *CHEK1*, *TP53I3*, *H2AFX*, *INIP*, *XRCC4*, *EYA4*, *RAD51AP1*, *RAD51*, *UBE2T*, *EYA1*, *NTHL1*, *CASP6*, *CASP3*, *CASP9* and *CASP1* whereas *EGLN3* is downregulated being a negative regulator of this pathway (Figure 5.39A). In addition, the DNA repair genes, *INIP*, *NUDT1*, *FANCC*, *BTG2*, *NSMCE4A*, *NEIL3*, *UBE2T*, *DDB2*, *JMY*, *UVSSA*, *INTS3*, *MDC1*, *RNF168*, *INO80B*, *RAD52* and *INO80D*, were also observed highly differentially expressed (Figure 5.39B).

Similar to investigation of DNA damage response regulators at protein level, this data is further evidence of delayed response in patient LCLs and adds that the DNA damage repair genes may also be playing a role in dysregulation of Wnt signaling.

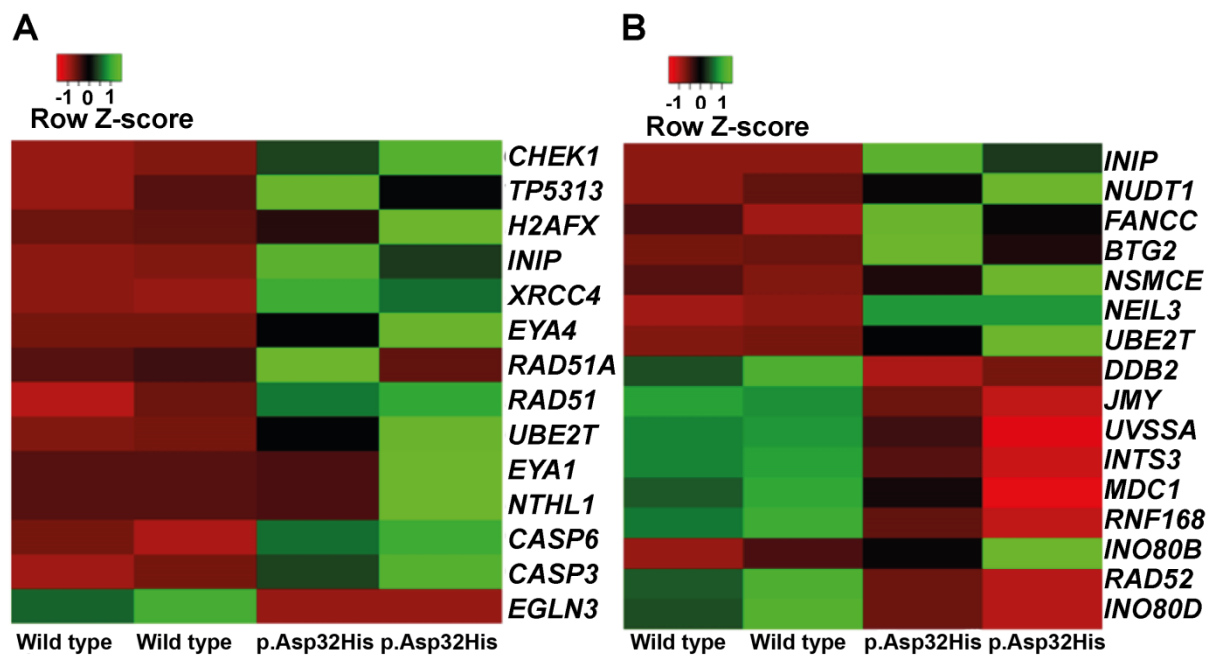


**Figure 5.39: Heat map of differentially regulated DNA damage and repair genes in p.Asp32His mutant LCLs compared to control.**

(A) Heatmap showing differentially expressed DNA damage regulator genes in wild-type LCLs as compared to mutant. Color code is mentioned on the top of the figure. Fold Change (FC) was >5, and *P* values <0.05. (B) Heatmap showing differentially expressed DNA repair related genes in wild-type LCLs as compared to mutant. Color code is mentioned on the top of the figure. Fold Change (FC) was >5, and *P* values <0.05).

#### **5.15.4 Transcription regulators**

As  $\beta$ -Catenin is a transcriptional co-factor and its investigation at protein level hinted a disturbance of transcriptional activities, on these grounds it was aimed to see the expression profiles of transcriptional regulators in RNA sequencing data. The data showed highly differentially expressed genes; those which were found downregulated were, *GATA4*, *DMRT1*, *FOS*, *TENM2*, *FOSB*, *TRIM29*, *EGFR*, *PADI2*, *HHEX*, *PRKCH*, *ASCL1*, *EOMES*, *DTX1*, *RIPK4* where *GATA4* was 50 times downregulated and showed maximum reduced expression among listed transcription regulators. Those genes which showed increased expression level were, *BHLHA15*, *TBX15*, *KLF2*, *MNX1*, *PTRF*, *EDNRB*, *PAX8*, *IFNG*, *TNF11*, *MYF6*, and *HGF* (Figure 5.40).

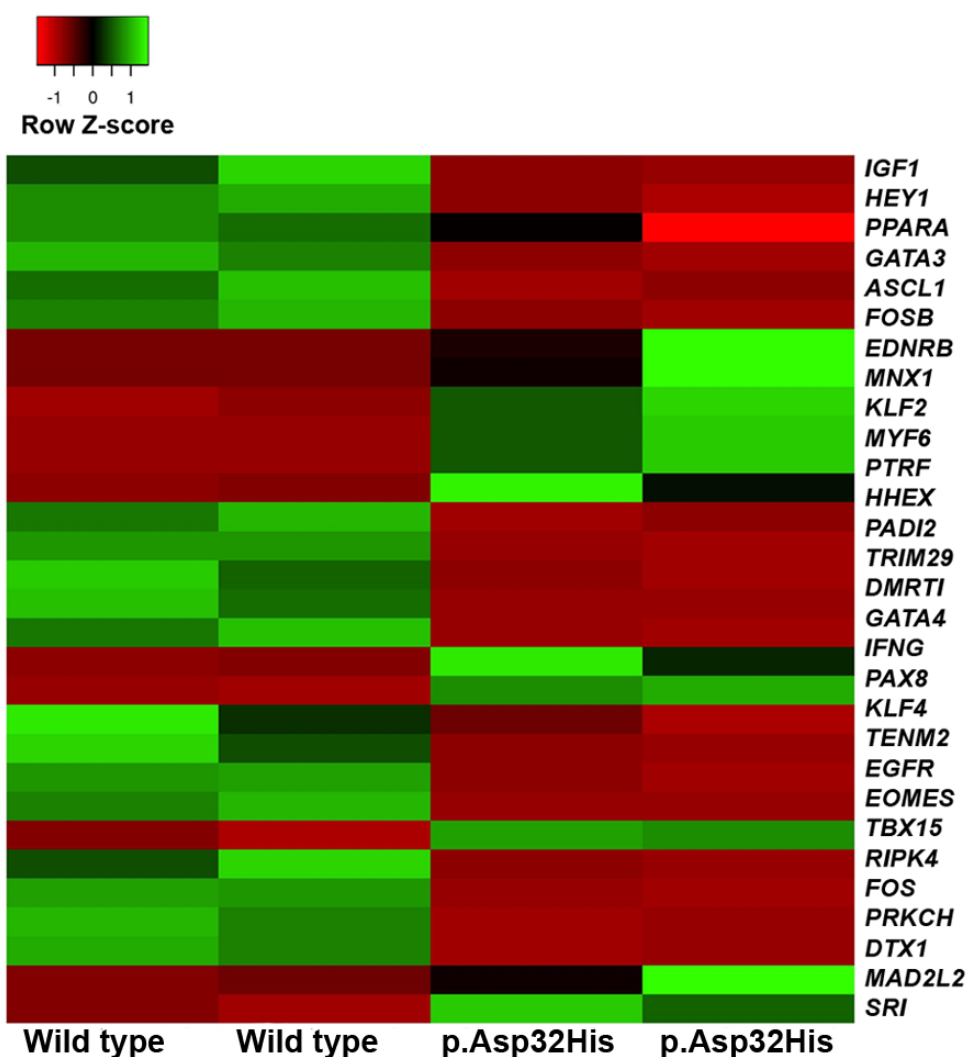


**Figure 5.40: Heatmap of differentially regulated transcription factors in p.Asp32His mutant LCLs compared to control.**

Color code is mentioned on the top side of the figure. Fold Change (FC) was >5, and  $p$  values <0.05.

### 5.15.5 Immune response genes

Regarding the maximum differential expression in whole transcriptome, highest number of genes were those, related to immune system response; *LILRA4*, *HAMP*, *TLR5*, *TREML4*, *IL18RAP*, *TNFRSF25*, *MASP2*, *CD4*, *EOMES*, *AIRE*, *THEMIS*, *VNN1*, *CCL1*, *F2RL1*, *CCR10OLR1*, *FCER1G*, *CHIA*, *ADGRE1*, *FCRL4*, *CCL25*, *PPARG*, *IL18*, *CD1A*, *TRIM31*, *CXCL13*, *CXCL10*, *CCL2*, *CCL4*, *IL12A*, *IL18*, *IL10*, *ILF2*, *IL17RE*, *IL1RAPL2*, *IL17A*, *IL6*, *IL19*, *ICAM2*, *TLR4*, *TLR2* and *SIX1*. As the differential expression was huge, it

was obligatory to review the phenotypic profile of patient for developing a link between differential expression of immune response genes and patient disease profile. For this purpose, blood profile of patient was obtained which showed comparatively high levels of IgM (immunoglobulin M); 253 mg/dL as compared to normal range which is 40-230 mg/dL and the only infection noticed was recurrent osiosis. This is a known fact that *CSNK2B* is a member of major histocompatibility complex and in that regard the differential expression can be related but further validation is also required (Gibson and Benveniste 2018).

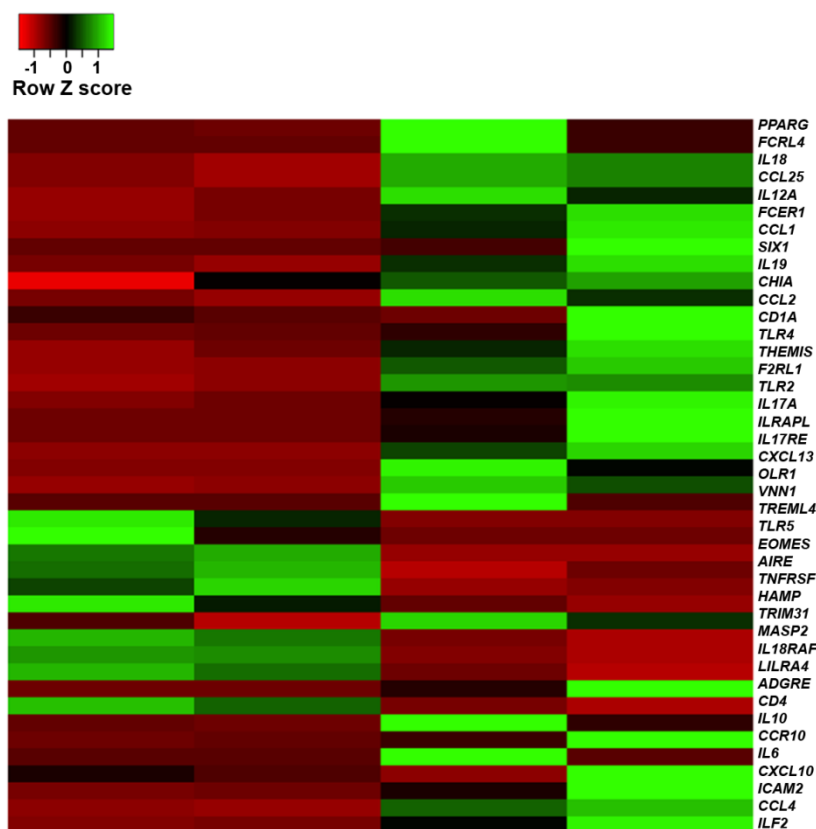


**Figure 5.41: Heatmap of differentially regulated immune response genes in p.Asp32His mutant and control LCLs.**

Color code is mentioned on the top of the figure. Fold Change (FC) was  $>5$ , and  $P$  values  $<0.05$ .

## 5.16 Proposed disease model

Based on all the investigations carried out, a disease model is being suggested (Figure 5.42). Disease model depicts that CK2 acts as a master regulator in the disease frame as the pathogenicity of disease is dependent on positive and negative regulation of CK2; due to mutation in *CSNK2B* the protein is abnormally high and presenting impaired function in the Wnt signaling pathway as well as DNA damage response pathway. In general, the mutations cause disturbances in whole proteomic and phosphoproteomic profiles of patients. Due to impaired phosphorylation activity of mutant CK2 and loss of interaction with crucial regulators of Wnt signaling,  $\beta$ -Catenin and DVL3, proteasomal degradation of  $\beta$ -Catenin and transcription wide events are being influenced which consequently resulted in severe clinical phenotype, Filippi syndrome. Though, the differences in the phenotype of patients can be explained by pleiotropic effects of the mutations.

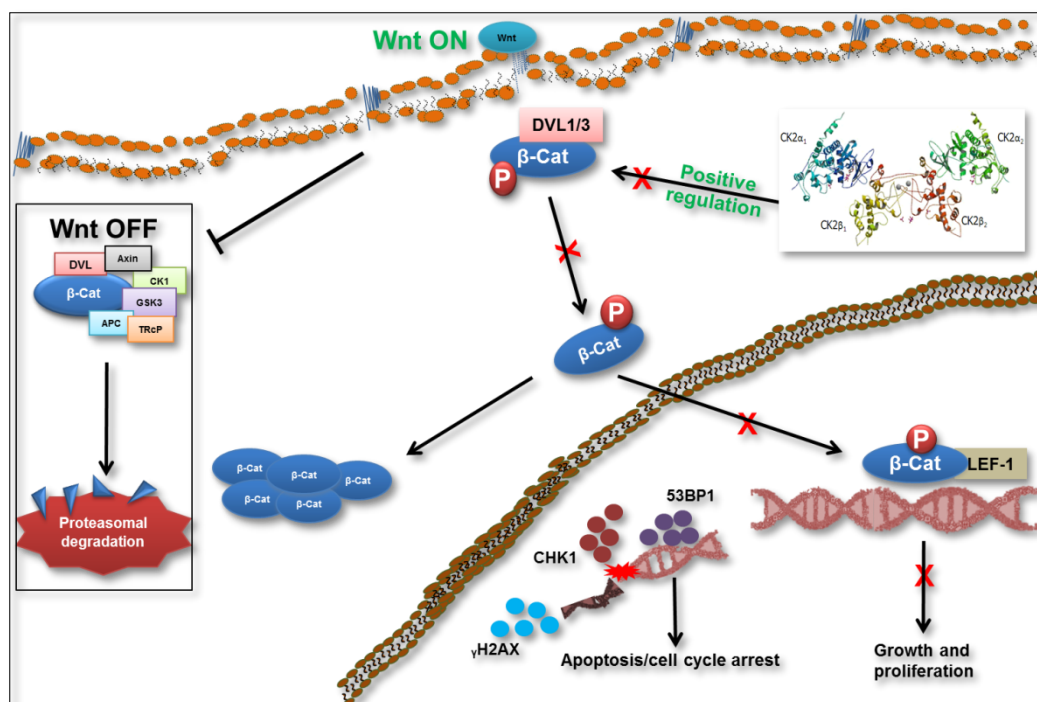


**Figure 5.42: Proposed disease model of FLPIS caused due to variations in *CSNK2B*.**

Note that in the center the structure of CK2 $\beta$  is adopted from SWISS Prot.

## 6. Discussion

Mendelian disorders are generally severe and unfathomed. As vast as oceans is human genome; identifying variants for these disorders remain as difficult as searching a pin dropped in an ocean. Although Mendelian disorders are rare, yet the cumulative incidence and associated social and economic impact is alarming. As a matter of fact, around 80% known rare diseases are covered under the title of single gene disorders (Blencowe, Moorthie et al. 2018). Based on the available public consortia (100,000 UK genome project, 1000 genome project, The Exome Aggregation Consortium (ExAC), DiscovEHR), sequencing of over 500,000 individuals revealed that genome of each individual contains ~100–300 autosomal recessive variants which are predicted to be damaging at protein level (Xue, Chen et al. 2012). Additionally, the updated version of ExAC called gnomAD (genome aggregation database) contains 125,748 exome sequences having 515,326 variants, this dataset is also helping scientific and researcher to find the culprit gene (Karczewski and Francioli 2017; Francioli, Tiao et al. 2018). Adding to this dilemma, the practice of consanguineous marriages increases the prevalence of rare recessive diseases (Modell and Darr 2002). Nevertheless, medical genetic anomalies are found in offsprings of unrelated parents as well. Mutations inherited in autosomal recessive manner had remained main focus for exploring genetic diseases due to their relative feasibility of identification, however, *de novo* mutations that are equally relevant for frequently contributing in sporadic cases of rare Mendelian diseases remain largely underexplored. With the advent of massively parallel sequencing technologies, identifying *de novo* variants, previously difficult to explore using conventional techniques, has become attainable. In addition, the revelation of genetic variants and disease pathogenesis is accelerated due to cost effectiveness of sequencing techniques and extensive collaborations established between clinicians and researchers.

For understanding the disease pathomechanism, functional characterization of a genetic variant is instrumental. Various animal models have been traditionally and successfully utilized to study phenotypic consequences of genetic variants. Notwithstanding, patient derived cells or organs depict more native context thus offers better insight into the pathogenesis. (Quadrato, Nguyen et al. 2017). Nevertheless, for reaching the milestone of treatment strategies, there is still a need of extensive clinical and genomic data as well as

deeper biochemical knowledge as reported cases of many rare diseases are still too scarce to be conclusive.

## **6.1 Prediction tools are effective for determining pathogenicity at gene and protein level**

The recent explosion in the availability and applications of bioinformatics tools has greatly facilitated the identification of potential candidate genes and their consequences at protein level. Based on available public databases of human genome variations, such as Genome Aggregation Database (gnomAD), Iranome, dbSNP and the Greater Middle Eastern (GME) Variome, neutral polymorphisms can be screened out. The effect of rare or previously undocumented variants can be predicted using multiple tools such as Combined Annotation Dependent Depletion (CADD), Mutation Taster and NetGene2 Server. Taking a step further, some bioinformatics tools such as PolyPhen-2, SIFT, PROVEAN and PyMOL can predict pathogenicity and structural defects in local context of the protein. This study also demonstrated the utility of these aforementioned tools that successfully identified novel genes of microcephaly and Filippi syndrome. These *in silico* predictions were authenticated by the downstream biochemical investigations.

## **6.2 Microcephaly — extensive phenotypic and genotypic spectra**

In this study, 16 families of different ethnicities and geographical territories have been investigated, covering Asian, European and Middle Eastern origins. Congenital microcephaly was consistently featured by all the patients, though some patients presented varying additional symptoms leading to be categorized in different syndromes. The phenotypic spectra in patients ranged from isolated primary microcephaly to association of specific kidney defects as well as global defects including facial dysmorphism, syndactyly and growth retardation.

Referring to the genetic underpinnings of primary microcephaly, 25 genes have previously been attributed to cause the disease and most of these encode centrosomal proteins (Chavali, Pütz et al. 2014). This study illustrates the contribution of non-centrosomal proteins, the nucleoporins, causing primary microcephaly. In addition, this study also supports the idea that syndromes of microcephaly show similarly heterogeneous genetic basis; investigations of Filippi syndrome show two different pathways being involved in disease manifestation; Wnt



signaling and DNA damage response pathway. Whereas, previously, Filippi syndrome was known to be only associated with cytoskeleton-associated protein 2-like (CKAP2L). Considering the above mentioned facts, it is evident that microcephaly is appearing to have heterogeneous genetic basis with multiple explanations of disease pathogenicity whereas traditionally it was known as centriolopathy (Jayaraman, Kodani et al. 2016).

### **6.2.1 A novel variant of *STIL* — addition to the existing knowledge**

As an addition to existing knowledge, whole-exome sequencing revealed a novel (and so far 12<sup>th</sup>) variant (c.3694C>T; p.(Arg1232\*)) of a previously reported gene, *STIL* (NM\_001048166.1), (Kumar, Girimaji et al. 2009) in a family afflicting primary microcephaly. *STIL* encodes SCL-interrupting locus protein, consists of 18 exons. It is ubiquitously expressed in proliferating cells and localizes on mitotic spindles and pericentriolar region and plays role in proper mitotic spindle organization in zebrafish and human (Pfaff, Straub et al. 2007). This mutation, presumably, results into truncated proteins, if being made, that lack C-terminal KEN box — a motif required for recognition by anaphase-promoting complex/cyclosome (APC/C) and degradation by proteasome. The disruption of this motif leads to accumulation of mutated protein product in cytoplasm that compromise the centrosomal amplification, though it does not affect the localization and function of protein *per se* (Cristofoli, De Keersmaecker et al. 2017).

### **6.2.2 *SH2D3C* is a promising novel candidate gene of primary microcephaly**

A family recruited from Pakistan presented two patients of typical MCPH. Careful analysis of WES revealed that *SH2D3C* is the strongest novel candidate gene. The candidate gene selection was based on stringent selection criteria. Initially, the variation(s) in genes falling within the homozygous regions were thoroughly studied with respect to functional relevance and allele frequency; as none was filtered out. Therefore, genes residing outside the linkage regions were further analyzed. Three genes *AJMI*, *DNHA11* and *SH2D3C* fulfilled the above-mentioned criteria but only *SH2D3C* was segregated in the family. *SH2D3C* is known to have multiple transcripts; the mutation found in my patients is a splice site mutation present only in one transcript (NM\_170600.3) which is 12 exons long. The mutation studies demonstrated that this *SH2D3C* (also known as Shep1) is highly expressed in brain and vasculature (Sakakibara and Hattori 2000; Wang, Vervoort et al. 2010).

Shep1 is a multidomain signaling protein, mainly involved in the regulation of cell morphology, adhesion and migration (Vervoort, Roselli et al. 2007). A very elegant study carried out by Wang et al comprehensively explained the role and expression of Shep1 in sensory axons extending to the forebrain of knockout mice. The homozygous knock-out mice were not viable, whereas the heterozygous were viable and fertile. The abnormalities noticed in the developing brain of the homozygotes were impaired sensory neuronal connections with the olfactory bulb, a visible reduction in the size of olfactory bulb size and disruption of bulb lamination (Wang, Vervoort et al. 2010). However, the study did not highlight phenotype of forebrain in specific.

Regarding my *SH2D3C* mutated patients, it is likely that the mutated transcript may have highest expression in brain and crucially required for embryonic brain development. Thus, on the basis of functional relevance demonstrated by previous studies and genetic underpinnings found in this study (splice variant having extremely low allele frequency), it is concluded that *SH2D3C* holds a great potential to be further explored as novel candidate gene of microcephaly.

### **6.2.3 Mutations in NUP genes — presenting non-syndromic and syndromic microcephaly**

In continuation of the arguments of syndromic and non-syndromic microcephaly, first family of primary microcephaly mutated with *NUP37* investigated in this study is a representative case. This family was afflicted with primary microcephaly and clinodactyly of both hands (Braun, Lovric et al. 2018). Linkage analysis and whole-exome sequencing analysis showed a nonsense variant (c.916C>T; p.(Arg306\*)) in *NUP37* gene. Sanger sequencing confirmed the co-segregation of this variant with the disease. This gene encodes for a nuclear pore protein and is a component of nuclear pore complex called Y complex located in the inner ring of the nuclear pore (Beck and Hurt 2016). This protein is involved in the protein trafficking across the nuclear envelop as well as in cell division (Chakraborty, Wang et al. 2008). As mutations in other nucleoporin proteins are known to impair renal function, these patients were also clinically investigated for kidney abnormalities (Braun, Lovric et al. 2018). All the three patients were found normal for renal function.

#### **6.2.4 Reduced nucleoporin proteins cause gross cellular abnormalities leading to disease phenotype**

Functional characterization of this variant showed significant reduction on the transcript and protein level in patient derived fibroblasts as compared to the wild type. The effect of reduced protein level was examined on the binding partners of NUP37 in Y complex, namely NUP107 and NUP160. It was observed that expression of binding partner proteins was reduced, they were also found mislocalised in the patient derived fibroblasts. An overall density of nuclear pores was also reduced. These results are consistent with previous studies reporting that the knockdown of *NUP107* and *NUP133* causes depletion of associated nucleoporins and effect nuclear pore density as a whole (Walther, Alves et al. 2003). Additionally, cellular abnormalities were also explored which showed that reduced NUP37 causes irregular heterochromatin arrangement. It also compromises the nuclear shape as the nucleus appeared distorted with bulbous invasions of nuclear envelope. These findings were also in line with the previous studies where depletion of nucleoporins, NUP133 and NUP107, caused similar nuclear abnormalities (Walther, Alves et al. 2003; Hetzer 2010). Moreover, mutation in *NUP37* indicated reduced growth rate of patient fibroblasts which hints that mutation impairs cell division dynamics. This finding further validates previous reports of NUPs including NUP37 being localized on the kinetochore during mitosis and maintaining the proper arrangement and segregation of chromosome. (Loiodice, Alves et al. 2004). Based on these facts, it is conceivable to say that hypomorphic mutation in NUP37 abrogates the nuclear pore complex assembly — an argument showing additional roles of NUP37 in cell division and might affect differentiation of neural progenitors during development (Lupu, Alves et al. 2008).

#### **6.2.5 Variable phenotypic spectra in NUP mutated individuals**

I also studied mutants of another nucleoporin gene and binding partner of *NUP37* protein — *NUP107* — to validate the findings of *NUP37* mutants. All the affected individuals segregating *NUP107* mutation (NM\_020401.4:c.303G>A; p.Met101Ile) were clinically diagnosed with microcephaly. The genetic investigation of *NUP107* mutated family is already published (Braun, Lovric et al. 2018). Clinical investigations of these patients showed that all the affected individuals manifested end stage renal failure – steroid resistant nephrotic syndrome (SRNS). The components of nuclear pore complex, NUP133 (direct binding partner of NUP107), NUP160 and NUP37 were examined in patient derived LCLs. It was observed

that mutation in *NUP107* leads to reduction of its protein product, similar to that of *NUP37* and all the investigated NUPs were downregulated and mislocalized at the nuclear envelop. These findings further validate the consequences of reduction of nuclear pore density due to hypomorphic mutation.

It was intriguing to observe that patients segregating *NUP37* mutation did not show any symptoms of steroid resistant nephrotic syndrome, diagnosed in *NUP107* mutated individuals. Instead, *NUP37* mutated individuals manifested clinodactyly which may be occurring due some variant being segregated in the family. Although both, *NUP37* and *NUP107*, have hypomorphic mutations as immunoblotting shows a certain amount of protein existing in *NUP37* mutated patient derived fibroblasts and *NUP107* mutated LCLs which could be still functional to perform low level of cellular activities. In this regard, a collaborative publication of this study and Braun et al (2018) must be mentioned here; both the hypomorphic and null mutations of *NUP107* were modeled in zebrafish by CRISPR/Cas/9 mediated genome editing, which showed that truncating mutation (c.50\_56del7; p.Thr81Argfs\*74) causes early lethality and developmental defects including microcephaly whereas in frame hypomorphic mutation (c.137\_139del; p.Ala46delAla) was compatible with embryonic survival. These findings, thus reflect the role of allelism in variable phenotypic spectra and inversely relate the residual function of gene with general severity of the disease (Duerinckx and Abramowicz 2018).

Interestingly, the published cases of impaired *NUP107* show predominantly SRNS phenotype, except one family of microcephaly associated SRNS segregating the mutation (c.303G>A, p.Met101Ile) in *NUP107* (Miyake, Tsukaguchi et al. 2015; Cragan, Isenburg et al. 2016; Braun, Lovric et al. 2018). In addition, hypomorphic mutations in other NUP genes such as *NUP85*, *NUP93*, *NUP205* and *NUP160* are also previously known to cause SRNS without microcephaly (Braun, Sadowski et al. 2016; Braun, Lovric et al. 2018). An exception however is exhibited in another NUP protein, *NUP133* — the direct binding partner of *NUP107* — where a loss-of-function mutation (c.3335-11T>A) leads to Galloway-Mowat syndrome which is characterized by early onset nephrotic syndrome, hiatus hernia and microcephaly. The mutation caused an abrogation of interaction between *NUP107* and *NUP133* leading to reduction of both proteins which can be related to the severity of the disease (Fujita, Tsukaguchi et al. 2018). However, the missense mutation in *NUP133* caused SRNS only (Braun, Lovric et al. 2018). Thus, it is convincing to deduce that hypomorphic mutations show milder phenotypes, whereas, loss-of-function mutations lead to severe medical

consequences affecting brain development along with other organs such as kidney in SRNS. Moreover, the age of onset of disease could also be one possible reason that *NUP37* mutated affected individuals did not show any symptoms of SRNS.

On the other hand, inherited variant of *NUP214* has shown phenotypic variability on the other end of the spectrum. A missense mutation in this gene is reported to cause severe encephalopathy and early death, whereas SRNS was not manifested (Shamseldin, Makhseed et al. 2019). The severity of disease here in case of *NUP214*, again, raises question on phenotypic spectra depicted by variations in other NUP genes. As a total exception, if I take *NUP93* into account, the reported variant shows no relevance with SRNS or microcephaly; instead it is reported for non-progressive congenital ataxia (Zanni, De Magistris et al. 2019). The phenotypic spectra of NUPs are given below (Table 6.1). Conclusively, it can be speculated that the demand for normal nucleocytoplasmic transport differs among organs, and that the brain may be particularly vulnerable to impairment of such a fundamental cellular function.

**Table 6.1: Reported phenotypes caused due to variations in NUP genes.**

Gene	Microcephaly	SRNS	Other reported phenotypes	Reference
<i>NUP107</i>	+	+	None	(Braun, Lovric et al. 2018)
<i>NUP133</i>	+	+	Galloway-Mowat syndrome	(Braun, Lovric et al. 2018; Fujita, Tsukaguchi et al. 2018)
<i>NUP93</i>	-	+	Congenital ataxia	(Braun, Sadowski et al. 2016; Zanni, De Magistris et al. 2019)
<i>NUP205</i>	-	+	None	(Braun, Sadowski et al. 2016)
<i>NUP160</i>	-	+	None	(Braun, Lovric et al. 2018)
<i>NUP85</i>	-	+	Short stature, hematuria	(Braun, Lovric et al. 2018)
<i>NUP37</i>	+	-	Clinodactyly	(Braun, Lovric et al. 2018)
<i>NUP214</i>	+	-	Severe encephalopathy	(Shamseldin, Makhseed et al. 2019)
<i>NUP62</i>	-	-	Bilateral striatal necrosis	(Basel-Vanagaite, Muncher et al. 2006)

The symbol of plus indicates presence of phenotype, whereas minus indicates otherwise.

### **6.3 The shift from non-syndromic to syndromic microcephaly remains unsolved**

Genetic etiology and phenotypic spectra of microcephaly and associated syndromes is heterogenous. The shift from primary microcephaly to syndromic microcephaly is evident in case of NUP mutations. This shift has been demonstrated by previous studies as well; a few genes, such as *CENPJ*, *CEP152* and *CEP135*, are known to cause primary microcephaly yet

also attributed to microcephaly associated with primordial dwarfism (MAPD) (Shaheen, Maddirevula et al. 2019). This genetic overlap suggested that microcephaly primordial dwarfism is a phenotypic continuum of primary microcephaly. The mechanism explaining variability of phenotypic spectra of closely related NUP proteins however remains debatable. The question still demands critical attention as to why some mutations cause mild isolated phenotypes in some case, whereas in other, these tend to appear in lethal syndromic form. Nonetheless, it can be assumed that the mutations causing complete loss of protein may increase the severity of the disease and manifests microcephaly associated syndrome, whereas, mutations compromising the function only partially, may only cause a brain restricted phenotype (Bettencourt-Dias, Hildebrandt et al. 2011). It is also noteworthy that on the basis of this controversy of phenotypic relation to genotype, the definition of primary microcephaly needs to be modified (Shaheen, Maddirevula et al. 2019).

Other speculation could be the role of modifying genetic factors (as explained in case of *WDR62* mutation causing microcephaly (Poulton, Schot et al. 2014) or epigenetic changes in addition to the causative gene. Furthermore, the phenomenon can also depend on the expression of protein; ubiquitously expressed protein and its high demand in the cellular activity might cause a severe phenotype as compared to the one which is exclusively expressed during brain development.

#### **6.4 Filippi Syndrome — microcephaly remains part of a severe syndrome**

The second domain of this study included families segregating a rare disorder Filippi syndrome. A cohort (13) of Filippi patients was recruited from different parts of the world. All (except FP16) FLPIS cases were born to non-consanguineous parents, with no prior history of FLPIS in extended family. As it is an extremely rare disorder, only 32 cases are reported throughout the world (Goyal, Goyal et al. 2015; Capecchi, Baldassarri et al. 2018; Sabir, Walker et al. 2019). Its genetic etiology remained unknown until Hussain et al, from our group, in 2014 performed the first thorough molecular genetic investigation of this syndrome. In that study, *CKAP2L* was shown as the first causative gene for this syndrome, explaining the pathogenic aspects of identified variants on protein level as well (Hussain, Battaglia et al. 2014).

#### **6.4.1 The wild card regulator of kinases, *CSNK2B*, is the second disease causing gene of Filippi syndrome**

This study investigated functional consequences of a *de novo* mutation of *CSNK2B* gene NM\_001320.5;c.94G>C;p.Asp32His, in an Italian patient (FP2) from the cohort of Hussain et al, 2014, showing typical features of FLPIS such as microcephaly, syndactyly of fingers and toes (fourth and fifth digits), facial dysmorphism and intellectual disability. Sanger sequencing of the proband excluded mutations in reported FLPIS gene *CKAP2L*. Trio whole-exome was later carried out which revealed *CSNK2B* as a potential candidate gene. It was already reported that knockout mouse model of *Csnk2b* is embryonic lethal (Homma and Homma 2008). This gene (NM\_001320.6) encodes a peptide of 215 amino acids known as the beta subunit (CK2 $\beta$ ) of casein kinase 2, that is a serine/threonine holoenzyme composed of two alpha and 2 beta subunits (Niefind, Guerra et al. 2001).

#### **6.4.2 Expanding the mutational and phenotypic horizon of *CSNK2B***

Through GeneMatcher, two further *de novo* variants of *CSNK2B* were identified in two patients (FP28 and FP30). Exome data showed that FP2 and FP28 mutants harbored mutations, c.94G>C;p.Asp32His and c.94G>A;p.Asp32Asn, respectively at the same codon. Mutated residue is highly conserved among different species. Finally, a truncating mutation c.374C>G;p.Ser125\* was identified in the third mutant, originated from Israel (FP30),

All of the three patients shared the phenotype of intellectual disability, facial dimorphism, short stature, developmental delay and epilepsy. However, phenotypic variability of craniodigital features was obvious. It was noticed that the phenotypic similarity in terms of facial gestalt was striking in FP2 and FP28; these features included deep set eyes, broad nasal bridge, thin lower lips, strawberry shaped chin and broad/square face. However, FP28 mutant did not show the phenotype of microcephaly and syndactyly observed in FP2 mutant only. Instead of syndactyly, the patient of FP28 family depicted the phenotype of hands which included clinodactyly and tapering of the fingers. Additionally, pronation of feet was also visible in FP28 mutant. Regarding FP30, no limb/digital or cranial deformity was noticed.

The phenotypic variability observed in all the cases can be related to the pleiotropic effects of the mutations. The data obtained from the ectopic expression of all the mutant proteins in HeLa cells showed that p.Asp32His and p.Asp32Asn caused accumulation of mutant CK2 $\beta$  whereas p.Ser125\* showed considerable reduction. The difference in the amount of CK2 $\beta$  in

all the mutants may show variable effects on the protein function and thus the phenotype of the patient as a whole.

Previously, *CSNK2B* variants has been reported with Poirier-Bienvenu neurodevelopmental syndrome (POBINDS; MIM 618732) (Poirier, Hubert et al. 2017). However, this study showed three patients (FP2, FP28 and FP30) afflicted with a syndrome distinguished from POBINDS phenotypically. It is also noteworthy that *CSNK2B* variants has always been related to epilepsy with or without associated abnormalities; a very recent publication (Alvarado, Bos et al. 2019) showed ten *de novo* variants of *CSNK2B* in nine patients manifested with epilepsy. My study further validates this fact as epilepsy is one of the clinical features of all the cases.

## **6.5 Why *CSNK2B* is chosen as the strongest candidate gene for this study?**

All the reasons for selecting *CSNK2B* as a candidate gene for Filippi syndrome would be addressed one by one as follow:

### **6.5.1 Extensive genetic investigations**

Three different approaches were adopted for revealing the genetic causes of disease afflicted patient (FP2). As first attempt, linkage analysis was carried out which did not provide with any homozygous region with significant LOD score due to small family size. Following that, exome sequencing and copy number variations (CNVs) analysis was conducted with no answers and the case remained unsolved. Additionally, trio whole-exome sequencing revealed a few numbers of recessive and compound heterozygous variants which were excluded on the basis of allele frequency. However, the list of *de novo* variants provided two variants (only); *CSNK2B* and *MTM1*. *CSNK2B* was chosen due to more functional bias as compared to *MTM1*. In case of FP30, chromosomal microarray analysis and fragile X syndrome analysis was also performed for further confirmation.

### **6.5.2 *In silico* prediction of pathogenicity of *CSNK2B* variants in relation with CK2 $\beta$ protein domains**

The potential of disease causation was indicated by the variant pathogenicity prediction tools; gnomAD showed that *CSNK2B* is highly intolerant to missense mutations ( $Z$  score= 3.0) as well as loss of function mutations (pLI score=0.92). Various other tools including Mutation



Taster, SIFT and PolyPhen-2, PROVEAN, SNAP2, Meta SNP, I-Mutant, PANTHER and MUpro also validated the pathogenicity of identified *de novo* variants of *CSNK2B*.

To gain further insight into the resultant structural changes caused due substituted amino acid, *in silico* protein model prediction using PyMOL was carried out.. Based on these *in silico* findings, it was hypothesized that the mutations (p.Asp32His and p.Asp32Asn) may impair the interaction with CK2 $\alpha$  — another subunit of a casein kinase 2 (CK2) holoenzyme. Interestingly, both missense mutations are located in the KEN box like sequence in CK2 $\beta$  (32-DKFNLTGLN-40) which was previously known for participating in cell cycle dependent protein degradation (Sajnaga, Szyszka et al. 2013). The exact role of KEN box has not been characterized in CK2 $\beta$  but considering its location in CK2 $\beta$  which is adjacent to the destruction box (attributed for proteasome degradation) it can be assumed that KEN box in CK2 $\beta$  may also be playing the same role in CK2 as in other kinases. In addition, the CK2 $\beta$  residues from position 20 to 33 are also reported for being important for functioning of CK2 $\beta$  as ectokinase (Rodriguez, Contreras et al. 2008). Interestingly, both mutations located in the same region might also have impact on the export of CK2 towards the external cell membrane.

Regarding the truncated protein produced due to p.Ser125\*, the loss of the CK2 $\alpha$  regulatory domain in truncated version would have definite effects on the overall catalytic activity of CK2 (Sajnaga, Szyszka et al. 2013).

### **6.5.3 CK2 $\beta$ being a chief regulatory subunit for many proteins indicates its functional relevance with a syndromic condition**

CK2 is a holoenzyme and functions to phosphorylate hundreds of substrates; beta subunit regulates the catalytic activity and efficiency of alpha subunit. Regarding the phosphorylation activity, it is well established fact that CK2 $\beta$  is capable of autophosphorylation and both subunits can function as independent entities (Pagano, Sarno et al. 2005). In this study, the protein-protein interactome data obtained by whole proteomic analysis of p.Asp32His mutant unravels 194 independent binding partners of beta subunit. These are classified on the basis of protein family and it was observed that most of these belonged to DNA/RNA binding proteins involved in protein expression or DNA/cellular damage response. In this regard, previously, a study conducted mass spectrometry combined with affinity chromatography of mouse brain to show that there are 144 CK2 independent binding partners of CK2 $\beta$ , out of which 32 are those

which are dedicated to protein formation and degradation (Arrigoni, Pagano et al. 2008). In addition to protein-protein interactome analysis, whole phosphoproteome data of p.Asp32His mutant also showed impaired phosphorylation of 362 substrates of CK2 out of which 75 are known substrates of CK2, verified by the previous studies (Bian, Ye et al. 2013; de Villavicencio-Díaz, Mazola et al. 2015; Franchin, Salvi et al. 2015) and online databases (PhosphositePlus and Phospho.ELM).

As proven by the previous studies and this study, CK2 is playing a leading role in the regulation of multiple proteins substrates, kinases and thus diverse cellular pathways. The following concept that may be built on this fact is that dysregulation in the phosphorylation activity may lead to disruption of more than one cellular pathway. Taken together, it may also be concluded that disturbances in the amount or functioning of free CK2 $\beta$  (or bound to the holoenzyme) may leave possible effects on interacting partners resulting in the syndromic phenotype.

## **6.6 Mutations in the beta subunit of CK2 — the master of all kinases — causes impaired Wnt signaling**

CK2 is known to be involved in regulation of diverse cellular pathways; the list of its substrates is growing, which makes it challenging to choose one pathway to follow. As a solution to this, protein-protein interactome was generated where a number of proteins were found to lose interaction with mutant CK2 $\beta$  (p.Asp32His). Interestingly, the enrichment of these proteins suggested that enriched proteins with the highest *p value* (determined by the tool FunRich 3.1.3) were involved in Wnt signaling, especially degradation of  $\beta$ -Catenin, and DNA Damage Response (DDR). The clue of these two pathways was taken into account for further investigations; Wnt signaling pathway is well known to orchestrate variety of cellular processes especially during the development. Any disturbance in Wnt signaling can lead to pathological conditions including microcephaly, limb malformations, dermal hypoplasia and Williams-Beuren Syndrome (Clevers and Nusse 2012; Kadir, Harel et al. 2016). Regarding the significance of  $\beta$ -Catenin, its function is previously explained in Wnt signaling as key player. It forms multiple complexes to control cell proliferation; in case of negative regulation when Wnt signaling is off, the cytoplasmic  $\beta$ -Catenin is associated with destruction complex (Axin, adenomatous polyposis coli (APC) and the kinases, glycogen synthase kinase-3 alpha/beta (GSK-3) and casein kinase-1 (CKI)) and undergoes proteasomal degradation

(Huelsenken and Behrens 2002). However, when Wnt signaling is on, the destruction complex is dismissed and free  $\beta$ -Catenin, after being phosphorylated by CK2, forms complex with DVL3; this CK2/Dvl and  $\beta$ -Catenin complex thereby allows  $\beta$ -Catenin to be transported into nucleus for binding with high-mobility-group-box transcription factors of the TCF/LEF family and carrying out transcription of target genes which are mostly related to growth and development (Song, Sussman et al. 2000). Previous studies also suggest that if CK2 phosphorylation is inhibited,  $\beta$ -Catenin no longer performs its transcriptional activities and at the same time, the balance in the pool of  $\beta$ -Catenin is also disturbed (Song, Sussman et al. 2000).

On the basis of potential involvement of Wnt signaling pathway and the functional relevance of CK2 with  $\beta$ -Catenin, I investigated the expression of  $\beta$ -Catenin in patient LCLs harboring p.Asp32His and p.Asp32Asn mutations. It was revealed that the cytoplasmic  $\beta$ -Catenin (non-active) was mislocalised and upregulated, whereas, the active/nuclear  $\beta$ -Catenin was drastically reduced in the patient LCLs. In addition, the increased amount of p- $\beta$ -Catenin (which signifies the phosphorylation at 37 to 42 amino acids) in p.Asp32His mutant clearly indicated that it is not being degraded rather accumulating in mutant cells and thus an imbalance in the maintenance of  $\beta$ -Catenin pool. These findings hinted that the CK2 mediated phosphorylation may be impaired due to reduced kinase activity of CK2 (containing mutant  $\beta$  subunit). The concept of CK2 mediated phosphorylation was proven by earlier studies; in case of positive regulation (when Wnt signaling is on)  $\beta$ -Catenin is phosphorylated by CK2, after CK2 association with Dvl. This phosphorylation maintains the stabilization and translocation of  $\beta$ -Catenin to nucleus to serve as a cofactor for transcription (Ahmed, Gerber et al. 2002). In this regard, the kinase activity of CK2 containing mutant beta subunit (p.Asp32His and p.Asp32Asn) was analyzed keeping  $\beta$ -Catenin as their substrates. The findings suggested a significant reduction of kinase activity of CK2, containing mutant beta subunit (p.Asp32His and p.Asp32Asn). Additionally, kinase activity was also checked in a separate experiment using a target peptide of CK2 which replicated the results of hypophosphorylation  $\beta$ -Catenin activity by CK2 containing p.Asp32His mutant beta subunit. However, CK2 containing p.Asp32Asn beta subunits showed normal kinase activity as wild type CK2. It could be assumed that p.Asp32Asn mutation may have milder effects on the efficiency of CK2 and could still phosphorylate selective substrates. This may explain comparatively milder phenotype of p.Asp32Asn patient compared to severe phenotype seen in patient carrying

p.Asp32His. Here, it was also considered that the reduced kinase activity could be due to the variable impact of both mutations on the structural changes and thus the interaction of both mutant beta subunits with its binding partners.

As the significance of DVL3 in Wnt signaling is mentioned earlier, I also conducted an experiment to analyze the interaction of CK2 with DVL3. It was evident from my findings that DVL3 also showed reduced interaction with endogenous mutant CK2 $\beta$  thereby suggesting an impairment in the formation of CK2 $\beta$ /DVL3/ $\beta$ -Catenin complex thus disturbing the whole positive regulation of Wnt signaling.

It was also interesting to know from whole phosphoproteomic profiling of p.Asp32His mutant that more than 300 CK2 substrates showed no phosphorylation in p.Asp32His mutant (discussed in the following section in detail). Further *in silico* functional enrichment of these proteins clearly showed that enriched proteins are related to regulation of nuclear  $\beta$ -Catenin and target genes expression. These results further strengthen and validate my findings of reduced kinase activity of CK2 containing mutant beta subunit. As shown by the functional enrichment, the importance of nuclear or active  $\beta$ -Catenin should be noted that it is a transcriptional co-activator and participates in diverse cellular pathways by positive and negative regulatory mechanisms of Wnt signaling (Huelsenken and Behrens 2002). This regulation is critical for maintaining the balance of  $\beta$ -Catenin, thus eventually controlling the homeostasis of transcriptional activities.

In the light of these findings, we speculate that CK2 $\beta$  might specifically mediate the nuclear translocation of  $\beta$ -Catenin. Dysregulation in kinase activity of CK2 containing mutant beta subunit or free mutant CK2 $\beta$  causes impairment of  $\beta$ -Catenin dependent Wnt signaling which globally effects the transcription of downstream target genes. A global transcriptional dysregulation may explain the severe developmental defects in my patient.

## **6.7 Delayed DNA damage response plays a significant role in pathogenicity of Filippi syndrome**

Regarding pathways being studied in Filippi patient, DNA damage response (DDR) was the second pathway suggested by the enrichment of proteins showing weakened interaction with CK2 $\beta$  mutant (p.Asp32His) obtained by protein-protein interactome. Involvement of CK2 in cell viability has already been reported; biallelic loss-of-functions of *Csnk2b* causes lethality

in embryonic stage in mice (Buchou, Vernet et al. 2003). In addition, the siRNA mediated depletion inhibits growth in human fibroblasts. Interestingly, overexpression of CK2 $\beta$  has also been shown to inhibit growth of mouse 3T3 cells (Homma and Homma 2008). We had consistent findings of overexpression of CK2 $\beta$  in my patient cells where the decreased cell proliferation was depicted by impaired DDR; the key regulators of this pathway, 53BP1,  $\gamma$ -H2AX and CHK1 proteins were examined after DNA damage induction in p.Asp32His mutant. Results demonstrated that all of these proteins were found upregulated, suggesting impaired DNA damage response. My results are consistent with the findings of a previous study carried out in *S. cerevisiae* which suggests involvement of *CKB2* in cell cycle arrest observed upon induction of double stranded DNA breaks (Toczyski, Galgoczy et al. 1997).

In addition, the involvement of CK2 $\beta$  in cell cycle regulation by interacting as a docking site for other kinases such as CHK1 is crucial (Guerra, Issinger et al. 2003). It has already been established that phosphorylation of H2AX results in the formation of DNA damage foci, which leads to activation of downstream kinases Chk1 and Chk2 and eventually p53, whereas, 53BP1 functions as mediator of the DDR pathway. Upregulation of these key players indicate cellular senescence or a delayed DNA damage response (Von Zglinicki, Saretzki et al. 2005). A similar picture was observed in my patient cells where upregulated DDR proteins were assumed to delay DNA repair activity. For further validation, I conducted experiments to demonstrate the effects of mutation on cell cycle and cellular fate decided by delayed DDR. Results showed that more mutant (p.Asp32His) cells were found in G0/G1 phase and lesser in S phase suggesting cell cycle arrest. In addition, cell death was also increased in the given mutant. Taking together all the findings obtained from biochemical investigations, it can be concluded that impaired DDR pathway contributes in manifestation of FLPIS.

## **6.8 Whole phosphoproteomic profiling validated and expanded knowledge to dysregulation of mutant CK2**

Whole cell phosphoproteome analysis was carried out to explore the consequences of mutation on phosphorylation activity of CK2 containing mutated  $\beta$  subunit. The hypophosphorylation observed on target peptides motifs of CK2 in patient cells indicated reduced kinase activity. Among these peptides, APC and DVL3 are also included and the loss of phosphorylation in patient cells once again validates my finding of impaired Wnt signaling. With special reference to calmodulin dependent casein kinase 2 (CaMKII), a drastic

hyperphosphorylation activity was observed which is an expected consequence as CK2 $\beta$ , in this case, works as inhibitor of CK2 $\alpha$  to control the normal activity of calmodulin (Meggio, Boldyreff et al. 1994). In addition, It is already reported that, genetically altered mice overexpressing calmodulin develop severe cardiac conditions caused by increased autonomous activity of CaMKII in vivo (Colomer and Means 2000; Alvarado, Bos et al. 2019). This observation thus explains the heart anomaly observed in FP2 patient.

The dysregulated phosphorylation of protein kinase A, kinase C and  $\beta$ -adrenergic receptor kinases also suggest abnormalities in the signal transduction in patient cells causing neurological conditions (Harms, Kloth et al. 2018; Orgah, Yu et al. 2018). Conclusively, phosphoproteome data strongly supports the impaired phosphorylation capacity of CK2 due to mutation in CK2 $\beta$ . It also extends the knowledge regarding dysregulation of other kinases in the patient LCLs.

## **6.9 Transcriptome profiling authenticates findings obtained at protein level**

The idea of RNA sequencing was useful to obtain a broader overview of global dysregulation in gene expression and connecting the dots with disease pathogenicity. It was interesting to observe striking relevance of results obtained on protein level with those found at transcript level in RNA sequencing data. The expression of investigated proteins of Wnt signaling and DDR was similar and in line with results at transcriptional level thus validating the expression trends at two different fronts.

Surprisingly, an elevated differential expression of genes involved in immune system was also observed in the transcriptome of patient, which directed me to review the phenotypic profile of patient for developing a link between differential expression of immune response genes and patient disease conditions. For this purpose, blood profile of patient was obtained which showed comparatively higher levels of IgM (immunoglobulin M); 253 mg/dL as compared to normal range which is 40-230 mg/dL and the only infection noticed during clinical investigation was recurrent osiosis. In addition, *CSNK2B* is a member of major histocompatibility complex and in this context the differential expression can be related to differential expression of genes involved in immune response, however, further validation is also required.

## 6.10 Implications of upregulated mutant CK2 $\beta$ (p.Asp32His and p.Asp32Asn) in patient LCLs

Experimental data showed an increased amount of mutant CK2 $\beta$  at both RNA and protein level. As both patients have heterozygous mutations, the abnormal protein product may interfere with the functioning of normal allele product implicating a dominant negative effect. A previous study demonstrated in the fission yeast *S. pombe* the increased expression of CK2 causes severe growth defects and a multiseptated phenotype (Roussou and Draetta 1994). On the other hand the truncated protein (p.Ser125\*) may cause the disease due to haploinsufficiency.

As I see that Wnt regulators are downregulated in my mutants yet the substrates of clomodulin-dependent substrates and DNA damage response regulators are upregulated, it must be taken into consideration that the interplay of mutated beta subunit may act differently in different pathways; in some case the loss of function or interference of upregulated mutant protein may impair the function of some interaction partners and on others it may depict a gain of function. Being the master regulator of many kinases, the implications may be observed variably in various cellular pathways.

## 6.11 Hunting novel candidate genes for FLPIS

My recruited FLPIS cohort comprised of total 16 cases out of which four cases remained unsolved and two cases harboured mutations in *CSNK2B*. For rest of the six cases, WES data analysis revealed likely pathogenic mutations in six different genes; *CDKL5*, *CDKL2*, *DNM3*, *PTPN23*, *PSEN1* and *TRIM35*. *CDKL5* and *DNM3* were segregating in the affected families, however, for the rest of the families, segregation could not be confirmed due to unavailability of DNA samples. All the proposed candidate genes have high pathogenicity scores predicted by *in silico* tools and very low allele frequency in gnomAD.

Like *CSNK2B*, *CDKL2* and *CDKL5* (cyclin dependent kinase like 2 and 5) are serine/therionine kinases. The role of both kinases is generally established in cell cycle pathway more specifically in regulation of the growth and functions of primary cilia (Canning, Park et al. 2018). A previous study also shows that cyclin dependent kinases are the phospho-regulators of  $\beta$ -Catenin dependent Wnt signaling in *Drosophilla* (Davidson and Niehrs 2010). Regarding *CDKL5*, defects in this protein has been associated with syndromes

(including microcephaly) such as Rett syndrome, neurodevelopmental disorder that exhibits epileptic seizures which is one of the prominent feature in my FLPIS cohort (Castrén, Gaily et al. 2011; Kilstrup-Nielsen, Rusconi et al. 2012; Yan, He et al. 2020). As a matter of fact DECIPHER, an online database of genetic diseases, have several entries of patients (having CDKL5 mutations) showing similar features to my CDKL5 mutated patient (<https://decipher.sanger.ac.uk/search?q=cdkl5#consented-patients/results>) such as syndactyly of finger or toes, facial dysmorphism and mental retardation. Regarding the effects of defective CDKL5, a previous study demonstrated that, CDKL5-deficient cells were found hypersensitive to DNA damage-associated stress indicated by  $\gamma$ H2AX positive and more susceptible to apoptosis which was shown by increased cell death of neurons of *Cdkl5* KO mice (Loi, Trazzi et al. 2020). Similar findings of DNA damage response were observed in one of my FLPIS patient (FP2).

Similarly, *PTPN23* also encoding tyrosine phosphatase non-receptor type 23 which maintains tyrosine phosphorylation of its substrates from diverse cellular pathways mainly including ciliogenesis, endosomal sorting and pre-mRNA splicing processing (Smigiel, Landsberg et al. 2018). Previously, *PTNP23* is associated with global developmental delay, epilepsy and brain atrophy (Alazami, Patel et al. 2015; Trujillano, Bertoli-Avella et al. 2017). A very recent study also demonstrates the consequences of mutated *PTPN23* observed in patients manifesting developmental delay, brain abnormalities including intellectual disability, language disorder, microcephaly and seizures (Bend, Cohen et al. 2020). These features are overlapping with the typical features of FLPIS cases.

*DNM3* encodes for a huge GTPase protein, dynamin 3, dedicated for endosomal trafficking especially in synaptic vesical endocytosis in neurons (Boumil, Letts et al. 2010). It is previously demonstrated by a study that the highest expression of dynamin 3 in humans is noted in all the studied tissues of central nervous system (Romeu and Arola 2014). Although, *DNM1* and *DNM2*, the isoforms of *DNM3* are reported to cause epilepsy and neurodegenerative diseases (Züchner, Nouredine et al. 2005; Boumil, Letts et al. 2010) yet the association of *DNM3* with rare disorders is not well established. It would be interesting to explore its role in a craniodigital condition in FLPIS. The mutation in my mutant may explain the consequences of aberrant protein in central nervous system leading to disease condition.

*PSEN1* encodes presenilin 1. MGI database showed that ablation of this gene in mice revealed phenotype of deformed axial skeletons as well as impaired brain growth with a deficiency of



neural stem cells. Furthermore deficiency of this gene in mice causes perinatal death (<http://www.informatics.jax.org/marker/MGI:1202717>). Due to these similar features of my FLPIS patient, I included it in the list of novel candidate gene.

Functional relevance illustrated by previous studies and strong genetic constrains for all identified variants is compelling to propose them as novel candidate genes of FLPIS.

## **6.12 Concluding remarks and future prospects**

This study answers many questions regarding the genetic etiology of microcephaly and associated syndromes, yet opens windows to the new quests. It shows the multiomics approach combining genomic, bioinformatic, transcriptomic and proteomic data is highly efficient to decipher disease pathogenicity of challengingly rare disorders. This is possible because of networking and collaborations between researchers of the aforementioned fields. The data obtained from this study will add knowledge and broaden my understanding for ultimately devising robust diagnostic tools and treatment strategies. It is further intended to investigate the mysteries of genetic factors involved in transforming an isolated phenotype into syndromic form, keeping microcephaly as model disease. Also, the unsolved cases of Filippi syndrome will be considered for further genetic and functional characterization.

## **7. Materials and Methods**

### **7.1 Data collection**

A total of 16 families were investigated in this study; All of the families were recruited from different parts of the world including, Pakistan, Italy, Germany, Mexico, Poland, Oman, New Zealand, Brazil, Finland, France and UK. Identification of these families were ascertained with the help of physicians, clinical laboratories, hospitals, and institutions for special children. Informed consent was taken from all the families under study with prior information of the purpose and expected benefits of this research project. Clinical information and photos of the affected individuals were also collected from concerned physician through electronic mails.

### **7.2 Pedigree Construction**

Pedigrees were constructed on the basis of information collected from the family members. Females, in the pedigrees, are indicated by circles and males by squares. Single line between male and female symbols showed mating between non-consanguineous couples whereas double lines are indicative of cousin marriage. For representation of unaffected individuals, clear circular symbols are used. Filled symbols denote affected ones and diagonal slashes on symbols are indicative of deceased individuals. In addition, a number enclosed within a symbol indicate the number of sibs. Generations number is indicated by Roman numerals and individuals within each generation in represented in Arabic numerals. Drawings of all pedigrees were done by software HaploPainter v.1.043 (Thiele and Nurnberg, 2005).

### **7.3 Genetic Investigations**

#### **7.3.1 Blood sampling and DNA extraction and quantification**

Peripheral blood was drawn by medical facility experts from all available affected and unaffected individuals, close relatives and parents. For this purpose, 10 ml BD vacutainer® (BD-Plymouth, UK) containing EDTA, were used for carrying and storing blood. Until further processing of blood samples, these were kept at 4 C<sup>0</sup>. Furthermore, Genomic DNA was extracted from blood samples using QIAamp®DNA Mini Kit (Qiagen, Germany, 69506). For knowing the integrity of dissolved DNA, it was run on 0.7% agarose gel followed by

quantification which was carried out by using NanoDrop-8000 Spectrophotometer (Thermo scientific).

### **7.3.2 Polymerase chain reaction (PCR) and gel electrophoresis**

PCR was employed for amplification of target genomic fragments. From each sample, 20 ng of genomic DNA was added to PCR ingredients; 1µl of 10X buffer, forward and reverse primer (10 pmol each), 2.5 mM of dNTPs. For amplification of target sequence, 0.15 U Taq DNA polymerase (Analytik Jena, 845-EZ-1000500), was used. Following to preparation of PCR mixture, it was subjected to thermocycling profile. The profile was optimized for temperatures and cycles for different sets of primers yet the commonly used profile is as follow: five minutes for template denaturation on 95 °C followed by 35-40 cycles of amplification. Each cycle consisted of 3 steps; DNA denaturation at 95°C for 35 seconds; 55-57°C (depending on the primers used) for 40 seconds for annealing of primers to target sequence; 72°C for 35 seconds for extension of complementary DNA strand from each primer. Finally, 5 minutes at 72°C for final extension of fragments that might were partially extended. PCR was performed using on the DNA Engine® Tetrad 2 Thermal Cycler (Bio-Rad).

Following to PCR reaction, PCR product was subjected to 0.7% to 2% agarose gel, agarose. The gel was prepared by melting agarose powder (Invitrogen) in IX TAE buffer (50X TAE, ROTH) and ethidium bromide (10 mg/mL) was added for DNA flourometrics. Horizontal gel electrophoresis chambers (Analytik Jena) were used to resolve PCR product on gel according to the size. For tracking the size of the amplicons, the DNA molecular weight marker, 1 kb Plus DNA Ladder (Invitrogen, SM0314) was used. Images of the gels were captured by Molecular Imager® Gel Doc™ XR System.

### **7.3.3 Homozygosity mapping**

Genome-wide linkage analysis for MCP2 family was conducted by genotyping the available family members with Affymetrix GeneChip® Axiom array PMRA. Genotype calling was accomplished by using the GeneChip® DNA Analysis Software (GDAS v3.0, 25 Affymetrix). Gender of each sample was confirmed by counting heterozygous SNPs on the X chromosome. Graphical Relationship Representation (Abecasis, Cherny et al. 2001) was used to examine any possible relationship errors. Regarding Mendelian errors, the program PedCheck for error detection as well as removing SNP error from the datasets (O'Connell and

Weeks 1998). On the other hand, the non-Mendelian errors were detected by the program MERLIN (Abecasis et al., 2002) and unlikely genotypes for related samples were deleted. Linkage analysis was based on the following factors: autosomal recessive inheritance, full penetrance, consanguinity and a disease gene frequency of 0.0001. Furthermore, for calculating the multipoint LOD score and reconstructing the haplotypes, the program ALLEGRO) was used (Gudbjartsson, Jonasson et al. 2000). Finally, the haplotypes were graphically presented using HaploPainter (Thiele and Nurnberg, 2005). It should be noted that ALOHOMORA was used as interface for all data handling (Rüschendorf and Nürnberg 2005).

#### **7.3.4 Whole-exome sequencing**

In this study, whole-exome sequencing (WES) was conducted for MCPH families and trio-WES for Filippi syndrome families at the Cologne Center for Genomics (CCG), Germany according to the set protocols. Ultrasonic treatment (Covaris, Inc., Woburn, MA 01801, USA) was performed for fragmentation of patient DNA (1 microgram). Further, the fragments obtained by ultrasonic treatment were end-repaired and adaptors were also ligated. For library preparation, Agilent (Santa Clara, CA) version 6 enrichment kit was used. For sequencing samples, Illumina HiSeq 4000 sequencing system (paired-end reads,  $2 \times 75\text{bp}$ ) was utilized which resulted in  $>30\times$  coverage for 81.9% of the target sequences. Data filtration and variation prioritization was performed by in-house designed pipeline named as VARBANK 2.0 ([https://varbank.ccg.uni-koeln.de/varbank 2](https://varbank.ccg.uni-koeln.de/varbank2)).

For the FP2, FP28 and FP30, trio-WES (sequencing patient and both parents) using SureSelect Human All Exons v5 kit without UTR (Agilent) was performed. Sequencing was carried out on an Illumina HiSeq 2500 (paired-end sequencing,  $2 \times 100\text{bp}$ ). Data analysis was performed by Illumina CASAVA (1.8.2) for demultiplex sequencing reads and adapters were detached using Skewer 0.1.116. The bundle of reads that were obtained were mapped against to the human reference genome (UCSC hg19) using the Burrows-Wheeler Aligner (BWA-mem 0.7.2) and variants were called using both samtools and varscan.

Data was filtered for identification of casual homozygous, compound heterozygous, and de novo variants; those, present in the coding region as well as flanking intronic regions ( $\pm 60\text{bp}$ ) showing minor allele frequency (MAF)  $< 1.5\%$  were considered. MAF was confirmed by using publicly available databases: 1000 Genomes, dbSNP, Exome Variant Server, gnomAD

(genome aggregation database), and an in-house database of CCG with >1,600 exomes. Known disease-causing variants (according to Human Genetic Variation Database) were assured to exclude before considering novel variants.

### **7.3.5 Sanger sequencing**

The candidate variants narrowed down from WES data were further confirmed for segregation by bidirectional Sanger sequencing. In this regard, specific primer sets were designed based on the site of mutation in particular exon/intron, using an online available tool/program of Primer3 (<http://bioinfo.ut.ee/primer3-0.4.0/>). For confirmation of efficiency, these primers were also validated from *in silico* PCR tool provided by UCSC genome browser (<https://genome.ucsc.edu/cgi-bin/hgPcr>).

#### ***Target DNA amplification***

Prior to sequencing, the region containing mutation was being amplified by taking six ng of genomic DNA. The procedure adopted for this PCR is already explained in section 7.3.2. Further, confirmation of the amplification was achieved by visualizing the PCR product on 1% agarose gel.

#### ***Exo-SAP treatment***

Depending on the approximate quantification, 0.5 to 1 µl of amplified product was cleaned to remove excess oligos and nucleotides. For this purpose, 0.25 µl each of Exonuclease I (20U/µl, New England Biolabs) and Shrimp Alkaline Phosphatase (SAP) (1U/µl, Promega) was mixed in the diluted PCR product keeping the total volume up to 6 µl by adding diH<sub>2</sub>O. Furthermore, the mixture was incubated in PCR thermocycler for 50 minutes at 37 °C, followed by enzyme inactivation at 95 °C for five minutes.

#### ***Sequencing PCR***

Cleaned product obtained from Exo-SAP treatment was further subjected to Sanger sequencing. For this purpose, reaction mixture was prepared by using 0.5 µl of the treated product, 2 µl of 5X BigDye sequencing buffer (Applied Biosystems), 1 µl BigDye® (V.1.1 cycle sequencing Kit, Applied Biosystems) along with 0.2 µl of 10 µM primers and making the volume up to 10 µl. In this way two reaction mixtures were made for both forward and reverse primer. Reaction mixture was further subjected to the thermocycler where denaturation at 96 °C for 10 seconds was set, followed by 55 °C for 5 seconds and 60 °C for 4 minutes having a total of 32 cycles. Sequences were analyzed using DNA Star (Lasergene) and Mutation Surveyor (SoftGenetics).

### **7.3.6 RNA isolation**

Cellular RNA from whole blood of patients and controls was isolated using PAXgene Blood RNA tubes (8.5ml). RNA was extracted and purified by using the PAXgene Blood RNA kit (PreAnalytiX, 762174) according to the manufacturer instructions. For RNA isolation from fibroblasts and LCLs, RNeasy Mini kit (Qiagen, 74104) was used according to the user's guide provided by the company.

### **7.3.7 Reverse transcriptase PCR (RT-PCR)**

Further to RNA isolation, complementary DNA (cDNA) was synthesized by using SuperScript II reverse transcriptase (RT) enzyme (Invitrogen, 18064014). A total of 1 µg RNA was mixed with 1 µl dNTPs (10 mM), 1 µl Oligo d(T)18-Primers (50 µM), and finally RNAase free water to make up to 11 µl of total volume. Further to this, the mixture was incubated for 5 minutes at 65 °C for removing the unopened RNA. After incubation, 4 µl of 5x First-Strand Buffer, 2 µl DTT (0.1 M) and 1 µl of SuperScript RTII (200 U/µl) were added to the mixture followed by incubation at 50 °C for 50 minutes and 70 °C for 15 minutes in thermal cycler. Finally, the samples were quantified using an Applied Biosystems 7900 Fast Real-time PCR System (Applied Biosystems Inc., Norwalk, CT, USA) and stored at -20C until further analysis.

### **7.3.8 Quantitative real-time PCR (qRT-PCR)**

For qRT-PCR, equal amount (150ng/µl) of cDNA from each patient and control sample was taken. Glyceraldehyde-3-phosphate dehydrogenase (*GAPDH*) was used as positive control. The mixture was prepared in 96-well microtiter, by mixing 15 µl PCR reaction with 3 µl cDNA template, 0.2 µM of forward and reverse primers and 7.5 µl PowerUp™ SYBR™ Green Master Mix (ThermoFisher Scientific, A25780). PCR amplification was performed according to the given profile: 95 °C for 5 min; 95 °C for 3 sec and 60 °C for 1 min; repeat 40 times stage "b" having melting curve analyzed at 60 °C to 95 °C with 2.3 °C increase in temperature per second at each step. After completion of PCR, data analysis was performed using the 7900 Fast System SDS Software (Applied Biosystems Inc.) and statistics was applied using Microsoft office Excel (Microsoft Corporation, Bellevue, WA, USA).

## **7.4 Functional studies**

### **7.4.1 Cell culture**

In this study, two different cell types — cell line and primary cells — were used; primary dermal fibroblasts derived from patient of *NUP37* mutated family and lymphoblastoid cell lines (LCLs) derived from *CSNK2B* (FP2 and FP28) and *NUP107* mutated patients. Centre d'Etude Polymorphisme Humain (CEPH) LCLs (Shukla and Dolan 2005) were also grown and used as healthy control for comparing them with patient derived LCLs. Unrelated healthy controls for respective cell lines were also established. In addition to these, I have also used HeLa cell line (Landry, Pyl et al. 2013).

### **7.4.2 Establishment of dermal fibroblasts from skin biopsies**

The skin biopsies were promptly placed in sterile 50 ml transport tube in 20 ml of DMEM media mixed with cocktail of antibiotics and fungicide (50 mg/ml gentamycin, (Sigma-Aldrich-G3632), 75 µg/ml of penicillin and 50 µg/ml of streptomycin (PAN Biotech) and amphotericin B, GIBCO). Skin biopsies were shipped from Pakistan to the recognized and well-managed cell culture labs in Institute for Biochemistry, Cologne. Biopsies were washed in 7-10 ml sterilizing reagent (Betaisodona, Povidon-Iodine) in a falcon and incubated in three series of falcon tubes containing 15 ml PBS supplemented with antibiotics and fungicide (50 mg/ml gentamycin (Sigma-Aldrich-G3632, USA), Penicillin/Streptomycin, each of 10.00 IE (µl)/ml, PAN Biotech and 250 µg/ml amphotericin B, GIBCO). Incubation time in each falcon will be maintained as 5, 10 and 20 minutes, respectively. Dispase II (1.5 U/ml, Roche) diluted in PBS was used to isolate epidermis at 4 °C overnight. Furthermore, the dermis was maintained at 37 °C in a small petri dish (60x15mm) in 10 ml DMEM (High Glucose (4.5 g/L) with L-Glutamine) media which was replaced by every three to four days. Growth of dermal cells was being observed under a light microscope regularly. On observing confluent growth of cells in small petri dish, the pool of primary fibroblasts was further increased by sub-culturing the cells.

### **7.4.3 Establishment of LCLs from blood**

Regarding the establishment of LCLs, blood samples were taken in BD Vacutainer® PST™ lithium heparin tubes and immediately processed by incubating the blood in lysis buffer (pH 7.4, 155 mM ammonium chloride, 10 mM potassium hydrogen carbonate and 0.1 mM disodium-EDTA) for 10 minutes. Blood containing lysis buffer was centrifuged and

supernatant was discarded. The pellet contained the white lymphocytes with residues of red blood cells on the walls of the tube which are cleaned with the help of a pipette tip and discarded. For immortalizing the lymphocyte cells in pellet, these were resuspended in 2 ml of EBV supernatant, obtained from an EBV stock culture. This suspension was incubated for 1 hour at 37 °C. In addition, cyclosporine was also added to selectively kill T-lymphocytes and generate a cell line of B-lymphocytes only.

#### **7.4.4 Cell culture conditions**

Human fibroblast cell lines were cultured in Dulbecco's Modified Eagle's Medium (DMEM, PAA), whereas LCLs, were grown in Gibco RPMI Media 1640. Both, RPMI and DMEM media were supplemented fortified with 10% fetal bovine serum (FBS, Biochrom), L-Glutamine (PAN Biotech, P04-80050) and antibiotics (Penicillin/Streptomycin, PAN Biotech, P06-07050). All cells were cultured and incubated at 37 °C in incubator supplied with 5% CO<sub>2</sub>.

Recipe used for media preparation is given as under:

1. DMEM/RPMI-----500ml
2. FBS (Fetal bovine serum) -----60ml
3. L-Glutamine (200 mM, 100X) -----6ml
4. Penicillin/Streptomycin (10.00 IE (µl)/ml) -----6ml

#### **7.4.5 Immunofluorescence of adherent cells**

Human fibroblasts were grown on 12 mm coverslips in 24-well plate. When cells achieved 70 % confluency, these were fixed by following two methods; (1) methanol fixation, using pre-chilled methanol for 10 minutes at -20 °C, (2) PFA fixation, with 3% paraformaldehyde - prepared in 1X phosphate buffer saline PBS - for 15 minutes at room temperature. After fixation, cells were washed three times with 1X PBS and permeabilized by treating the cells with 0.5% Triton X-100 in PBS for 10 minutes at room temperature. To be noted here is that this step was not followed for cells subjected for methanol fixation, as the cells are permeabilized by treatment with methanol. Subsequently, the cells were incubated three times with 1X PBS (each for 5 minutes) and blocked for 1 to 2 hours, with blocking buffer (5% FBS diluted in PBS). Next to this, cells were incubated with primary antibodies diluted in blocking buffer overnight at 4 °C in a dark chamber. Following to this, cells were washed with 1x PBS three times for 5 minutes and then incubated with secondary antibodies for an



hour at room temperature. DNA contents of cells were stained using 4', 6-Diamidino-2'-phenylindole (DAPI, Sigma-Aldrich, D9572). Finally, the cells were mounted on glass slides by using gelvatol. Primary and secondary antibodies used in this study are given in the table (Table 7.1 and 7.2).

#### **7.4.6 Immunofluorescence of cell suspension (LCLs)**

As LCLs are not adherent cells, Poly-L-lysine hydrobromide 0.1 % (Sigma-Aldrich, P5899-5MG) was used for attachment of LCLs in the cover slips. For that purpose, autoclaved coverslips were incubated with Poly-L-lysine solution for 10 minutes and then incubated with diH<sub>2</sub>O two times. After washing, LCLs in RPMI media were grown overnight and later subjected for immunocytochemistry by following the aforementioned method.

Recipes of solutions prepared for immunofluorescence are as under.

#### **PBS (pH 7.2)**

1. 10 mM NaCl
2. 10 mM KCl
3. 32 mM KH<sub>2</sub>PO<sub>4</sub>
4. 16 mM Na<sub>2</sub>HPO<sub>4</sub>

#### **3% paraformaldehyde (pH 6.1, 100 ml)**

1. Paraformaldehyde powder-----3g
2. 1X PBS-----80ml
3. 0.4 M NaOH (to adjust pH 6.1)
4. deionized H<sub>2</sub>O (final volume)

#### **10X Triton X-100 (25ml)**

1. Triton X-100 -----3 ml
2. PBS-----22 ml

#### **0.5% Triton X-100 (50ml)**

3. 10X Triton X-100----- 2.5 ml
4. 1X PBS----- 47.5 ml

#### **Gelvatol**

1. Polyvinyl alcohol (87%-89%, Sigma P8136)
2. 12 g of Glycerol

3. 12 ml of Ionized water, (RT, 10hr)
4. 24 ml of 0.2 MTris-HCl (pH 8.5)
5. 2.5% Diazabicyclooctan (DABCO, Sigma Aldrich, D252)

## **7.5 Microscopy**

### **7.5.1 Electron microscopy**

Transmission electron microscopy (TEM) was used for imaging of NUP37 mutated fibroblast. For this purpose, imaging facility of Cologne Excellence Cluster on Cellular Stress Responses in Aging-associated Diseases (CECAD) was used. Samples were visualized by using transmission electron microscope (JEOL JEM2100PLUS) with 200 kV for RT having GATAN OneView camera. The procedure was carried out according to the set protocol of CECAD imaging facility described elsewhere (Stoffel, Hammels et al. 2016).

### **7.5.2 Confocal imaging**

Images, after immunofluorescence, were acquired using confocal laser scanning microscopy (Leica, LSM TCS SP5) with 60X and 100X objectives, depending on the cell type used in the experiment. Images were captured using Leica-TCS-SP5/LAS-AF-Lite\_2.0.2\_2038 software and were labeled and edited, accordingly, using Adobe Photoshop.

### **7.5.3 Confocal laser scanning microscope**

Confocal laser scanning microscope (TCS SP8 gSTED, Leica Microsystems) service provided by CECAD imaging facility was used for imaging of nuclear pore density of wild-type and NUP37 mutated fibroblasts. Further, Nuclear pore density was analyzed using the “particle analysis” tool of ImageJ (version 1.51z; NIH) as instructed by the user guide (Ferreira and Rasband 2012).

## **7.6 Cell cycle assay by FACS**

A specific number,  $5 \times 10^5$ , of LCLs derived from patient mutated with *CSNK2B* and from control individual were dissolved in 500 $\mu$ l of RPMI media. After incubation with Nuclear-ID™ Red DNA stain (Enzo Life Sciences, 52406), dilution 1:250 for 5 minutes on 37°C, the cells were sorted immediately by using BD FACSAira III cell sorter (BD Bioscience USA).

## **7.7 Proliferation assay**

Proliferation assay was performed to analyse the growth rate of *NUP37* mutated fibroblasts according to the protocol defined in the previous study (Hussain, Baig et al. 2013). In short, equal amounts of cells, derived from patient and wild-type individual, were grown in eight different plates. Cells were counted and documented daily for designing final graph.

## **7.8 TUNEL assay**

TUNEL assay was performed to examine apoptosis in *CSNK2B* mutated patient (FP2) by using commercially available kit, DeadEnd™ Fluorometric TUNEL System (Promega, G3250). All the steps were carried out according to the user's manual provided by the company.

## **7.9 Investigating DNA Damage response**

For inducing DNA damage the cultured wild-type and *CSNK2B* mutated LCLs were treated with hydroxyurea (1.5µl/ml) for 24 hours and followed as comprehended elsewhere (Szczepanski, Hussain et al. 2016) and later on subjected to immunofluorescence and western blot.

## **7.10 Immunoblot analysis**

### **7.10.1 Protein extraction from eukaryotic cells**

Cells were washed with ice-cold 1X PBS supplemented with protease inhibitor cocktail (PIC, Sigma-Aldrich, P8340) and inhibitors (Dithiothreitol (DTT), Benzamidine, and Phenylmethylsulfonylfluorid (PMSF) at 1 mM each). After washing, centrifugation was carried out at 1,100 rpm at 4 °C. Cell pellet was washed with PBS and lysed by using RIPA buffer containing 50 mM Tris/HCl (pH 7.5), 0.1% Triton™ X-100 (Sigma Aldrich), 150 mM NaCl, 0.5% Na-deoxycholate, 0.1% Sodium Dodecyl Sulfate (SDS) and PIC, also supplemented with 1 mM each of protease inhibitors DTT, Benzamidine, and PMSF. The quantity of RIPA buffer was kept 2-4 folds higher than the volume of the cell pellet and homogenized using syringe 0.4x19 mm needles (27Gx3/4", Nr.20, BD Macrolane TM3). The homogenized mixture was incubated on ice for 15 minutes, centrifuged at 16,000 g for 15 minutes. Finally, for denaturation of proteins, the supernatant was taken and heated in 5x SDS

sample buffer (recipe is given below) at 95°C for 10 minutes. Obtained protein samples were subjected for immunoblotting for using specific antibodies (Table 7.1 and 7.2).

### **5X SDS-sample buffer (10ml)**

1. 0.125M Tris/HCl
2. (pH 6.8) [0.5M]-----2.5 ml
3. 4% SDS [10%]-----4 ml
4. 20% Glycerol-----2 ml
5. 10%  $\beta$ -mercaptoethanol-----1 ml
6. Bromophenol blue-----0.005% (w/v)

### **7.10.2 Immunoblotting**

Two gels, 10% (depending upon the size of protein) resolving gel and 4% stacking gel was prepared for running equal amounts of denatured protein samples and Page Ruler Plus Prestained Protein Marker (Fermentas, 26619) were loaded on sodium dodecyl sulfate-polyacrylamide gel electrophoresis (SDS-PAGE) system. For resolving proteins by electrophoresis, MiniPROTEAN® (BioRad, Munich, Germany) system was used at 100-120 voltage supply for 2-3 hours. 1x SDS (25 mM Tris-base, 192 mM Glycine and 0.1% SDS) was used as sample running buffer. Following to electrophoresis, proteins were transferred to the nitrocellulose membrane (PROTRANR, Germany) was placed under the gel and both were sandwiched between blotting papers and sponges. The nitrocellulose membrane, gel, and blotting papers were soaked in blotting buffer thoroughly and pressed tightly to avoid bubbles and ensure proper transfer of proteins. The composition of wet blot buffer is: 48 mM Tris-base, 39 mM glycine, and 100% ethanol. The positive terminal (red) and the negative terminal (black) were connected in the right order. This sandwich was kept in wet blot transfer buffer at 4 °C overnight with a supply of 15 V and stirred at 700 rpm with a magnetic stirrer placed inside the buffer tank. After one night, the membrane was taken out and successful transfer of proteins to the membrane was revealed by staining the membrane with Ponceau S, composition is given below. Blocking was performed with 5 % milk powder dissolved in TBS-T buffer (Tris-buffered saline, with a composition of 15 mM NaCl, 1 mM Tris-HCl, pH 8.0, 0.04% Tween 20) under constant shaking for 1 h, at room temperature. Following to blocking, the membrane was incubated with primary antibody (on optimized dilution) for overnight at 4 °C . The following day, the membrane was washed with 1X TBST for three times each for five minutes. Next to this, the membrane was incubated with respective secondary antibody for one hour. It was then washed again with 1X TBST three times each

for five minutes. Finally, antibody signal was captured on X-ray films using Enhanced chemiluminescence (ECL) solution, composition is given below.

#### **10x Ponceau S (1 L)**

1. Ponceau S concentrate 0.03 M
2. Trichloroacetic acid 1.84 M
3. Suldodalicylic acid 1.37 M
4. Volume was increased to 1 L by adding ddH<sub>2</sub>O.

#### **ECL solution (20ml)**

1. 1 M Tris-HCl (pH 8.0)-----2 ml
2. Luminol (0.25 M in DMSO) 3-aminonaphthylhydrazide-200 µl
3. p-cumaric acid (0.09 M in DMSO)-----89 µl
4. dH<sub>2</sub>O-----18 ml
5. 30% H<sub>2</sub>O<sub>2</sub>-----6.3 µl

#### **Resolving gel 12% for western blotting (10ml)**

1. 1.5M Tris/HCl (pH 8.8)----- 2.5ml
2. 30% Polyacrylamide----- 4ml
3. 10% SDS----- 100µl
4. Water----- 3.4ml
5. 10% APS----- 22µl
6. TEMED----- 10µl

#### **Stacking gel 4% for western blotting (10ml)**

1. 0.5M Tris/HCl (pH 6.8) ----- 2ml
2. 30% Polyacrylamide----- 1.33ml
3. 10% SDS-----100µl
4. Water----- 6.56ml
5. 10% APS----- 22µl (in 3ml of total)
6. TEMED----- 10µl (in 3ml of total)

## **7.11 Site-directed mutagenesis to generate mutant constrcuts**

Prokaryotic and eukaryotic expression plasmids, pGEX-4T-1 (GE Healthcare GmbH) and pEGFP-C1, respectively, containing ORF (NM\_001320.6) of wild-type *CSNK2B* were further taken to generate the mutations of interests — c.94G>C, c.94G>A and c.374G>C — by using a site-directed mutagenesis kit (Promega). These wild-type plasmids along with prokaryotic expression plasmid, pGEX-4T-1 containing ORF (NM\_177559.3) of *CSNK2A1* used in this

study were taken from published data (<http://kups.ub.uni-koeln.de/id/eprint/8139>). Oligonucleotides (Table 7.3) containing particular mutations was designed individually with the help of Agilent primer design tool available online (<https://www.agilent.com/store/primerDesignProgram.jsp>). Mutant strand synthesis reaction was performed by PCR. The recipe for reaction mixture and program are given below:

### PCR master-mix composition

1. x  $\mu$ l (5-50 ng) template DNA
2. 2.5  $\mu$ l (125 ng) forward primer
3. 2.5  $\mu$ l (125 ng) reverse primer
4. 1  $\mu$ l dNTP-mix
5. 5  $\mu$ l 10x reaction buffer
6. 1  $\mu$ l PfuUltra HF DNA polymerase (2.5U/ $\mu$ l)
7. 50  $\mu$ l dH<sub>2</sub>O

### PCR program for site-directed mutagenesis

PCR program	Temp. (°C)	Time	Cycles
Initial denaturation	95	30 sec	x 1
Denaturation	95	30 sec	x12-18
Annealing	55	60 sec	
Extension	68	60 sec	
Final extension	68	10 min	x 1
Hold	4		

#### 7.11.1 Growing bacterial culture

For growing bacterial cells, lysogeny broth (LB) medium supplemented with appropriate antibiotics was used. The concentration of antibiotics added is as follows; Ampicillin, 100  $\mu$ g/ml and Kanamycin, 50  $\mu$ g/ml.

The LB and agar media were prepared as described below:

#### LB medium (1L) (pH 7.0)

1. Tryptone enzymatic digest from Casein (Fluka, BioChemika) -----10 g
2. Yeast extract (Fluka, BioChemika) -----5 g
3. NaCl-----5 g

#### LB agar plates (1L) (pH 7.0)

1. Tryptone enzymatic digest from Casein (Fluka, BioChemika) -----10 g
2. Yeast extract (Fluka, BioChemika) -----5 g
3. NaCl -----5 g
4. Bacto Agar (Becton, Dickinson and Company, France) -----15g

### **7.11.2 Transformation of competent bacterial cells**

All the prokaryotic and eukaryotic expression plasmids containing wild-type and mutant ORFs of *CSNK2B* were introduced into competent bacterial cells. For this purpose, the standard heat shock transformation method was followed {Hanahan, 1983 #252}. Two different types of bacterial cells were used; arctic cells for prokaryotic plasmids and XL1 Blue cells for eukaryotic expression plasmids. Notably, pGEX-4T1-CTNNB1 plasmid containing ORF (NM\_001904.4) was a kind gift from Prof. Dr. Catherin Niemann (CMMC, University of Cologne). For transforming the cells, 1-2  $\mu$ l of plasmid DNA (50 ng/ $\mu$ l) was mixed with 200  $\mu$ l of the bacterial cells. Then, the mixture was kept on ice for 30 minutes followed by heat-pulsed at 42°C in a water bath for 90 seconds. The mixture was immediately transferred to ice for two minutes. Super Optimal broth with Catabolite repression (SOC) medium was used to multiply the transformed bacterial cells. For that purpose, 0.9 ml of preheated at 42 °C SOC medium was added in the mixture and incubated at 37 °C for one hour on shaker (225–250 rpm). After one hour, the mixture was spread onto agar plate (containing agar supplemented with antibiotic) in using heat sterile glass spreader and incubated at 37 °C overnight. The following day, the transformed colonies showing growth on agar plate were picked and subcultured in LB broth supplemented with appropriate antibiotic respective to plasmid. Stock was being stored in glycerol at -80 °C. Plasmid DNA were purified from all kinds of bacterial cells by miniprep method and were further subjected for Sanger sequencing to confirm the site of desired mutation.

### **7.11.3 Plasmid DNA purification from prokaryotic cells**

Plasmid purification for validation of site directed mutagenesis with Sanger sequencing was performed manually by mini prep method. For that, 1 ml LB media (containing antibiotics) was inoculated with bacterial clone with vigorous shaking at 37 °C for 14-16 hrs. Next, 1.5 ml to 2 ml culture was transferred into microcentrifuge tube, and centrifuged at 20,000 rpm for 15 min to obtain the cell pellet. After discarding the LB media in supernatant, the cell pellet was resuspended in lysis buffer (25mM Tris-HCl, pH8.0, 10mM EDTA). It was made sure that the bacteria were completely resuspended and no clumps were visible. After this, the lysis buffer (50  $\mu$ l 400 mM NaOH, 50  $\mu$ l 2% SDS) was added, inverting 5-6 times and kept at RT for no longer than 5 min. Further, 120  $\mu$ l solution K (neutralization buffer) (5M potassium acetate, pH 5.5) was added, gently mixed and incubated at room

temperature for 3 min. At this point, the solution contained flocculent white precipitate consisting of bacterial DNA and protein which was removed by centrifugation at 12000rpm for 15 min. Following to this, the supernatant was carefully transferred to fresh tube avoiding the flakes. For precipitating the plasmid DNA 600  $\mu$ l isopropanol was added to the supernatant and mixed thoroughly by inverting 10 times. This DNA was collected as pellet by centrifugation of tubes at 14000 rpm for 10 min. For washing the DNA pellet obtained after centrifugation, 500  $\mu$ l 70% ethanol was added and re-spun the DNA down at 14000 rpm (full speed) for 10 min. The tubes were then kept for drying and later on the DNA was dissolved in 50  $\mu$ l ddH<sub>2</sub>O. The dissolved plasmid was used for downstream experiments.

In case of ultra-pure DNA needed for transfection, midi prep kit (Macherey-Nagel™ NucleoBond™ Xtra Midi - ThermoFisher Scientific, 740410.50) was used according to the set protocol of manufacturers.

## **7.12 Expression and purification of recombinant GST fused proteins from prokaryotic cells**

The transformed cells, containing the plasmids of wild-type and mutant pGEX-4T-1-CSNK2B, pGEX-4T-1-CTNNB1, and pGEX-4T-1 empty vector were grown in 10 ml LB media supplemented with Ampicillin at 37 °C, over the night. The following day, culture was diluted 1:25 by adding 240 ml LB media in 5 ml of bacterial culture. This diluted culture was grown without antibiotic at 37 °C until OD<sub>600</sub> reached 0.6-0.8 measured by spectrophotometer. Further, induction of protein expression was carried out by adding 0.5 mM of Isopropyl beta-D-1-thiogalactopyranoside (IPTG) and incubated overnight at 10 °C on shaker (225–250 rpm). The following day, induced culture was centrifuged at 5000 rpm for 15 min at 4°C. Supernatant was discarded and pellet was dissolved in bacterial lysis buffer (10 mM Tris-HCl, pH 8, 150 mM NaCl, and 1 mM EDTA) along with PIC and protease inhibitors (1 mM DTT, 1 mM benzamidine, 1 mM PMSF), lysozyme (1 mg/ml) and 1% sarcosyl. Further, the bacterial cells were lysed by pottering them 20 times in a glass potter followed by incubation on ice for 20 min. Additional 10 strokes were also performed after incubation on ice. Then, centrifugation of cell lysate was performed at 4 °C for 15 min at 15,000 rpm. Supernatant was taken and incubated overnight with Glutathione Sepharose® 4B



beads (GE Healthcare GmbH, GE17-0756-01) on a rolling rotator at 4 °C. The following day, sample was centrifuged at 500 rpm for 2 minutes to obtain protein bound GST beads. Then, beads were washed with lysis buffer containing inhibitors, 5 times for two minutes each. Further, 20 µl of the beads slurry was taken to boil with 5X SDS sample buffer at 95 °C for 5 min. Finally, for confirmation of purified protein, samples were loaded on a thin SDS-PAGE gel and subjected for staining proteins with Coomassie-Brilliant-Blue R 250, recipe is given below. The stock of beads bound protein was kept at 4 °C for later use in pull-down experiments.

#### **Coomassie-Brilliant-Blue R 250 staining solution (1L)**

1. Methanol 50 %
2. Acetic acid 10 %
3. Coomassie brilliant blue G-2500 0.1 %
4. Volume was increased to 1L by adding ddH<sub>2</sub>O and stirred gently

#### **7.12.1 Thrombin cleavage of GST tag from fusion proteins**

In order to cleave off the GST tag from the purified proteins, 10 units (1U/ul) of thrombin enzyme from bovine plasma (Sigma-Aldrich, T6634) was added to the beads containing fusion proteins and kept on the shaker for overnight at 4°C. After incubation, the supernatant was run on SDS-PAGE for confirmation of cleaved protein product. The thrombin cleavage buffer contained 500 mM Tris-HCl, pH 8.0, 150 mM NaCl and 100 mM CaCl<sub>2</sub>.

#### **7.13 Transient transfection of GFP-tagged constructs in eukaryotic cells**

For transient expression of purified protein, 70-80 percent confluent HeLa cells were transfected with the wild-type and mutant GFP-tagged *CTNNB1* cloned pEGFP-C1 and *CSNK2B*, both wild type and all three mutants, also cloned in pEGFP-C1 plasmids. Two different methods were followed for this purpose; electroporation by Amaxa Cell line Nucleofector (R) Kit V (LONZA, VCA-1003) and chemical transfection using 1mg/ml polyethylenimine (PEI, Polysciences, 23966) and lipofectamine 2000 (ThermoFisher Scientific, 11668019).

In case of electroporation done by Amaxa, the cultured cells were trypsinized and centrifuged at 1,100 rpm for 6 mins. The cell pellet was shifted to Amaxa cuvette (provided with the kit) and mixed with a pre-made solution of plasmid DNA (10 µg in 1 x 10<sup>6</sup>- 5 x 10<sup>6</sup> cells) and

nucleofactor buffer (100  $\mu$ l Nucleofector®Solution). Following to this, the cuvette containing cells and plamid DNA mix was placed in the Amaxa electroporator and the appropriate Nucleofector® program. After this, cells were dispersed in the media and kept in the incubator for 16- 24 hours for transfection.

For the chemical transfection carried out by PIE or lipofectamine 3000, the transfection reagent was mixed with DMEM media (without antibiotics and FBS), transfection buffer provided by the company, and purified plasmid DNA (30 $\mu$ g in 13cm dish). The mixture was incubated for 30 minutes for complex formation of transfection reagent and plasmid DNA. Total amount of this mixture was 1 ml, depending on the amount of transfection reagent (three folds of the amount of plasmid DNA) and plasmid DNA. After incubation of 30 min, the cells were supplemented with fresh media and the DNA mixture was thoroughly mixed into it and left for 16-24 hours.

After 16-24 hours of transfection, cells were harvested and lysed to get the protein for downstream processes. The process of protein purification from eukaryotic cells is already discussed.

#### **7.14 Pull-down assay**

This assay was conducted to reveal the binding association of GST-tagged CK2 $\beta$  wild-type and mutants with GFP-tagged  $\beta$ -Catenin and also with whole HeLa cell lysates. For this purpose, proteins obtained from overexpressed GFP-CTNNB1 and whole HeLa cell lysates were precleared by mixing glutathione sepharose beads for 4 hours at 4 °C. The pre-cleared lysates were then mixed with wild-type and mutant GST coupled CK2 $\beta$  proteins. GST protein coupled with GST beads was also prepared and mixed with lysate to be used as a control (in every assay). Further, the samples were incubated at 4 °C overnight with gentle shaking. The following day beads in the lysate were settled down by centrifugation at 500 rpm for 2 minutes. Washing of the beads was then carried out 5 times with BPS buffer. Beads containing CK2 $\beta$  proteins pulldown with GFP- $\beta$ -Catenin lysate were boiled at 95 °C in SDS sample buffer and resolved on 10-12% SDS-PAGE gel. Anti-GFP antibody was used for further western blot analysis and visualization of GFP-tagged  $\beta$ -Catenin. In addition, lysate of non-transfected LCLs and HeLa cells were also prepared and pulled down with wild-type and mutant GST tagged CK2 $\beta$  for detection of endogenous DVL3 protein using appropriate antibody.

## 7.15 Mass spectrometry analysis

For determining the interaction of cellular proteins with CK2 $\beta$  and to examine the effects of identified *CSNK2B* mutations, the purified wild-type and mutant GST-CK2 $\beta$  were incubated with HeLa cell lysate overnight at 4 °C. GST protein was used as negative control. The following day, beads were washed for all samples, 5 times with washing buffer containing 50 mM Tris-HCl; pH 7.5, 150 mM NaCl and inhibitors cocktail. Then DTT was added to reduce the samples, to a final concentration of 5 mM. For reducing the samples, 30 minutes incubation was carried out at 60 °C. Then, CAA was added to alkylate cysteines followed by incubation at room temperature (preferably in dark). Further, Lamieli buffer was added to the samples and boiled at 95 °C for 5-10 minutes. Samples were then analyzed by liquid chromatography-tandem mass spectrometry (LC-MS/MS) at CECAD proteomics facility according to the set protocol (Kallabis, Abraham et al. 2020).

## 7.16 Experiments conducted for determining the kinase activity of CK2 $\beta$ variants

For determining the kinase activity of CK2 $\beta$  variants as compared to wild type, two different strategies were adopted. Both of them are discussed as under.

### 7.16.1 ADP-Glo assay

The kinase activity of CK2 $\beta$  wild type and mutants was measured using ADP-Glo assay. For this purpose, kinase reaction was performed in 5  $\mu$ L volume containing 100 nM CK2 $\alpha$  and 200 nM CK2 $\beta$  (wild type and both mutants, p.Asp32His and p.Asp32Asn) in 80 mM NaCl, 280 mM Tris/HCl (pH 8.0), 50 mM CaCl<sub>2</sub>, 7.5 mM MgCl<sub>2</sub> and 1 mM ATP. After the addition of 6  $\mu$ M  $\beta$ -Catenin the reaction mixture was incubated for 25 min at 37 °C and 300 rpm. After 5 min re-tempering to room temperature, 5  $\mu$ L of ADP-Glo reagent was added to the samples for terminating the kinase reaction and depleting the remaining ATP for 1 h at room temperature. Afterwards 10  $\mu$ L kinase detection reagent was added to convert the generated ADP, into ATP. In this way synthesized ATP was measured in a luciferase/luciferin reaction. Luminescence was detected with a Tecan Infinite M200 Pro after 1 hour. A sample without the addition of CK2 $\alpha$  and CK2 $\beta$  variants was used as blank and its luminescence signal was subtracted from the luminescence intensities of the other samples. The

luminescence intensity of the sample containing CK2 $\beta$  wild type was set to 100 % and the luminescence intensities of the CK2 $\beta$  mutants were related to it.

### **7.16.2 Capillary Electrophoresis**

For the kinase reaction 80  $\mu$ L kinase buffer (50 mM Tris/HCl pH 7.5, 100 mM NaCl, 10 mM MgCl<sub>2</sub>) containing 70 nM CK2 $\alpha$  and 140 nM CK2 $\beta$  (wild type, and mutants p.Asp32His and p.Asp32Asn) were pre-incubated for 10 min on ice followed by 10 min incubation at 37°C. The reaction was started by the addition of 120  $\mu$ L assay buffer (25 mM Tris/HCl (pH 8.5), 150 mM NaCl, 5 mM MgCl<sub>2</sub>, 190  $\mu$ M substrate peptide RRRDDDSDDD (Wünsch, Kröger et al. 2020) and 60  $\mu$ M of ATP). The samples were incubated at 37 °C for 1 min, 2 min, 3 min, 4 min and 5 min. The reaction was stopped by reducing the temperature to 4°C and addition of 5  $\mu$ L EDTA (0.5 M).

Samples were analyzed by Beckman Coulter pa800 plus (Krefeld, Germany) CE system. With 2 M acetic acid (pH 2.0) as background electrolyte and a constant current of 30  $\mu$ A. Peptides were detected at a wavelength of 195 nm.

### **7.17 Microscale thermophoresis (MST)**

For investigating the interaction of alpha with wild type and mutant beta subunit of CK2, microscale thermophoresis was performed. The experiment was performed and  $K_D$  values were calculated by the previously defined protocol (Wünsch, Kröger et al. 2020)

### **7.18 Whole transcriptome analysis**

Whole transcriptome profiling of RNA obtained from *CSNK2B* mutated patient (FP2) LCLs and from control LCLs was carried out at CCG sequencing facility. Initially, 2  $\mu$ g of RNA was submitted for further sequencing. The samples were proceeded according to the established protocol of the facility (Wagle, Nikolić et al. 2015). Resultant reads were mapped to the *Homo sapiens* reference genome with the help of Tophat (version 2.0.10) and abundance estimation with Cufflinks (Version 2.1.1). Differential gene expression analysis was performed by DESeq2. QuickNGS database of CCG/CECAD was used for further analyses.

## 7.19 Whole phosphoproteome analysis

A total of 3 mg of protein lysates obtained from *CSNK2B* mutated patient (FP2) along with wild type was submitted to CECAD's proteomic facility. All the steps were followed according to their established protocol (Rinschen, Pahlmeyer et al. 2015).

**Table 7.1: List of primary antibodies used in this study**

Target antigen	Species	Company	Catalogue number	Concentration
NUP107	Rabbit polyclonal antibody	Sigma-Aldrich, St. Louis, USA	SAB2702098	1:1,000 - WB 1:200 - IF
NUP85	Mouse monoclonal antibody	Santa Cruz biotechnologies, Dallas, USA	sc-376111	1:1,000 - WB 1:200 - IF
NUP133	Mouse monoclonal antibody	Santa Cruz biotechnologies, Dallas, USA	sc-376763	1:1,000 - WB 1:200 - IF
NUP160	Rabbit polyclonal antibody	Abcam, Cambridge, USA	ab151563, EPR10291(B)	1:1,000 - WB
NUP37	Rabbit polyclonal antibody	Abcam, Cambridge, USA	ab201161	1:1,000 - WB 1:100 - IF
NUP93	Mouse monoclonal antibody	Santa Cruz biotechnologies, Dallas, USA	sc-374400	1:1,000 - WB
Fibrillarin	Rabbit polyclonal antibody	Abcam, Cambridge, USA	ab5821	1:100 - IF
HP1 $\beta$	Rabbit polyclonal antibody	Sigma Aldrich, St. Louis, USA	H2039	1:200 - IF
mAb414 (FG-repeat NUPs)	Mouse monoclonal antibody	Abcam, Cambridge, USA	ab24609	1:1,000 - WB 1:400 - IF
$\alpha$ -tubulin	Mouse monoclonal antibody	Sigma Aldrich, St. Louis, USA	T8328	1:3,000 - WB
CK2 $\beta$	Mouse monoclonal antibody	Santa Cruz biotechnologies, Dallas, USA	Sc-12739	1:1,000 - WB
CK2 $\beta$	Rabbit polyclonal antibody	Abcam, Cambridge, USA	Ab76025	1:100 - IF
CKAP2L	Rabbit polyclonal	Novusbiological	NBP1-83450	1:1500 - WB
CK2 $\alpha$	Mouse monoclonal antibody	Jena Biosciences	ABD-019	1:500 - WB
GM130	Rabbit polyclonal antibody	Abcam, Cambridge, USA	ab52649	1:300 - IF
DVL3	Rabbit monoclonal	Abcam, Cambridge, USA	ab76081	1:1000 - WB 1:200 - IF
H2AX (Ser139)	Mouse monoclonal antibody	Millipore	05-636	1:2000 - WB 1:200 - IF
CHK1 (2G1D5)	Mouse monoclonal antibody	Cell signalling technology	2360	1:500 - WB
CHK (Ser345)	Rabbit monoclonal antibody	Cell signalling technology	2348	1:250 - WB
$\beta$ -Catenin	Rabbit monoclonal antibody	Abcam, Cambridge, USA	ab32572	1:1000 - WB 1:100 - IF
Active $\beta$ -Catenin	Mouse monoclonal antibody	Millipore	05-665	1:50 - IF
GFP	Mouse monoclonal, K3-184-2	-	(Noegel, Rivero et al. 1999)	1:5 - WB 1:20 - IF
GAPDH	Mouse monoclonal GAPDH POD, monoclonal	Sigma-Aldrich Corp.	G8795	1:1000

WB = western blotting, IF = immunofluorescence

**Table 7.2: List of secondary antibodies used in this study**

Target antigen	Species	Company	Catalogue number	Concentration
<b>For immunofluorescence</b>				
Alexa Fluor 488 anti-rabbit IgG	Donkey	Invitrogen	A21206	1:10,000
Alexa Fluor 568 anti-mouse IgG	Goat	Invitrogen	A11004	1:10,000
Fluor 568 anti-rabbit IgG	Donkey	Abberior Star	635P	1:1000
<b>For immunoblotting</b>				
Anti-mouse IgG peroxidase conjugate	Mouse	Sigma Aldrich	A4416	1:10,000
Anti-rabbit IgG peroxidase conjugate	Rabbit	Sigma Aldrich	A6154	1:10,000

**Table 7.3: List of primers used in this study**

Gene	Forward primer, 5' to 3'	Reverse primer, 5' to 3'	Purpose
<i>PTPN23</i>	GGGACTCCCTCTCCTCACTC	GAGTGGATCCAGAAGGCTGA	CSA
<i>CDKL2</i>	ACCACCCTTTCCAAACTGC	TTTGCTCACTGCTCAGAAAAC	CSA
<i>CDKL5</i>	ATAAGAAAATATAAGCAGGAA GTCAAG	GAAACAGCCTTAAATAAAAG AATCG	CSA
<i>DNM3</i>	GGGTTGGAGTTGTTCAGATAC AC	GGCTTAGAAATGCCTGTTTTTC	CSA
<i>TRIM35</i>	CCGCTCTCCAAGATTTCC	GCTTCTCCACCAGGTTGTTG	CSA
<i>STIL</i>	CCTCCCGACAATGCAGATAG	AAGGGCAGGGAGTTAAAAGG	CSA
<i>AJM1</i>	ACGAGAACCTGCTGGGGCGC	ATGACCAGGTCCGTGATGAG	CSA
<i>DNAH11</i>	CTGCAAATTGTCAGGGAAGG	CCTCAAGCAGCAGCCATTAT	CSA
<i>SH2D3C</i>	ATGTGCTGGGCACAATGG	GTTGCCCAGGCTCAAGTG	CSA
<i>NUP37-RT</i>	CGTTGCAGGAAATGATTGG	AAAAGCAACTGAGACATTTTC TAAAG	RT PCR
<i>CSNK2B</i> c.94G>C	GTGGATGAAGACTACATCCAG CACAAATTTAATCTTACTGGAC	GTCCAGTAAGATTAAATTTGT GCTGGATGTAGTCTTCATCCA C	SDM
<i>CSNK2B</i> c.94G>A	GTGGATGAAGACTACATCCAG AACAAATTTAATCTTACTGGA C	GTCCAGTAAGATTAAATTTGT TCTGGATGTAGTCTTCATCCA C	SDM
<i>CSNK2B</i> c.374C>G	GCTTCCCATTGGCCTTTGAGAC ATCCCAGG	CCTGGGATGTCTCAAAGGCCA ATGGGAAGC	SDM
<i>CSNK2B</i> c.94G>A	TCTTCTGTGAAGTGGATGAAG AC	CCTTGCTGGTACTTTTCCAAC	qRT PCR
<i>CSNK2B</i> c.94G>A	GTGAAGCCATGGTGAAGCTC	GACTGGGCTCTTGAAGTTGC	qRT PCR
<i>GAPDH</i>	TGACAACAGCCTCAAGATCAT CAGCAA	GTTTTTCTAGACGGCAGGTCA GGTCCA	qRT PCR

CSA = Co-segregation analysis, RT = Reverse transcriptase, qRT = Quantitative RT, SDM= Site directed mutagenesis

## 8. Web resources

gnomAD: <https://gnomad.broadinstitute.org/>

PANTHER: <http://www.pantherdb.org/>

GORilla: <http://cbl-gorilla.cs.technion.ac.il/>

MUpro: <http://mupro.proteomics.ics.uci.edu/>

SNAP2: <https://roslab.org/services/snap2web/results.php?id=320f1b4c-ec5b-4f88-bcb4-efb56856fd2f>

PROVEAN: [http://provean.jcvi.org/seq\\_submit.php](http://provean.jcvi.org/seq_submit.php)

Meta SNP: <https://snps.biofold.org/meta-snp/>

HOPE: <https://www3.cmbi.umcn.nl/hope/input/>

I-Mutant: [https://folding.biofold.org/i-mutant/pages/I-Mutant2.0\\_Tutorial.html](https://folding.biofold.org/i-mutant/pages/I-Mutant2.0_Tutorial.html)

FunRich tool: <http://www.funrich.org/>

PyMOL: <https://pymol.org/2/>

PhosphoSitePlus: <https://www.phosphosite.org/homeAction>

Phospho.ELM: <http://phospho.elm.eu.org/dataset.html>

## 9. Abbreviations

APS	Ammonium persulfate
ATP	Adenosine triphosphate
cDNA	Complementary DNA
CM	Congenital microcephaly
CWS	Canonical wnt signaling
ddH <sub>2</sub> O	Double-distilled water
<i>CSNK2B</i>	Casein kinase 2 beta
DAPI	4', 6-Diamidino-2'-phenylindole
DDR	DNA damage response
DMEM	Dulbecco's Modified Eagle's Medium
DMSO	Dimethylsulfoxide
DNA	Deoxyribonucleic acid
dNTP	Deoxyribonucleotidetriphosphate
DTT	Dithiothreitol
ECL	Enhanced chemiluminescence
EDTA	Ethylenediaminetetraacetic acid
FBS	Fetal bovine serum
FLPIS	Filippi syndrome
FLS	Filippi-like syndrome
GAPDH	Glyceraldehyde-3-phosphate dehydrogenase
gnomAD	Genome Aggregation Database
GST	Glutathione-S-Transferase
HC	Head circumference
HSF	Human Splice Finder (HSF)
LB	Luria Bertani
LCLs	lymphoblastoid cell lines
LOD	Logarithm of the odds
MOPD	Microcephaly associated with primordial dwarfism



MCPH	Autosomal recessive primary microcephaly
MIM	Mendelian Inheritance in Man
MRI	Magnetic resonance imaging
NCBI	National Center for Biotechnology Information
NUPs	Nucleoporins
OD	Optical density
ORF	Open Reading Frame
PBS	Phosphate buffered saline
PCR	Polymerase chain reaction
PIC	Proteinase Inhibitor Cocktail
PMSF	Phenylmethanesulfonylfluoride
POBINDS	Poirier-Bienvenu neurodevelopmental syndrome
rpm	Revolutions per minute
RNA	Ribonucleic acid
RPMI	Roswell Park Memorial Institute
RT-PCR	Reverse transcriptase PCR
SAP	Shrimp Alkaline Phosphatase
SD	Standard deviation
SEM	Standard error of the mean
Taq	Thermus aquaticus
TEM	Transmission electron microscopy
TEMED	N,N,N',N'-Tetramethyl-ethylendiamin
SDS-PAGE	SDS-polyacrylamide gel electrophoresis
SRNS	Steroid resistant nephrotic syndrome
TBS-T	Tris-buffered saline-Tween-20
ZIKV	Zika virus

## 10. References

- Abecasis, G. R., S. S. Cherny, et al. (2001). "GRR: graphical representation of relationship errors." Bioinformatics **17**(8): 742-743.
- Abuelo, D. (2007). Microcephaly syndromes. Seminars in pediatric neurology, Elsevier.
- Acuna-Hidalgo, R., J. A. Veltman, et al. (2016). New insights into the generation and role of de novo mutations in health and disease. Genome Biology. **17**: 241.
- Ahmad, I., S. Baig, et al. (2017). "Genetic heterogeneity in Pakistani microcephaly families revisited." Clinical genetics **92**(1): 62-68.
- Ahmad, K. A., G. Wang, et al. (2005). "Targeting CK2 for cancer therapy." Anti-cancer drugs **16**(10): 1037-1043.
- Ahmed, K., D. A. Gerber, et al. (2002). "Joining the cell survival squad: an emerging role for protein kinase CK2." Trends in cell biology **12**(5): 226-230.
- Ahmed, K., O.-G. Issinger, et al. (2015). Protein Kinase CK2 Cellular Function in Normal and Disease States, Springer.
- Alakbarzade, V., A. Hameed, et al. (2015). "A partially inactivating mutation in the sodium-dependent lysophosphatidylcholine transporter MFSD2A causes a non-lethal microcephaly syndrome." Nature genetics **47**(7): 814.
- Alazami, A. M., N. Patel, et al. (2015). "Accelerating novel candidate gene discovery in neurogenetic disorders via whole-exome sequencing of prescreened multiplex consanguineous families." Cell reports **10**(2): 148-161.
- Alcantara, D. and M. O'driscoll (2014). Congenital microcephaly. American Journal of Medical Genetics Part C: Seminars in Medical Genetics, Wiley Online Library.
- Alvarado, F. J., J. M. Bos, et al. (2019). "Cardiac hypertrophy and arrhythmia in mice induced by a mutation in ryanodine receptor 2." JCI insight **4**(7).
- Aparicio-Siegmund, S., J. Sommer, et al. (2014). "Inhibition of protein kinase II (CK2) prevents induced signal transducer and activator of transcription (STAT) 1/3 and constitutive STAT3 activation." Oncotarget **5**(8): 2131.
- Arrigoni, G., M. A. Pagano, et al. (2008). "Mass spectrometry analysis of a protein kinase CK2 $\beta$  subunit interactome isolated from mouse brain by affinity chromatography." The Journal of Proteome Research **7**(3): 990-1000.
- Awad, S., M. S. Al-Dosari, et al. (2013). "Mutation in PHC1 implicates chromatin remodeling in primary microcephaly pathogenesis." Human molecular genetics **22**(11): 2200-2213.

- Bakrania, P., M. Efthymiou, et al. (2008). "Mutations in BMP4 cause eye, brain, and digit developmental anomalies: overlap between the BMP4 and hedgehog signaling pathways." The American Journal of Human Genetics **82**(2): 304-319.
- Barbelanne, M. and W. Y. Tsang (2014). "Molecular and cellular basis of autosomal recessive primary microcephaly." BioMed research international **2014**.
- Barbosa-Morais, N. L., M. Irimia, et al. (2012). "The evolutionary landscape of alternative splicing in vertebrate species." Science **338**(6114): 1587-1593.
- Barkovich, A. J., R. Guerrini, et al. (2012). "A developmental and genetic classification for malformations of cortical development: update 2012." Brain **135**(5): 1348-1369.
- Barrangou, R. and P. Horvath (2017). "A decade of discovery: CRISPR functions and applications." Nature microbiology **2**(7): 17092.
- Basel-Vanagaite, L., L. Muncher, et al. (2006). "Mutated nup62 causes autosomal recessive infantile bilateral striatal necrosis." Annals of Neurology: Official Journal of the American Neurological Association and the Child Neurology Society **60**(2): 214-222.
- Basit, S., K. M. Al-Harbi, et al. (2016). "CIT, a gene involved in neurogenic cytokinesis, is mutated in human primary microcephaly." Human genetics **135**(10): 1199-1207.
- Basto, R., K. Brunk, et al. (2008). "Centrosome amplification can initiate tumorigenesis in flies." Cell **133**(6): 1032-1042.
- Battaglia, A., T. Filippi, et al. (2008). "Filippi syndrome: further clinical characterization." American Journal of Medical Genetics Part A **146**(14): 1848-1852.
- Beck, M. and E. Hurt (2016). "The nuclear pore complex: understanding its function through structural insight." Nature Reviews Molecular Cell Biology **18**: 73.
- Beck, M. and E. Hurt (2017). "The nuclear pore complex: understanding its function through structural insight." Nature Reviews Molecular Cell Biology **18**(2): 73.
- Bend, R., L. Cohen, et al. (2020). "Phenotype and mutation expansion of the PTPN23 associated disorder characterized by neurodevelopmental delay and structural brain abnormalities." European Journal of Human Genetics **28**(1): 76-87.
- Bennett, H., A. Presti, et al. (2014). "A prenatal presentation of severe microcephaly and brain anomalies in a patient with novel compound heterozygous mutations in the STIL gene found postnatally with exome analysis." Pediatric neurology **51**(3): 434-436.
- Bettencourt-Dias, M., F. Hildebrandt, et al. (2011). "Centrosomes and cilia in human disease." Trends in Genetics **27**(8): 307-315.
- Bhat, V., S. Girimaji, et al. (2011). "Mutations in WDR62, encoding a centrosomal and nuclear protein, in Indian primary microcephaly families with cortical malformations." Clinical genetics **80**(6): 532-540.

- Bian, Y., M. Ye, et al. (2013). "Global screening of CK2 kinase substrates by an integrated phosphoproteomics workflow." Scientific reports **3**: 3460.
- Bilgüvar, K., A. K. Öztürk, et al. (2010). "Whole-exome sequencing identifies recessive WDR62 mutations in severe brain malformations." Nature **467**(7312): 207.
- Bittles, A. (2008). "A community genetics perspective on consanguineous marriage." Public Health Genomics **11**(6): 324-330.
- Bittles, A. H. (1990). "Consanguineous marriage: current global incidence and its relevance to demographic research."
- Bittles, A. H. and M. Black (2010). "Consanguinity, human evolution, and complex diseases." Proceedings of the National Academy of Sciences **107**(suppl 1): 1779-1786.
- Blencowe, H., S. Moorthie, et al. (2018). "Rare single gene disorders: estimating baseline prevalence and outcomes worldwide." Journal of community genetics **9**(4): 397-406.
- BODENBACH, L., J. FAUSS, et al. (1994). "Recombinant human casein kinase II: A study with the complete set of subunits ( $\alpha$ ,  $\alpha'$  and  $\beta$ ), site-directed autophosphorylation mutants and a bicistronically expressed holoenzyme." European journal of biochemistry **220**(1): 263-273.
- Bond, J., S. Scott, et al. (2003). "Protein-truncating mutations in ASPM cause variable reduction in brain size." The American Journal of Human Genetics **73**(5): 1170-1177.
- Bond, J. and C. G. Woods (2006). "Cytoskeletal genes regulating brain size." Current opinion in cell biology **18**(1): 95-101.
- Borrell, V. and I. Reillo (2012). "Emerging roles of neural stem cells in cerebral cortex development and evolution." Developmental neurobiology **72**(7): 955-971.
- Boumil, R. M., V. A. Letts, et al. (2010). "A missense mutation in a highly conserved alternate exon of dynamin-1 causes epilepsy in fitful mice." PLoS genetics **6**(8).
- Boycott, K. M., M. R. Vanstone, et al. (2013). "Rare-disease genetics in the era of next-generation sequencing: discovery to translation." Nature Reviews Genetics **14**(10): 681.
- Branzei, D. and M. Foiani (2010). "Maintaining genome stability at the replication fork." Nature Reviews Molecular Cell Biology **11**(3): 208.
- Braun, D. A., S. Lovric, et al. (2018). "Mutations in multiple components of the nuclear pore complex cause nephrotic syndrome." Journal of Clinical Investigation **128**(10): 4313-4328.
- Braun, D. A., C. E. Sadowski, et al. (2016). "Mutations in nuclear pore genes NUP93, NUP205 and XPO5 cause steroid-resistant nephrotic syndrome." Nature genetics **48**(4): 457.
- Buchman, J. J., O. Durak, et al. (2011). "ASPM regulates Wnt signaling pathway activity in the developing brain." Genes & development **25**(18): 1909-1914.

- Buchou, T., M. Vernet, et al. (2003). "Disruption of the regulatory  $\beta$  subunit of protein kinase CK2 in mice leads to a cell-autonomous defect and early embryonic lethality." Molecular and cellular biology **23**(3): 908-915.
- Canning, P., K. Park, et al. (2018). "CDKL family kinases have evolved distinct structural features and ciliary function." Cell reports **22**(4): 885-894.
- Capecchi, G., M. Baldassarri, et al. (2018). "CKAP2L mutation confirms the diagnosis of Filippi syndrome." Clinical genetics **93**(5): 1109-1110.
- Castrén, M., E. Gaily, et al. (2011). "Epilepsy caused by CDKL5 mutations." European journal of paediatric neurology **15**(1): 65-69.
- Chakraborty, P., Y. Wang, et al. (2008). "Nucleoporin levels regulate cell cycle progression and phase-specific gene expression." Developmental cell **15**(5): 657-667.
- Chavali, P. L., M. Pütz, et al. (2014). "Small organelle, big responsibility: the role of centrosomes in development and disease." Philosophical Transactions of the Royal Society B: Biological Sciences **369**(1650): 20130468.
- Chellas-Gery, B., K. Wolf, et al. (2011). "Biochemical and localization analyses of putative type III secretion translocator proteins CopB and CopB2 of Chlamydia trachomatis reveal significant distinctions." Infection and immunity **79**(8): 3036-3045.
- Chial, H. (2008). "DNA sequencing technologies key to the Human Genome Project." Nature Education **1**(1): 219.
- Christianson, A., C. P. Howson, et al. (2006). "March of Dimes." Global report on birth defect. The hidden toll of dying and disabled children. New York.
- Clevers, H. and R. Nusse (2012). "Wnt/ $\beta$ -catenin signaling and disease." Cell **149**(6): 1192-1205.
- Collins, F. S., M. Morgan, et al. (2003). "The Human Genome Project: lessons from large-scale biology." Science **300**(5617): 286-290.
- Colomer, J. M. and A. R. Means (2000). "Chronic elevation of calmodulin in the ventricles of transgenic mice increases the autonomous activity of calmodulin-dependent protein kinase II, which regulates atrial natriuretic factor gene expression." Molecular Endocrinology **14**(8): 1125-1136.
- Consortium, G. P. (2015). "A global reference for human genetic variation." Nature **526**(7571): 68.
- Corry, P. C. (2014). "Consanguinity and prevalence patterns of inherited disease in the UK Pakistani community." Human heredity **77**(1-4): 207-216.
- Cox, J., A. P. Jackson, et al. (2006). "What primary microcephaly can tell us about brain growth." Trends in molecular medicine **12**(8): 358-366.

- Cragan, J. D., J. L. Isenburg, et al. (2016). "Population-based microcephaly surveillance in the United States, 2009 to 2013: An analysis of potential sources of variation." Birth Defects Research Part A: Clinical and Molecular Teratology **106**(11): 972-982.
- Cristofoli, F., B. De Keersmaecker, et al. (2017). "Novel STIL compound heterozygous mutations cause severe fetal microcephaly and centriolar lengthening." Molecular syndromology **8**(6): 282-293.
- Darvish, H., S. Esmaeeli-Nieh, et al. (2010). "A clinical and molecular genetic study of 112 Iranian families with primary microcephaly." Journal of medical genetics **47**(12): 823-828.
- Davidson, G. and C. Niehrs (2010). "Emerging links between CDK cell cycle regulators and Wnt signaling." Trends in cell biology **20**(8): 453-460.
- de Villavicencio-Díaz, T. N., Y. Mazola, et al. (2015). "Predicting CK2 beta-dependent substrates using linear patterns." Biochemistry and biophysics reports **4**: 20-27.
- de Vries, B. B., W. G. van't Hoff, et al. (2001). "Diagnostic dilemmas in four infants with nephrotic syndrome, microcephaly and severe developmental delay." Clinical dysmorphology **10**(2): 115-121.
- de Vries, T. I., G. R. Monroe, et al. (2016). "Mosaic CREBBP mutation causes overlapping clinical features of Rubinstein-Taybi and Filippi syndromes." European Journal of Human Genetics **24**(9): 1363.
- del Viso, F., F. Huang, et al. (2016). "Congenital heart disease genetics uncovers context-dependent organization and function of nucleoporins at cilia." Developmental cell **38**(5): 478-492.
- Desmet, F.-O., D. Hamroun, et al. (2009). "Human Splicing Finder: an online bioinformatics tool to predict splicing signals." Nucleic acids research **37**(9): e67-e67.
- DiStasio, A., A. Driver, et al. (2017). "Copb2 is essential for embryogenesis and hypomorphic mutations cause human microcephaly." Human molecular genetics **26**(24): 4836-4848.
- Dobzhansky, T. (2013). "Nothing in biology makes sense except in the light of evolution." The american biology teacher **75**(2): 87-92.
- Duerinckx, S. and M. Abramowicz (2018). The genetics of congenitally small brains. Seminars in cell & developmental biology, Elsevier.
- Dyer, O. (2005). MP is criticised for saying that marriage of first cousins is a health problem, British Medical Journal Publishing Group.
- Farooq, M., A. Fatima, et al. (2016). "A novel splice site mutation in CEP135 is associated with primary microcephaly in a Pakistani family." Journal of human genetics **61**(3): 271.
- Fei, J.-F., C. Haffner, et al. (2014). "3' UTR-dependent, miR-92-mediated restriction of Tis21 expression maintains asymmetric neural stem cell division to ensure proper neocortex size." Cell reports **7**(2): 398-411.

- Ferreira, T. and W. Rasband (2012). "ImageJ user guide." ImageJ/Fiji **1**: 155-161.
- Filippi, G., F. C. Fraser, et al. (1985). "Unusual facial appearance, microcephaly, growth and mental retardation, and syndactyly. A new syndrome?" American journal of medical genetics **22**(4): 821-824.
- Fish, J. L., C. Dehay, et al. (2008). "Making bigger brains—the evolution of neural-progenitor-cell division." Journal of cell science **121**(17): 2783-2793.
- Fish, J. L., Y. Kosodo, et al. (2006). "Aspm specifically maintains symmetric proliferative divisions of neuroepithelial cells." Proceedings of the National Academy of Sciences **103**(27): 10438-10443.
- Franchin, C., M. Salvi, et al. (2015). "Proteomics perturbations promoted by the protein kinase CK2 inhibitor quinalizarin." Biochimica et Biophysica Acta (BBA)-Proteins and Proteomics **1854**(10): 1676-1686.
- Francioli, L., G. Tiao, et al. (2018). "gnomAD v2. 1." MacArthur Lab.
- Fujita, A., H. Tsukaguchi, et al. (2018). "Homozygous splicing mutation in NUP133 causes Galloway–Mowat syndrome." Annals of neurology **84**(6): 814-828.
- Gao, C., G. Xiao, et al. (2014). "Regulation of Wnt/ $\beta$ -catenin signaling by posttranslational modifications." Cell & bioscience **4**(1): 13.
- Garty, B. Z., B. Eisenstein, et al. (1994). "Microcephaly and congenital nephrotic syndrome owing to diffuse mesangial sclerosis: an autosomal recessive syndrome." Journal of medical genetics **31**(2): 121-125.
- Genin, A., J. Desir, et al. (2012). "Kinetochore KMN network gene CASC5 mutated in primary microcephaly." Human molecular genetics **21**(24): 5306-5317.
- Gibson, S. A. and E. N. Benveniste (2018). "Protein kinase CK2: an emerging regulator of immunity." Trends in immunology **39**(2): 82-85.
- Gibson, S. A., W. Yang, et al. (2017). "Protein kinase CK2 controls the fate between Th17 cell and regulatory T cell differentiation." The Journal of Immunology **198**(11): 4244-4254.
- Gilissen, C., J. Y. Hehir-Kwa, et al. (2014). "Genome sequencing identifies major causes of severe intellectual disability." Nature **511**(7509): 344.
- Gilissen, C., A. Hoischen, et al. (2012). "Disease gene identification strategies for exome sequencing." European Journal of Human Genetics **20**(5): 490.
- Gilmore, E. C. and C. A. Walsh (2013). "Genetic causes of microcephaly and lessons for neuronal development." Wiley Interdisciplinary Reviews: Developmental Biology **2**(4): 461-478.
- Götz, M. and W. B. Huttner (2005). "Developmental cell biology: The cell biology of neurogenesis." Nature Reviews Molecular Cell Biology **6**(10): 777.

- Goyal, L., J. P. Goyal, et al. (2015). "Filippi Syndrome: Report of a Rare Case." Journal of Clinical and Diagnostic Research: JCDR **9**(12): SD01.
- Griffiths, A. J., S. R. Wessler, et al. (2005). An introduction to genetic analysis, Macmillan.
- Grove, E. A., B. P. Williams, et al. (1993). "Multiple restricted lineages in the embryonic rat cerebral cortex." Development **117**(2): 553-561.
- Gudbjartsson, D. F., K. Jonasson, et al. (2000). "Allegro, a new computer program for multipoint linkage analysis." Nature genetics **25**(1): 12-13.
- Guernsey, D. L., H. Jiang, et al. (2010). "Mutations in centrosomal protein CEP152 in primary microcephaly families linked to MCPH4." The American Journal of Human Genetics **87**(1): 40-51.
- Guerra, B., O.-G. Issinger, et al. (2003). "Modulation of human checkpoint kinase Chk1 by the regulatory  $\beta$ -subunit of protein kinase CK2." Oncogene **22**(32): 4933.
- Harms, F. L., K. Kloth, et al. (2018). "Activating mutations in PAK1, encoding p21-activated kinase 1, cause a neurodevelopmental disorder." The American Journal of Human Genetics **103**(4): 579-591.
- Haubensak, W., A. Attardo, et al. (2004). "Neurons arise in the basal neuroepithelium of the early mammalian telencephalon: a major site of neurogenesis." Proceedings of the National Academy of Sciences **101**(9): 3196-3201.
- Hebsgaard, S. M., P. G. Korning, et al. (1996). "Splice site prediction in Arabidopsis thaliana pre-mRNA by combining local and global sequence information." Nucleic acids research **24**(17): 3439-3452.
- Hetzer, M. W. (2010). "The nuclear envelope." Cold Spring Harbor perspectives in biology **2**(3): a000539.
- Hirano, S. and M. Takeichi (2012). "Cadherins in brain morphogenesis and wiring." Physiological Reviews **92**(2): 597-634.
- Hoischen, A., B. W. van Bon, et al. (2010). "De novo mutations of SETBP1 cause Schinzel-Giedion syndrome." Nature genetics **42**(6): 483.
- Homma, M. K. and Y. Homma (2008). "Cell cycle and activation of CK2." Molecular and cellular biochemistry **316**(1-2): 49-55.
- Huelsken, J. and J. Behrens (2002). "The Wnt signalling pathway." Journal of cell science **115**(21): 3977-3978.
- Hussain, M. S., S. M. Baig, et al. (2012). "A truncating mutation of CEP135 causes primary microcephaly and disturbed centrosomal function." The American Journal of Human Genetics **90**(5): 871-878.



- Hussain, M. S., S. M. Baig, et al. (2013). "CDK6 associates with the centrosome during mitosis and is mutated in a large Pakistani family with primary microcephaly." Human molecular genetics **22**(25): 5199-5214.
- Hussain, M. S., A. Battaglia, et al. (2014). "Mutations in CKAP2L, the human homolog of the mouse Radmis gene, cause Filippi syndrome." The American Journal of Human Genetics **95**(5): 622-632.
- Hussain, R. and A. H. Bittles (1998). "The prevalence and demographic characteristics of consanguineous marriages in Pakistan." Journal of biosocial science **30**(2): 261-275.
- Issa, L., K. Mueller, et al. (2013). "Clinical and cellular features in patients with primary autosomal recessive microcephaly and a novel CDK5RAP2 mutation." Orphanet journal of rare diseases **8**(1): 59.
- Jackson, A. P., D. P. McHale, et al. (1998). "Primary autosomal recessive microcephaly (MCPH1) maps to chromosome 8p22-pter." The American Journal of Human Genetics **63**(2): 541-546.
- Javed, A. O., Y. Li, et al. (2018). "Microcephaly modeling of kinetochore mutation reveals a brain-specific phenotype." Cell reports **25**(2): 368-382. e365.
- Jayaraman, D., B.-I. Bae, et al. (2018). "The genetics of primary microcephaly." Annual review of genomics and human genetics **19**: 177-200.
- Jayaraman, D., A. Kodani, et al. (2016). "Microcephaly proteins Wdr62 and Aspm define a mother centriole complex regulating centriole biogenesis, apical complex, and cell fate." Neuron **92**(4): 813-828.
- Johnson, D. E. (1998). "Regulation of survival pathways by IL-3 and induction of apoptosis following IL-3 withdrawal." Front Biosci **3**: d313-d324.
- Jordan, D., S. Hindocha, et al. (2012). "The Epidemiology, Genetics and future Management of Syndactyly, The Open Orthop." J **6**: 14-27.
- Kadir, R., T. Harel, et al. (2016). "ALFY-controlled DVL3 autophagy regulates Wnt signaling, determining human brain size." PLoS genetics **12**(3): e1005919.
- Kaindl, A. M., S. Passemard, et al. (2010). "Many roads lead to primary autosomal recessive microcephaly." Progress in neurobiology **90**(3): 363-383.
- Kallabis, S., L. Abraham, et al. (2020). "High-throughput proteomics fiber typing (ProFiT) for comprehensive characterization of single skeletal muscle fibers." Skeletal muscle **10**(1): 1-18.
- Karczewski, K. and L. Francioli (2017). "The Genome Aggregation Database (gnomAD)." MacArthur Lab.
- Keaney, J. and M. Campbell (2015). "The dynamic blood–brain barrier." The FEBS journal **282**(21): 4067-4079.

- Kelley, K., K. E. Knockenhauer, et al. (2015). "Atomic structure of the Y complex of the nuclear pore." Nature structural & molecular biology **22**(5): 425.
- Khan, M. A., V. M. Rupp, et al. (2014). "A missense mutation in the PISA domain of HsSAS-6 causes autosomal recessive primary microcephaly in a large consanguineous Pakistani family." Human molecular genetics **23**(22): 5940-5949.
- Kilstrup-Nielsen, C., L. Rusconi, et al. (2012). "What we know and would like to know about CDKL5 and its involvement in epileptic encephalopathy." Neural plasticity **2012**.
- Komai, T., K. I. Kishimoto, et al. (1955). "Genetic study of microcephaly based on Japanese material." American journal of human genetics **7**(1): 51.
- Kousar, R., M. J. Hassan, et al. (2011). "Mutations in WDR62 gene in Pakistani families with autosomal recessive primary microcephaly." BMC neurology **11**(1): 119.
- Kraemer, N., S. Picker-Minh, et al. (2016). "Genetic causes of MCPH in consanguineous Pakistani families." Clinical genetics **89**(6): 744-745.
- Kriegstein, A., S. Noctor, et al. (2006). "Patterns of neural stem and progenitor cell division may underlie evolutionary cortical expansion." Nature Reviews Neuroscience **7**(11): 883.
- Kriegstein, A. R. and S. C. Noctor (2004). "Patterns of neuronal migration in the embryonic cortex." Trends in neurosciences **27**(7): 392-399.
- Kuijpers, M. and C. C. Hoogenraad (2011). "Centrosomes, microtubules and neuronal development." Molecular and Cellular Neuroscience **48**(4): 349-358.
- Kumar, A., S. C. Girimaji, et al. (2009). "Mutations in STIL, encoding a pericentriolar and centrosomal protein, cause primary microcephaly." The American Journal of Human Genetics **84**(2): 286-290.
- Landry, J. J., P. T. Pyl, et al. (2013). "The genomic and transcriptomic landscape of a HeLa cell line." G3: Genes, Genomes, Genetics **3**(8): 1213-1224.
- Lazier, J., J. Chernos, et al. (2014). "A 2q24. 3q31. 1 microdeletion found in a patient with Filippi-like syndrome phenotype: A case report." American Journal of Medical Genetics Part A **164**(9): 2385-2387.
- Lenkkeri, U., M. Männikkö, et al. (1999). "Structure of the gene for congenital nephrotic syndrome of the Finnish type (NPHS1) and characterization of mutations." The American Journal of Human Genetics **64**(1): 51-61.
- Létard, P., S. Drunat, et al. (2018). "Autosomal recessive primary microcephaly due to ASPM mutations: An update." Human mutation **39**(3): 319-332.
- Lewis, R. (2016). Human genetics: the basics, Garland Science.
- Li, H., L. Saucedo-Cuevas, et al. (2016). "Zika virus infects neural progenitors in the adult mouse brain and alters proliferation." Cell stem cell **19**(5): 593-598.

- Lin, S.-Y., R. Rai, et al. (2005). "BRIT1/MCPH1 is a DNA damage responsive protein that regulates the Brca1–Chk1 pathway, implicating checkpoint dysfunction in microcephaly." Proceedings of the National Academy of Sciences **102**(42): 15105-15109.
- Liu, C., Y. Li, et al. (2002). "Control of  $\beta$ -catenin phosphorylation/degradation by a dual-kinase mechanism." Cell **108**(6): 837-847.
- Logan, C. Y. and R. Nusse (2004). "The Wnt signaling pathway in development and disease." Annu. Rev. Cell Dev. Biol. **20**: 781-810.
- Loi, M., S. Trazzi, et al. (2020). "Increased DNA Damage and Apoptosis in CDKL5-Deficient Neurons." Molecular neurobiology: 1-19.
- Loiodice, I., A. Alves, et al. (2004). "The entire Nup107-160 complex, including three new members, is targeted as one entity to kinetochores in mitosis." Molecular biology of the cell **15**(7): 3333-3344.
- Lupski, J. R., J. W. Belmont, et al. (2011). "Clan genomics and the complex architecture of human disease." Cell **147**(1): 32-43.
- Lupu, F., A. Alves, et al. (2008). "Nuclear pore composition regulates neural stem/progenitor cell differentiation in the mouse embryo." Developmental cell **14**(6): 831-842.
- Lynch, M. (2010). "Rate, molecular spectrum, and consequences of human mutation." Proceedings of the National Academy of Sciences **107**(3): 961-968.
- Machon, O., M. Backman, et al. (2007). "A dynamic gradient of Wnt signaling controls initiation of neurogenesis in the mammalian cortex and cellular specification in the hippocampus." Developmental biology **311**(1): 223-237.
- Marin, O., F. Meggio, et al. (1997). "Physical dissection of the structural elements responsible for regulatory properties and intersubunit interactions of protein kinase CK2  $\beta$ -subunit." Biochemistry **36**(23): 7192-7198.
- Mason, H. (2011). Investigating the role of 53BP1 in regulating gene transcription, University of Birmingham.
- Meggio, F., B. Boldyreff, et al. (1994). "Casein Kinase 2 Down-Regulation and Activation by Polybasic Peptides Are Mediated by Acidic Residues in the 55-64 Region of the  $\beta$ -Subunit. A Study with Calmodulin As Phosphorylatable Substrate." Biochemistry **33**(14): 4336-4342.
- Mirzaa, G. M., B. Vitre, et al. (2014). "Mutations in CENPE define a novel kinetochore-centromeric mechanism for microcephalic primordial dwarfism." Human genetics **133**(8): 1023-1039.
- Miyake, N., H. Tsukaguchi, et al. (2015). "Biallelic mutations in nuclear pore complex subunit NUP107 cause early-childhood-onset steroid-resistant nephrotic syndrome." The American Journal of Human Genetics **97**(4): 555-566.

- Mlakar, J., M. Korva, et al. (2016). "Zika virus associated with microcephaly." New England Journal of Medicine **374**(10): 951-958.
- Modell, B. and A. Darr (2002). "Genetic counselling and customary consanguineous marriage." Nature Reviews Genetics **3**(3): 225-229.
- Mora-Bermúdez, F., M. T. García, et al. (2013). "Stem cells: neural stem cells in cerebral cortex development." Neuroscience in the 21st Century: From Basic to Clinical: 137-159.
- Mouden, C., M. de Tayrac, et al. (2015). "Homozygous STIL mutation causes holoprosencephaly and microcephaly in two siblings." PloS one **10**(2): e0117418.
- Nakashima, M., J. Tohyama, et al. (2019). "Identification of de novo CSNK2A1 and CSNK2B variants in cases of global developmental delay with seizures." Journal of human genetics **64**(4): 313.
- Narayanaswamy, P. B., S. Tkachuk, et al. (2016). "CHK1 and RAD51 activation after DNA damage is regulated via urokinase receptor/TLR4 signaling." Cell death & disease **7**(9): e2383.
- Nicholas, A. K., M. Khurshid, et al. (2010). "WDR62 is associated with the spindle pole and is mutated in human microcephaly." Nature genetics **42**(11): 1010.
- Niefind, K., B. Guerra, et al. (2001). "Crystal structure of human protein kinase CK2: insights into basic properties of the CK2 holoenzyme." The EMBO journal **20**(19): 5320-5331.
- Noegel, A. A., F. Rivero, et al. (1999). "Assessing the role of the ASP56/CAP homologue of Dictyostelium discoideum and the requirements for subcellular localization." Journal of cell science **112**(19): 3195-3203.
- O'Connell, J. R. and D. E. Weeks (1998). "PedCheck: a program for identification of genotype incompatibilities in linkage analysis." The American Journal of Human Genetics **63**(1): 259-266.
- O'Driscoll, M. and P. A. Jeggo (2008). "The role of the DNA damage response pathways in brain development and microcephaly: insight from human disorders." DNA Repair **7**(7): 1039-1050.
- Orgah, J. O., J. Yu, et al. (2018). "Danhong Injection Reversed Cardiac Abnormality in Brain–Heart Syndrome via Local and Remote  $\beta$ -Adrenergic Receptor Signaling." Frontiers in pharmacology **9**: 692.
- Organization, W. H. (1985). "Advisory Group on Hereditary Diseases. Community approaches to the control of hereditary diseases." Unpublished WHO document: HMG/WG/85.10. Available at [https://whqlibdoc.who.int/hq/1985-86/HDP-WG\\_85\\_10](https://whqlibdoc.who.int/hq/1985-86/HDP-WG_85_10).
- Orrico, A. and G. Hayek (1997). "An additional case of craniodigital syndrome: variable expression of the Filippi syndrome?" Clinical genetics **52**(3): 177-179.

- Pagano, M. A., S. Sarno, et al. (2005). "Autophosphorylation at the regulatory  $\beta$  subunit reflects the supramolecular organization of protein kinase CK2." Molecular and cellular biochemistry **274**(1-2): 23-29.
- Palm, L., I. Hägerstrand, et al. (1986). "Nephrosis and disturbances of neuronal migration in male siblings--a new hereditary disorder?" Archives of disease in childhood **61**(6): 545-548.
- Papari, E., M. Bastami, et al. (2013). "Investigation of primary microcephaly in Bushehr province of Iran: novel STIL and ASPM mutations." Clinical genetics **83**(5): 488-490.
- Passemard, S., A. M. Kaindl, et al. (2013). Microcephaly. Handbook of Clinical neurology, Elsevier. **111**: 129-141.
- Passemard, S., L. Titomanlio, et al. (2009). "Expanding the clinical and neuroradiologic phenotype of primary microcephaly due to ASPM mutations." Neurology **73**(12): 962-969.
- Pelvig, D., H. Pakkenberg, et al. (2008). "Neocortical glial cell numbers in human brains." Neurobiology of aging **29**(11): 1754-1762.
- Perez, D. I., C. Gil, et al. (2011). "Protein kinases CK1 and CK2 as new targets for neurodegenerative diseases." Medicinal research reviews **31**(6): 924-954.
- Perez, Y., R. Bar-Yaacov, et al. (2019). "Mutations in the microtubule-associated protein MAP11 (C7orf43) cause microcephaly in humans and zebrafish." Brain **142**(3): 574-585.
- Pfaff, K. L., C. T. Straub, et al. (2007). "The zebra fish cassiopeia mutant reveals that SIL is required for mitotic spindle organization." Molecular and cellular biology **27**(16): 5887-5897.
- Poirier, K., L. Hubert, et al. (2017). "CSNK2B splice site mutations in patients cause intellectual disability with or without myoclonic epilepsy." Human mutation **38**(8): 932-941.
- Pompolo, S. and V. Harley (2001). "Localisation of the SRY-related HMG box protein, SOX9, in rodent brain." Brain research **906**(1-2): 143-148.
- Posey, J. E., J. A. Rosenfeld, et al. (2016). "Molecular diagnostic experience of whole-exome sequencing in adult patients." Genetics in Medicine **18**(7): 678.
- Poulton, C. J., R. Schot, et al. (2014). "Severe presentation of WDR62 mutation: is there a role for modifying genetic factors?" American Journal of Medical Genetics Part A **164**(9): 2161-2171.
- Preston, R., H. M. Stuart, et al. (2019). "Genetic testing in steroid-resistant nephrotic syndrome: why, who, when and how?" Pediatric Nephrology **34**(2): 195-210.
- Quadrato, G., T. Nguyen, et al. (2017). "Cell diversity and network dynamics in photosensitive human brain organoids." Nature **545**(7652): 48.
- Riazuddin, S., M. Hussain, et al. (2017). "Exome sequencing of Pakistani consanguineous families identifies 30 novel candidate genes for recessive intellectual disability." Molecular psychiatry **22**(11): 1604.

- Rinschen, M. M., C. Pahmeyer, et al. (2015). "Comparative phosphoproteomic analysis of mammalian glomeruli reveals conserved podocin C-terminal phosphorylation as a determinant of slit diaphragm complex architecture." Proteomics **15**(7): 1326-1331.
- Rodriguez, F. A., C. Contreras, et al. (2008). "Protein kinase CK2 as an ectokinase: The role of the regulatory CK2 $\beta$  subunit." Proceedings of the National Academy of Sciences **105**(15): 5693-5698.
- Romeu, A. and L. Arola (2014). "Classical dynamin DNM1 and DNM3 genes attain maximum expression in the normal human central nervous system." BMC research notes **7**(1): 188.
- Roussou, I. and G. Draetta (1994). "The Schizosaccharomyces pombe casein kinase II alpha and beta subunits: evolutionary conservation and positive role of the beta subunit." Molecular and cellular biology **14**(1): 576-586.
- Rüschendorf, F. and P. Nürnberg (2005). "ALOHOMORA: a tool for linkage analysis using 10K SNP array data." Bioinformatics **21**(9): 2123-2125.
- Rusin, S. F., M. E. Adamo, et al. (2017). "Identification of candidate casein kinase 2 substrates in mitosis by quantitative phosphoproteomics." Frontiers in cell and developmental biology **5**: 97.
- Sabir, A., J. K. Walker, et al. (2019). "Expanding the phenotype of Filippi Syndrome: a patient with early onset puberty." Clinical dysmorphology.
- Sajid Hussain, M., S. Marriam Bakhtiar, et al. (2013). "Genetic heterogeneity in Pakistani microcephaly families." Clinical genetics **83**(5): 446-451.
- Sajnaga, E., R. Szyszka, et al. (2013). Site-Directed Mutagenesis in the Research of Protein Kinases-The Case of Protein Kinase CK2. Genetic Manipulation of DNA and Protein-Examples from Current Research, IntechOpen.
- Sakakibara, A. and S. Hattori (2000). "Chat, a Cas/HEF1-associated adaptor protein that integrates multiple signaling pathways." Journal of Biological Chemistry **275**(9): 6404-6410.
- Ségurel, L., M. J. Wyman, et al. (2014). "Determinants of mutation rate variation in the human germline." Annual review of genomics and human genetics **15**: 47-70.
- Shaheen, R., G. M. Abdel-Salam, et al. (2015). "Mutation in WDR4 impairs tRNA m<sup>7</sup>G 46 methylation and causes a distinct form of microcephalic primordial dwarfism." Genome Biology **16**(1): 210.
- Shaheen, R., S. Maddirevula, et al. (2019). "Genomic and phenotypic delineation of congenital microcephaly." Genetics in Medicine **21**(3): 545.
- Shamseldin, H. E., N. Makhseed, et al. (2019). "NUP214 deficiency causes severe encephalopathy and microcephaly in humans." Human genetics **138**(3): 221-229.

- Sharif, S. and D. Donnai (2004). "Filippi syndrome: two cases with ectodermal features, expanding the phenotype." Clinical dysmorphology **13**(4): 221-226.
- Sheffield, L. G., H. B. Miskiewicz, et al. (2006). "Nuclear pore complex proteins in Alzheimer disease." Journal of Neuropathology & Experimental Neurology **65**(1): 45-54.
- Shukla, S. J. and M. E. Dolan (2005). "Use of CEPH and non-CEPH lymphoblast cell lines in pharmacogenetic studies."
- Siomi, H., M. Choi, et al. (1994). "Essential role for KH domains in RNA binding: impaired RNA binding by a mutation in the KH domain of FMR1 that causes fragile X syndrome." Cell **77**(1): 33-39.
- Smigiel, R., G. Landsberg, et al. (2018). "Developmental epileptic encephalopathy with hypomyelination and brain atrophy associated with PTPN23 variants affecting the assembly of UsnRNPs." European Journal of Human Genetics **26**(10): 1502-1511.
- Song, D. H., D. J. Sussman, et al. (2000). "Endogenous protein kinase CK2 participates in Wnt signaling in mammary epithelial cells." Journal of Biological Chemistry **275**(31): 23790-23797.
- Souza, B. S., G. L. Sampaio, et al. (2016). "Zika virus infection induces mitosis abnormalities and apoptotic cell death of human neural progenitor cells." Scientific reports **6**: 39775.
- Speicher, M., S. E. Antonarakis, et al. (2009). Vogel and Motulsky's Human Genetics: Problems and Approaches, Springer Science & Business Media.
- Stoffel, W., I. Hammels, et al. (2016). "Neutral sphingomyelinase (SMPD3) deficiency disrupts the Golgi secretory pathway and causes growth inhibition." Cell death & disease **7**(11): e2488-e2488.
- Sudmant, P. H., T. Rausch, et al. (2015). "An integrated map of structural variation in 2,504 human genomes." Nature **526**: 75.
- Szczepanski, S., M. S. Hussain, et al. (2016). "A novel homozygous splicing mutation of CASC5 causes primary microcephaly in a large Pakistani family." Human genetics **135**(2): 157-170.
- Taverna, E., M. Götz, et al. (2014). "The cell biology of neurogenesis: toward an understanding of the development and evolution of the neocortex." Annual review of cell and developmental biology **30**: 465-502.
- Thornton, G. K. and C. G. Woods (2009). "Primary microcephaly: do all roads lead to Rome?" Trends in Genetics **25**(11): 501-510.
- Toczyski, D. P., D. J. Galgoczy, et al. (1997). "CDC5 and CKII control adaptation to the yeast DNA damage checkpoint." Cell **90**(6): 1097-1106.

- Tolmie, J., M. McNay, et al. (1987). "Microcephaly: genetic counselling and antenatal diagnosis after the birth of an affected child." American journal of medical genetics **27**(3): 583-594.
- Trujillano, D., A. M. Bertoli-Avella, et al. (2017). "Clinical exome sequencing: results from 2819 samples reflecting 1000 families." European Journal of Human Genetics **25**(2): 176-182.
- Valencia, C. A., A. Husami, et al. (2015). "Clinical Impact and Cost-Effectiveness of Whole Exome Sequencing as a Diagnostic Tool: A Pediatric Center's Experience." Frontiers in Pediatrics **3**(67).
- Van den Bosch, J. (1958). "Microcephaly in the Netherlands: a clinical and genetical study." Annals of human genetics **23**(2): 91-116.
- Vervoort, V. S., S. Roselli, et al. (2007). "Splice variants and expression patterns of SHEP1, BCAR3 and NSP1, a gene family involved in integrin and receptor tyrosine kinase signaling." Gene **391**(1-2): 161-170.
- Vogel, F. and A. G. Motulsky (1997). History of Human Genetics. Human Genetics, Springer: 11-23.
- von Appen, A., J. Kosinski, et al. (2015). "In situ structural analysis of the human nuclear pore complex." Nature **526**(7571): 140.
- Von Zglinicki, T., G. Saretzki, et al. (2005). "Human cell senescence as a DNA damage response." Mechanisms of ageing and development **126**(1): 111-117.
- Wagle, P., M. Nikolić, et al. (2015). "QuickNGS elevates Next-Generation Sequencing data analysis to a new level of automation." BMC genomics **16**(1): 487.
- Walther, T. C., A. Alves, et al. (2003). "The conserved Nup107-160 complex is critical for nuclear pore complex assembly." Cell **113**(2): 195-206.
- Wang, J. and A. Wynshaw-Boris (2004). "The canonical Wnt pathway in early mammalian embryogenesis and stem cell maintenance/differentiation." Current opinion in genetics & development **14**(5): 533-539.
- Wang, L., V. Vervoort, et al. (2010). "The SRC homology 2 domain protein Shep1 plays an important role in the penetration of olfactory sensory axons into the forebrain." Journal of Neuroscience **30**(39): 13201-13210.
- Warejko, J. K., W. Tan, et al. (2018). "Whole exome sequencing of patients with steroid-resistant nephrotic syndrome." Clinical Journal of the American Society of Nephrology **13**(1): 53-62.
- Weischenfeldt, J., O. Symmons, et al. (2013). "Phenotypic impact of genomic structural variation: insights from and for human disease." Nature Reviews Genetics **14**(2): 125.
- Weldon, W. F. R. (1902). "Mendel's laws of alternative inheritance in peas." Biometrika **1**(2): 228-254.



- Wisniewska, M. B. (2013). "Physiological role of  $\beta$ -catenin/TCF signaling in neurons of the adult brain." Neurochemical research **38**(6): 1144-1155.
- Woods, C., M. Crouchman, et al. (1992). "Three sibs with phalangeal anomalies, microcephaly, severe mental retardation, and neurological abnormalities." Journal of medical genetics **29**(7): 500.
- Woods, C. G. (2004). "Human microcephaly." Current opinion in neurobiology **14**(1): 112-117.
- Woods, C. G., J. Bond, et al. (2005). "Autosomal recessive primary microcephaly (MCPH): a review of clinical, molecular, and evolutionary findings." The American Journal of Human Genetics **76**(5): 717-728.
- Wünsch, B., L. Kröger, et al. (2020). "Synthesis and SAR of tetracyclic inhibitors of protein kinase CK2 derived from furocarbazole W16." ChemMedChem.
- Wynbrandt, J. and M. D. Ludman (2010). The encyclopedia of genetic disorders and birth defects, Infobase Publishing.
- Xue, Y., Y. Chen, et al. (2012). "Deleterious-and disease-allele prevalence in healthy individuals: insights from current predictions, mutation databases, and population-scale resequencing." The American Journal of Human Genetics **91**(6): 1022-1032.
- Yalçinkaya, F., N. Tümer, et al. (1994). "Congenital microcephaly and infantile nephrotic syndrome—a case report." Pediatric Nephrology **8**(1): 72-73.
- Yamamoto, S., M. Jaiswal, et al. (2014). "A drosophila genetic resource of mutants to study mechanisms underlying human genetic diseases." Cell **159**(1): 200-214.
- Yan, Y., D. He, et al. (2020). "Novel CDKL5 mutations were found in patients in China: retrospective investigation in cases of CDKL5-related disorders." Italian Journal of Pediatrics **46**(1): 1-6.
- Yang, Y., D. M. Muzny, et al. (2014). "Molecular findings among patients referred for clinical whole-exome sequencing." Jama **312**(18): 1870-1879.
- Yang, Y. J., A. E. Baltus, et al. (2012). "Microcephaly gene links trithorax and REST/NRSF to control neural stem cell proliferation and differentiation." Cell **151**(5): 1097-1112.
- Yeo, G. and C. B. Burge (2004). "Maximum entropy modeling of short sequence motifs with applications to RNA splicing signals." Journal of computational biology **11**(2-3): 377-394.
- Yumoto, T., K. Nakadate, et al. (2013). "Radmis, a novel mitotic spindle protein that functions in cell division of neural progenitors." PloS one **8**(11): e79895.
- Zanni, G., P. De Magistris, et al. (2019). "Biallelic Variants in the Nuclear Pore Complex Protein NUP93 Are Associated with Non-progressive Congenital Ataxia." The Cerebellum **18**(3): 422-432.

Zaqout, S., D. Morris-Rosendahl, et al. (2017). "Autosomal Recessive Primary Microcephaly (MCPH): An Update." Neuropediatrics **48**(03): 135-142.

Zecevic, N., Y. Chen, et al. (2005). "Contributions of cortical subventricular zone to the development of the human cerebral cortex." Journal of Comparative Neurology **491**(2): 109-122.

Zhang, L., X. Yang, et al. (2011). "The Wnt/ $\beta$ -catenin signaling pathway in the adult neurogenesis." European Journal of Neuroscience **33**(1): 1-8.

Zhao, F., J.-y. Zhu, et al. (2019). "Mutations in NUP160 Are Implicated in Steroid-Resistant Nephrotic Syndrome." Journal of the American Society of Nephrology **30**(5): 840-853.

Zheng, X., S. Yang, et al. (2012). "Loss of zygotic NUP107 protein causes missing of pharyngeal skeleton and other tissue defects with impaired nuclear pore function in zebrafish embryos." Journal of Biological Chemistry **287**(45): 38254-38264.

Züchner, S., M. Noureddine, et al. (2005). "Mutations in the pleckstrin homology domain of dynamin 2 cause dominant intermediate Charcot-Marie-Tooth disease." Nature genetics **37**(3): 289-294.

# 11. Erklärung

Ich versichere, dass ich die von mir vorgelegte Dissertation selbständig angefertigt, die benutzten Quellen und Hilfsmittel vollständig angegeben und die Stellen der Arbeit – einschließlich Tabellen, Karten und Abbildungen –, die anderen Werken im Wortlaut oder dem Sinn nach entnommen sind, in jedem Einzelfall als Entlehnung kenntlich gemacht habe; dass diese Dissertation noch keiner anderen Fakultät oder Universität zur Prüfung vorgelegen hat; dass sie – abgesehen von unten angegebenen Teilpublikationen – noch nicht veröffentlicht worden ist sowie, dass ich eine solche Veröffentlichung vor Abschluss des Promotionsverfahrens nicht vornehmen werde.

Die Bestimmungen der Promotionsordnung sind mir bekannt. Die von mir vorgelegte Dissertation ist von **Prof. Dr. Peter Nürnberg** betreut worden.

## **Teilpublikationen:**

Braun DA, Lovric S, Schapiro D, Schneider R, Marquez J, Asif M, Hussain MS, Daga A, Widmeier E, Rao J, et al. Mutations in multiple components of the nuclear pore complex cause nephrotic syndrome. **J Clin Invest.** (2018); 128: 4313-4328.

Köln, den 27. April 2020



---

**Maria Asif**

## 12. Lebenslauf

### Persönliche Daten

Name: Maria Asif  
Geburtsdatum: 06. Juni 1989  
Geburtsort: Peshawar, Pakistan  
Staatsangehörigkeit: Pakistani  
Anschrift: Kölner Str. 175, 51149, Köln

### Bildung

2017- 2020 Doktorand am Cologne Center for Genomics (CCG) und Institut für Biochemie I, Medizinische Fakultät, Universität zu Köln, Deutschland.

#### **Dissertationsthema;**

“Delineating genetic underpinnings and disease pathogenesis of primary microcephaly associated syndromes”.

2013-2016 Wissenschaftliche Mitarbeiter im Bereich des projektes “Autosomal rezessive primäre Mikrozephalie” am NIBGE (National Institute for Biotechnology and Genetic Engineering), Faisalabad, Pakistan.

2011-2013 M.Phil (Master of Philosophy) im Bereich der Biotechnologie am NIBGE (National Institute for Biotechnology and Genetic Engineering), Institute of Engineering and Applied Sciences (PIEAS), Islamabad, Pakistan.

#### **Masterarbeit;**

“Genetic analysis of autosomal recessive deafness and dyslexia in Pakistani kindred”.

2007-2011 BS (Hons) im Bereich der Biotechnologie, University of Peshawar, Pakistan.

2005-2007 F.Sc (Faculty of Science), Board of Intermediate and Secondary Education, Peshawar.